University of Groningen

Towards control over motion at the molecular and submolecular level

Bauer, Jurica

IMPORTANT NOTE: You are advised to consult the publisher's version (publisher's PDF) if you wish to cite from it. Please check the document version below.

Document Version
Publisher's PDF, also known as Version of record

Publication date:
2013

Link to publication in University of Groningen/UMCG research database

Towards Control over Motion at the Molecular and Submolecular Level

Jurica Bauer

university of
groningen

RIJKSUNIVERSITEIT GRONINGEN

Towards Control over Motion at the Molecular and Submolecular Level

Proefschrift

ter verkrijging van het doctoraat in de
Wiskunde en Natuurwetenschappen
aan de Rijksuniversiteit Groningen
op gezag van de
Rector Magnificus, dr. E. Sterken,
in het openbaar te verdedigen op
vrijdag 13 december 2013
om 14:30 uur

door

Jurica Bauer

geboren op 7 december 1982

te Zagreb, Kroatië

Promotor : Prof. dr. B.L. Feringa

Beoordelingscommissie : Prof. dr. A.J. Minnaard
Prof. dr. W.R. Browne
Prof. dr. D.J. Broer

Contents

Chapter 1

Controlling Molecular Motion

This chapter aims to give an overview of the numerous attempts by scientists to develop artificial motor systems, the vast majority of which draw inspiration from natural dynamic systems. The focus is set on rotary motion and responsive molecules on surfaces. The former describes the development of molecular rotors and the attempts to control them while the latter aims to show how the field progressed from the investigation of small and simple functional molecules to nanovehicles of gradually increasing complexity.

Introduction

Despite all the scientific advances over the years, scientists still remain puzzled when it comes to some of the most basic features of biological systems that life is based upon. The way biologically important molecules perform their functions in a highly complex system like a cell still remains to a large extent a mystery. Understanding natural systems at the molecular and even submolecular level is crucial if these systems are to be affected and altered in a controlled way. Interfering with these systems, however, is essential for treating certain diseases and improving the life of many[1,2].

Getting to understand how biological systems exactly work and manipulating them at the molecular level has proven extremely difficult, not only due to the minuscule size of these highly complex molecules but also due to the prevalence of different physical phenomena at that level[3]. Whereas macroscopic objects follow Newtonian mechanics governed by forces like gravity and friction, these forces become negligible at the molecular level. Movement of molecules is rather governed by noncovalent interactions including van der Waals interactions and electrostatic interactions, as well as molecular vibrations and Brownian motion. In stark contrast to the macroscopic world, molecular systems never remain stationary, not even at the temperature of 0 K where vibrational motion is still present. At temperatures above 0 K, molecular motion is mostly governed by random and thermal movements (Brownian motion) and, under these conditions, molecular motion in a straight line (or any directed motion) seems like „walking in a hurricane"[7] (apart from thermal translational motion molecules also exhibit thermal conformational motion). Harnessing molecular motion at the nanoscale is therefore an extremely difficult task[4,5,6,7].

Nevertheless, one of modern chemistry's main objectives is gaining control over molecular motion[3,8,9,10,11]. Taking inspiration from nature, scientists have started developing simple artificial systems with the goal of developing controlled motion at the (sub)molecular level. Molecular rotors, motors, shuttles and switches have extensively been used in numerous attempts to bring molecular motion under control. In the next sections some of the most prominent examples of natural as well as entirely artificial rotors will be discussed.

Gaining complete control over molecular motion, however, is an endeavor that faces many challenges, the biggest of which is often considered to be competing with Brownian motion[3,4]. In order to control movement at the molecular level, Brownian motion needs to be either exploited or overcome. A way of overcoming Brownian motion is immobilization of molecular machinery on a surface. Artificial systems designed for the study of molecular motion on surfaces will be discussed at the end of this chapter.

Natural rotary motors

ATP synthase

Life implies movement and most forms of movement in the living world are powered by protein machines known as molecular motors[1,2,12]. These important biomolecules transport cargo, power cell locomotion, drive cell division and allow organisms to move. Three types of cytoplasmic motors are known: myosins which move on actin filaments, and dyneins and kinesins, which use microtubules as tracks. All three classes of motors use ATP hydrolysis to convert chemical energy into mechanical work. ATP, the main biological energy currency, is synthesized from ADP and inorganic phosphate, catalyzed by ATP synthase. The F_1 portion of ATP synthase, also known as F_1–ATPase, functions as a rotary molecular motor; as depicted in Fig 1, its γ-subunit rotates against the surrounding $\alpha_3\beta_3$ subunits, hydrolysing ATP in three separate catalytic sites on the β-subunits. The reverse rotation of the γ-subunit, driven by proton flow through the associated F_0 portion of ATP synthase, leads to ATP synthesis in biological systems[13,14,15,16,17]. One ATP synthase can hydrolyze 390 molecules of ATP per second which corresponds to 130 revolutions per second[18].
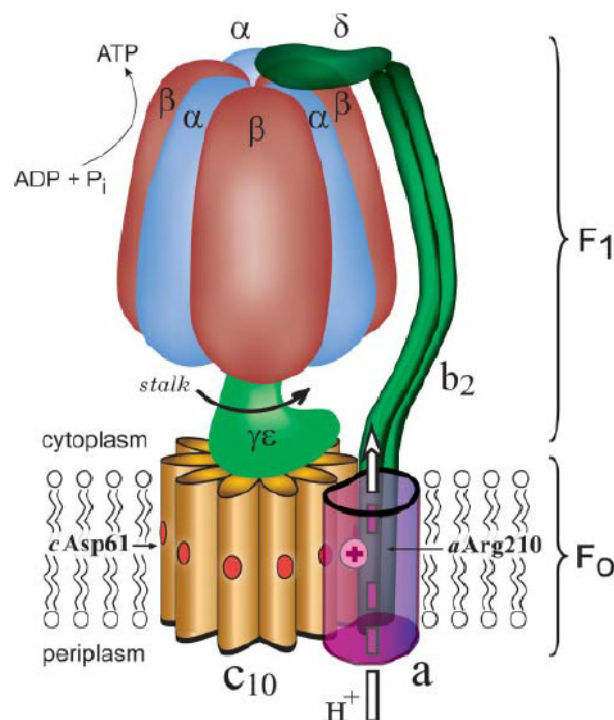
Figure 1. Schematic view of the *E. coli* ATP synthase[15]. The solvent exposed F_1 unit (*top*) consists of subunits $\alpha_3\beta_3\gamma\delta\varepsilon$; the membrane F_0 unit (*bottom*) consists of subunits ab_2c_{10}.

Bacterial flagellar motor

Another well-known rotary mechanism in the biological world is the bacterial flagellar motor[2,19,20,21]. A flagellum is a lash-like appendage that protrudes from the cell body of certain prokaryotic and eukaryotic cells. This motor is responsible for the locomotion of the bacterium cell. The flagellar filament (propeller) is a 10 μm-long, thin, rigid, corkscrew-shaped structure, with a helical period of about 2 μm. The filament is connected to the hook by two junctional proteins. The flexible hook acts as a universal joint permitting the filament and motor to rotate about different axes. The remaining flagellar parts are rings. A schematic representation of the flagellum is given in Fig 2. The bacterial flagellum is driven by a rotary engine made up of protein, located at the flagellum's anchor point on the inner cell membrane. The engine is powered by the flow of protons across the bacterial cell membrane due to a concentration gradient set up by the cell's metabolism. The rotor transports protons across the membrane and is turned in the process. The direction of rotation can be switched almost instantaneously, caused by a slight change in the position of a protein in the rotor. The flagellum can spin at a rate of 350 Hz[22] and achieve linear locomotion of the bacterium as fast as 25 μm s^{-1}.[23]
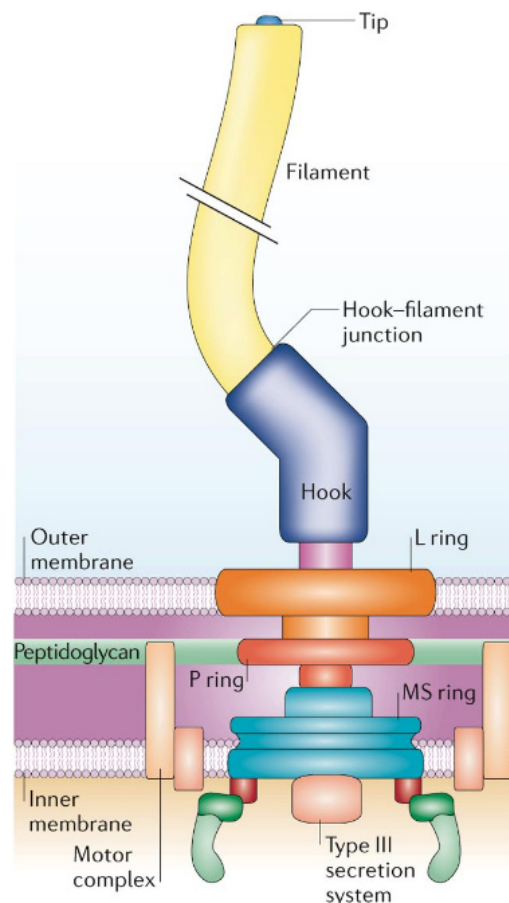
Figure 2. Schematic view of the bacterial flagellum from *Salmonella typhimurium*[21].

Natural motors like the abovementioned ATP synthase or the bacterial flagellum are often taken by scientists as a source of inspiration for making analogous, yet entirely synthetic, systems[3]. It is obvious that the complexity and efficiency of natural systems cannot be easily reproduced. Many attempts of making artificial systems, however, have been realized and some of them are potentially useful in the growing field of nanotechnology[9]. In the next sections the most prominent examples of artificial molecular rotors as well as control over their rotary behaviour are reviewed.

Artificial molecular rotors

Before describing any of the examples from the literature it may be wise to define some of the terms that are commonly used to describe these rotary systems.

A *molecular rotor* is a molecular system in which a molecule or part of a molecule rotates against another part of the molecule or against a macroscopic entity such as a surface or a solid[24]. It is common to call the part of the molecule that rotates against the rest the *rotator* and the stationary part of the system with respect to which the rotator turns the *stator*. If the rotor is not mounted on a solid support, it is common to view the part with the larger moment of inertia as stationary (the stator) and the part with the smaller moment of inertia as the rotator. The *axle* is the portion of the molecule that carries the rotator and about which the rotator turns. A molecular *rotary motor* is a molecular rotor capable of producing useful work. Useful work is not easily defined at the nanoscale but may in this context be described as a process that starts with the system at thermal equilibrium with its surroundings and at the end leaves a measurable and desired difference in the system after it is once again in thermal equilibrium[24].

Molecular rotors have been studied extensively due to their applications as molecular machines[3,9,11,24,25,26]. These promising systems are being investigated for their use in the most recent generations of nanoscale electronics[10]. The construction and operation of nanoscale machines and devices[3,10,27,28], in which the molecular motion is controlled with the goal of performing a specific function, has been the focus of many research groups. Triggering these devices by external stimuli such as electricity, light or chemical reagents gives rise to various functions including those of diodes, rectifiers, memories, resonant tunnel junctions and single settable molecular switches that can be electronically configured for logic gates[25]. A task of a molecular machine is to perform an action leading to a desired function following the input of a signal with a supply of energy. It is often desirable to have a molecular machine performing mechanical movements under control of appropriate energy inputs[3,9,10,26]. Achieving unidirectional motion has been one of the primary objectives of nanotechnology[3,11,29] and examples of realizing such systems will be discussed in the next sections.

Biaryl rotors

Biaryl rotors are one of the simplest classes of these systems[24,30]. They comprise two aryl groups connected by a C–C bond of an aryl–aryl type. The rotation about the aryl–aryl bond in biaryl rotors has no directional preference. Most investigated of all biaryl rotors are biphenyl rotors as depicted in Fig 3a.

a **b**
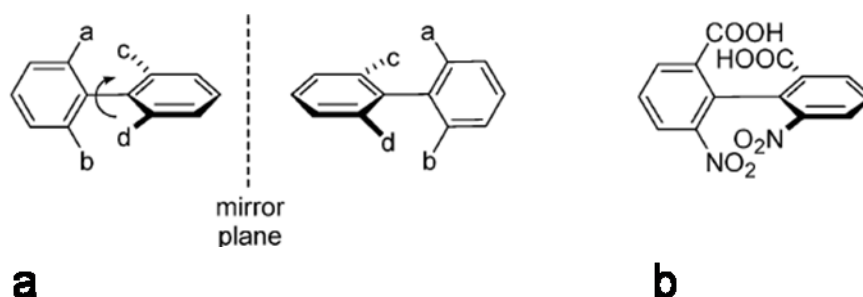
Figure 3. a: Atropisomers of a biphenyl molecule, **b:** 6,6'-dinitro-2,2'-diphenic acid; the first resolution of enantiomers of a biphenyl molecule[24,31].

Hindered rotation of groups within a molecule, if slow enough on the time scale of observation, can render a molecule chiral. This is the case for biphenyl molecules where the rotation about the C–C bond is hindered (Fig 3). The resolution of enantiomers was first realized for 6,6'-dinitro-2,2'-diphenic acid (Fig 3b) and the resolution of a number of other sterically hindered biphenyls followed. The ability of compounds to possess chirality due to restricted rotation is termed *atropisomerism*[24,30]. Rotational processes are related to the energy difference between the ground-state and transition-state geometries of the molecules in question. For biphenyl-type molecules, for rotation to proceed, the two aryl groups must pass through a geometry in which they are coplanar (some computational results indicate, however, that the transition state is somewhat twisted and not perfectly coplanar which decreases steric hindrance when the aryl rings go through the same plane in the transition state[30]). Depending on the substituents at the positions located *ortho* to the aryl–aryl bond, the transition state may be low enough in energy such that rotation occurs rapidly at room temperature. If sterically demanding groups are introduced in these positions, isomers will result which do not rotate at room temperature and may be isolated as single enantiomers. Most tri- and tetra-*ortho*-substituted biphenyls are conformationally stable and can be conveniently resolved into enantiomers at room temperature unless small fluoro or methoxy *ortho*-substituents are present. With the exception of 2,2'-disubstituted biphenyls bearing bulky isopropyl, phenyl or *tert*-butyl groups, axially chiral biphenyls bearing fewer than three *ortho*-substituents are often not stable to racemization at room temperature.

Rotation about the chiral axis in 2,2'-disubstituted biphenyls can in principle occur via two different transition states (Fig 4[30], in which the substituents pass either one another or a hydrogen atom of the adjacent aryl ring. The latter entails

significantly less steric repulsion and is the energetically favoured and therefore predominant pathway of atropisomerization in biphenyl systems.
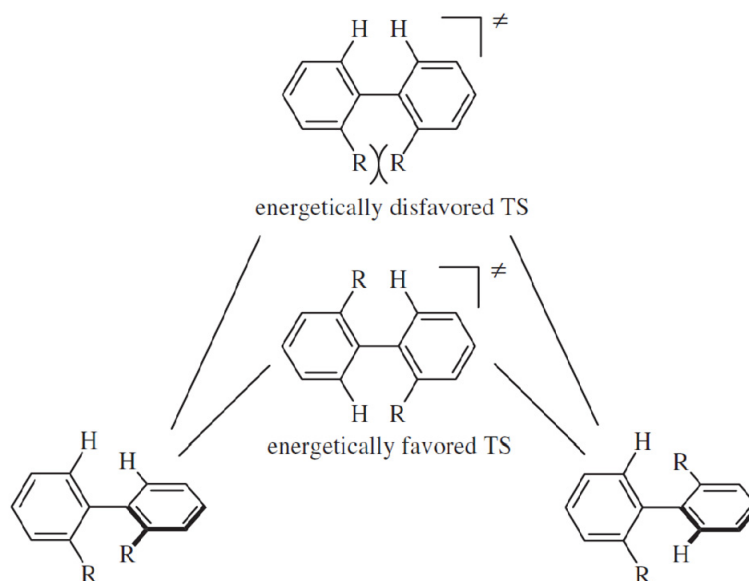
Figure 4. Rotation in a 2,2'-disubstituted biphenyl and two possible transition states for the process[30].

Substituents in the *meta*-position exhibit a so-called *buttressing effect*[30]: they reduce the flexibility of the adjacent *ortho*-substituent and therefore enhance steric repulsion during rotation about the chiral axis. The buttressing effect may provide a significant contribution to the overall steric hindrance to rotation; the effect depends on the size and geometry of the *meta*-group and on the bulkiness of the adjacent *ortho*-substituent. Electronic effects of *para*-substituents are less pronounced than steric interactions and alter the rotational energy barrier of 2,2'-disubstituted biphenyls by up to 10 %[30].

Molecular propellers and gears

Work on biphenyls and related atropisomeric systems led to the discovery of propeller-like molecules (molecules having a helical propeller structure)[24]. Two propeller conformations with all or some of the rings twisted in the same sense are depicted in Fig 5. Molecular propellers are still being investigated[32].
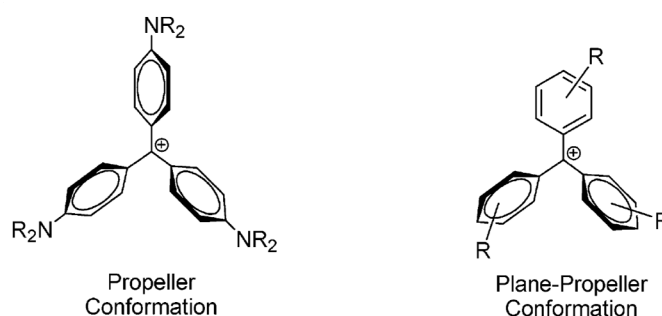
Figure 5. Proposals for the stereochemistry of molecular propeller systems[24].

Soon after the discovery of propeller systems, researchers began to discover that the rotation in one part of the molecule could affect the rotation of other parts in a correlated fashion. In molecules like dimesitylcarbonium ions (Fig 6a) the *ortho*-methyl groups were found to exchange rapidly even at low temperatures. This exchange can be due to nearly unhindered rotation about the axle or to a concerted rotation of the arene rings wherein the torsional motion of one ring mandates the turning of the second in the opposite direction (disrotation). Steric arguments make the former highly unlikely and the latter is supported by calculations. This type of motion has been termed the „cogwheel effect". A broader concept of a molecular gear was developed with the intention of invoking images of the macroscopic analogues. Some of the gear classes are shown in Fig 6b–e. Despite the conceptual analogy, the physical phenomena related to these macroscopic systems may not translate to the molecular scale[24].

a   **b**   **c**   **d**   **e**
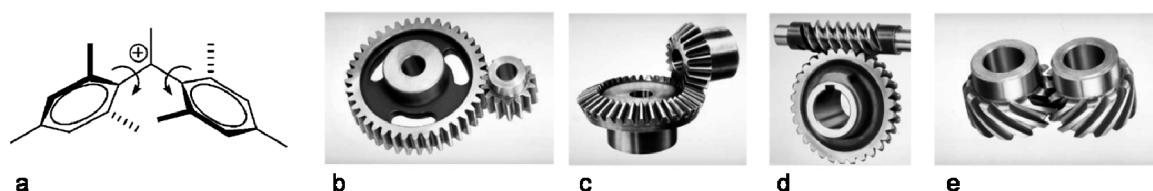
Figure 6. a: A gear-like molecule displaying concerted rotational motion, **b:** spur gears, **c:** bevel gears, **d:** worm gears, **e:** spiral or helical gears[24].

It can be argued, however, that the molecular gear was the first mechanical molecular device as it is one of simplest devices that can be designed from molecules[9,24]. The first examples of truly geared rotation (bevel gears, Fig 6c), however, were ditriptycyl ethers and ditriptycylmethanes depicted in Fig 7. These molecules consist of two three-toothed gears and the intermeshing between the phenyl groups on the two triptycenes leads to little or no slippage of the gears. In these systems there is no doubt that rotation of one triptycene unit causes the disrotation of the other in a frame of reference that keeps the central linker atom static[24]. There is, however, no control over the direction of rotation in these examples.
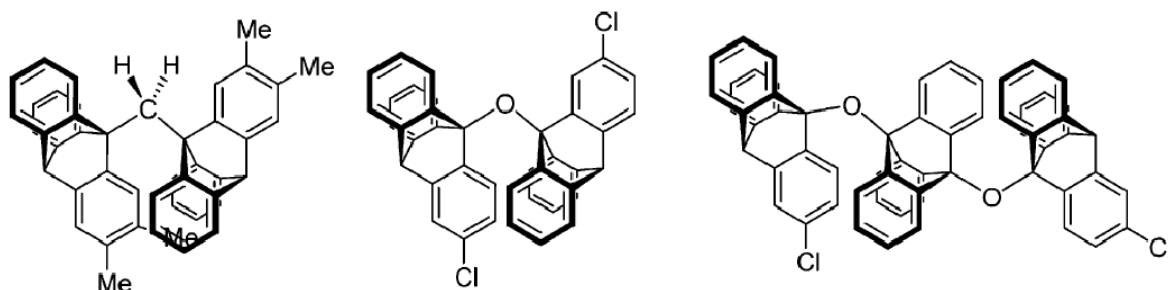
Figure 7. Triptycene-based molecular bevel gears[24].

Formal rotation about triple bonds

Biaryl rotors as well as molecular propellers and gears discussed above are examples of the rotation about single bonds. There has also been a substantial amount of research about formal rotation about triple bonds[24]; in a rotary system with a triple bond there are actually two single and a triple bond separating the rotator from the stator. The rotation actually takes place around the single bonds and not around the triple bond and the large distance (around 4 Å) between the two parts rotating with respect to one another results in a low energy barrier for the rotation. In order to measure energy barriers for rotations about triple bonds by conventional techniques, such as dynamic NMR spectroscopy, sterically hindered analogues need to be synthesized. Figure 8 shows some of the sterically hindered diphenylacetylenes investigated both experimentally and theoretically.
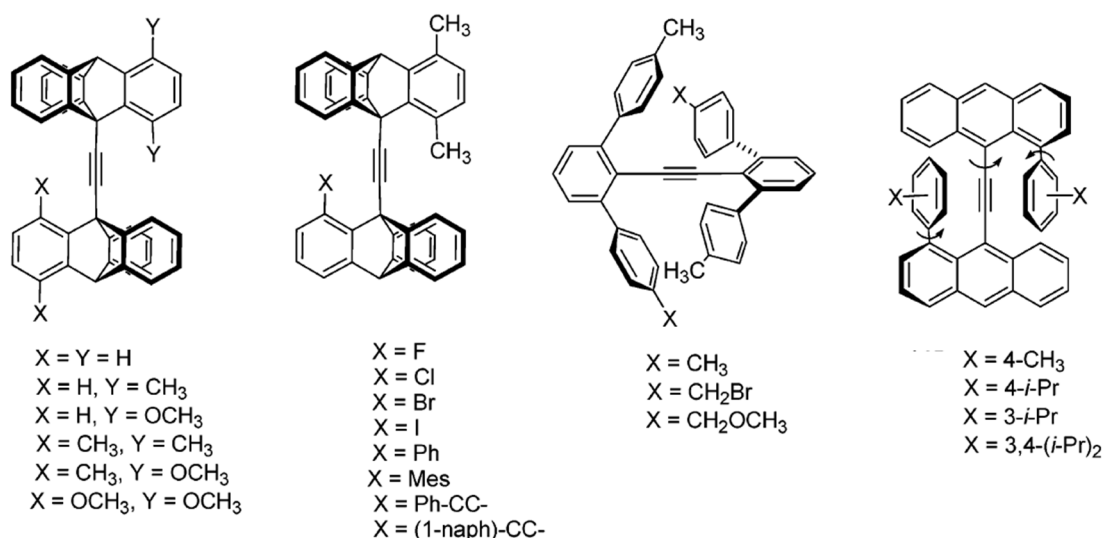
Figure 8. Sterically hindered diphenylacetylenes designed for the investigation of the rotation about the triple bond[24].

The barrier is found to increase with increasing steric size of the substituent X (Fig 8), for example on going from fluorine to iodine. It is also worth noting that it is not just the absolute steric size of X that needs to be taken into account but its flexibility as well. For example, a methyl group raises the energy barrier more than a methoxy group which is likely due to the ability of the latter to avoid steric interactions by rotations around the aryl–O and methyl–O bonds. The methyl group, on the other hand, is more rigid and cannot avoid steric interactions as easily[24]. This work shows how rotation rates may be tuned by changing the structure of the molecular rotor and this will be crucial for the design of future rotational devices. The direction of rotation, however, is random. These and similar systems are still widely investigated[33].

Rope-skipping rotors, turnstiles and gyroscopes

A „rope-skipping" rotor, as depicted in Fig 9, consists of a cyclic core to opposite ends of which are attached the two ends of a chain that can swing around the core[24]. Taking the core of such a system as an immobile reference frame, this evokes images of children skipping rope in the street. The parent rope-skipper is cyclophane (Fig 9).
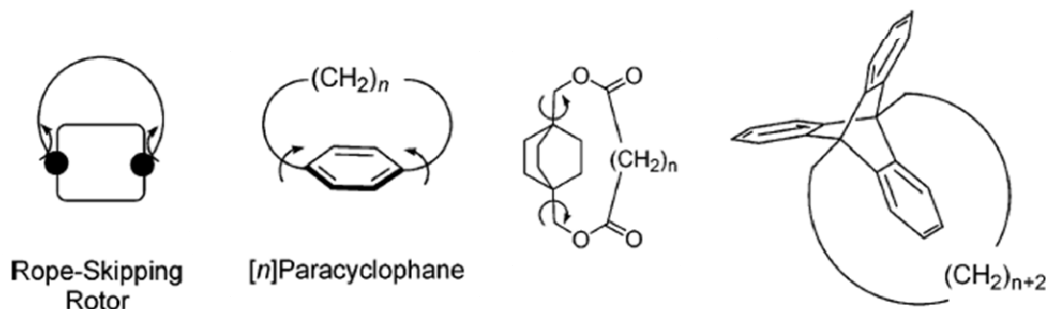
Figure 9. Rope-skipping rotors[24].

Two other examples of rope-skipping rotors are shown in Fig 9. The investigation of rotors with the triptycene central unit (Fig 9) showed that the triptycenes could not rotate inside the cavity of the chain for any length. Models indicated that the chain was wedged between two phenyl groups of the triptycene; this was evidenced by the NMR spectra which showed two phenyl groups to be equivalent and the third one to be in a magnetically different environment. Similar results were also found for a triptycene-based cyclophane.

The first rationally designed molecular turnstile[24,34] is shown in Fig 10. A substituted *p*-diethynylbenzene group is attached to the interior of a phenylethynyl macrocyclic framework and the rotation of the internal phenylene group is observed as a function of its substituents.
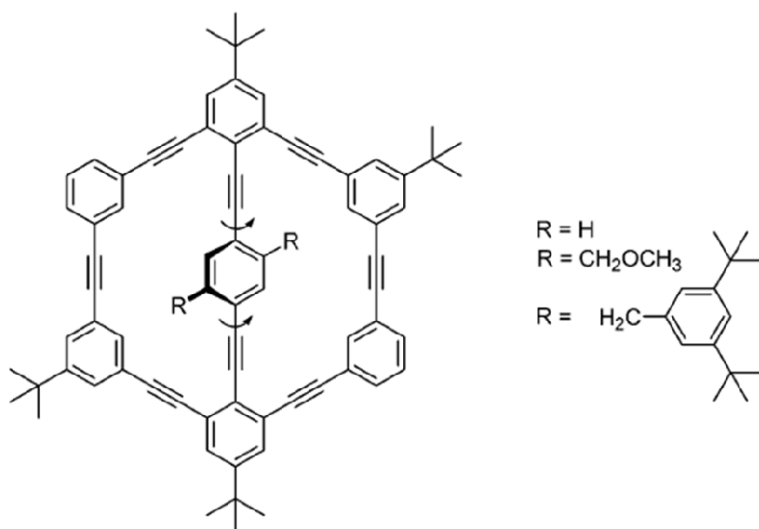
Figure 10. Molecular turnstile[24,34].

When R = H the rotation of the phenylene group is too fast to be studied by NMR methods (the energy barrier to rotation is likely below 4 kJ mol^{-1}). For the compound with R = CH$_2$OCH$_3$ the rotation is still very fast and the barrier to rotation is determined to be 56 kJ mol^{-1}. The barrier is higher than for the compound with R = H due to steric interactions between the methoxymethylene groups and the macrocyclic framwork. When R = (3,5-di-*tert*-butylphenyl)methylene no rotation is observed. The R group is very bulky rendering the compound conformationally locked[34]. This is yet another example how the rotation rate of a rotor molecule may be tuned by careful design. The rotary system still lacks directional preference.

A simple gyroscope (Fig 11a) is a device with one degree of freedom consisting of a spinning mass (rotator) with its spinning axis positioned through the centre of the mass and mounted within a rigid frame (stator). When mounted on gimbals, gyroscopes have up to three degrees of freedom and form the basis of inertial navigation systems used in airplanes and satellites. A molecular gyroscope is a molecular rotor similar to a rope-skipping rotor but carrying more than one chain around the central core. The surrounding chains provide a shield/cage around the rotor in the interior (Fig 11). In an isolated molecule the core and the shield will both rotate and it will not be easy to tell the stator apart from the rotor[9,24,35,36,37,38].
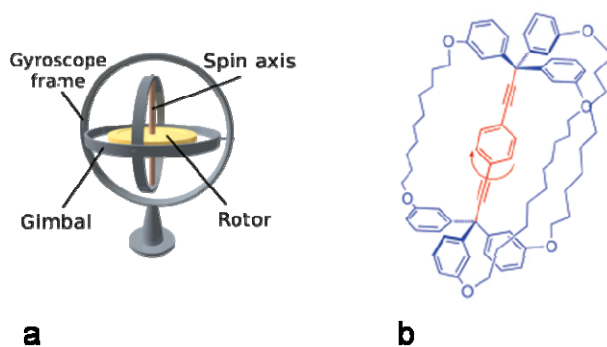
Figure 11. a: Gyroscope **b:** Molecular gyroscope[35].

An example of a molecular gyroscope, prepared for the study of rotation in the crystalline state, is given in Fig 11b. It consists of an intrinsically barrierless 1,4-dialkynylbenzene rotator and two triarylmethyl (trityl) groups acting as a stator. In addition to providing steric shielding, the stator serves as a frame of reference to define the dynamics of the rotator in the crystal. As revealed by X-ray analysis the steric shielding provided by three alkyl chains in not ideal. While the three bridges curve away from the centre to maximize the space around the rotator, bridges from neighbouring molecules and included solvent molecules reduce the free volume about the prospective rotator. This suggests that bulkier chains will be necessary to create the shielding needed to prevent close packing interactions and the inclusion of solvent molecules.

Structure-function relationships for crystalline molecular machines, including molecular gyroscopes and compasses, can now be employed in the design of novel amphidynamic systems (systems able to make up supramolecular assemblies with structurally programmed molecular dynamics). Recent progress in multicomponent amphidynamic molecular machines has led to the development of strategies to not only rationally engineer functional structures but also to modulate their dynamic behavior through the presence of chemical and electric stimuli[37,38,39,40,41,42,43].

Molecular carousels

A molecular carousel is defined as a compound whose molecules consist of two or more (nearly) planar „decks" which rotate and remain parallel to each other[24]. Metallocenes are the simplest type of molecular carousel and ferrocene is possibly the best-known one (Fig 12). The energy barrier for the rotation in ferrocene, as well as in ruthenocene, cobaltocene, nickelocene and chromocene, is around 8 kJ mol^{-1}. As can be seen from Fig 12, inserting bulky groups on the cyclopentadiene rings increases the barrier to rotation.

$\Delta^{\ddagger}G = 8$ kJ mol^{-1}
(M = Fe, Ru, Cr, Co, Ni)

$\Delta^{\ddagger}G = 46$ kJ mol^{-1}

$\Delta^{\ddagger}G = 54$ kJ mol^{-1}
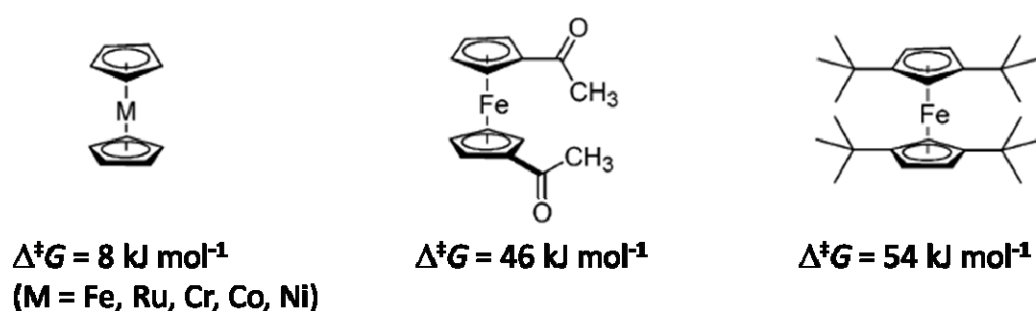
Figure 12. Metallocenes and some of their derivatives with corresponding rotation energy barriers[24].

Bis(tetraphenylcyclopentadienyl)iron(II) was synthesized to investigate both the rotation of the cyclopentadienyl rings and the reorientation of the phenyl groups in the process in an attempt to determine if they were correlated (Fig 13a). The barrier to rotation of phenyl groups (cogwheeling) was found to be 8 kJ mol^{-1} at −95 °C while the cyclopentadienes were still rotating rapidly.
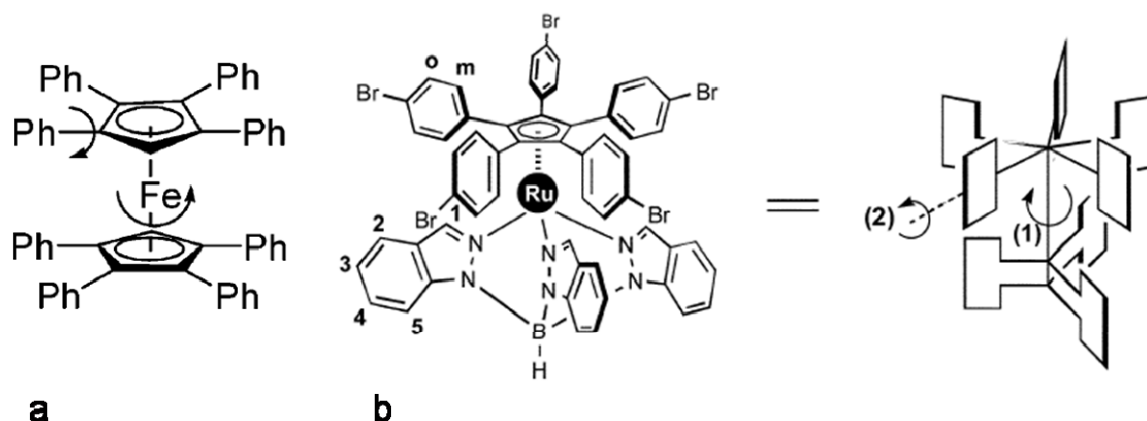
Figure 13. a: Octaphenylated ferrocene for the study of coupled rotation, **b:** molecular turnstile with a scheme representing its coupled rotation[24,44].

Interestingly, polyphenylated metallocene molecules do not have very high barriers to rotation as one might expect for such a crowded system. It was postulated that the phenyl rings can rotate slightly out of their preferred geometry to allow for passage of the other substituents, which corresponds to a geared („concerted") rotation. This was also observed for a „molecular turnstile", shown in Fig 13b[24,44]. The rotation of the cyclopentadiene ligand was not hindered nor was the rotation of the phenyl rings on the cyclopentadienyl ring. It was indicated by NMR that the indazolyl groups fit into the pockets created by the phenyl groups on the opposite deck, as evidenced by their greater shielding. A rotational mechanism was proposed wherein the phenyl rings twist out of their nearly perpendicular arrangement as the indazolyl rings pass and then settle back into their perpendicular state[24,44]. Molecular carousels of this type exhibit no directional preference for rotation.

Electrically controlled molecular rotors

A molecular rotor was reported recently consisting of a five-arm rotator mounted on a tripodal stator[45] (Fig 14a). Rotation of the rotator is enabled by the central ruthenium atom acting as an atomic ball bearing between the stator and the central cyclopentadienyl ring in the rotator. Four of the rotator arms have a ferrocene group attached at their ends, and the fifth arm is truncated beyond the phenyl ring. This provides a structural dissymmetry that helps in the detection of discrete rotation steps or the rotator relative to the stator.
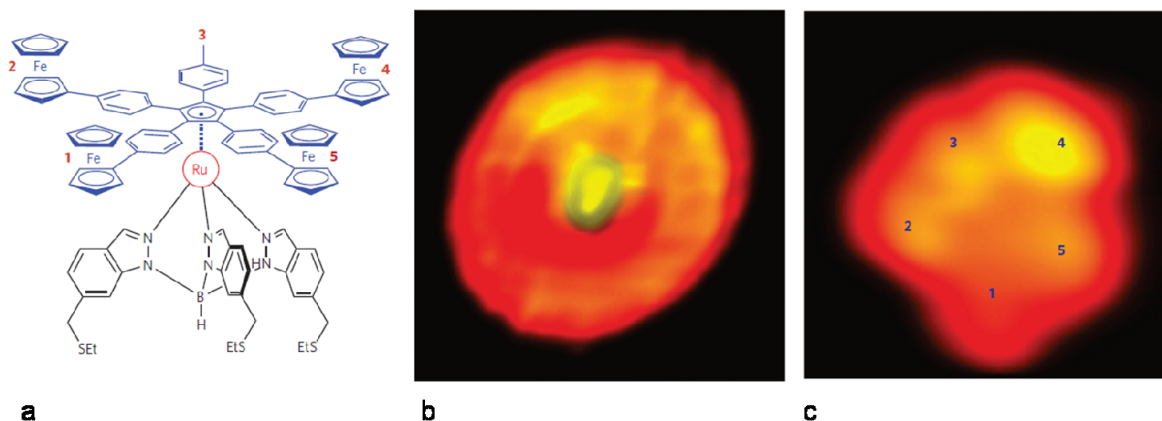
Figure 14. a: Structure of the electrically driven rotary motor, **b:** STM image of a rotating motor, **c:** STM image of a stationary motor[45].

The rotor was mounted on a Au(111) surface and observed by scanning tunneling microscopy (STM) as shown in Fig 14b,c. By selective inelastic electron tunneling through different subunits of the molecule the rotor can be made to rotate in a clockwise or counterclockwise direction. The rotation takes place in rotational increments of 24° and the direction of the rotation is determined from the change in the position of the truncated arm (Fig 14a). The ability to undergo directional rotation makes the described molecule not only function as a rotor but also as a rotary motor. The mean rotation is predominantly clockwise if electrons are passing through the truncated arm position and mostly counterclockwise if electron excitation takes place via a ferrocene arm. Excitation of a specific subunit of the motor therefore enables a controlled unidirectional rotation provided the excitation period is sufficiently long. The directional rotation arises from sawtooth-like rotational potentials which are solely determined by the internal molecular structure and are independent of the surface adsorption site[45]. The system described here is a significant step forward in the development of complex and automated nanomachinery that can be operated on a material surface.

The first example of a ferrocene-based redox-responsive molecular carousel was recently reported[46]. Its rotary motion is triggered by simple electron transfers centred on π-dimerizable bipyridinium fragments introduced on both cyclopentadienyl rings (Fig 15). In the tetracationic form the molecule adopts the „open state" as governed by the tendency of the molecule to keep the repelling charges as far apart as possible. In the reduced dicationic form the charges do not repel each other as severely and the bipyridyl arms come together in the „closed state". The driving force for this is the π–π stacking of the bipyridyl groups which overrides the destabilizing effect of having both charges on the same side of the rotor.
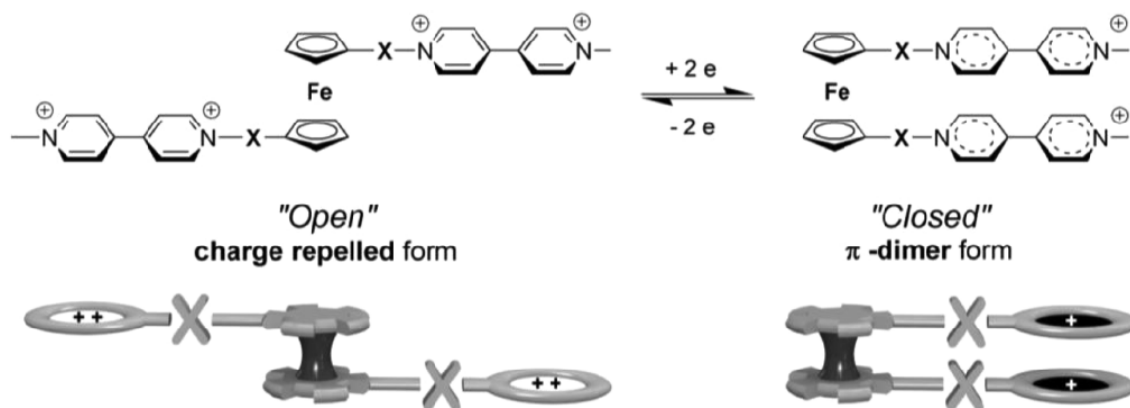
Figure 15. Reversible conversion of a ferrocene-based pivot between "open" charge-repelled form and a "closed" π-dimerized state[46]. "X" represents an organic linker.

In the work described above no directionality of the rotary motion is achieved but it nevertheless provides an elegant method of controlling rotary motion in a molecular carousel. As such this work undoubtedly contributes to the development of molecular devices.

Apart from electrically controlled molecular rotors that show no directional preference of rotation[46,47,48], there have also been examples of directional electric molecular rotary motors. An example where rotation induced by the electric field has been experimentally realized is shown in Fig 16b; mounted on a Au(111) surface, the molecules act as altitudinal rotors and the rotation is controlled by the electric field of an STM tip[49,50,51]. The rotation has been observed by tunneling barrier height imaging (BHI) and confirmed by molecular dynamics calculations. Unidirectional rotation of certain stereoisomers is predicted in the presence of an alternating electric field but has not been observed experimentally[49,50,51]. Based on quantum chemistry calculations, another organic molecule with a rotator having a permanent dipole moment was proposed (Fig 16a)[52]. Attaching this molecule to electrodes, as shown in Fig 16a, an electric field might be used to drive the molecular dipole motor with unidirectionality and complete control over the rotation rate while the conductance should provide a real-time measure of the motion[52]. Despite the clever design, however, this system has not been put into practice yet. Another example is a molecule of butyl-methyl sulfide that becomes chiral once mounted on a Cu(111) surface[53,54]. Electrons from an STM tip are used to drive the directional rotation of the molecule on the surface (Fig 16c). It was shown that the direction and rate of the rotation were related to the chiralities of both the molecule on the surface and the STM tip[53,54]; it is known that regular STM tips can be intrinsically chiral[55] and the investigation described here showed that any tip used affected opposite enantiomers in a different but not opposite way and different tips also affected the same enantiomer in a different way. This led to the conclusion that the observed rotational directionality and changes in the rotation rate are a result of a diastereomeric effect brought upon by the combination of the chirality of the molecules on the surface and that of the STM tip[53,54].
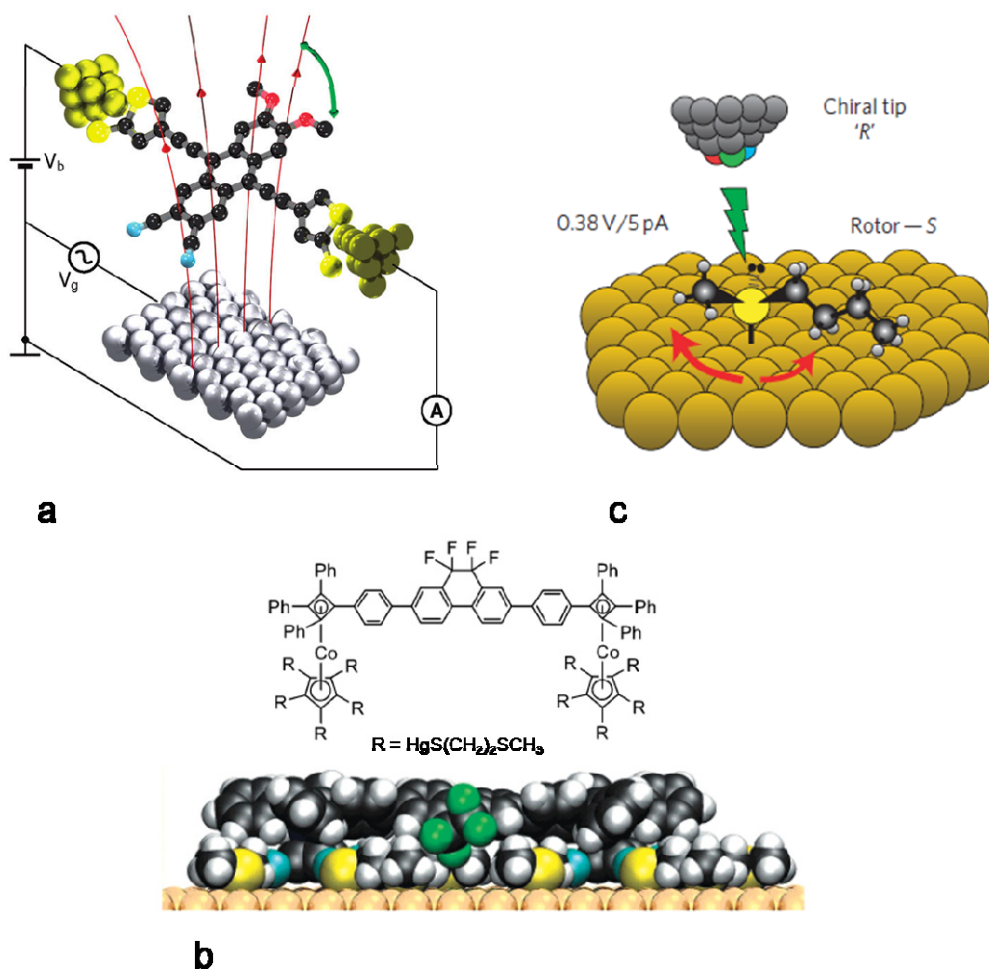
Figure 16. a: A rotor being operated by electric field[52], **b:** An altitudinal rotor on Au(111)[49], **c:** A surface-mounted rotor being operated by an STM tip[54].

Chemically controlled molecular rotors

Controlling and tuning the rotation rate by chemical stimuli is highly important due to its applicability in molecular devices[3,9,24,26]. The design of a first molecular brake[26] is shown in Fig 17.

a

activate
brake

(brake off)   (brake on)

b

add Hg++
EDTA

(brake off)   (brake on)
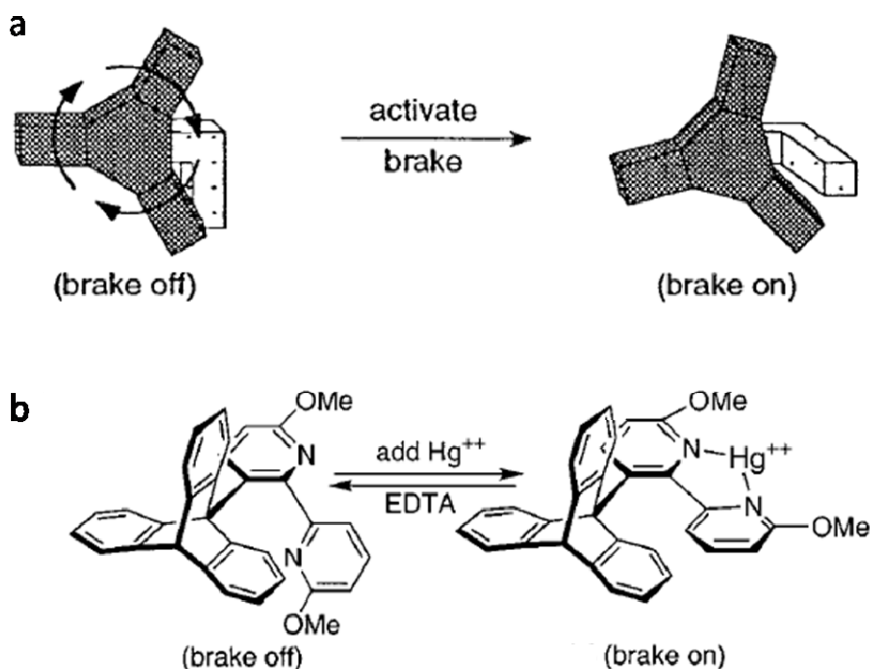
Figure 17. Design of a triptycene rotator with a molecular brake. **a:** A schematic representation of the molecular brake, **b:** The mechanism of action of the molecular brake[9,24,26].

The triptycene rotator rotates rapidly in the absence of Hg^{2+} ions. Upon addition of Hg^{2+} ions, the bipyridine moiety coordinates to a Hg^{2+} ion and gets positioned between the two blades of the rotator bringing the triptycene rotator to a halt and therefore acting as a brake. The removal of Hg^{2+} ions restores the rotation. The rotation in this system shows no directional preference. The importance of the concept of a molecular brake is evidenced by the continued research on this topic[56]; a dual ion-switched molecular brake in a ferrocene-based rotary system was synthesized and operated by chemical reagents (H^+/OH^- and $Zn^{2+}/EDTA$)[57], a photo- and thermoaddressable azobenzene-based molecular brake was used in a cyclic azobenzenophane to control the rotation of a dioxynaphthalene rotator[58], a stilbene-based molecular brake[59] was used as part of a molecular antilock braking system (ABS) to control the rotation of the pentiptycene rotator (the light-driven brake has a proton-gated antilock function to control the braking time)[60].

A design similar to the molecular brake shown in Fig 17 was used by the Kelly group to achieve chemically driven directional rotary motion[26,29,61], as shown in Scheme 1. Phosgene was used as fuel for this process much like ATP is used to drive biochemical motors. In the first step phosgene reacts with an amino group in molecule **1** to form isocyanate **2** which then needs to undergo rotation before reacting (intramolecularly) with the hydroxyl group to afford urethane **4**. The urethane molecule **4** thermally relaxes to give the more stable conformation **5**. The rotation proceeds in one direction only as the reverse direction is restricted by the newly formed urethane bond. Addition of water then cleaves the urethane to afford **6**, a rotamer of the starting molecule **1**.
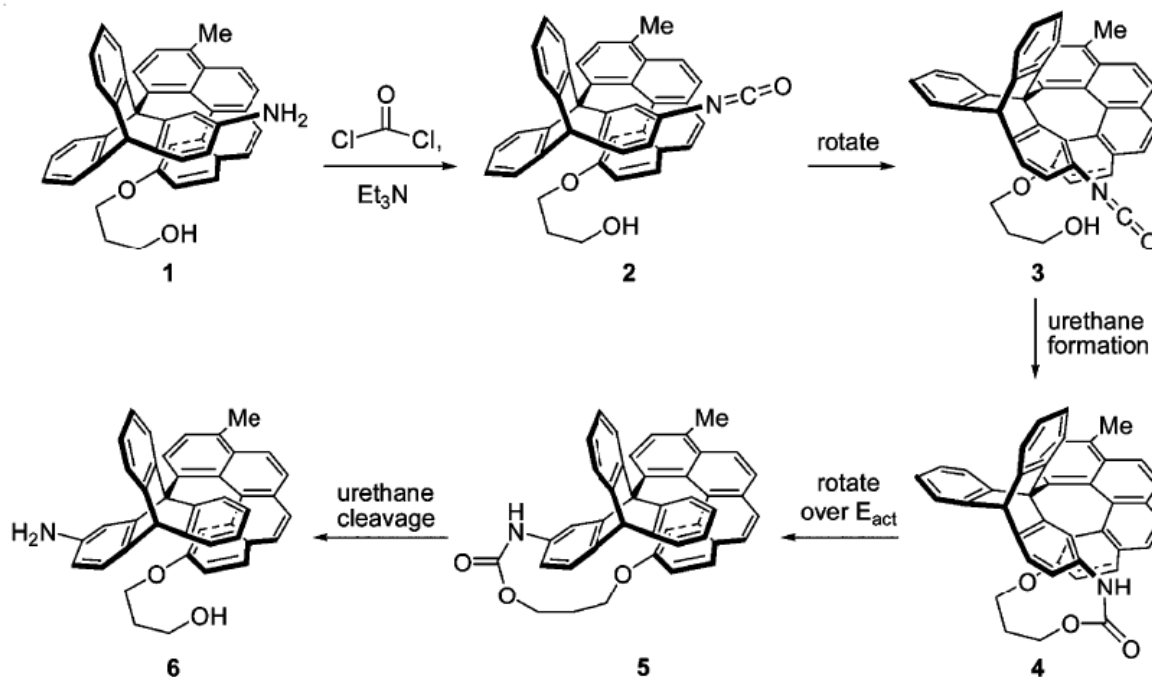
Scheme 1. Chemically driven unidirectional molecular rotor[61].

Although the system described in Scheme 1 seems rather simple, it provides the proof of concept that unidirectional motion can be realized using chemical compounds as energy input. As can be seen from Scheme 1, the rotor discussed here undergoes net unidirectional rotation of 120°. There have also been other reports of chemically driven unidirectional rotary motion where a system undergoes net directional rotation of 180°[62] and even 360°[63,64]. The rotors in the latter case also function as molecular motors as they meet the requirement of being able to perform a full 360° unidirectional rotation which can be continued repeatedly.

In Fig 17 we described a „molecular brake", namely a system where the presence of an additive causes the rotational motion to stop[26]. There have also been examples of the rotation rate of molecular rotors being increased by an additive. Figure 18a shows a rotor whose rotation rate may be increased by seven orders of magnitude upon protonation of the molecule[65]. The protonated quinoline nitrogen forms an intramolecular hydrogen bond with an imide carbonyl stabilizing the planar transition state and therefore accelerating the rotation. The acid catalyzed acceleration can easily be reverted by the increase in pH. The rotation exhibits no directional preference.

$\Delta^{\ddagger}G = 93 \text{ kJ mol}^{-1}$ $\Delta^{\ddagger}G = 54 \text{ kJ mol}^{-1}$

a

$\Delta^{\ddagger}G = 133 \text{ kJ mol}^{-1}$ $\Delta^{\ddagger}G = 113 \text{ kJ mol}^{-1}$

b
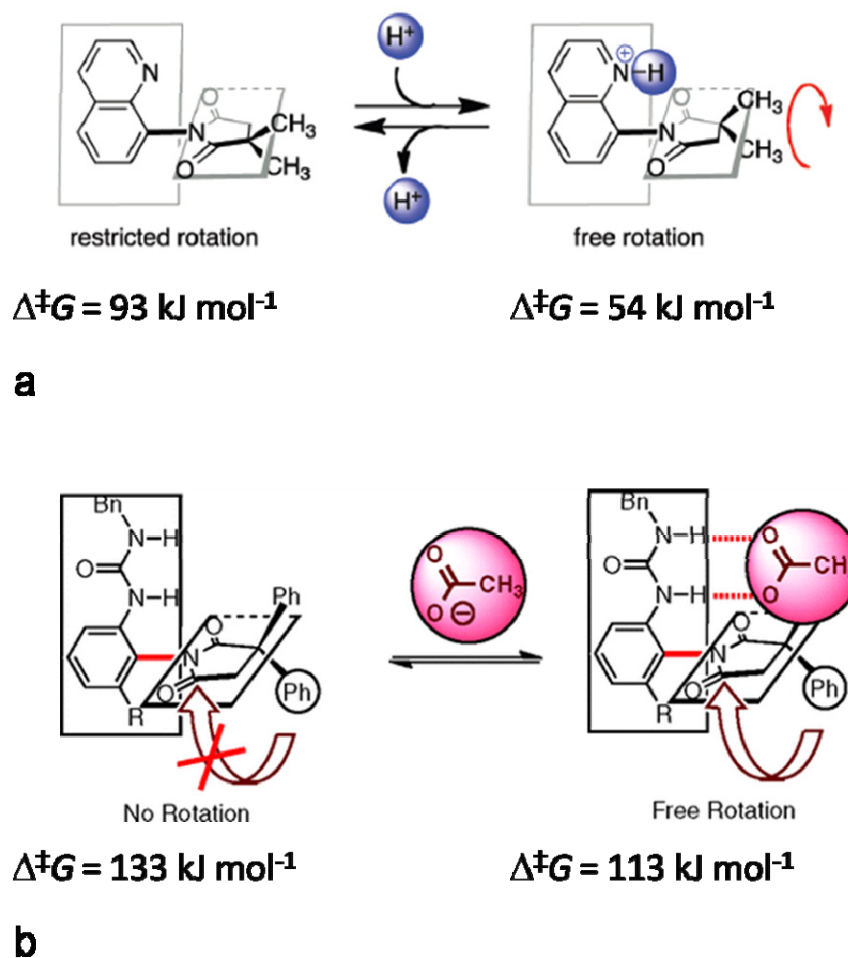
Figure 18. Acceleration of a molecular rotor by the addition of **a**: acid[65], **b**: acetate[66].

Another example of regulating the rotation rate of a rotor is shown in Fig 18b. The rotor accelerates upon the addition of acetate[66]. The additive appears to form hydrogen bonds with the rotor and in turn stabilize the planar transition state leading to the lowering of the rotational energy barrier. Much like in the previous example, the rotary system lacks directional preference.

Photochemically controlled molecular rotors

Using light as the energy source to fuel unidirectional motion has enabled continuous rotary motion in a molecular system[67,68]. In order to function as a molecular motor the system needs to undergo repetitive 360° rotation, use light as the source of energy and undergo unidirectional rotary motion. The developed first and second generation systems are depicted in Fig 19.
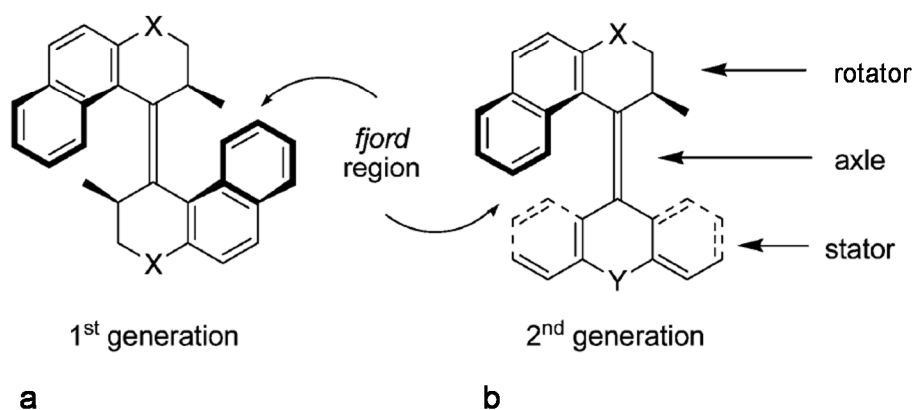
Figure 19. Design of a light-driven molecular rotary motor[68]; **a:** first generation, **b:** second generation.

The so-called first generation molecular motors (Fig 19a) comprise two identical halves connected by a central double bond, which is the axis of rotation. Due to the large sizes of the substituents on the double bond these compounds are often referred to as overcrowded alkenes. The large substituents disrupt the planarity of the central double bond forcing the molecule to adopt a variety of twisted or folded helical conformations. Each half features a stereogenic centre which dictates the conformation of that part of the molecule and is a key element in controlling the direction of the rotation process. In second generation molecular motors (Fig 19b) the two halves connected by the central bond are different as one half in the corresponding first generation molecule is replaced by a tricyclic aromatic group. This also means that there is only one stereogenic centre present in a second generation motor molecule. Although, in the rotary cycle, the two halves rotate relative to each other, the lower half (tricyclic aromatic group) is arbitrarily termed the stator and the upper half (bearing a stereogenic centre) the rotator. The second generation molecular motor may be connected to surfaces or other molecules through the stator with the rotator still functioning as a propeller[68,69]. The region in the molecule where the substituents from both halves come into proximity is often referred to as the *fjord* region.

The rotary cycle of a typical second generation molecular motor is depicted in Scheme 2. By applying light and heat, the unidirectional rotation of the upper half with the respect to the lower half proceeds in a four-step cycle which includes two reversible photochemical steps each followed by a thermal step. The photochemical steps are extremely fast (picosecond timescale)[70] making the thermal processes the rate-determining steps in the cycle. In each step the helicity of the molecule is changed[68].
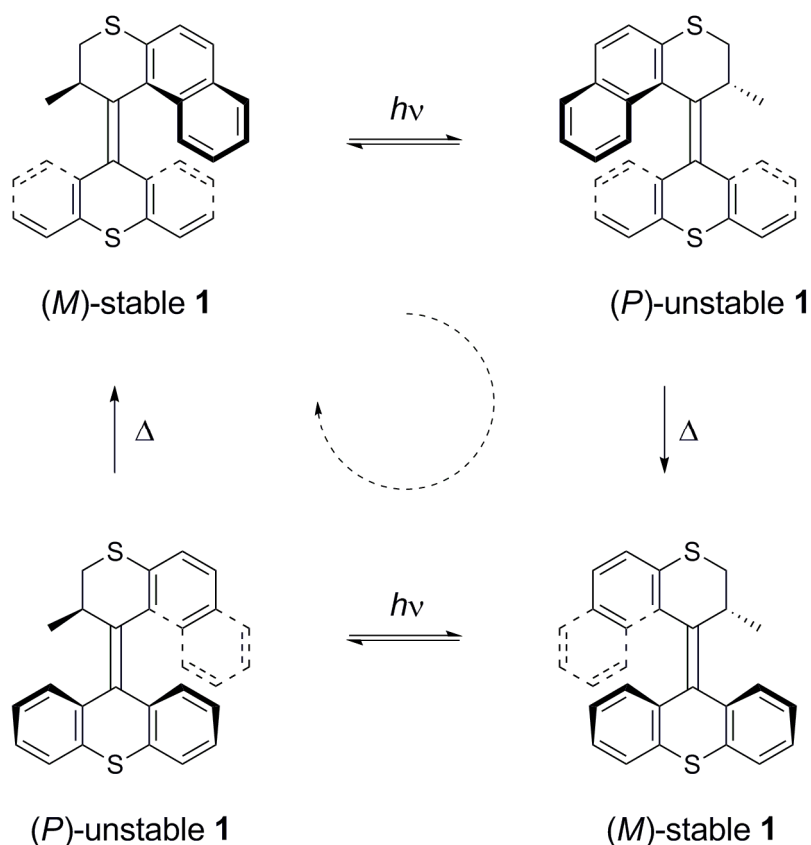
Scheme 2. The rotary cycle of a photochemically driven unidirectional molecular motor.

As shown in Scheme 2, the photochemical step converts the stable isomer into the unstable isomer. In the unstable form the methyl group at the stereogenic centre is forced to adopt a sterically unfavourable pseudoequatorial orientation. The strain is released in the thermal helix inversion process which affords the stable form again with the methyl group adopting a more favourable pseudoaxial orientation. This two-step process has resulted in a net 180° rotation of the rotator with respect to the stator. The photochemical and thermal process are repeated to complete a full 360° rotation.

As the photochemical steps are equilibria, the directionality of the rotation process comes from the thermal steps. The thermal helix inversion process is irreversible as the molecule relaxes from the unstable form to the stable form; the directionality in this step is provided by the tendency of the methyl substituent to adopt a more favourable pseudoaxial orientation. The unidirectionality of the rotation process is governed by the configuration of the stereogenic centre; the two enantiomers will undergo rotation in opposite directions.

It has already been mentioned that the thermal helix inversion process is the rate-determining step in the rotary cycle. In order to accelerate the motor, the major challenge is to reduce the energy barrier to the thermal helix inversion without compromising unidirectionality. The rate of the thermal step strongly depends on the steric interactions in the fjord region. By modifying the molecular design of these

molecules, the rate of the thermal step may be affected which in turn allows for the tuning of the rotation rate of molecular motors[68,71,72].

The remarkable properties of overcrowded alkene based molecular motors, like the capability of undergoing continuous unidirectional rotation if light and thermal energy are supplied simultaneously[73], render these molecules highly useful in a variety of applications[74]. Some of them have already been realized. First generation molecular motors have been applied for the precise positioning of functional groups and the most prominent example is the photoswitchable organocatalyst which allows for the photocontrol of the stereoselectivity of the catalyzed reaction[75]. Second generation molecular motors have been immobilized on surfaces for various applications, changing the properties of the surface being only one of them[69,76,77,78]. The molecular motor has also been used to control the chirality of a polymer chain[79] as well as the chirality of the cholesteric phase of a liquid crystal doped with the motor[80,81]. It was also found that microscale objects placed on top of the motor-doped liquid crystal rotated along with the liquid crystal phase during switching, demonstrating the impressive transfer of a conformational effect from the molecular level, through the organization of the liquid crystalline molecules, to directed motion at the microscale. The most prominent application of the molecular motor up to date, however, is its incorporation as engine into a nanocar[82]. The molecule, equipped with four molecular motors, was shown to undergo directed movement across a surface by means of a repetitive isomerization process. The last two applications clearly demonstrate the capability of these systems to perform work as the word "motor" suggests.

There have also been examples of a rotor function coupled to a separate light-driven rotary motor function[83,84] (Fig 20); if a unidirectional molecular motor is used, it might be possible to induce directionality in a geared system[24]. In Fig 20a one can see a second generation molecular motor with a xylyl unit (rotator) attached to the stator. The unidirectional rotation of the motor can be observed as a sequential interconversion between four isomers; two stable forms and two unstable forms. Different isomers of the molecular motor have been found to exhibit different rotation rates of the rotor function, namely in the order cis_{stable} > $cis_{unstable}$ > $trans_{stable}$ > $trans_{unstable}$ on going from high to low rates.
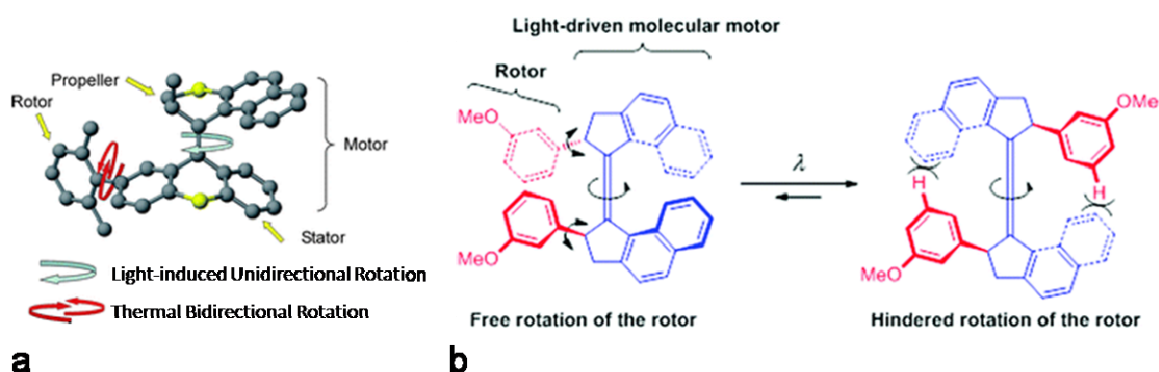
Figure 20. A rotor function coupled to a motor function based on **a:** a second generation molecular motor[83], **b:** a first generation molecular motor[84].

In Fig 20b one can see a first generation molecular motor equipped with a *m*-methoxyphenyl rotator in each half. It was found that the bidirectional rotation of the *m*-methoxyphenyl rotator is unhindered (fast) in the stable *trans*, unstable *cis* and stable *cis* isomers but hindered (slow) in the unstable *trans* isomer.

The rotation rate of the bidirectional rotor, in both examples, may therefore be tuned by controlling the motor function with light and heat. The control of the rotation rate is realized through steric interactions in the immediate vicinity of the rotator; a change in the conformation and/or configuration of the molecule brings about a change in the interactions with the rotator which in turn alters the rotation rate.

Responsive and functional molecules on surfaces

Due to their remarkable molecular properties, azobenzene compounds[85] are among the most widely used molecular switches in various applications[86,87]. They have also been frequently used on surfaces. Various studies on switching behaviour of azobenzene compounds on surfaces have been reported[88,89,90,91,92,93,94,95].

Electrical isomerization of azobenzenes on surfaces

In Fig 21 one can see the scanning tunneling microscopy (STM) study of a tetra-*tert*-butylazobenzene molecule on Au(111) surface[89]. This azobenzene derivative molecule (Fig 21a) was chosen for the study for several reasons. The substitution pattern increases the separation between the surface and the π-system of the molecule leading to increased surface mobility and potentially lower electronic coupling without significantly altering the electronic properties of the azobenzene unit or imparting steric hindrance upon the isomerization process. Furthermore, its set of four symmetrically positioned labels facilitates conformational analysis[89,90].
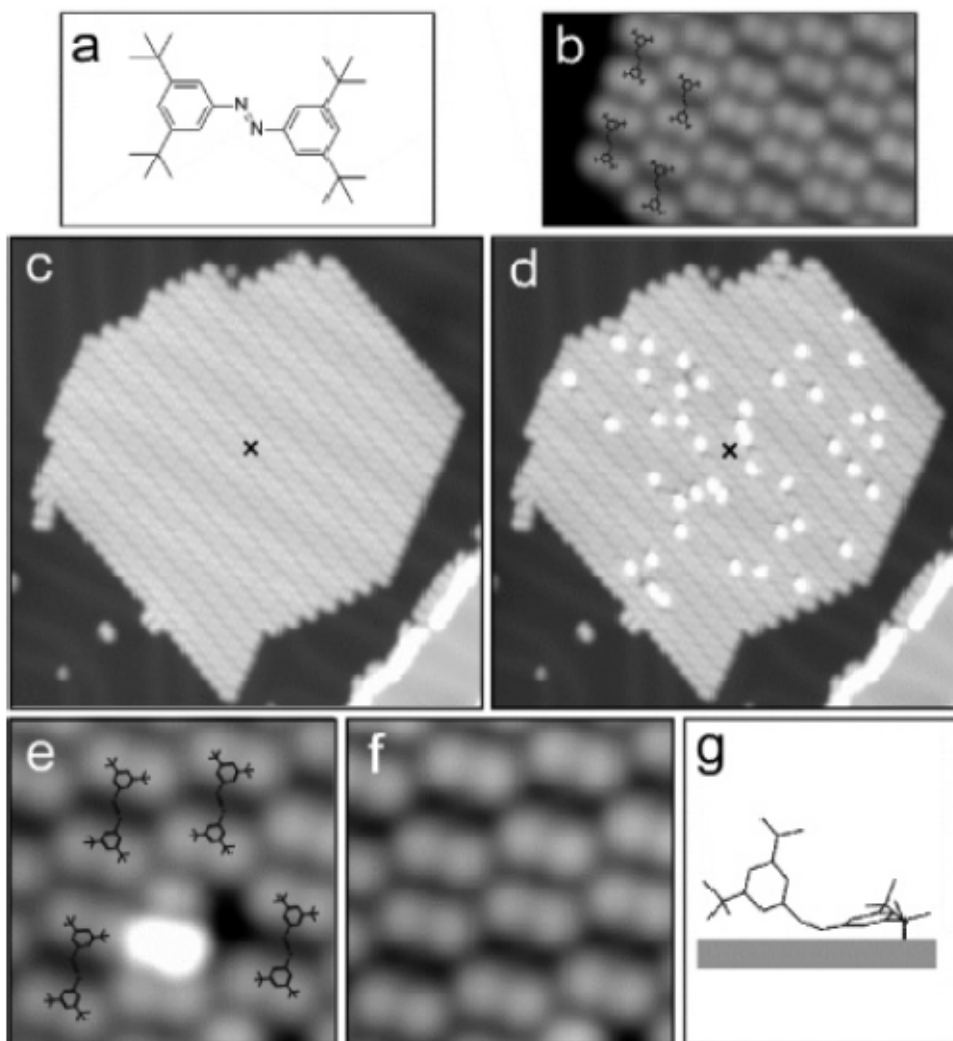
Figure 21. a: *trans*-3,3',5,5'-Tetra-*tert*-butylazobenzene, **b:** STM image of a corner of a molecular island; the molecular adsorption geometry is indicated by structural models, **c:** STM image of an island containing about 400 molecules; subsequent voltages are applied at the position indicated by the cross, **d:** STM image of the island from **c** after nine pulses, **e:** zoomed STM image of a molecular island, **f:** zoomed image of the island from **e** after a voltage pulse, **g:** schematic model of an adsorbed *cis*-3,3',5,5'-tetra-*tert*-butylazobenzene molecule[89].

The experiments were performed in ultrahigh vacuum at 5 K and representative STM images are shown in Fig 21. In Fig 21b one can see a corner of a molecular island with structural models indicating the molecular adsorption geometry; each molecule appears as four lobes corresponding to the *tert*-butyl groups while the central azobenzene part is not visible. All observed molecules were found in the same planar *trans* configuration. The isomerization experiments were performed by positioning the STM tip at a fixed height above a molecular island with the feedback loop switched off (Fig 21c) and applying subsequent voltage pulses. A collection of STM images was recorded after the pulsing (Fig 21d). As one can see in Fig 21d, many molecules have changed their appearance showing a larger apparent height of (4.1 ± 0.3) Å. Typically, the application of a single voltage pulse causes the

switching of several molecules in a radius up to 500 Å around the position of the tip. The bright molecules are stable and their initial appearance can be restored by applying another pulse as shown in Fig 21e,f. Such switching experiments could be reproduced several hundred times which led to the conclusion that the observed changes corresponded to the isomerization of single molecules from the *trans* to the *cis* form, and *back* to the trans form. The *cis*-isomer appears with a bright central intensity maximum, while three lateral lobes in triangular shape can be resolved (Fig 21e). From the STM images a structural model was proposed in which one phenyl ring remains on the surface while the second one points upwards (Fig 21g) which is in agreement with the non-planar conformation of the molecules of the *cis*-isomer in the gas phase[89].

In conclusion, this work shows for the first time that the reversible isomerization of specifically designed azobenzene molecules can be induced on Au(111) by the electric field in the STM junction, without tunneling of electrons[89,90].

Photochemical isomerization of azobenzenes on surfaces

Another study of *tert*-butylated azobenzene molecules on Au(111) surface was undertaken, here with the focus on the photochemical switching of the molecules[93]. Azobenzene molecules were designed with a varying number of *tert*-butyl „legs" with the goal of increasing their surface photomechanical activity. STM images showed that increasing the number of *tert*-butyl legs lifts the azobenzene molecules from the substrate, thereby increasing molecular photomechanical activity by decreasing molecule–surface coupling. When irradiated with UV light, azobenzene molecules with no or two *tert*-butyl legs did not undergo photoisomerization when deposited on a gold surface but azobenzene molecules with four legs did. Single molecule photoisomerization was confirmed unambiguously by the reversibility of the photoreaction and by comparing experimentally resolved intramolecular features of single *trans* and *cis* azobenzene molecules with *ab initio* simulations.

The *trans*-3,3',5,5'-tetra-*tert*-butylazobenzene molecules were deposited onto clean Au(111) substrates at 30 K and the STM images were acquired in the temperature range from 25 to 30 K. As seen in Fig 22a individual *trans*-molecules appear as four-lobed structures. Before any UV exposure the island of molecules is uniformly composed of the *trans* isomer. After UV exposure for 3 h the emergence of new, bright protrusions can be seen in the island; the UV-transformed molecules display only three peripheral lobes along with a new, bright (i.e. "tall") feature near the centre of the molecule. Approximately 4 % of the *trans*-molecules photoswitch after a 1 h UV exposure at 90 mW cm^{-2}.
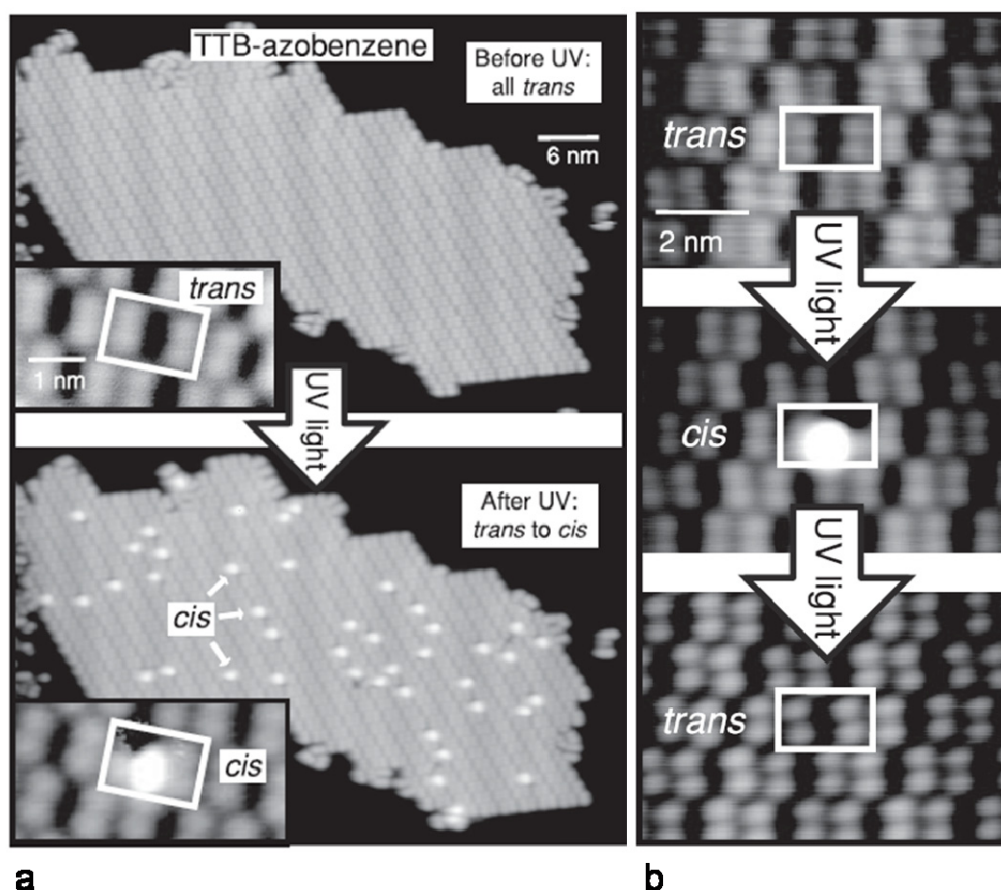
Figure 22. a: STM images showing the photoisomerization of individual *trans*-3,3',5,5'-tetra-*tert*-butylazobenzene molecules on Au(111). Same island of molecules is shown before and after exposure to UV irradiation at 375 nm. Inset zoom-in images show UV-induced switching for a single molecule, **b:** STM images showing reversible photoinduced switching of a single molecule; the same individual molecule is shown before and after two successive exposures to UV light[93].

As shown in Fig 22b, the observed photochemical switching can be reversed for single molecules by reexposing them to UV light. The reversibility of the photoswitching provides strong evidence that the three-lobe state is indeed the *cis*-isomer of the 3,3',5,5'-tetra-*tert*-butylazobenzene molecule. *Ab initio* density functional theory (DFT) calculations of the two isomeric molecules predict structures very similar to the experimentally observed molecules[93].

In conclusion, reversible photochemical switching of specifically designed individual azobenzene molecules has been experimentally observed on Au(111). The investigation has also revealed the significance of environmental coupling in determining molecular photoswitching behaviour.

Thermal isomerization of azobenzenes on surfaces

Azobenzene molecules on surfaces have not only been investigated by means of scanning tunneling microscopy (STM). There are also spectroscopic techniques that can provide valuable information about surface-adsorbed molecules. The

photoinduced and thermally activated switching of 3,3',5,5'-tetra-*tert*-butylazobenzene molecules on Au(111) were investigated by means of two-photon photoemission (2PPE) and high-resolution electron energy loss spectroscopy (HREELS)[94,96,97,98].

Two-photon photoemission (2PPE) is a variant of photoelectron spectroscopy which allows for investigation of unoccupied electronic states between the Fermi level and the vacuum level of a metal or semiconductor[99,100]. This technique can be used to analyze changes in the electronic structure of the molecule adsorbed on a surface. Dynamical information may be obtained with time-resolved 2PPE.

High-resolution electron energy loss spectroscopy (HREELS) is a high-sensitivity, non-destructive technique for the study of surface and adsorbate vibrations and low-energy electronic excitations. It is based on the energy losses of electrons when inelastically scattered on matter[101]. As a surface vibrational spectroscopic technique, HREELS can provide information about chemical reactions of molecules adsorbed on a surface.

The reversible isomerization of the investigated 3,3',5,5'-tetra-*tert*-butylazobenzene molecules is accompanied by geometrical and electronic changes in the structure of the molecules allowing to gain mechanistic and quantitative insight into the switching process by means of 2PPE and HREELS.

The isomerization process can be followed by HREELS as shown in Fig 23. Exposure to UV light at 355 nm leads to a significant intensity decrease of the elastic peak and all dipole active modes, most demonstrative for the phenyl torsion vibrations, τ(C−C). This is a direct result of the photoinduced *trans*-to-*cis* isomerization. Annealing the surface at 300 K restores the original spectrum demonstrating the thermal *cis*-to-*trans* isomerization process[98].
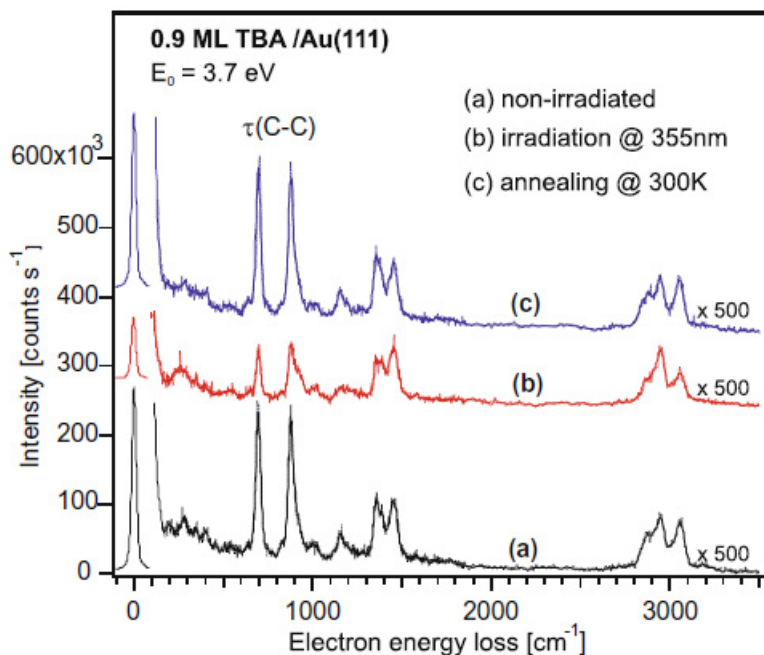
Figure 23. Reversible isomerization of 3,3',5,5'-tetra-*tert*-butylazobenzene molecules on Au(111) followed by HREEL spectra; **a:** before UV-light exposure, **b:** after UV-light exposure at 355 nm, **c:** after annealing the irradiated sample at 300 K for 300 s[94,98].

The same isomerization process can also be followed by 2PPE as shown in Fig 24. The two-color 2PPE spectra shown in Fig 24 provide access to the molecular LUMO levels. From the „1 scan" spectrum of the adsorbate-covered surface an intense feature is observed which is attributed to the LUMO level of the *trans*-isomer. Irradiation with UV light leads to an intensity loss of this peak whereas at lower energy a new feature emerges which is assigned to the LUMO level of the *cis*-isomer. These different 2PPE spectra for the two isomers allow for the isomerization process to be followed by this technique. In addition, it allows one to make a quantitative analysis of the amount of switched molecules as well as to follow the process of isomerization in time[94,96,97].
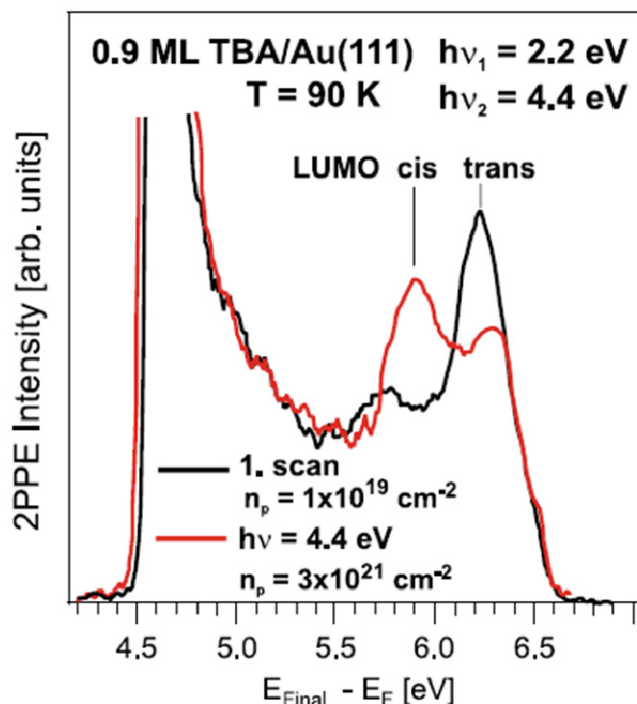
Figure 24. Two-color 2PPE spectra of 3,3',5,5'-tetra-*tert*-butylazobenzene molecules on Au(111); before and after irradiation[94,96].

The photostationary state was thus determined to consist of 55 % of the *cis*-isomer and 45 % of the *trans*-isomer (a low-temperature STM study reported 50 %). The kinetics of the thermal *cis*-to-*trans* isomerization at different temperatures were also followed by 2PPE to give a value of 240 meV for the Arrhenius activation energy. For comparison, an activation energy of 1.0 eV was obtained by studying the reaction in a solution of cyclohexane. The frequency factor (pre-exponential factor) was three orders of magnitude higher in solution than on the surface, reflecting the influence of the solvent on the degrees of freedom in the transition state. Both the activation energy and the reaction rate for the surface-bound molecules are strongly reduced compared to the values obtained in solution. The different value of the activation energy reflects the electronic coupling between the molecules and the metal surface which is rather surprising since it was believed that the four *tert*-butyl groups should significantly lift the azobenzene unit from the metal surface and reduce the coupling. Furthermore, the mechanism of photoexcitation and switching of the molecules on Au(111) has been identified to arise from a substrate-mediated charge transfer process which is completely different from the well-known direct (intramolecular) excitation mechanism operative in the photoisomerization of molecules in solution. These results clearly demonstrate the feasibility of molecular switching on metal surfaces but also indicate that the switching properties of the surface-bound species are strongly modified by the interaction with a metal substrate[94,96].

In conclusion, apart from microscopic techniques, there are also some powerful spectroscopic techniques at our disposal for following chemical reactions and processes taking place on surfaces. Two of such spectroscopic techniques are two-photon photoemission and high-resolution electron energy loss spectroscopy which are essentially electronic and vibrational spectroscopic techniques, respectively. These allow not only for qualitative monitoring of chemical transformations on surfaces but quantitative as well. The kinetics of the thermal isomerization of 3,3',5,5'-tetra-*tert*-butylazobenzene molecules on Au(111) were followed and the kinetic parameters obtained significantly differ from those determined in solution. This reminds us how differently molecules behave on surface than in solution and it is certainly something that needs to be kept in mind when designing new molecules intended for surface systems studies.

Bisazobenzenes on surfaces

Having thoroughly studied simple azobenzene compounds on surfaces, it becomes interesting to investigate more complex molecules. Three different molecules (Fig 25a), each containing a bisazobenzene switching unit and a number of *tert*-butyl groups, were successfully deposited onto a Au(111) surface and studied by STM under ultrahigh vacuum conditions (Fig 25b)[102].

a   b
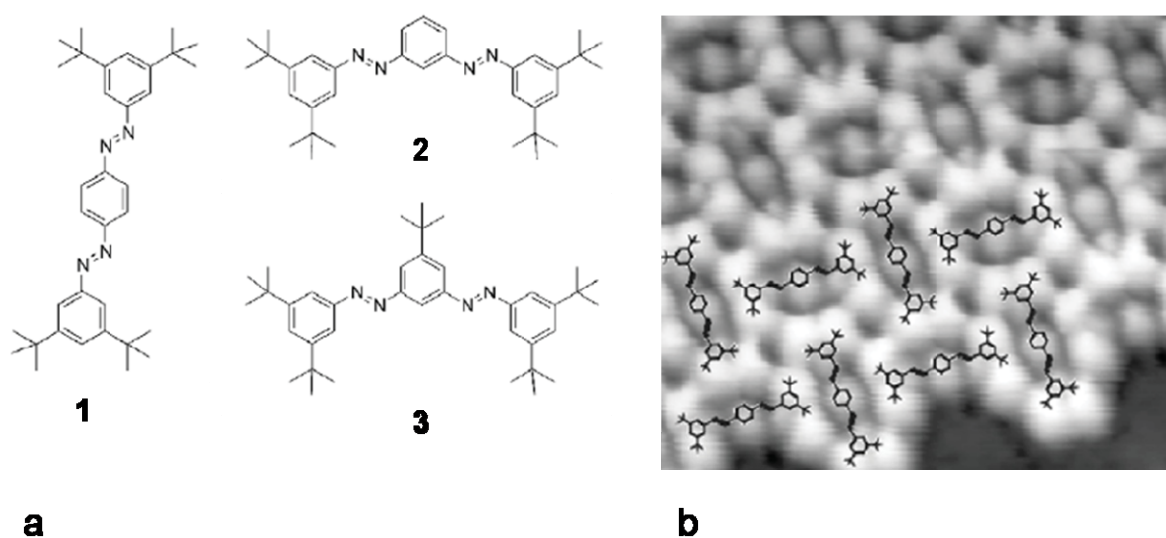
Figure 25. a: Three bisazobenzene molecules investigated, **b:** STM image of an island containing molecules of **1** on Au(111); the molecular adsorption geometry is indicated by structural models[102].

All three molecules were found in self-organized molecular arrangements that reflected their chemical structures. Single molecules could be observed and identified by their characteristic appearance in STM images (Fig 25b). The isomerization processes, typical of azobenzene compounds, could not be induced however, by voltage pulses over different parts of the molecules and in different environments. There are two possible reasons for the observed behaviour: (1) the

motion of the molecule is sterically constrained either by the surface or by the neighbouring molecules, and/or (2) the electronic coupling with the metal surface reduces the lifetime of excited states in the molecule and when the lifetime becomes too short, the isomerization process is quenched. For the molecules studied here, steric hindrance by the surrounding molecules is unlikely as switching was attempted in large islands as well as with isolated molecules. According to the authors, the origin of the suppressed switching could indeed be found in overly strong binding of specific parts of the molecule or in electronic effects due to the coupling with the metal substrate[102]. However, given that the switching process in the analogous 3,3',5,5'-tetra-*tert*-butylazobenzene molecules on Au(111) has thoroughly been documented[88,89,90,91,92,93,94,95], it might be necessary to look for the reason for the different behaviour in bisazobenzenes elsewhere.

Even though simple azobenzene molecules on surfaces are considered to be well-understood, similar molecules of (slightly) higher degree of complexity may behave in an unexpected manner. The bisazobenzene molecules studied here were successfully deposited onto a surface but failed to undergo the isomerization process. The reason for this behaviour is not entirely clear at this point and reminds one of how much more work needs to be done in this area before being able to fully understand the dynamic behaviour of molecules on surfaces.

Azobenzene-based cargo lifter

Inspired by the successful realization of a pH-addressable molecular elevator in solution based on a triple bistable [2]rotaxane[103,104,105], it was attempted to design and develop a conceptually similar albeit simpler system mounted on a surface. A tightly packed self-assembled monolayer (SAM) of azobenzenes was developed on Au(111) (SAM$_{AZO}$). Scanning tunneling microscopy (STM) studies revealed that upon irradiation of the chemisorbed SAMs, a collective isomerization of entire molecular-crystalline domains occurred with an outstandingly high directionality. Based on these results, a cooperative nature of the isomerization of adjacent azobenzene molecules was proposed[106]. This was used to demonstrate that, upon irradiation, azobenzene SAMs, incorporated in a junction between a Au(111) surface and a mercury drop, are able to lift the „heavy" Hg drop and reversibly photoswitch the current flowing through the junction[107] (Fig 26).
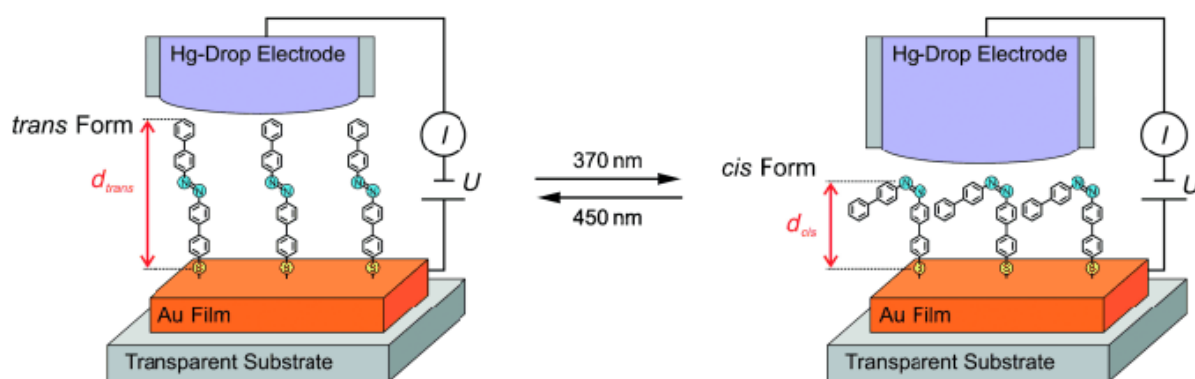
Figure 26. The SAM$_{AZO}$ immobilized between a transparent Au surface and a Hg drop electrode. As a result of the light-triggered isomerization between the rod-like *trans*-isomer and the more compact *cis*-isomer, the distance between both electrodes varies, thus providing both an optoelectronic switch and an optomechanical cargo lifter[107].

A metal–molecule–metal junction was used, based on a Hg top electrode (Fig 26). The junction incorporated the SAM$_{AZO}$ chemisorbed on a transparent Au(111) electrode on a quartz support and a Hg drop as the top electrode[107]. The current density increased and decreased reversibly over one order of magnitude upon alternating irradiation at 370 nm and 450 nm, respectively. The switching behaviour can be explained in terms of the SAM$_{AZO}$ reversibly lifting and lowering the Hg drop on top of the monolayer as depicted in Fig 26. The collective nature of the azobenzene molecules in the SAM$_{AZO}$ is used to provide work.

The work described here demonstrates that by harnessing the collective nature of the isomerization of azobenzene molecules, it is possible to photoswitch the current going through a molecular junction and to develop a prototypical molecular machine that acts as a cargo lifter. The ability of the system to provide work is clearly demonstrated. The system described here holds potential as a photoswitchable monolayer for nanoelectronics. Furthermore, these findings pave the way towards the fabrication of a new class of devices based on the force expressed by molecules organized in films.

Molecular wheel

Surpassing the mere study of switching behaviour on surfaces described in the previous sections, recent advances in surface engineering have led to the attempts to mimic the motion from the macroscopic world right down to the molecular level[108,109,110,111,112,113,114,115,116,117,118,119].

A report of a triptycene molecular wheel that could be moved across a surface by rolling rather than by hopping or sliding paved the way for future developments[120]. The molecular design of the wheel is shown in Fig 27a. Two triptycene units act as wheels and can freely rotate about a diacetylenic axle. Fig 27a also gives a schematic representation of the proposed movement of the wheels; the molecule can be manipulated by the STM tip in such a way to induce rolling motion.
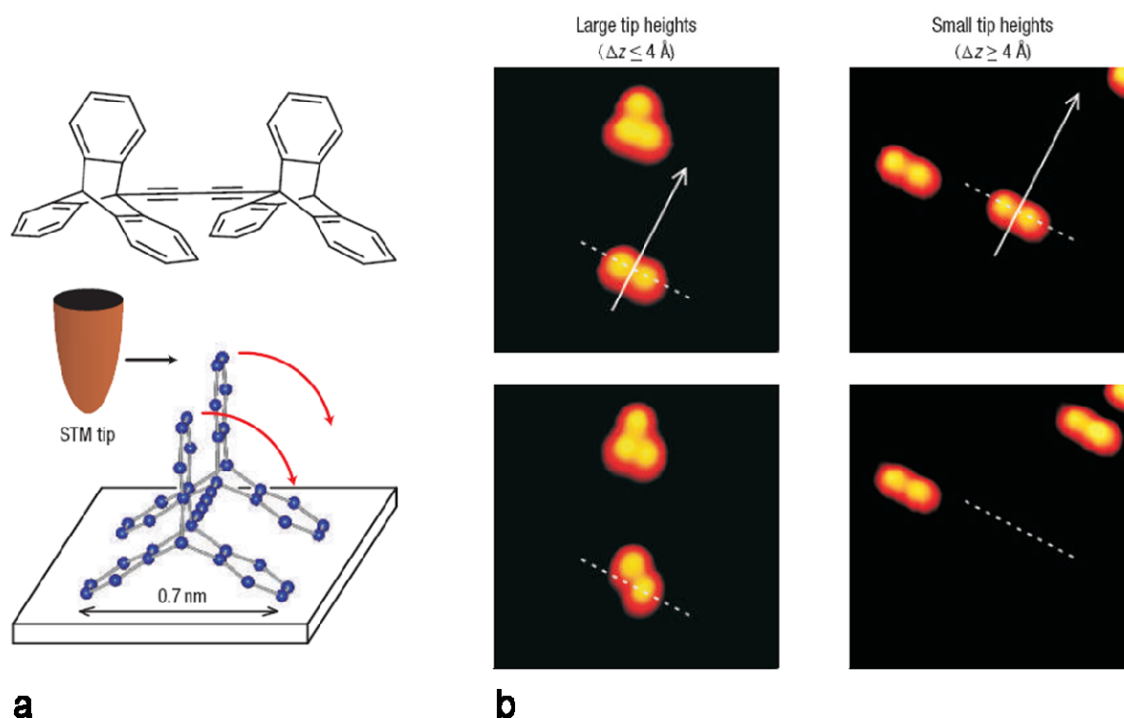
Figure 27. a: Ditriptycene wheels and a scheme showing their movement on a surface, **b:** STM images of the wheels moving on Cu(110) as induced by the STM tip; the arrows mark the pathway of the tip apex during the manipulation and the dashed lines indicate the initial position of the molecules[120].

The manipulation of the molecules on copper was followed by STM and is shown in Fig 27b at two different tip heights. It was shown that in the pushing mode the molecule follows the complete pathway of the tip (small tip heights in Fig 27b). In the rolling mode, on the other hand, the molecule does not follow the tip apex up to the end. Instead, one wheel moves and the other remains in its initial position (large tip heights in Fig 27b). These findings were confirmed by the analyses of the electric current signals. The work described here demonstrates how the rolling mechanism can be mastered at the molecular scale paving the way for the development of more complex dynamic systems.

Nanovehicles

A growing interest in making analogues of vehicles at the moleculer level is evidenced by numerous literature reports of various designs of nanovehicles[108,109,110,111]. In Fig 28a one can see one of the first designs of a nanovehicle[111,121]. The molecule is based on a rigid oligo(phenylene ethynylene) (OPE) frame to which four fullerene wheels are attached. By means of rolling, the molecule can only move in the two directions indicated by the red arrows (Fig 28a); there is no preference for either one of the two indicated directions, however.

The molecules were deposited onto a Au(111) surface and could be observed under ultrahigh vacuum conditions by STM. Due to their rectangular constitution, determination of the chassis and axle orientation of the four-lobed molecules was

possible through peak-to-peak length versus width measurements. The fullerene wheels appear brightly imaged and thereby provide a definitive indication of the molecule and it orientation. After initial imaging at room temperature, the substrate temperature was slowly increased until the molecules started moving through a combination of translation and pivoting. The translational movement of the nanocars, however, occurred in the direction perpendicular to their axles as predicted by the model in Fig 28a, indicating movement by rolling of the wheels and not by stick-slip or sliding motion[111,121].

a

b
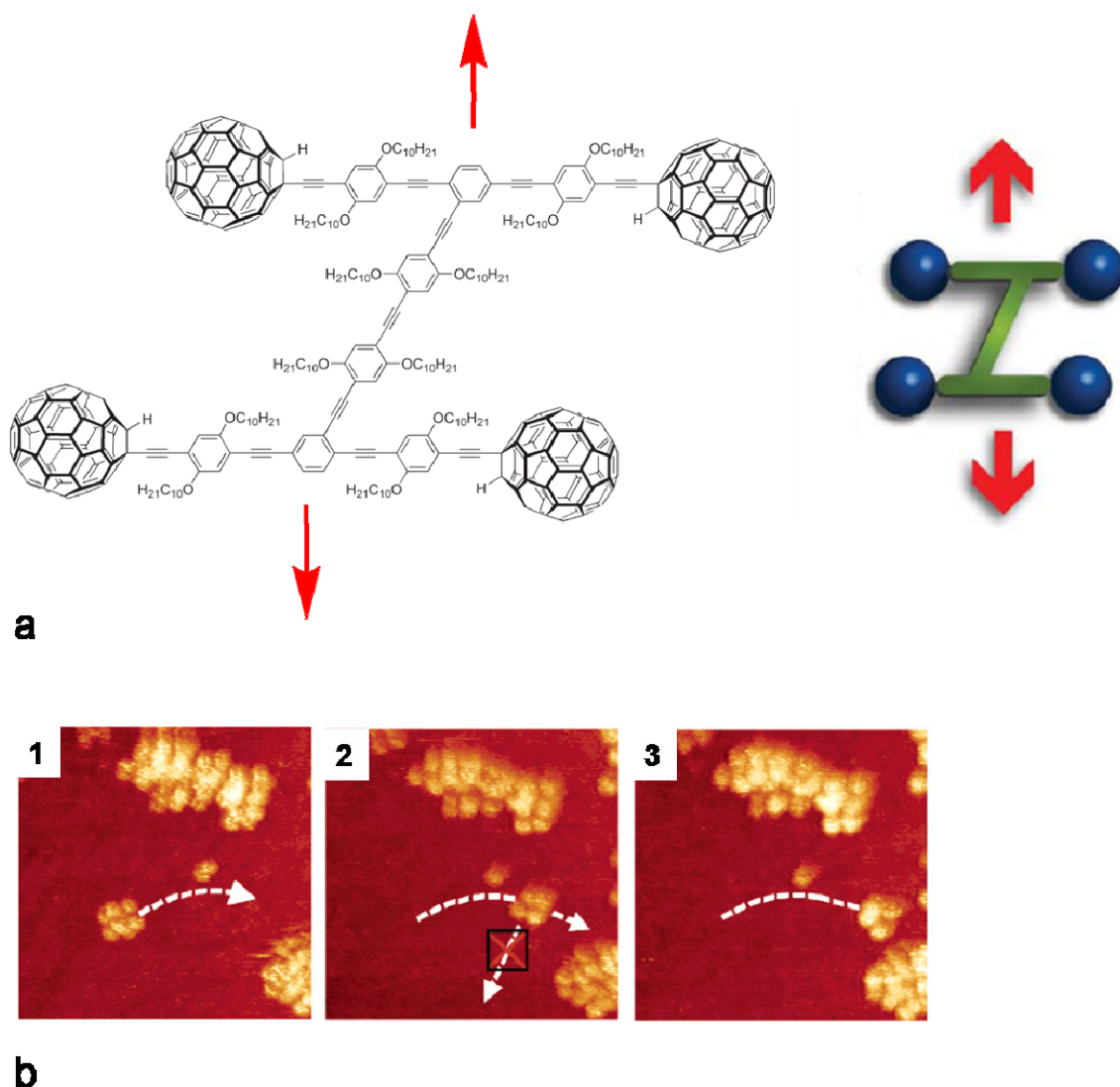
Figure 28. a: Molecular structure of a nanocar along with a schematic representation showing the directional preference of its motion, **b:** STM images of the molecule moving on Au(111) as a result of direct manipulation with the STM tip[121].

Additionally, direct manipulation of the molecules by the STM tip was performed in order to further explore the hypothesis that the motion of these molecules is facilitated by rotation of the fullerene wheels about the alkynyl axles. An example of this manipulation is shown in Fig 28b. The tip was lowered in front of the molecule in the direction of motion, pulling the molecule by the tip. As seen in Fig 28b (image 1),

the molecule was successfully pulled in a shallow arc in a direction parallel to its axles. Pulling it at 90° to its former path (Fig 28b, image 2), however, did not result in any movement of the molecule. The molecule could then again be pulled further along its initial path (Fig 28b, image 3). This strong directional preference favouring motion perpendicular to the axles further supports movement by means of fullerene-facilitated rolling[111,121].

Two three-wheeled molecules (Fig 29a) were prepared to further examine the nature of moving these molecules across the surface. They are designed in such a way that their axles inhibit any translational rolling. When these molecules were slowly heated on Au(111), the majority of observed motion for **1** was pivoting in place around a central pivot point (Fig 29b). No translation or pivoting was observed for **2**. This behaviour of the trimer molecules is in further support of motion by means of rolling of the wheels in the original nanovehicle[121].
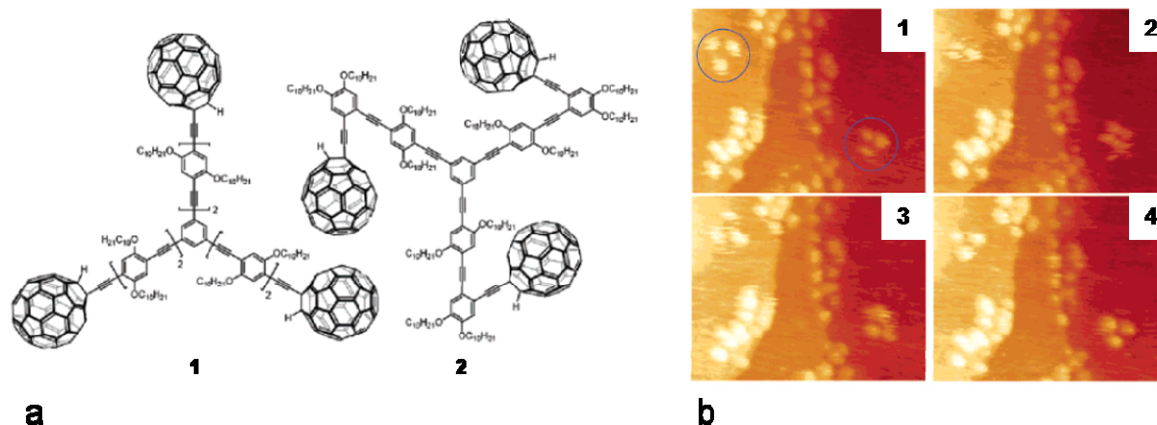
Figure 29. a: Molecular structures of the trimers **1** and **2**. **b:** A sequence of STM images of trimer **1** on Au(111) during annealing at 225 °C[121].

Although directed motion was clearly demonstrated, the molecules could not undergo autonomous motion; instead they underwent directed thermal motion or had to be pulled by the STM tip. The next generation of nanovehicles was therefore equipped with an engine that was envisaged to power the motion of the molecule. One of the first molecules in this generation was the so-called „nanoworm"[122] whose design can be seen in Fig 30a. The molecule has a rigid oligo(phenylene ethynylene) (OPE) frame with an azobenzene group as a part of the chassis. The molecule is also equipped with four wheels. Two different molecules were made; one with fullerene wheels and one with carborane wheels. Fullerene wheels were replaced for carborane wheels due to their ability to quench photochemical processes as well as for synthetic and solubility reasons.
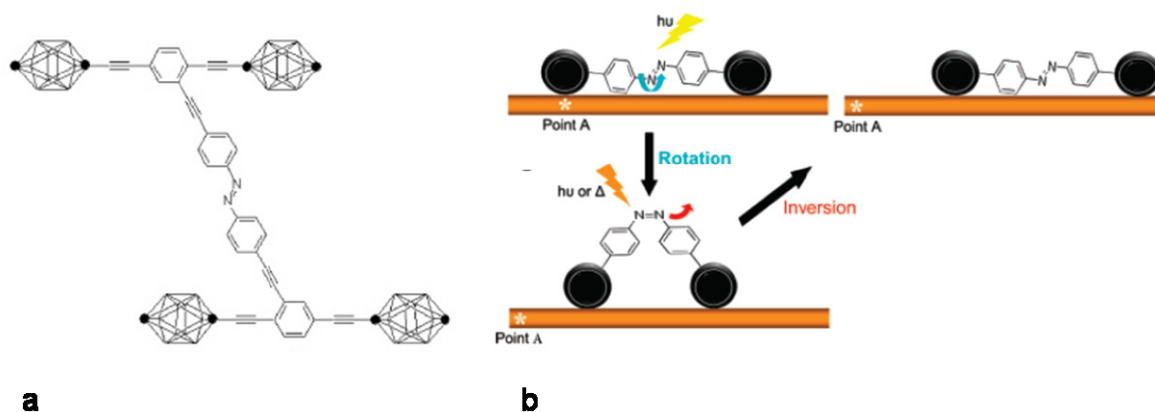
Figure 30. a: Molecular structure of nanoworm. **b:** Side view model of the nanoworm and its envisaged means of motion[122].

As depicted in Fig 30b, undergoing photoisomerization and thermal isomerization via two different pathways, the switching motion on a surface was envisaged to be accompanied by a translational component propelling the nanoworm[122]. This seemed like an interesting concept but no surface studies have been reported up to date.

Another design of a nanocar came equipped with a unidirectional light-driven rotary molecular motor[68] (Fig 31a) that was supposed to propel the vehicle in a paddlewheel-like motion[123,124] (Fig 31b). The four-wheeled molecule had a unidirectional light-driven molecular motor incorporated in its chassis (Fig 31a). It was envisaged that, upon exposing the molecule to UV-light and heat, the rotator would repeatedly sweep across the surface propelling the nanocar forward as depicted in Fig 31b.
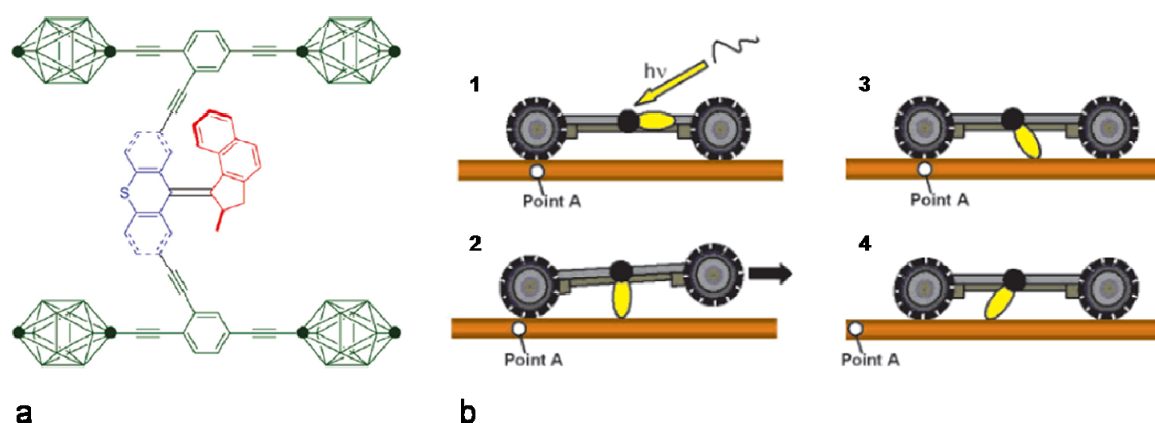
Figure 31. a: Molecular structure of a motorized nanovehicle. **b:** Proposed propulsion scheme for the motorized nanovehicle[123,124].

The nanocar was evaporated thermally onto a clean Cu(111) surface under ultrahigh vacuum conditions and studied by STM. The molecules could be observed as five-lobed protrusions, with four lobes coming from the wheels and one from the motor (Fig 32). Their appearance in the STM images is in good agreement with the

molecular dimensions in the gas phase, and according to their chemical structure, two typical conformations are identified (Fig 32b,c). As some of the bonds in the chassis of the nanocar allow for rotation, the two axles of the molecule can be either crossed or parallel giving rise to two possible conformations[124].
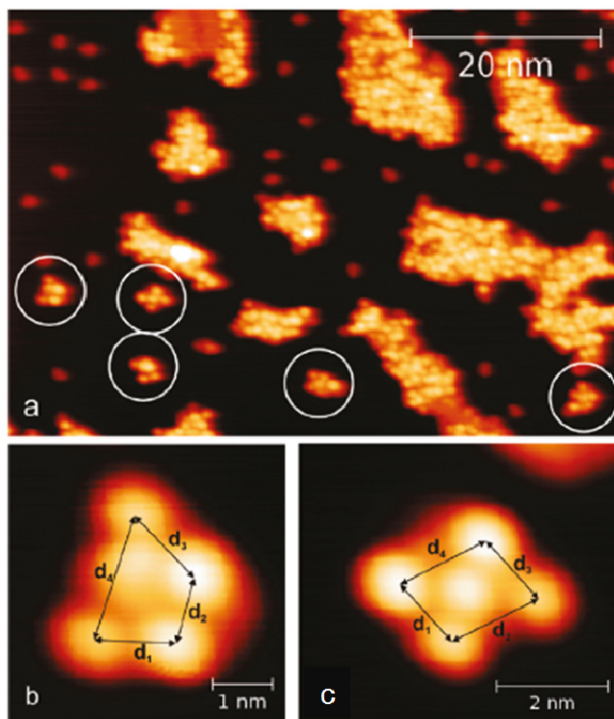
Figure 32. a: STM images of the nanocar on Cu(111).
b,c: Single molecules in different conformations[124].

Irradiation experiments were also performed but irradiation of the covered surface with light at 248 nm did not result in any changes on the surface as observed by STM. Lateral motion could not be induced by STM manipulation (using the STM tip) either indicating a rather strong molecule-surface interaction.

In order to benefit from an alternative technique for following molecules on surfaces, the newest generation of nanovehicles is equipped with a fluorophore that allows for the imaging of single molecules by the use of fluorescence microscopy[125,126,127,128,129]. Even though this technique does not provide the atomic resolution offered by STM, it allows localization of individual fluorophores within a few nanometers and also yield rapid results. Molecules **1** and **2** (Fig 33a) were prepared with the goal of investigating molecular motion across a surface by means of fluorescence microscopy. Molecule **1** serves as a reference compound and contains a fluorescent BODIPY moiety and three adamantane wheels. Nanocar **2** contains two BODIPY moieties and four adamantane wheels. For the study on glass surfaces the motion of nanocars was found to be hindered by stronger interactions between carborane wheels and the glass surface. In order to maximize the number of moving molecules, adamantane was used as a new design of a molecular wheel[125].
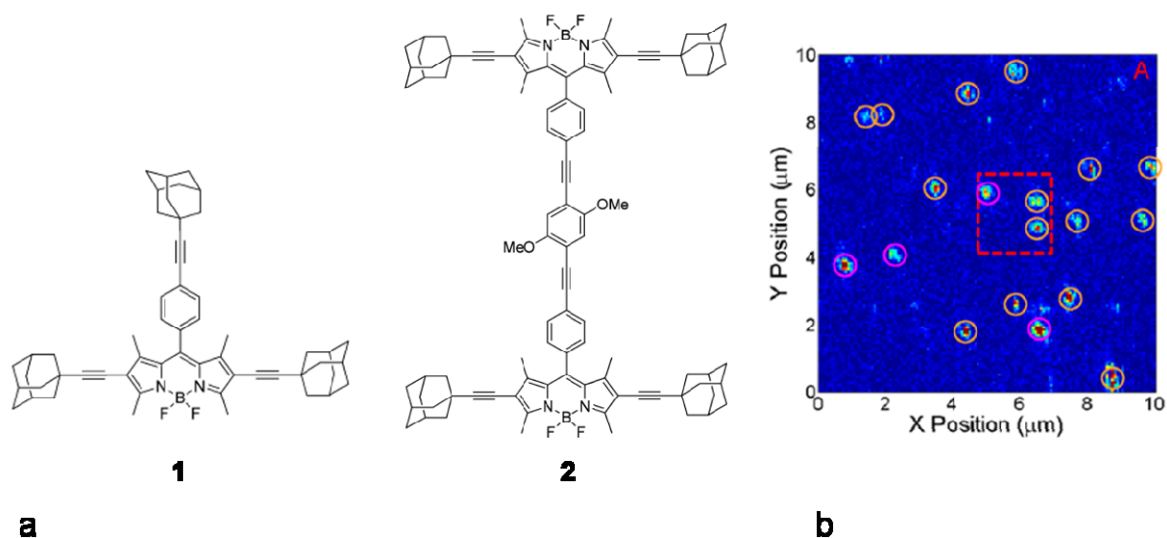
Figure 33. a: Molecular structure of fluorescent nanovehicles **1** and **2**, **b:** Fluorescence image of the fluorescent nanocar **2**; the yellow circles indicate moving molecules and purple circles indicate stationary molecules[125].

A study of nanocar **2** on a glass surface by means of single molecule fluorescence microscopy (SMFM) was carried out and a representative image is shown in Fig 33b. The bright spots in the image represent individual nanocar molecules which are identified based on an intensity threshold and the shape of the fluorescent spot. This method allows for simultaneous determination of multiple trajectories of single molecules from sequential fluorescence images. Molecules were categorized into „moving", highlighted in yellow circles in Fig 33b, and „stationary" nanocars, highlighted in purple circles in Fig 33b, and their ratio was found to be 15:4. Molecules of **1** were also studied on a glass surface and showed significantly reduced mobility compared to the molecules of **2**. This is in support of the rolling mechanism of molecular motion on the surface because if the molecules moved across the surface by hopping or sliding, a higher mobility of **1**, having one fewer wheel, would be expected due to the weaker interactions of the molecules with the surface[125].

The work presented here shows that the choice of wheels can be used to tune the strength of the molecule-surface interaction and in turn adjust the mobility of molecules on the surface. Furthermore, it is demonstrated that the molecules move across the surface by rolling of the wheels.

An alternative means of fuelling the propulsion of nanovehicles has also been proposed; active Hoveyda–Grubbs catalyst nanocars are envisaged to engage in surface-initiated ring-opening metathesis polymerization (ROMP) triggering polymer chain growth which should in turn propel the nanovehicle[130].
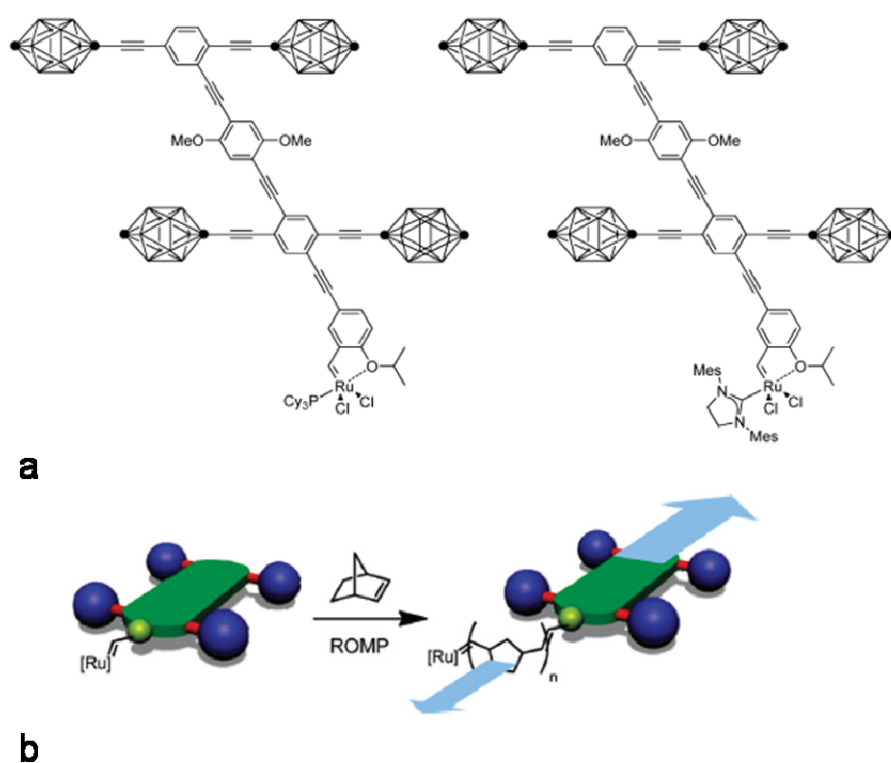
Figure 34. a: Molecular structures of Ru-based metathesis catalyst nanocars,
b: Proposed propulsion scheme for Ru-based metathesis catalyst nanocars[130].

The molecular design can be seen in Fig 34a; carborane-wheeled nanocars are functionalized with ruthenium-based metathesis catalysts at the rear end. As depicted in Fig 34b, by feeding the nanocar with fuel, such as norbornene, a ROMP reaction should occur on the surface and the energy liberated is envisaged to provide the thrust needed to propel the nanocar forward. Concurrently, the ruthenium catalyst and the nanocar will move away from each other. The catalytic activities of the nanocars were tested in solution and remained high which makes them good candidates for surface-initiated ROMP[130]. No studies of ROMP reactions on a surface have yet been reported.

The newest design of a nanocar appeared in the literature recently[82]. It is a molecule equipped with four functional units – unidirectional rotary motors[3,68], attached to two rigid carbazole cores, as shown in Fig 35a. These motor units serve multiple purpose in the molecular design; through continuous and well-defined conformational and configurational changes they act as molecular wheels as well as the engine of the nanovehicle. These structural changes arise through sequential electronic and vibrational excitation. The molecule is envisaged to move across the surface in a unidirectional fashion through a paddlewheel type motion, as depicted in Fig 35b.

Meso-(R,S-R,S) isomer

a **b**
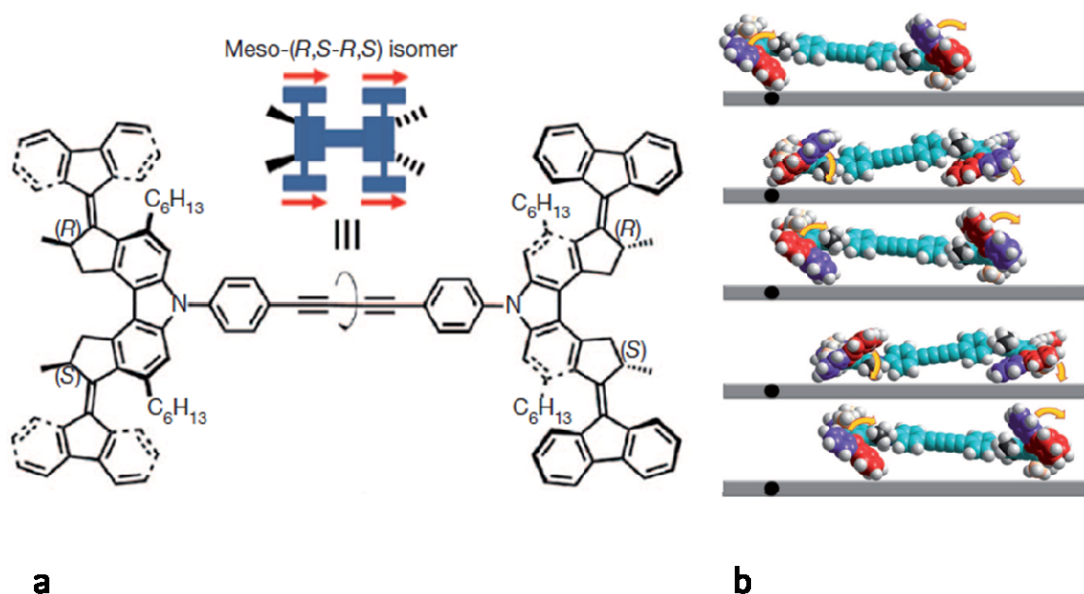
Figure 35. Electrically driven nanocar; **a:** molecular structure, **b:** paddlewheel type motion[82].

From the design of the molecule it is clear that there is free rotation around single C−C bonds of the chassis (Fig 35a). This means that only some of the *meso*-molecules, once landed on the surface, will have the motor units properly aligned to work in concert and propel the molecule in one direction by their conrotatory motion. In contrast, the remainder of the *meso*-molecules will land on the surface so that the combined effects of the motor units cancel out and preclude any translational motion of the molecule. In addition, the (*R,R−R,R*) and (*S,S−S,S*) molecules, with the motor units on opposite sides of the molecule rotating in a disrotatory fashion should undergo spinning and/or random translational motion[82].

The molecules were deposited onto a Cu(111) surface and examined by STM in ultrahigh vacuum at a temperature of 7 K. Single molecules appeared as three or four joint lobes, each corresponding to a motor unit. By repeatedly applying voltage to some of the molecules, they moved forward across the surface with directional preference (Fig 36). These correspond to the „correctly landed" *meso*-molecules having all four motor units rotating in a conrotatory fashion.

10 excitation steps

Final position

10-step trajectory

6 nm

Starting position
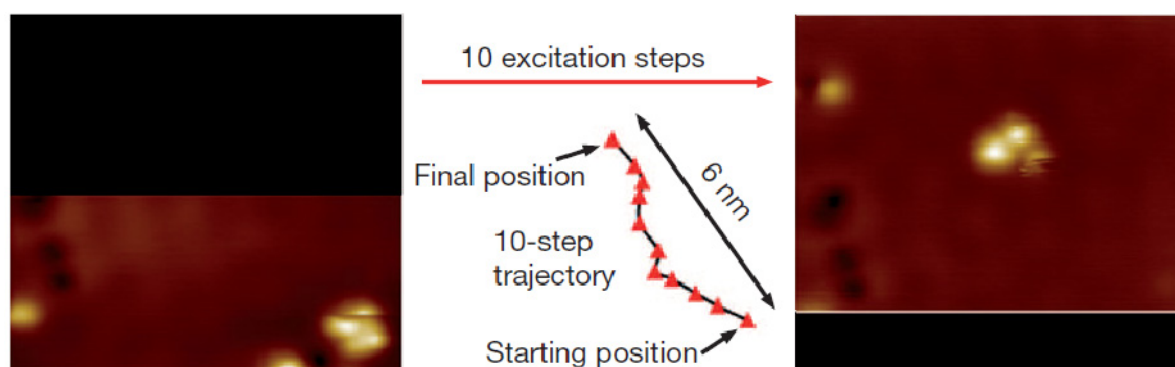
Figure 36. STM images of the nanocar undergoing directed motion on Cu(111)[82].

Some other molecules did not show any translational movement when exposed to electrical pulsing and those were assigned as the „wrongly landed" *meso*-molecules. In addition, there were also other molecules that exhibited random motion and these correspond to the all-*R* or all-*S* molecules. The observation of the three different categories of surface behaviour corresponding to the three different stereoisomers of the nanocar provide compelling evidence that the translational movement originates from the concerted action of the molecular motor units[82].

In conclusion, the directional and exclusively forward movement of an electrically driven nanocar has been realized. By tuning of the chirality of the individual motor units the system may be adapted to follow either linear or random surface trajectories or to remain stationary. This is also the first example of the unidirectional character of the rotation of a molecular motor to be applied for achieving translational motion.

Although autonomous directional movement on a surface has been realized with the design depicted in Fig 35a, there is still room for improvement[108]. Despite being equipped with light-driven rotary motors, the current nanocar is driven electrically *i.e.* by pulsing it with an STM tip. Light is still considered as the ultimate fuel for severals reasons: it can be switched on and off quite easily and rapidly, the system can be operated from a distance, lasers allow for working in a very small space and very short time domains, photons can be useful to „read" the state of the system and control the operation of the machine in addition to supplying energy for work[8]. The idea of a light-driven nanovehicle is therefore still highly appealing. Furthermore, future application of these devices will require them to be more efficient which undoubtedly requires more research in this area[3].

Aims of the research and outline of the thesis

This chapter describes how scientists draw inspiration from natural dynamic systems and make attempts to develop artificial motor systems mimicking the remarkable features present in their biological analogues[2,3,8,9,11]. As this is a truly vast field of research, in this thesis the focus is set on rotary motion and responsive molecules on surfaces. Some of the previous sections of this chapter aim to describe the development of molecular rotors and the attempts to control them. A number of examples of influencing the rotation behaviour by adapting the design of the rotor system are described as well as methods of affecting the rotation by applying external stimuli (chemical, electrochemical and photochemical methods). Also given are several examples of rotor systems that display unidirectional rotation and at the same time function as molecular motors. The remainder of the sections in this chapter deals with responsive and functional molecules on surfaces. It is described how the field progressed from the investigation of small and simple functional molecules to nanovehicles of gradually increasing complexity. The successes and failures in the field are both described in order to show the gradual development in this area.

As much as has already been done in this field, there is still plenty of room for improvements and further developments. Dynamic systems exhibiting coupled rotary motion have not been studied extensively and selectively addressing only one of multiple rotors within a complex molecular system still remains a challenge. Likewise, although an electrically driven nanocar has been realized, it still fails to use light as fuel for motion despite being equipped with light-driven molecular motors.[82] Moreover, future application of these devices (both molecular rotors and devices operating on surfaces) will require them to be more efficient which undoubtedly requires more research in this area[108].

This thesis deals with attempts to control motion at the molecular and submolecular level. The design, preparation and solution-study of new molecules is described with the goal of getting a better understanding of the motion-related behaviour of molecules and molecular devices on surfaces. Furthermore, the design, preparation and study of new molecular rotors with the aim of tuning the rotation rate in these systems is also described.

In Chapter 2 of this thesis, the design and preparation of novel multiazobenzene molecules are described as well as their properties in solution. The molecules are designed to have multiple photoswitching units with the goal of studying their surface-behaviour as this type of molecular multiswitches has not been studied extensively and does not appear to be well-understood[102].

Chapter 3 deals with the design, preparation and solution-study of light-driven molecular vehicles equipped with an azobenzene unit and two wheels. A new design of the molecular wheel is introduced. The molecules are designed for surface studies with the aim of investigating their surface-traversing properties.

In Chapter 4 a new design of a light-driven surface-traversing molecule is introduced. The molecules are equipped with two wheels and two azobenzene switching units. Due to the known ability of the azobenzene switches to act in concert and provide work[107], the newly designed molecule, having two switching units, is envisaged to display different surface-behaviour than the molecules described in Chapter 3.

Chapter 5 of this thesis deals with unidirectional light-driven rotary molecular motors. Due to their remarkable properties, these molecules have proven highly useful to various applications in nanotechnology[3,82]. For many applications, however, molecular motors exhibiting higher rotation rates are more appealing. To this end a new molecular motor is designed, prepared and thoroughly studied.

Chapter 6 describes the design, preparation and study of a set of novel binaphthyl-based molecular rotors with the goal of tuning their rotation rate by means of direct steric control as well as by allosteric regulation. Having multiple rotors makes these molecules excellent candidates for the study of coupled rotation

as well as for exploring the possibilities of selectively affecting only one of the multiple rotors.

References

1. M. Schliwa, G. Woehlke *Nature* **2003**, *422*, 759−765.

2. *Molecular motors* (Ed: M. Schliwa), Wiley−VCH, Weinheim, Germany **2003**.

3. W. R. Browne, B. L. Feringa *Nature Nanotechnol.* **2006**, *1*, 25−35.

4. R. D. Astumian *Phys. Chem. Chem. Phys.* **2007**, *9*, 5067−5083.

5. R. D. Astumian *Nature Nanotechnol.* **2012**, *7*, 684−688.

6. R. F. Ismagilov, A. Schwartz, N. Bowden, G. M. Whitesides *Angew. Chem. Int. Ed.* **2002**, *41*, 652−654.

7. G. M. Whitesides *Sci. Am.* **2001**, *285*, 78−83.

8. V. Balzani, A. Credi, M. Venturi *Molecular Devices and Machines – A Journey into the Nano World*, Wiley−VCH, Weinheim, Germany **2003**.

9. E. R. Kay, D. A. Leigh, F. Zerbetto *Angew. Chem. Int. Ed.* **2007**, *46*, 72−191.

10. J. F. Stoddart *Acc. Chem. Res.* **2001**, *34*, 410−411.

11. J. Michl, E. C. H. Sykes *ACS Nano* **2009**, *3*, 1042−1048.

12. R. D. Vale, R. A. Milligan *Science* **2000**, *288*, 88−95.

13. H. Itoh, A. Takahashi, K. Adachi, H. Noji, R. Yasuda, M. Yoshida, K. Kinosita Jr. *Nature* **2004**, *427*, 465−468.

14. K. Kinosita Jr., R. Yasuda, H. Noji, S. Ishiwata, M. Yoshida *Cell* **1998**, *93*, 21−24.

15. A. Aksimentiev, I. A. Balabin, R. H. Fillingame, K. Schulten *Biophys. J.* **2004**, *86*, 1322−1344.

16. P. D. Boyer *Nature* **1999**, *402*, 247−249.

17. J. E. Walker *Biochem. Soc. Trans.* **2013**, *41*, 1−16.

18. K. Kinosita, Jr., K. Adachi, H. Itoh *Annu. Rev. Biophys. Biomol. Struct.* **2004**, *33*, 245−268.

19. D. J. DeRosier *Cell* **1998**, *93*, 17−20.

20. R. M. Macnab *Annu. Rev. Microbiol.* **2003**, *57*, 77−100.

21. M. J. Pallen, N. J. Matzke *Nature Rev. Microbiol.* **2006**, *4,* 784−790.

22. X. Chen, H. C. Berg *Biophys. J.* **2000**, *78*, 1036−1041.

23. T. C. Elston, G. Oster *Biophys. J.* **1997**, *73*, 703−721.

24. G. S. Kottas, L. I. Clarke, D. Horinek, J. Michl *Chem. Rev.* **2005**, *105*, 1281−1376.

25. M. Xue, K. L. Wang *Sensors* **2012**, *12*, 11612−11637.

26. T. R. Kelly *Acc. Chem. Res.* **2001**, *34*, 514−522.

27. V. Balzani, M. Gómez-López, J. F. Stoddart *Acc. Chem. Res.* **1998**, *31*, 405−414.

28. B. L. Feringa *Acc. Chem. Res.* **2001**, *34*, 504−513.

29. C. P. Mandl, B. König *Angew. Chem. Int. Ed.* **2004**, *43*, 1622−1624.

30. C. Wolf *Dynamic Stereochemistry of Chiral Compounds: Principles and Applications* 1st ed; Royal Society of Chemistry, Cambridge, UK **2008**.

31. G. H. Christie, J. Kenner *J. Chem. Soc., Trans.* **1922**, *121*, 614–620.

32. T. Benincori, V. Bonometti, R. Cirilli, P. R. Mussini, A. Marchesi, M. Pierini, T. Pilati, S. Rizzo, F. Sannicolò *Chem. Eur. J.* **2013**, *19*, 165–181.

33. D. K. Frantz, A. Linden, K. K. Baldridge, J. S. Siegel *J. Am. Chem. Soc.* **2012**, *134*, 1528–1535.

34. T. C. Bedard, J. S. Moore *J. Am. Chem. Soc.* **1995**, *117*, 10662-10671.

35. J. E. Nuñez, A. Natarajan, S. I. Khan, M. A. Garcia–Garibay *Org. Lett.* **2007**, *9*, 3559–3561.

36. T.-A. V. Khuong, J. E. Nuñez, C. E. Godinez, M. A. Garcia–Garibay *Acc. Chem. Res.* **2006**, *39*, 413–422.

37. C. S. Vogelsberg, M. A. Garcia–Garibay *Chem. Soc. Rev.* **2012**, *41*, 1892–1910.

38. K. Skopek, M. C. Hershberger, J. A. Gladysz *Coord. Chem. Rev.* **2007**, *251*, 1723–1733.

39. T.-A. V. Khuong, H. Dang, P. D. Jarowski, E. F. Maverick, M. A. Garcia–Garibay *J. Am. Chem. Soc.* **2007**, *129*, 839–845.

40. M. A. Garcia–Garibay, C. E. Godinez *Cryst. Growth Des.* **2009**, *9*, 3124–3128.

41. A. Stopin, M. A. Garcia–Garibay *Cryst. Growth Des.* **2012**, *12*, 3792–3798.

42. C. Lemouchi, C. Mézière, L. Zorina, S. Simonov, A. Rodríguez–Fortea, E. Canadell, P. Wzietek, P. Auban–Senzier, C. Pasquier, T. Giamarchi, M. A. Garcia–Garibay, P. Batail *J. Am. Chem. Soc.* **2012**, *134*, 7880–7891.

43. S. D. Karlen, M. A. Garcia–Garibay *Top. Curr. Chem.* **2005**, *262*, 179–227.

44. A. Carella, J. Jaud, G. Rapenne, J.–P. Launay *Chem. Comm.* **2003**, 2434–2435.

45. U. G. E. Perera, F. Ample, H. Kersell, Y. Zhang, G. Vives, J. Escheverria, M. Grisolia, G. Rapenne, C. Joachim, S.–W. Hla *Nature Nanotechnol.* **2013**, *8*, 46–51.

46. A. Iordache, M. Oltean, A. Milet, F. Thomas, B. Baptiste, E. Saint–Aman, C. Bucher *J. Am. Chem. Soc.* **2012**, *134*, 2653–2671.

47. K. Tashiro, K. Konishi, T. Aida *J. Am. Chem. Soc.* **2000**, *122*, 7921–7926.

48. B. L. Feringa *Nature* **2000**, *408*, 151–154.

49. X. Zheng, M. E. Mulcahy, D. Horinek, F. Galeotti, T. F. Magnera, J. Michl *J. Am. Chem. Soc.* **2004**, *126*, 4540–4542.

50. D. Horinek, J. Michl *Proc. Natl.Acad. Sci. USA* **2005**, *102*, 14175–14180.

51. J. Vacek, J. Michl *Adv. Funct. Mater.* **2007**, *17*, 730–739.

52. J. S. Seldenthuis, F. Prins, J. M. Thijssen, H. S. J. van der Zant *ACS Nano* **2010**, *4*, 6681–6686.

53. B. L. Feringa *Nature Chem.* **2011**, *3*, 915–916.

54. H. L. Tierney, C. J. Murphy, A. D. Jewell, A. E. Baber, E. V. Iski, H. Y. Khodaverdian, A. F. McGuire, N. Klebanov, E. C. H. Sykes *Nature Nanotechnol.* **2011**, *6*, 625–629.

55. H. L. Tierney, C. J. Murphy, E. C. H. Sykes *Phys. Rev. Lett.* **2011**, *106*, 010801.

56. K. Hirose *J. Incl. Phenom. Macrocycl. Chem.* **2010**, *68*, 1–24.

57. D. Zhang, Q. Zhang, J. Su, H. Tian *Chem. Comm.* **2009**, 1700–1702.

58. M. C. Basheer, Y. Oka, M. Mathews, N. Tamaoki **2010**, *16*, 3489–3496.

59. J.–S. Yang, Y.–T. Huang, J.–H. Ho, W.–T. Sun, H.–H. Huang, Y.–C. Lin, S.–J. Huang, S.–L. Huang, H.–F. Lu, I. Chao *Org. Lett.* **2008**, *10*, 2279–2282.

60. W.–T. Sun, S.–L. Huang, H.–H. Yao, I.–C. Chen, Y.–C. Lin, J.–S. Yang *Org. Lett.* **2012**, *14*, 4154–4157.

61. T. R. Kelly, X. Cai, F. Damkaci, S. B. Panicker, B. Tu, S. M. Bushell, I. Cornella, M. J. Piggott, R. Salives, M. Cavero, Y. Zhao, S. Jasmin *J. Am. Chem. Soc.* **2007**, *129*, 376–386.

62. Y. Lin, B. J. Dahl, B. P. Branchaud *Tetrahedron Lett.* **2005**, *46*, 8359–8362.

63. S. P. Fletcher, F. Dumur, M. M. Pollard, B. L. Feringa *Science* **2005**, *310*, 80–82.

64. J. V. Hernández, E. R. Kay, D. A. Leigh *Science* **2004**, *306*, 1532–1537.

65. B. E. Dial, P. J. Pellechia, M. D. Smith, K. D. Shimizu *J. Am. Chem. Soc.* **2012**, *134*, 3675–3678.

66. B. E. Dial, R. D. Rasberry, B. N. Bullock, M. D. Smith, P. J. Pellechia, S. Profeta Jr., K. D. Shimizu *Org. Lett.* **2011**, *13*, 244–247.

67. N. Koumura, R. W. J. Zijlstra, R. A. van Delden, N. Harada, B. L. Feringa *Nature* **1999**, *401*, 152–155.

68. B. L. Feringa *J. Org. Chem.* **2007**, *72*, 6635–6652.

69. R. A. van Delden, M. K. J. ter Wiel, M. M. Pollard, J. Vicario, N. Koumura, B. L. Feringa *Nature* **2005**, *437*, 1337–1340.

70. J. Conyard, K. Addison, I. A. Heisler, A. Cnossen, W. R. Browne, B. L. Feringa, S. R. Meech *Nature Chem.* **2012**, *4*, 547–551.

71. J. Vicario, M. Walko, A. Meetsma, B. L. Feringa *J. Am. Chem. Soc.* **2006**, *128*, 5127–5135.

72. M. M. Pollard, M. Klok, D. Pijper, B. L. Feringa *Adv. Funct. Mater.* **2007**, *17*, 718–729.

73. E. M. Geertsema, S. J. van der Molen, M. Martens, B. L. Feringa *Proc. Natl. Acad. Sci. U. S. A.* **2009**, *106*, 16919–16924.

74. A. Coskun, M. Banaszak, R. D. Astumian, J. F. Stoddart, B. A. Grzybowski *Chem. Soc. Rev.* **2012**, *41*, 19–30.

75. J. Wang, B. L. Feringa *Science* **2011**, *331*, 1429–1432.

76. G. London (2011) *Light–Driven Molecular Motors and Switches in Confined Environments* PhD Thesis, University of Groningen, The Netherlands.

77. M. M. Pollard, M. K. J. ter Wiel, R. A. van Delden, J. Vicario, N. Koumura, C. R. van den Brom, A. Meetsma, B. L. Feringa *Chem. Eur. J.* **2008**, *14*, 11610–11622.

78. G. T. Carroll, M. M. Pollard, R. A. van Delden, B. L. Feringa *Chem. Sci.* **2010**, *1*, 97–101.

79. D. Pijper, B. L. Feringa *Angew. Chem. Int. Ed.* **2007**, *46*, 3693–3696.

80. R. Eelkema, M. M. Pollard, J. Vicario, N. Katsonis, B. Serrano Ramon, C. W. M. Bastiaansen, D. J. Broer, B. L. Feringa *Nature* **2006**, *440*, 163.

81. R. Eelkema, M. M. Pollard, N. Katsonis, J. Vicario, D. J. Broer, B. L. Feringa *J. Am. Chem. Soc.* **2006**, *128*, 14397–14407.

82. T. Kudernac, N. Ruangsupapichat, M. Parschau, B. Maciá, N. Katsonis, S. R. Harutyunyan, K.–H. Ernst, B. L. Feringa *Nature* **2011**, *479*, 208–211.

83. M. K. J. ter Wiel, R. A. van Delden, A. Meetsma, B. L. Feringa *Org. Biomol. Chem.* **2005**, *3*, 4071–4076.

84. A. S. Lubbe, N. Ruangsupapichat, G. Caroli, B. L. Feringa *J. Org. Chem.* **2011**, *76*, 8599–8610.

85. *Molecular Switches* (Ed: B. L. Feringa and W. R. Browne), Wiley–VCH, 2nd edition, Weinheim, Germany **2011**.

86. E. Merino, M. Ribagorda *Beilstein J. Org. Chem.* **2012**, *8*, 1071–1090.

87. J. García–Amorós, D. Velasco *Beilstein J. Org. Chem.* **2012**, *8*, 1003–1017.

88. K. Morgenstern *Acc. Chem. Res.* **2009**, *42*, 213–223.

89. M. Alemani, M. V. Peters, S. Hecht, K.–H. Rieder, F. Moresco, L. Grill *J. Am. Chem. Soc.* **2006**, *128*, 14446–14447.

90. M. Alemani, S. Selvanathan, F. Ample, M. V. Peters, K.–H. Rieder, F. Moresco, C. Joachim, S. Hecht, L. Grill *J. Phys. Chem. C* **2008**, *112*, 10509–10514.

91. B.–Y. Choi, S.–J. Kahng, S. Kim, H. Kim, H. W. Kim, Y. J. Song, J. Ihm, Y. Kuk *Phys. Rev. Lett.* **2006**, *96*, 156106.

92. J. Henzl, M. Mehlhorn, H. Gawronski, K.–H. Rieder, K. Morgenstern *Angew. Chem. Int. Ed.* **2006**, *45*, 603–606.

93. M. J. Comstock, N. Levy, A. Kirakosian, J. Cho, F. Lauterwasser, J. H. Harvey, D. A. Strubbe, J. M. J. Fréchet, D. Trauner, S. G. Louie, M. F. Crommie *Phys. Rev. Lett.* **2007**, *99*, 038301.

94. M. Wolf, P. Tegeder *Surf. Sci.* **2009**, *603*, 1506–1517.

95. D. Bléger, A. Ciesielski, P. Samorì, S. Hecht *Chem. Eur. J.* **2010**, *16*, 14256–14260.

96. S. Hagen, P. Kate, M. V. Peters, S. Hecht, M. Wolf, P. Tegeder *Appl. Phys. A* **2008**, *93*, 253–260.

97. S. Hagen, F. Leyssner, D. Nandi, M. Wolf, P. Tegeder *Chem. Phys. Lett.* **2007**, *444*, 85–90.

98. L. Óvári, M. Wolf, P. Tegeder *J. Phys. Chem. C* **2007**, *111*, 15370–15374.

99. P. M. Echenique, R. Berndt, E. V. Chulkov, T. Fauster, A. Goldmann, U. Höfer *Surf. Sci. Rep.* **2004**, *52*, 219–317.

100. M. Weinelt *J. Phys.: Condens. Matter* **2002**, *14*, R1099–R1141.

101. J. L. Erskine *J. Vac. Sci. Technol. A* **1986**, *4*, 1282–1288.

102. J. Mielke, S. Selvanathan, M. Peters, J. Schwarz, S. Hecht, L. Grill *J. Phys.: Condens. Matter* **2012**, *24*, 394013.

103. V. Balzani, M. Clemente–León, A. Credi, J. N. Lowe, J. D. Badjić, J. F. Stoddart, D. J. Williams *Chem. Eur. J.* **2003**, *9*, 5348–5360.

104. J. D. Badjić, V. Balzani, A. Credi, S. Silvi, J. F. Stoddart *Science* **2004**, *303*, 1845–1849.

105. J. D. Badjić, C. M. Ronconi, J. F. Stoddart, V. Balzani, S. Silvi, A. Credi *J. Am. Chem. Soc.* **2006**, *128*, 1489–1499.

106. G. Pace, V. Ferri, C. Grave, M. Elbing, C. von Hänisch, M. Zharnikov, M. Mayor, M. A. Rampi, P. Samorì *Proc. Natl. Acad. Sci. U. S. A.* **2007**, *104*, 9937–9942.

107. V. Ferri, M. Elbing, G. Pace, M. D. Dickey, M. Zharnikov, P. Samorì, M. Mayor, M. A. Rampi *Angew. Chem. Int. Ed.* **2008**, *47*, 3407–3409.

108. C. Joachim, G. Rapenne *ACS Nano* **2013**, *7*, 11–14.

109. Y. Shirai, J.-F. Morin, T. Sasaki, J. M. Guerrero, J. M. Tour *Chem. Soc. Rev.* **2006**, *35*, 1043–1055.

110. G. Vives, J. M. Tour *Acc. Chem. Res.* **2009**, *42*, 473–487.

111. Y. Shirai, A. J. Osgood, Y. Zhao, Y. Yao, L. Saudan, H. Yang, C. Yu–Hung, L. B. Alemany, T. Sasaki, J.–F. Morin, J. M. Guerrero, K. F. Kelly, J. M. Tour *J. Am. Chem. Soc.* **2006**, *128*, 4854–4864.

112. J. K. Gimzewski, C. Joachim *Science* **1999**, *283*, 1683–1688.

113. F. Chiaravalloti, L. Gross, K.–H. Rieder, S. M. Stojkovic, A. Gourdon, C. Joachim, F. Moresco *Nature Mater.* **2007**, *6*, 30–33.

114. K. L. Wong, G. Pawin, K.–Y. Kwon, X. Lin, T. Jiao, U. Solanki, R. H. J. Fawcett, L. Bartels, S. Stolbov, T. S. Rahman *Science* **2007**, *315*, 1391–1393.

115. L. Gross, K.–H. Rieder, F. Moresco, S. M. Stojkovic, A. Gourdon, C. Joachim *Nature Mater.* **2005**, *4*, 892–895.

116. W. Auwärter, A. Schiffrin, A. Weber–Bargioni, Y. Pennec A. Riemann, J. V. Barth *Int. J. Nanotechnol.* **2008**, *5*, 1171–1193.

117. S.–W. Hla, K.–H. Rieder *Annu. Rev. Phys. Chem.* **2003**, *54*, 307–330.

118. L. Bartels, G. Meyer, K.–H. Rieder *Appl. Phys. Lett.* **1997**, *71*, 213–215.

119. L. Gross, K.–H. Rieder, F. Moresco, S. M. Stojkovic, A. Gourdon, C. Joachim *Nature Mater.* **2005**, *4*, 892–895.

120. L. Grill, K.–H. Rieder, F. Moresco, G. Rapenne, S. Stojkovic, X. Bouju, C. Joachim *Nature Nanotechnol.* **2007**, *2*, 95–98.

121. Y. Shirai, A. J. Osgood, Y. Zhao, K. F. Kelly, J. M. Tour *Nano Lett.* **2005**, *5*, 2330–2334.

122. T. Sasaki, J. M. Tour *Org. Lett.* **2008**, *10*, 897–900.

123. J.–F. Morin, Y. Shirai, J. M. Tour *Org. Lett.* **2006**, *8*, 1713–1716.

124. P.–T. Chiang, J. Mielke, J. Godoy, J. M. Guerrero, L. B. Alemany, C. J. Villagómez, A. Saywell, L. Grill, J. M. Tour *ACS Nano* **2012**, *6*, 592–597.

125. P.–L. E. Chu, L.–Y. Wang, S. Khatua, A. B. Kolomeisky, S. Link, J. M. Tour *ACS Nano* **2013**, *7*, 35–41.

126. J. Godoy, G. Vives, J. M. Tour *Org. Lett.* **2010**, *12*, 1464–1467.

127. K. Claytor, S. Khatua, J. M. Guerrero, A. Tcherniak, J. M. Tour, S. Link *J. Chem. Phys.* **2009**, *130*, 164710.

128. G. Vives, J. M. Guerrero, J. Godoy, S. Khatua, Y.-P. Wang, J. L. Kiappes, S. Link, J. M. Tour *J. Org. Chem.* **2010**, *75*, 6631–6643.

129. S. Khatua, J. M. Guerrero, K. Claytor, G. Vives, A. B. Kolomeisky, J. M. Tour, S. Link *ACS Nano* **2009**, *3*, 351–356.

130. J. Godoy, G. Vives, J. M. Tour *ACS Nano* **2011**, *5*, 59–90.

Chapter 2

Molecular Multiswitches for the Study of the Switching Behaviour on Surfaces

This chapter describes the design, preparation and solution-properties of novel multiazobenzene molecules. The molecules are equipped with multiple photoswitching units and designed with the aim of evaluating the surface-behaviour of this type of molecular multiswitches. As discussed in Chapters 3 and 4, these (multi)switching units may be used in the design of future surface-traversing molecules.

Introduction

One of modern chemistry's main objectives is gaining control over molecular motion. This endeavor faces many challenges, the biggest of which is often considered to be overcoming Brownian motion. A way of addressing this issue is immobilization of molecular machinery on a surface[1]. Molecular motors and switches have extensively been used in attempts to bring molecular motion under control[1,2,3,4,5,6,7,8,9].

Azobenzene compounds are among the most frequently used switches for this purpose due to their unique properties[7]. They can exist in two isomeric forms, namely the *E*–isomer and the *Z*–isomer which can interconvert both photochemically and thermally (Scheme 1). Since the *E*–azobenzene group is planar and the *Z*–azobenzene group is not, their interconversion brings about a significant geometric change; the shape of the molecule and the intramolecular distances change (Scheme 1 shows how the distance between the opposite ends of the molecule changes upon switching). This is accompanied by a significant change in the dipole moment (μ_E = 0 D, μ_Z = 3.0 D for azobenzene)[7]. These effects make azobenzene compounds excellent candidates for use in building dynamic molecular devices that can be addressed and controlled by light[7].
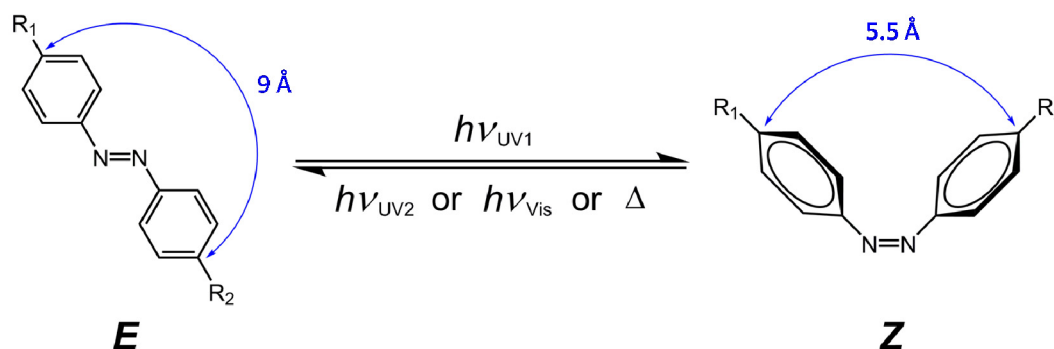
Scheme 1. Typical switching behaviour of azobenzenes.

A polymer containing an azobenzene group in its repeating unit has been reported[10]. The polymer molecule was investigated by means of single-molecule force spectroscopy in combination with optical excitation in total internal reflection; by switching the azobenzene units between their *E* and *Z* states, individual molecules could be optically extended and contracted. The molecule was also found to contract against an external force acting along a polymer backbone, thus delivering mechanical work at the molecular level.

Azobenzene compounds have also been used on surfaces quite extensively. There have been contributions where these switches were mounted on surfaces and used to perform work and/or induce molecular movements[11,12,13,14]. Azobenzene compounds have also been studied on metal surfaces in ultrahigh vacuum where reversible electrical[15,16,17,18] and photochemical[19,20] as well as thermal[20] switching of

individual molecules was observed by scanning tunneling microscopy (STM). Switching studies of azobenzene self-assembled monolayers at the solid-liquid interface are also known[21].

Due to their special switching properties azobenzene compounds have also been envisaged to provide a means of propelling nanovehicles[5,22,23]. We deal with this idea in Chapters 3 and 4. It is likely however that only multiazobenzene molecules will show movement on surfaces as the collective nature of the azobenzene isomerization has already been harnessed to provide work[12,13]. In order to utilize azobenzene compounds for these purposes a more thorough fundamental understanding of the behaviour of these molecules on surfaces is needed. Apart from azobenzene-containing dendrimeric structures[24,25], multiazobenzene compounds have not been studied extensively in solution[26,27,28,29,30] nor on surfaces[31].

To this end we set out to prepare and study molecules **1** and **2** (Fig 1), containing three and four azobenzene groups, respectively. In the all–*E* form the molecules are planar and once the azobenzene groups are switched to the *Z*–form the molecules lose their planarity as one phenyl ring from each *Z*–azobenzene group flips out of plane[7]. This also renders the *Z*–azobenzene group clearly distinguishable from the *E*–azobenzene group by means of scanning tunneling microscopy[15,16,18,19,20]. The molecular backbone is based on oligo(phenylene ethynylene)s (OPEs) which have extensively been used as organic building blocks for molecular devices due to their shape-persistent nature and relatively simple synthetic accessibility[32,33]. The rigidity of the scaffold should therefore ensure that the only geometrical changes come from the isomerization of the azobenzene groups. The azobenzene units are equipped with long alkyl chains. Their purpose is twofold: they should increase the solubility of the molecules[5,6] and through interchain van der Waals interactions they should facilitate self-assembly of the molecules for the study at the solid-liquid interface[34,35,36].
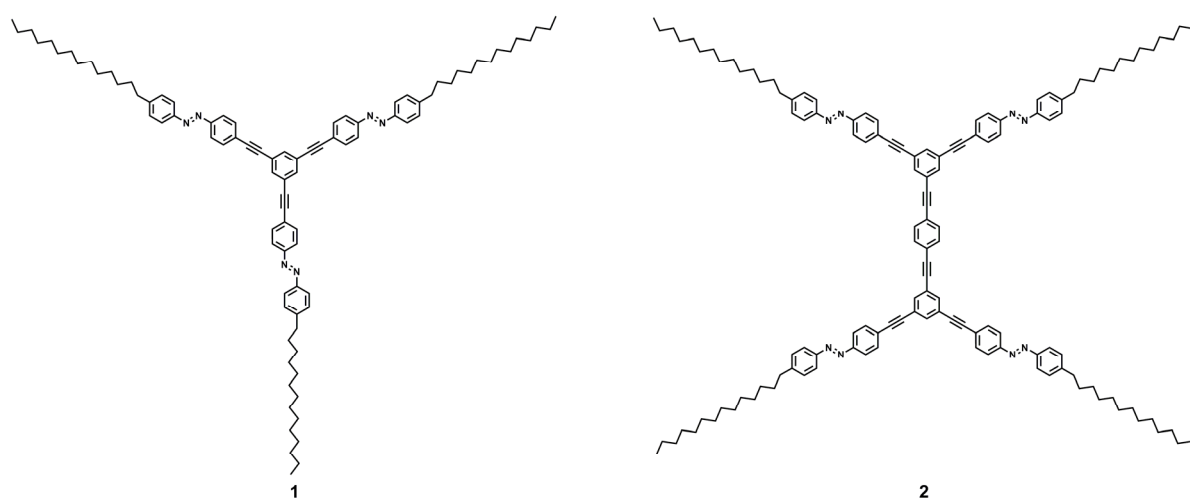
Figure 1. Design of multiazobenzene switches **1** and **2**.

Furthermore, for **1** the trigonal symmetry of the molecule and the underlying three-fold symmetry of the substrate should enhance self-assembly and organization and lead to the formation of hexagonal patterns at the solid-liquid interface (if, for instance, HOPG is used) [37,38,39,40,41,42]. Molecule **2**, although in the absence of trigonal symmetry like **1**, might still engage in self-assembly due to its star-shaped appearance[40]. It is designed in this way, however, to resemble various nanovehicle designs recently reported in the literature[5,6,22,26]. As an analogue having four azobenzene switches in place of molecular wheels or motors, its behaviour on a surface might be rather interesting to compare to other nanovehicle designs. It should be noted that a „molecular arachnoid", resembling our design of **2**, has been reported by Bonifazi and co-workers[26]. No thorough photochemical characterization or any surface studies have been reported up to date however.

The objectives of the research described in this chapter are to synthesize compounds **1** and **2**, characterize them and study their switching properties in solution. This should allow us to compare the behaviour of these novel molecules to simple azobenzenes and related compounds reported in the literature. The results should already give an indication about their utility for any surface studies. Ultimately, we would like to study these molecules on surfaces, be it in self-assembled monolayers or as individual molecules. The first step would be the visualization of individual molecules or domains of molecules by STM. This would provide information about possible interactions between molecules and their packing mode on the surface. The next step would be to follow the dynamic processes triggered by irradiation (changes in molecular geometry, orientation, position, etc.) by means of STM. Visualizing the isomerization process on the surface would allow us to gain insight into the switching process on the surface. How many molecules would be affected by irradiation? How many azobenzene units per molecule can be switched? What would the distribution of isomers be? Is it possible to reversibly switch the azobenzene groups? Does surface assembly affect the switching behaviour? Will there be any cooperative effects? These are but a few questions that we would ultimately like to address. Furthermore, reversible switching of azobenzenes on a surface by electrical pulsing is also known[15,16,18]. It would be highly interesting to see if it is possible to selectively switch only a single azobenzene unit in the molecule by positioning the STM tip directly above a certain part of the molecule and leave the remaining azobenzene groups unaffected. This would give us complete control over the switching process on the surface. The surface investigations indicated above should provide insight into the behaviour of these molecules on the surface and possibly pave the way for the development of a new generation of nanovehicles (Chapters 3 and 4).

Results and discussion

Synthesis and characterization

Despite the apparently large sizes of molecules **1** and **2**, due to their high symmetry, they could be synthesized in a convergent manner reducing the number of synthetic steps and increasing the efficiency of the syntheses.

The trisazobenzene molecule **1** was synthesized according to Scheme 2. The unsymmetrically substituted azobenzene unit **5** was prepared by the coupling of the corresponding nitroso compound **4** with 4-iodoaniline following a literature procedure for an analogous azobenzene derivative differing from **5** only in the alkyl chain length[43]. 1-Nitroso-4-tetradecylbenzene **4** was prepared by the oxidation of 4-tetradecylaniline **1** with oxone (2 KHSO$_5$ · KHSO$_4$ · K$_2$SO$_4$) and was subsequently coupled to 4-iodoaniline in acetic acid. This reaction afforded the iodo-functionalized azobenzene molecule **5** which was used as the main building block in the syntheses of both target molecules **1** and **2**. Molecule **1** was then obtained in a triple Sonogashira coupling reaction between the iodo-functionalized azobenzene **5** and 1,3,5-triethynylbenzene.
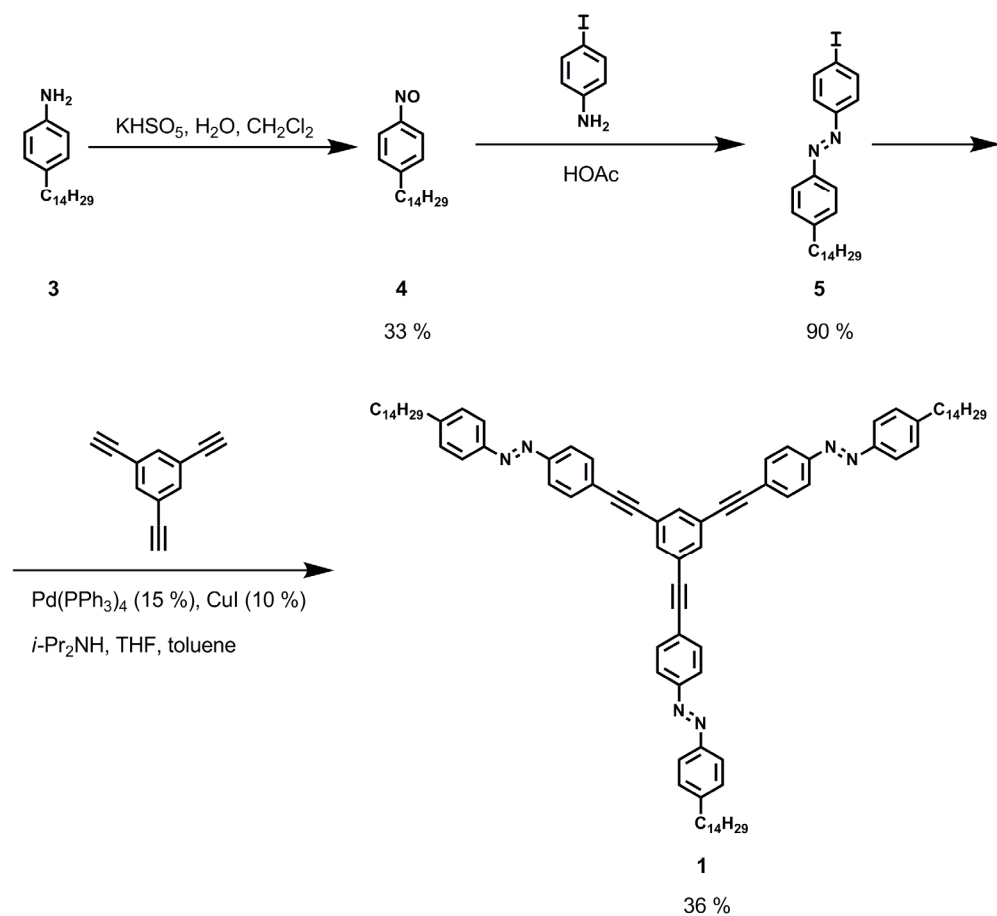
Scheme 2. Synthesis of the trisazobenzene **1**.

The tetrakisazobenzene molecule **2** was synthesized according to Scheme 3. The synthesis started with 1,3,5-tribromobenzene **6** which was converted into 1-bromo-3,5-diiodobenzene **7** following a literature procedure[44]. Compound **7** was then reacted with triisopropylsilylacetylene in a double Sonogashira reaction followed by the removal of the TIPS-groups to afford 1-bromo-3,5-diethynylbenzene **9**. These two synthetic steps were adapted from a literature procedure reporting a synthesis of a similar compound[45] and the NMR spectra of intermediate **9** compared well to those reported in the literature[46]. Molecule **9** was then coupled to two molecules of the iodo-functionalized azobenzene **5** in a double Sonogashira reaction affording the bromo-functionalized bisazobenzene **10**. This reaction is a fine example of different reactivities of bromo- and iodo-functionalized aromatics in the Sonogashira coupling reactions. The coupling reaction was carried out at room temperature to prevent the polymerization reaction of 1-bromo-3,5-diethynylbenzene **9** from taking place; under those conditions only the iodo-compound reacted affording the desired product **10**. The last step of the synthesis was a convergent coupling of two molecules of **10** to a molecule of 1,4-diethynylbenzene in another Sonogashira reaction; this time the less reactive bromo-functionalized **10** had to react so the reaction was carried out at elevated temperature. This afforded the target molecule **2**.
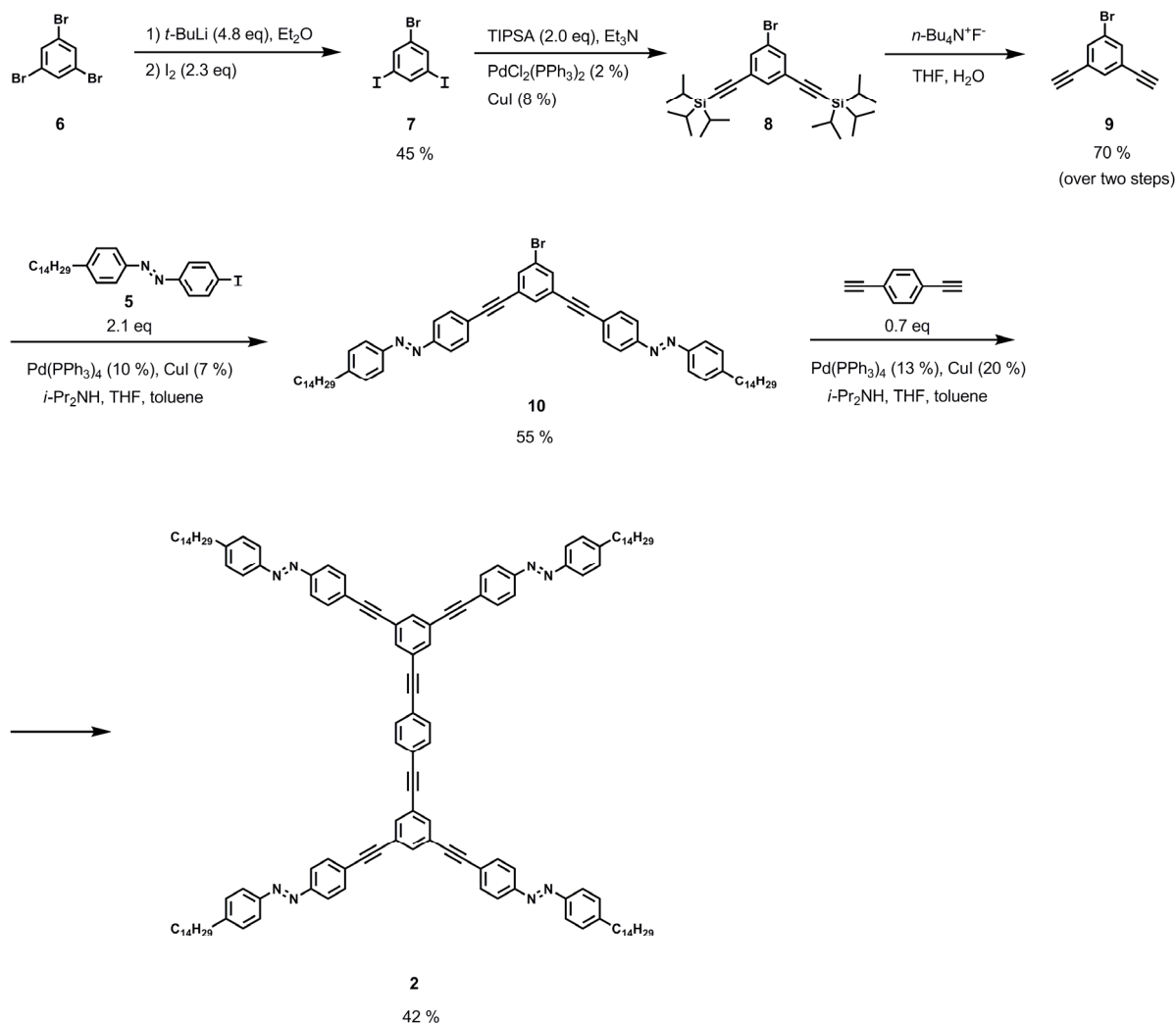
Scheme 3. Synthesis of the tetrakisazobenzene **2**.

All the synthetic intermediates and the target molecules **1** and **2** were characterized by ^{1}H–NMR and APT NMR spectroscopic techniques as well as by high resolution mass spectrometry. In addition to the signals corresponding to the azobenzene units, the aromatic region of the ^{1}H–NMR spectrum of **1** also shows a singlet signal, in support of the newly formed connection between the azobenzene units. The ^{13}C–NMR spectrum of **1** also shows two signals in the region 90–91 ppm which correspond to two C–atoms belonging to a C≡C bond. The aromatic region of the ^{1}H–NMR spectrum of **2**, in addition to the signals corresponding to the azobenzene units, also shows three singlet signals with the integral ratio of 4:4:2, in support of the newly formed connection between the azobenzene units. The ^{13}C–NMR spectrum of **2** shows four signals in the region 89–91 ppm which correspond to the C–atoms belonging to C≡C bonds. Furthermore, two of the signals show approximately double the intensity of the remaining two indicating the presence of two magnetically different C≡C bonds in 2:1 ratio. This again is in strong support of the structure of the target molecule **2**. In mass spectrometry the final products **1** and **2** give the masses that correspond to the protonated molecules, [M+H]+. Molecules of **1** could be observed by using the electrospray ionization

55

technique whereas molecules of **2** could only be observed using MALDI as the ionization technique.

Photochemical characterization

Trisazobenzene 1

UV−Vis spectroscopic study

Photochemical properties of switch **1** were examined in solution (*n*-heptane) by means of UV−Vis spectroscopy, as shown in Fig 2. The UV−Vis spectrum of **1** shows a strong absorption band with λ_{max} = 365 nm. Upon irradiation of the sample at λ = 365 nm, the band drops in intensity and two new bands appear simultaneously, one with λ_{max} = 321 nm and another with λ_{max} = 450 nm. Subsequent irradiation with light at λ = 312 nm or λ > 420 nm, or an increase in temperature causes the newly formed bands to disappear again and the original band with λ_{max} = 365 nm to reappear in its original intensity. A total of four isosbestic points is identified from Fig 2, namely at 232, 245, 330 and 416 nm. The described isomerization behaviour is typical of azobenzene compounds[7,47].
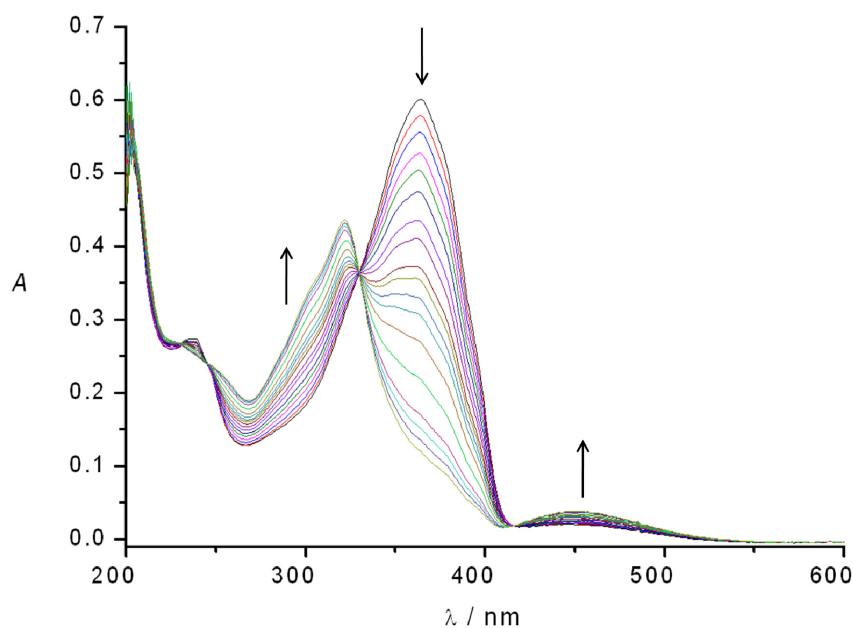
Figure 2. UV−Vis spectra of switch **1**, c = 5.2·10^{-6} mol dm^{-3}; in *n*-heptane, at −10 ˚C. Irradiation with light at 365 nm, 312 nm and > 420 nm.

Irradiation of the sample kept in the dark (*E*−isomer) with light at 365 nm establishes a photoequilibrium between the *E*−isomer and the *Z*−isomer of the azobenzene (Scheme 1). The change in the composition of the solute (the ratio of the *E*− and *Z*−isomer) is reflected in the UV−Vis spectrum of the solution; the spectrum changes during irradiation until a photoequilibrium has been reached. The exact composition of the solute at the photoequilibrium cannot be estimated at this

point but will be addressed at a later stage. Irradiation of the solution with light at λ = 312 nm or λ > 420 nm causes a new photoequilibrium to be established which is again reflected in the UV$-$Vis spectra of the solution. Since the spectrum taken at the new photoequilibrium appears identical to the one of the *E*$-$isomer it can be concluded that the photostationary state (at λ = 312 nm or λ > 420 nm) consists predominately of the *E*$-$isomer. This also makes sense since it is the *Z*$-$isomer that absorbs to a greater extent at those wavelengths.

After the photostationary state has been reached by irradiation of the *E*$-$isomer with light at 365 nm, the change can not only be reversed photochemically (at λ = 312 nm or λ > 420 nm) but thermally as well *i.e.* by warming up the sample. The spectrum of the pure *E*$-$isomer is once again recovered. This complete thermal reversal of the changes brought about by irradiation with light at 365 nm makes sense since the less stable *Z*$-$isomer is well known to thermally convert to the more stable *E*$-$isomer[7,47] (Scheme 1). The time it takes for the full recovery of the original spectrum of the *E*$-$isomer will depend on the temperature of the system. This phenomenon will be studied and described in more detail at a later stage.

^{1}H$-$NMR spectroscopic study

The switching behaviour of molecule **1** was also studied in CD_2Cl_2 by means of ^{1}H$-$NMR spectroscopy (Fig 3). Irradiation of the solution containing only the *E*$-$isomer of **1** with light at 365 nm was accompanied by the appearance of new signals in both the aromatic as well as in the aliphatic region of the spectrum, Fig 3b (the assignment of the ^{1}H$-$NMR signals in the aliphatic region of the spectrum is given in Fig 4). It was proceeded with the irradiation until no further changes could be observed in the spectrum, Fig 3c. The photostationary state had been reached at that point and the solute contained 75 % of the newly formed species. Irradiation of the sample now at the photostationary state with light at 312 nm resulted in the decrease in the intensity of the new signals. Even after prolonged irradiation, however, the new signals did not disappear completely and the original spectrum (of the *E*$-$isomer) could not be restored, as shown in Fig 3d. At the photostationary state reached by irradiation with light at 312 nm the sample contained a total of 30 % of the new species and the rest was the *E*$-$isomer.
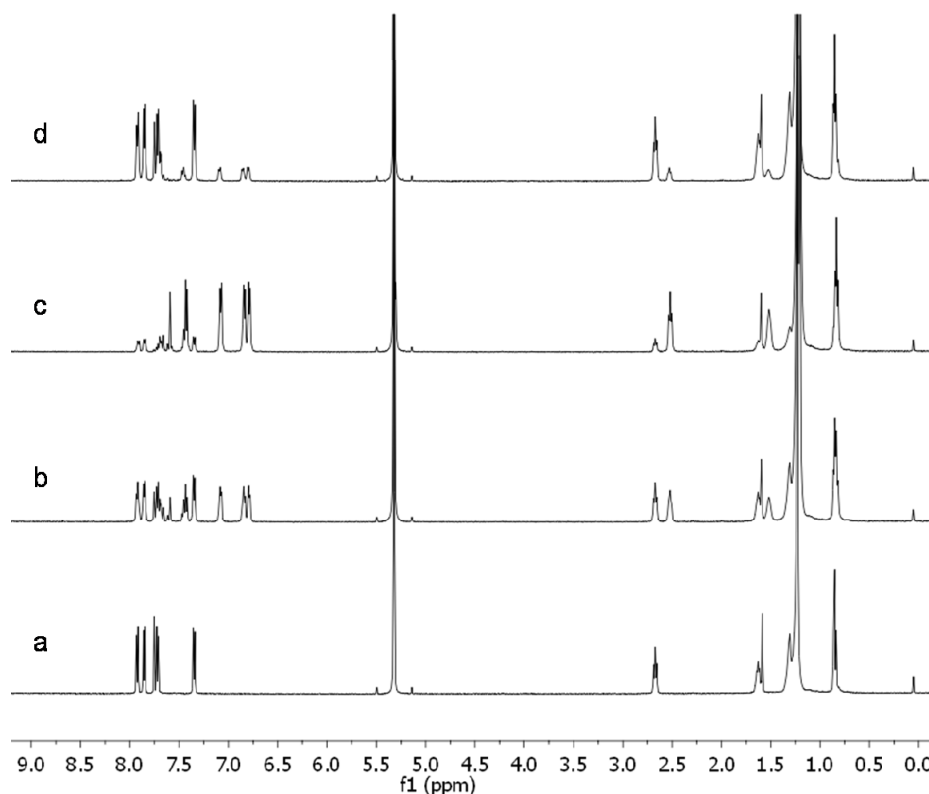
Figure 3. ^{1}H–NMR spectra of switch **1**, in CD$_2$Cl$_2$, at –10 °C (irradiation was performed at 4 °C); **a:** in the dark, **b:** sample from **a** irradiated at 365 nm for 0.5 h, **c:** sample from **a** irradiated at 365 nm for 3 h (PSS), **d:** sample from **c** irradiated at 312 nm for 3 h (PSS).

It should be noted that the NMR experiments were performed in CD$_2$Cl$_2$ whereas the UV–Vis experiments were conducted in *n*-heptane. Furthermore, the concentrations differed by 2 to 3 orders of magnitude (roughly 10^{-5} mol dm^{-3} for UV–Vis spectroscopy and 10^{-3} mol dm^{-3} for NMR spectroscopy) and the irradiation was conducted in an NMR tube in the former case and in a cuvette in the latter case; the results can therefore not be directly compared. The data obtained by the two spectroscopic studies do however give an idea of where the photoequilibria lie *i.e.* the data give an indication of the compositions of the mixtures at the photostationary states. The NMR study suggests that a large part of the azobenzene switches goes from the *E*– to the *Z*–configuration upon irradiation with light at 365 nm (until the photostationary state is reached) and the UV–Vis experiments seem to be in accordance with that finding as the most intense band (λ_{max} = 365 nm) of the *E*–isomer almost entirely disappears at the photostationary state. If, at this photostationary state, the system is irradiated with light at 312 nm, this brings it to another photostationary state where a significant percentage of the *Z*–isomers is converted back to their original *E*–configuration. The UV–Vis study suggests that the photoequilibrium lies completely on the side of the *E*–isomer whereas the ^{1}H–NMR study clearly shows some remaining molecules of the *Z*–isomer at photoequilibrium. It is known for azobenzene compounds to have a different ratio of *E*– and *Z*–isomers at the photostationary state in different

solvents[48,49]. Besides the possibility of a solvent effect, it is also possible that the irradiation of an NMR sample is not as efficient as the irradiation of a UV–Vis sample. An NMR sample is 2 to 3 orders of magnitude more concentrated than a UV–Vis sample needing light of stronger intensity for maximum absorption by the sample. Furthermore, an NMR tube has a smaller cross section than a cuvette allowing less light to reach the sample. For these reasons it might be possible that in an NMR tube the true photostationary state is never actually reached due to inefficient irradiation (even after prolonged irradiation times). This could cause a discrepancy in the results obtained from the two spectroscopic techiques.

The NMR signals that shift (most) upon irradiation are those corresponding to the protons that are in immediate vicinity of the azobenzene unit that undergoes the isomerization process. As seen in Fig 3, the aromatic signals undergoing most change upon irradiation are the ones corresponding to the aromatic protons of the azobenzene unit. There are also some changes in the aliphatic region of the spectrum however. In Fig 4 one can see the aliphatic region of the ^{1}H–NMR spectra of **1** in more detail; Fig 4a shows the spectrum of **1** that has been kept in the dark (*E*–isomer), Fig 4b shows the spectrum of the same sample after having been exposed to irradiation with light at 365 nm for 0.5 h and Fig 4c depicts the structure of the azobenzene unit of **1**, highlighting the aliphatic protons of relevance.
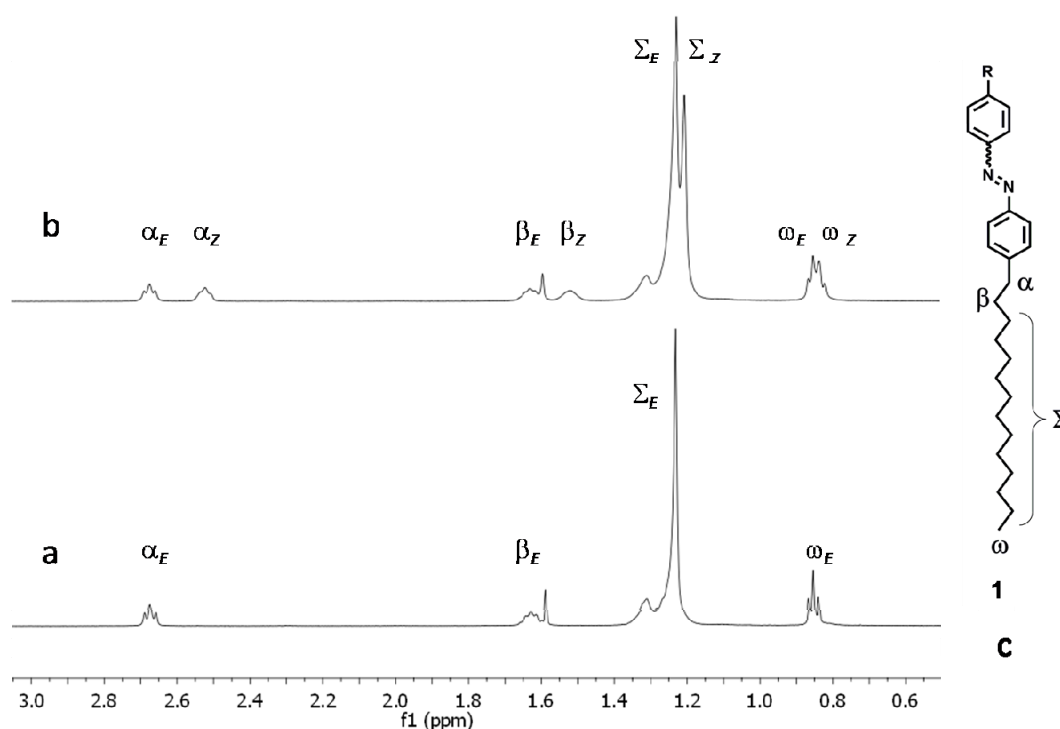
Figure 4. The aliphatic region of ^{1}H–NMR spectra of switch **1**, in CD_2Cl_2, at −10 °C; **a:** in the dark, **b:** sample from **a** irradiated at 365 nm for 0.5 h, **c:** the structure of an azobenzene unit of **1** with the aliphatic protons of interest highlighted.

The signal appearing at δ = 2.70 ppm in Fig 4a,c corresponds to the protons of the methylene group adjacent (in the α–position) to the phenyl ring of the *E*–azobenzene group of **1**; these protons are denoted α_E. The protons of the methylene group adjacent to the α–protons are denoted β_E and appear at δ = 1.66 ppm. The remaining methylene groups of the alkyl chain are rather indistinguishable and appear as a broad signal in the range δ = 1.41–1.22 ppm; they are denoted Σ_E, Fig 4 a,c. The terminal methyl group with its ω_E protons appears at δ = 0.88 ppm.

After irradiating **1** with light at 365 nm for 0.5 h, approximately half of the total azobenzene groups have switched as evidenced by the appearance of new peaks corresponding to the aliphatic protons of the *Z*–isomer, Fig 4b. All the new signals appear at lower chemical shifts (δ) than their corresponding signals from the *E*–isomer which is typical of azobenzene compounds[7]. The appearance of separate signals for α_Z and β_Z protons is expected since these protons are in proximity to the switching azobenzene unit. Somewhat less expected is the finding that there is also a separate set of signals for Σ_Z and ω_Z protons since some of these are quite remote from the switching azobenzene group. Furthermore, the alkyl chain is expected to be quite flexible and therefore free to take almost any conformation and position in space regardless the configuration of the N=N bond. In compound **1**, rather surprisingly, the effect of switching of the azobenzene group seems to extend further away from the switching unit.

This finding clearly indicates some sort of a communication between the azobenzene groups and the most remote atoms of the alkyl chains, at least under the NMR conditions. It is not entirely clear at this point by which mechanism this communication arises. It is possible that the long alkyl chains interact with one another or with other parts of the molecule(s), be it in an intermolecular or intramolecular manner (Fig 5). If the alkyl chains were held together by van der Waals forces in an intermolecular way, this would fix the position of molecules to a certain extent *i.e.* reduce their degrees of freedom. Even though various modes of intermolecular interactions can be thought of, a simple in–plane alignment of molecules is suggested in Fig 5b (one could also imagine another layer of molecules coming on top of the one depicted in the figure, interacting with the bottom layer not only through the van der Waals interactions but through π–π stacking of the aromatic cores as well). Changing the configuration of the azo-groups from the planar *E* to the nonplanar *Z* would undoubtedly also change the intermolecular distances between the interacting molecules. This would in turn also alter the interaction between the alkyl chains (and therefore between the molecules as whole as well). It is not difficult to imagine that this different interaction would lead to a shift of the NMR signals corresponding even to the remotest protons in the alkyl chains. Such aggregation of molecules would however be expected to be concentration dependent; a systematic dilution experiment should therefore be conducted to check for the concentration dependence of the spectra at the photostationary state. Alternatively, the alkyl chains might interact with one another

(or with the phenyl rings or N=N groups) intramolecularly as indicated in Fig 5a. Switching an azobenzene group from the planar *E*–configuration to the nonplanar *Z*–configuration would severely change the geometry of the molecule allowing for new interactions; as indicated in Fig 5a, the alkyl chains of *E*–azo units can only interact (in an intramolecular manner) with the conjugated system of the molecule but the alkyl chains of the *Z*–azo units can also engage in interactions with alkyl chains of adjacent azobenzene units. This change in interaction is expected to be observed in the NMR spectra, even with the signals corresponding to the remotest protons in the alkyl chains. Such intramolecular interactions would, however, be entropically less favourable than the intermolecular interactions and therefore also less likely.

a

b
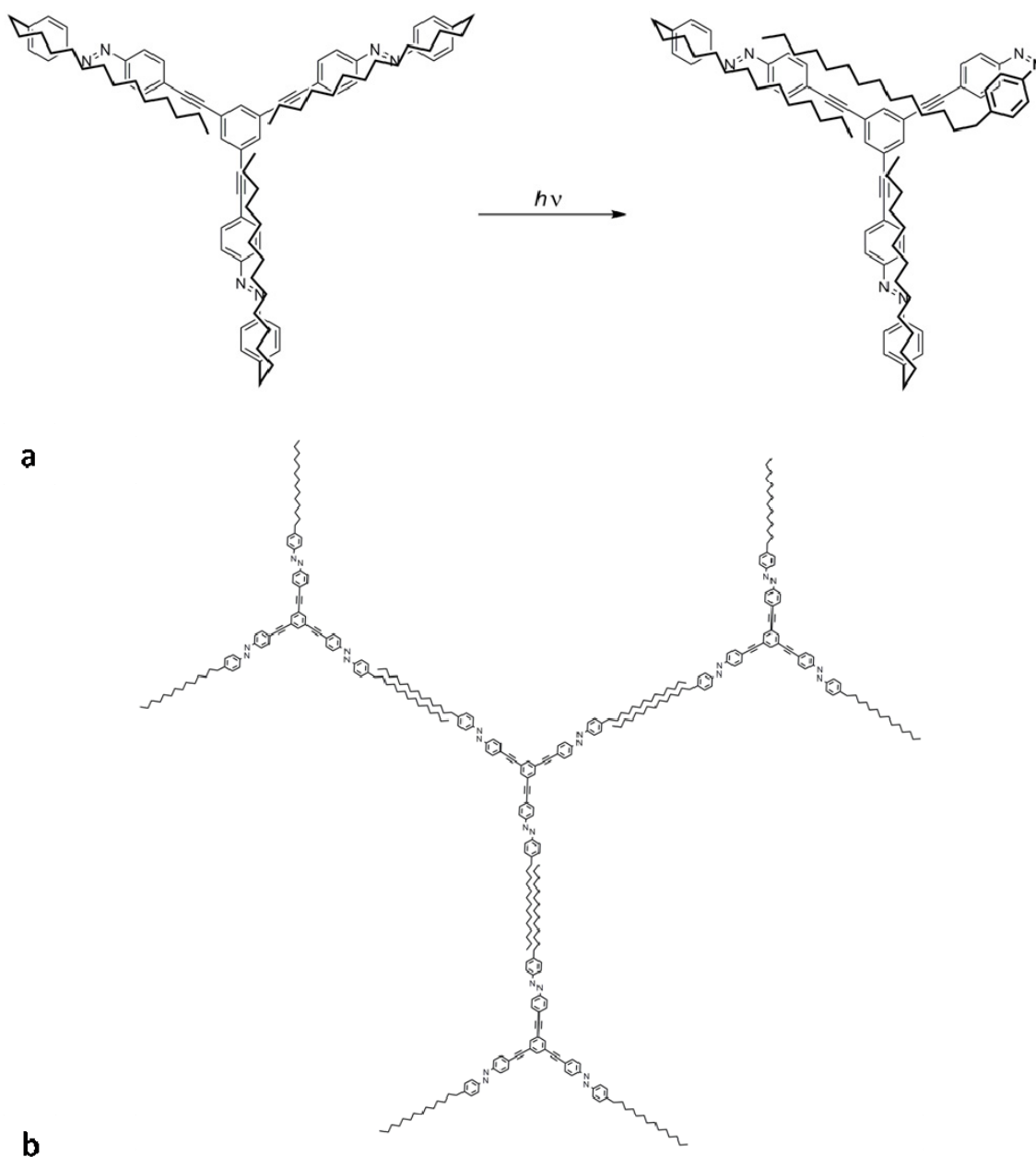
Figure 5. A model by which the alkyl chains of **1** interact with each other **a:** intramolecularly, **b:** intermolecularly.

There is another issue worth addressing. So far we have termed different isomers of molecule **1** as the *E*– or *Z*–isomer. This is quite unclear as each molecule of **1** contains three separate azobenzene units. As evidenced by the NMR spectra the most stable form of **1** (kept in the dark) is the all–*E*–isomer as only a single *E*–configured azobenzene group is observed in the spectrum which is in accordance with the symmetry of the molecule. Irradiation with light at 365 nm yields 75 % of the "other isomer" at the photostationary state. This means that 75 % of all azobenzene groups are *Z*–configured and 25 % are *E*–configured. This, however, says nothing about the distribution of those azobenzene groups in molecules. Do these numbers mean that 75 % of the molecules is all–*Z* and 25 % is all–*E* or is there a mixture of (*E,E,E*), (*E,E,Z*), (*E,Z,Z*) and (*Z,Z,Z*) molecules with a total of 75 % of all the azobenzene groups *Z*–configured and 25 % *E*–configured? And in the latter case, what would the distribution of these isomers be in the mixture?

In an attempt to address these questions an expansion of the aromatic region of spectra from Fig 3 is shown in Fig 6.
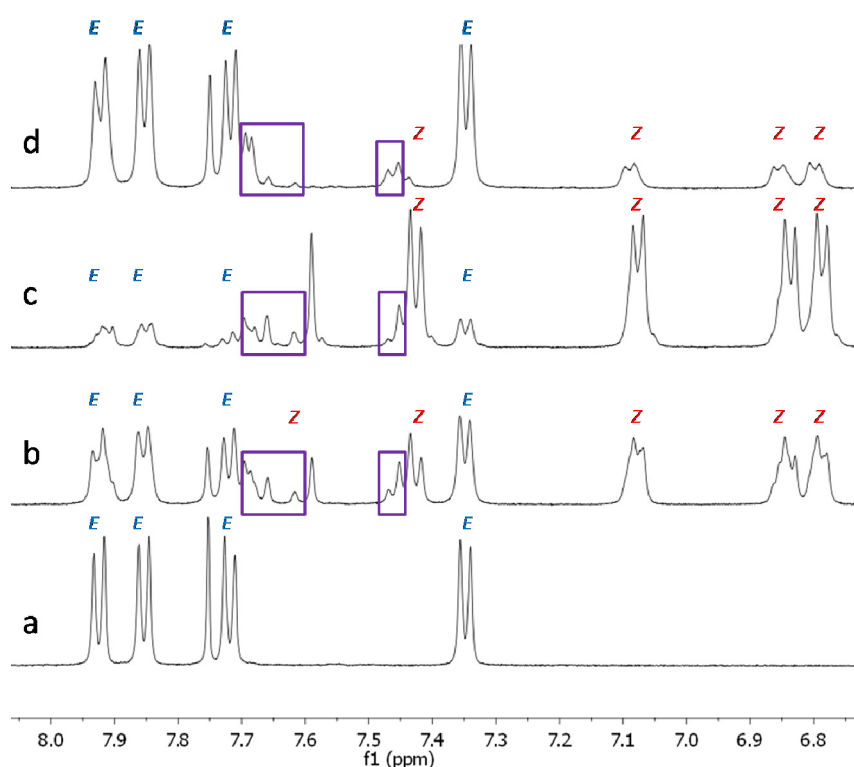
Figure 6. An expansion of the aromatic region of spectra depicted in Fig 3.

The spectrum of *E,E,E*–**1** is shown in Fig 6a; four doublets represent four different protons of the *E*–azobenzene group and a singlet represents the proton of the central benzene ring in the molecule. At the photostationary state (Fig 6c), where 75 % of the azobenzene groups are *Z*–configured, a new set of doublets is present; these correspond to the four different protons of the *Z*–azobenzene group. The singlet of the central benzene ring has now shifted from 7.75 ppm to 7.59 ppm.

It seems reasonable to assume that the chemical shift of that singlet will depend on the number of *Z*–azobenzene groups surrounding the proton in question. Due to the overlap with other peaks, however, the integration is unreliable in determining how many protons correspond to the singlet peak. It is therefore not possible to say if the dominant species at the PSS contains two or three *Z*–azobenzene groups. It is also worth noting that the other PSS, containing only 30 % of the *Z*–azobenzene groups, Fig 6d) no longer contains the species with the singlet at 7.59 ppm. Furthermore, there are more singlet signals in the spectrum present in lower intensities (highlighted in purple frames in Fig 6) revealing the presence of multiple species in the mixture despite the appearance of a dominant species. This seems to indicate that upon irradiation a mixture of all possible isomers of **1** is formed and not a mixture of only the all–*E* and all–*Z* isomers of **1**.

As concluded above, upon irradiation of **1**, a mixture of isomers of **1** is formed at the photostationary state. With the exception of the singlet peak corresponding to the proton of the central benzene ring of **1**, only one set of peaks in the ^{1}H–NMR is obtained for the *E*–azobenzene group and only one set for the *Z*–azobenzene group regardless which isomers are present in the equilibrium mixture and at which quantities. In other words, any *E*–azobenzene group will always be characterized by the same set of ^{1}H–NMR peaks and any *Z*–azobenzene group will always be characterized by the same (but different than for the *E*–azobenzene group) set of ^{1}H–NMR peaks regardless of how many other *E*– or *Z*–azobenzene groups are present in the molecule. This finding demonstrates that the three switching groups in a molecule do not "feel" one another. Furthermore, the observation that a mixture of isomers is obtained upon irradiation suggests that the three azobenzene groups in the same molecule switch independently of one another. These conclusions are also supported by the UV−Vis spectroscopic study of the switching phenomenon of **1** which shows the same switching pattern in the spectrum as a typical monoazobenzene molecule[7] (positions of absorption bands and isosbestic points, Fig 2). This behaviour has also been reported for some azobenzene-containing dendrimers[25].

Kinetics of the thermal isomerization

As already mentioned before, the *Z*–isomer may be isomerized to the *E*–isomer photochemically (irradiation with either UV light at 312 nm or visible light) or thermally. The driving force for the latter process comes from the relative instability of the *Z*–isomer[7,47]; if kept in the absence of light the less stable *Z*–isomer will spontaneously isomerize to the more stable *E*–isomer. The rate at which it undergoes the thermal process depends on the temperature but is always much slower than the photochemical isomerizations[7]. In order to gain more insight into the behavior of **1**, we opted to follow the kinetics of the thermal isomerization step. Temperature dependent UV−Vis spectroscopy was used to follow the process in time (Fig 7).
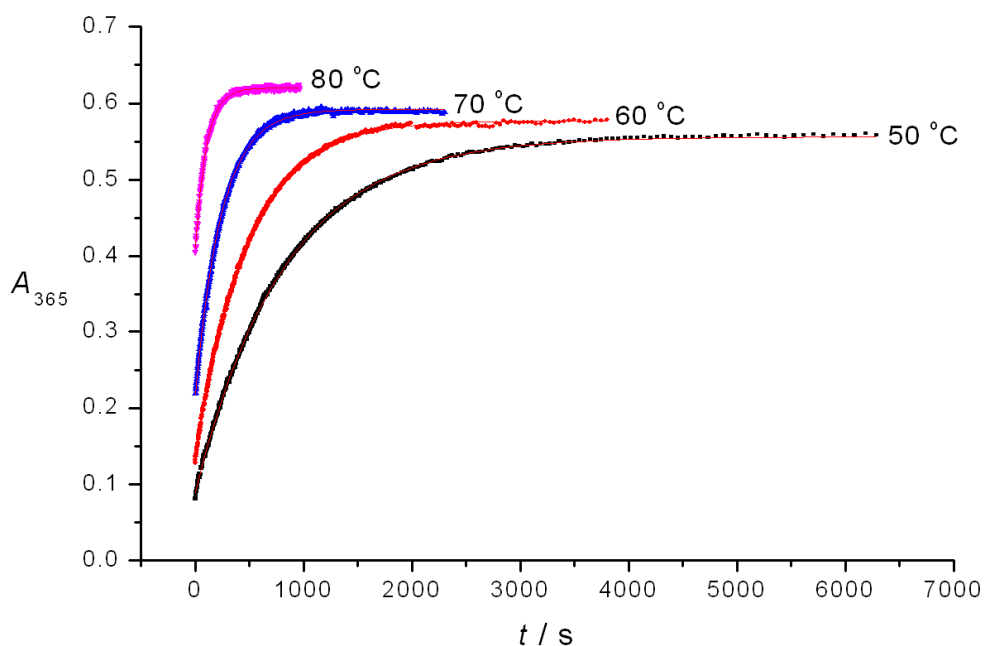
Figure 7. The data points collected by following the absorbance at 365 nm of a sample of **1** over time at different temperatures, c = 1.1·10^{-5} mol dm^{-3} in *n*-heptane, and the calculated values (–) as obtained by nonlinear regression analyses.

A sample of a solution of **1** in *n*-heptane was irradiated with light at 365 nm to the photostationary state and the absorbance was followed at maximum absorption (λ_{max} = 365 nm) over time in the temperature range 50–80 °C. The collected data were fitted to the exponential function assuming first-order kinetics for the thermal step[50]. The collected data as well the fits are shown in Fig 7 and the parameters from the fits are given in Table 1. Good fits to the monoexponential function, like the ones shown in Fig 7 and described in Table 1, suggest that all the *Z*–azobenzene groups in **1** exhibit the same kinetics in the process of isomerization regardless of the configuration of the adjacent azobenzene units in the molecule indicating independent switching behaviour of the azobenzene switching units.

Table 1. The half-lives, $t_{1/2}$, at different temperatures as obtained from the regression analyses of the data in Fig 7.

Θ / °C	$t_{1/2}$ / min	R^2
50	9.5	0.99969
60	5.5	0.99978
70	2.8	0.99938
80	1.2	0.99761

From Table 1 it can be seen that the half-life for the thermal isomerization, $t_{1/2}$, ranges from 9.5 min at 50 °C to 1.2 min at 80 °C.

The data from Table 1 can be analyzed according to the Eyring equation to obtain the activation parameters, $\Delta^{\ddagger}H$ and $\Delta^{\ddagger}S$ (Fig 8).
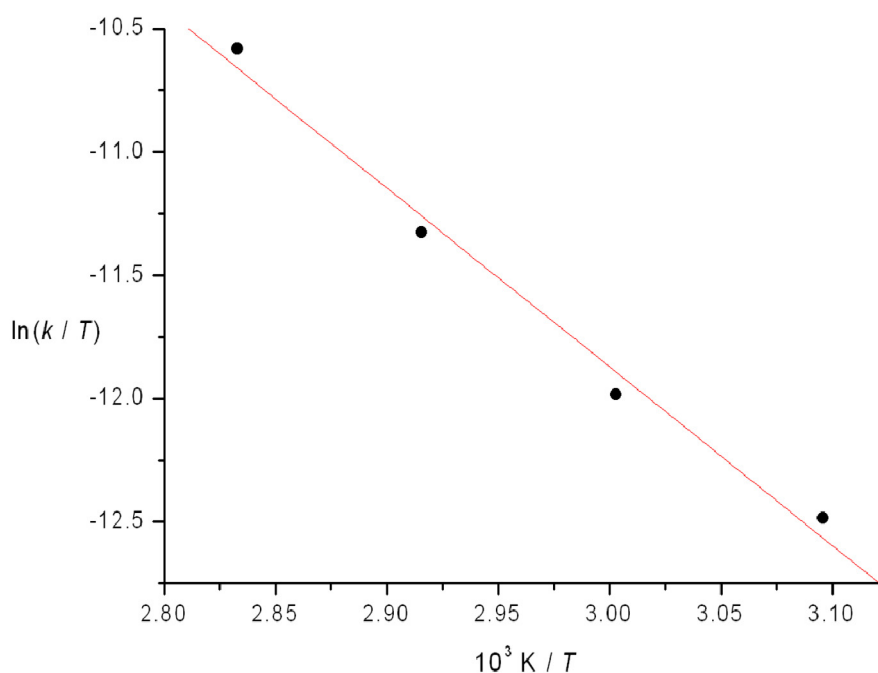
Figure 8. The data points from Table 1 analyzed according to the Eyring equation and the calculated values (–) as obtained by linear regression analysis.

From the analysis in Fig 8 the following activation parameters were obtained: $\Delta^{\ddagger}H$ = (60 ± 5) kJ mol^{-1}, $\Delta^{\ddagger}S$ = (−115 ± 14) J K^{-1} mol^{-1}. Previously reported values for

these parameters for different azobenzene systems are roughly in the range 35 − 100 kJ mol^{-1} and −200 − 50 J K^{-1} mol^{-1}, respectively, depending on the exact structure of the azobenzene compounds as well as the solvent used during the measurements[51,52,53,54]. Our values for **1** are well within that range. The activation parameters allow for the calculation of the half-life for the thermal isomerization in *n*-heptane, at 25 °C, $t_{1/2}$ = 70 min. Furthermore, these parameters can give some information about the mechanism of the thermal isomerization but this will be discussed at a later stage.

Tetrakisazobenzene 2

UV−Vis spectroscopic study

Photochemical properties of switch **2** were examined in solution (*n*-heptane) by means of UV−Vis spectroscopy, as shown in Fig 9. The UV−Vis spectrum of **2** shows a strong absorption band with λ_{max} = 360 nm. Upon irradiation of the sample with light at λ = 365 nm, the band drops in intensity and two new bands appear simultaneously, one with λ_{max} = 327 nm and another with λ_{max} = 446 nm. Subsequent irradiation with light at λ = 312 nm or λ > 420 nm, or an increase in temperature will cause the newly formed bands to disappear again and the original band with λ_{max} = 360 nm to reappear in its original intensity. Compound **2** appears to behave the same way as compound **1** and such behaviour is typical of azobenzene compounds[7,47].
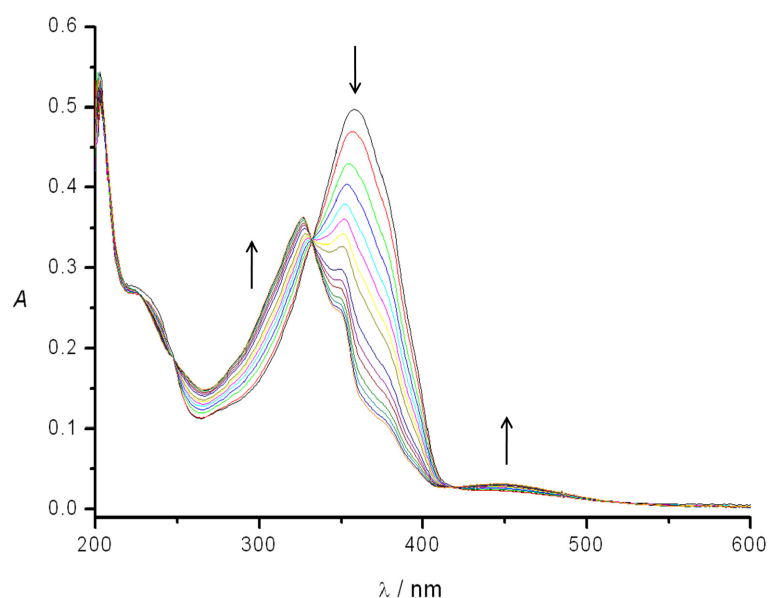
Figure 9. UV−Vis spectra of switch **2**, c = 5.0·10^{-6} mol dm^{-3}; in *n*-heptane, at −10 °C. Irradiation with light at 365 nm, 312 nm and > 420 nm.

Just like with compound **1**, irradiation of the sample of **2** kept in the dark (*E*−isomer) with light at 365 nm establishes a photoequilibrium between the

E–isomer and the *Z*–isomer of the azobenzene, Scheme 1. The change in the composition of the solute (the ratio of the *E*– and *Z*–isomer) is reflected in the UV–Vis spectrum of the solution; the spectrum changes during irradiation until a photoequilibrium has been reached. Irradiation with light at λ = 312 nm or λ > 420 nm causes a new photoequilibrium to be established which is again reflected in the UV–Vis spectra of the solution. The spectrum taken at photoequilibrium appears identical to the one of the *E*–isomer so it can be concluded that the photostationary state (at λ = 312 nm or λ > 420 nm) consists predominately of the more stable *E*–isomer. This seems reasonable since it is the *Z*–isomer that absorbs to a greater extent at those wavelengths.

After the photostationary state has been reached by irradiation of the *E*–isomer with light at 365 nm, the change can also be reversed thermally *i.e.* by warming up the sample. The spectrum of the pure *E*–isomer will once again be recovered as the less stable *Z*–isomer thermally converts to the more stable *E*–isomer[7,47], Scheme 1. The kinetics of the thermal isomerization step will be discussed later.

^{1}H–NMR spectroscopic study

The switching behaviour of molecule **2** was also studied in $CDCl_3$ by means of ^{1}H–NMR spectroscopy (Fig 10). Irradiation of the solution containing only the *E*–isomer of **2** with light at 365 nm was accompanied by the appearance of new signals in both the aromatic as well as in the aliphatic region of the spectrum (Fig 10b,c). Irradiation was continued until no further changes could be observed in the spectrum. The photostationary state had been reached at that point and the solute contained 72 % of the newly formed species. Irradiation of the sample at the photostationary state with light at 312 nm resulted in the decrease in the intensity of the new signals (Fig 10d). Even after prolonged irradiation, however, the new peaks did not disappear completely and the original spectrum (of the *E*–isomer) could not be fully restored indicative of a photostationary state that still contains some *Z*–isomer. If a sample containing both *E*– and *Z*–isomer was left in the absence of light at room temperature overnight or at 40 °C for 90 min, it was completely depleted of the *Z*–isomer, Fig 10e.
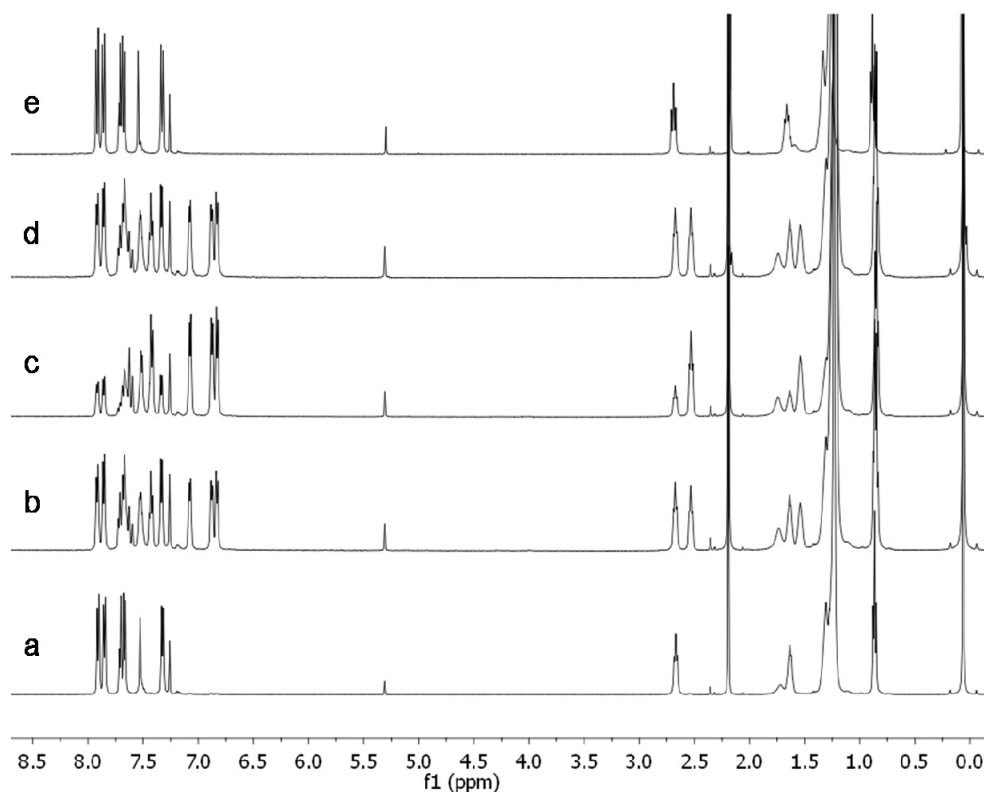
Figure 10. ^{1}H–NMR spectra of switch **2**, in CDCl$_3$, at –10 °C (irradiation was performed at 4 °C); **a:** in the dark, **b:** sample from **a** irradiated at 365 nm for 0.5 h, **c:** sample from **a** irradiated at 365 nm for 1:15 h, **d:** sample from **c** irradiated at 312 nm for 15 min, **e:** sample from **d** left in the dark at room temperature overnight.

It should be noted that the NMR experiments were performed in CDCl$_3$ whereas the UV–Vis experiments were conducted in *n*-heptane. Additional differences between the two spectroscopic investigations as well as the consequences these may have on the results are discussed in the section of this chapter that deals with the spectroscopic investigation of molecule **1** (*vide supra*). Similar to what was found for molecule **1**, the NMR study of molecule **2** revealed a total of 72 % of the azobenzene groups in the *Z*–configuration at the photostationary state reached by irradiation of the sample with light at 365 nm. The NMR study seems to suggests that a large part of the azobenzene switches goes from the *E*– to the *Z*–configuration upon irradiation with light at 365 nm (until the photostationary state is reached) and the UV–Vis experiments seem to be in accordance with that finding as the most intense band (λ_{max} = 360 nm) of the *E*–isomer almost entirely disappears at the photostationary state. The equilibrium between the differently configured isomers may again be shifted to the *E*–isomer either photochemically or thermally as evidenced by both UV–Vis and NMR experiments.

A total of 72 % of the *Z*–configured azobenzene units in **2** and 75 % in **1** at the photostationary state (with the experimental uncertainty around 5 %) upon irradiation with light at 365 nm is a very good photochemical property as azobenzene derivatives containing oligo(phenylene ethynylene)s (OPEs) have been

reported to have much poorer photostationary states; the higher the number of OPEs the lower the photoconversion at the photostationary state[33]. The main difference between molecules **1** and **2** and the ones reported is that **1** and **2** are multiazobenzene compounds whereas the reported ones contain a single azobenzene group.

The change in the aliphatic region of the NMR spectrum of **2** upon irradiation with light at 365 nm is shown in Fig 11.
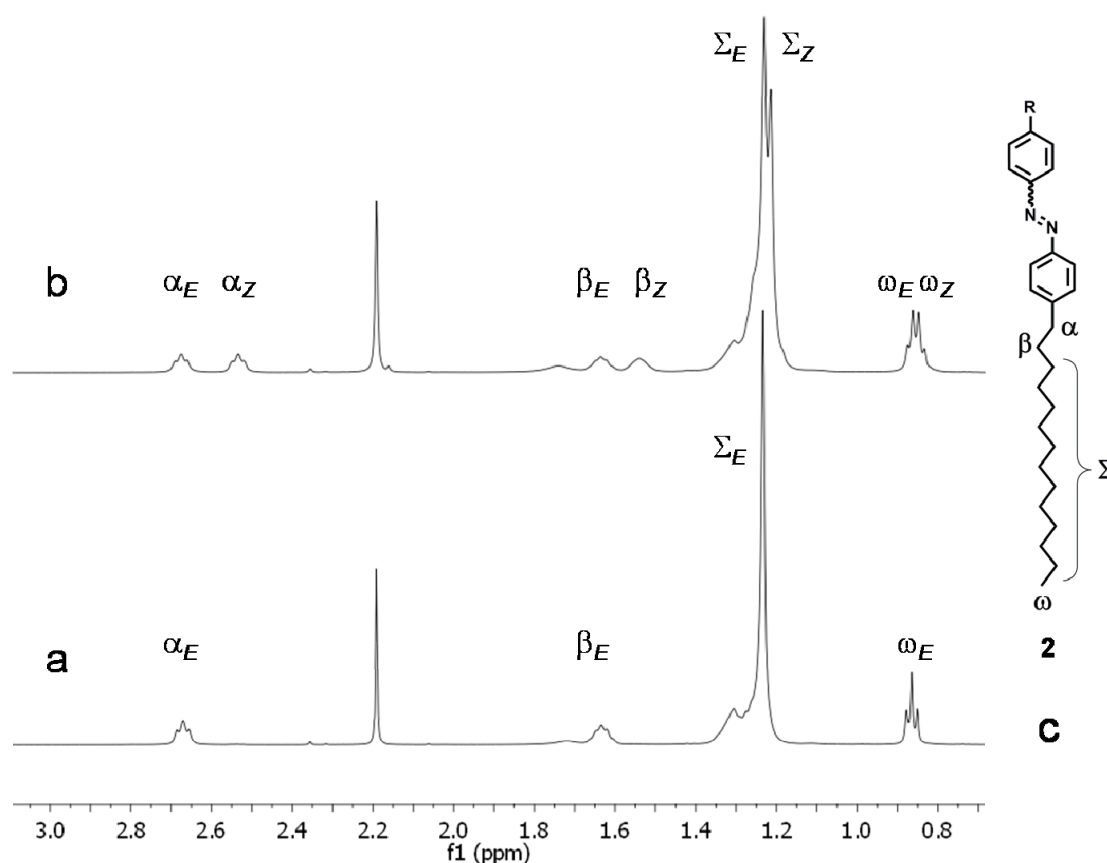
Figure 11. The aliphatic region of ^{1}H–NMR spectra of switch **2**, in CDCl$_3$, at –10 °C; **a:** in the dark, **b:** sample from **a** irradiated at 365 nm till approximately 50 % photoconversion, **c:** the structure of an azobenzene unit of **2** with the aliphatic protons of interest highlighted.

The signal appearing at δ = 2.67 ppm in Fig 11a,c corresponds to the protons of the methylene group adjacent (in the α–position) to the phenyl ring of the *E*–azobenzene group of **2**; these protons are denoted α_E. The protons of the methylene group adjacent to the α–protons are denoted β_E and appear at δ = 1.62 ppm. The remaining methylene groups of the alkyl chain are rather indistinguishable and appear as a broad signal in the range δ = 1.37–1.17 ppm; they are denoted Σ_E, Fig 11a,c. The terminal methyl group with its ω_E protons appears at δ = 0.86 ppm.

Once irradiated, compound **2** undergoes a change that may be followed by the appearance of new peaks in the NMR spectrum. Much like in the case of **1** and

typical of azobenzene behaviour[7] for each signal from the original NMR spectrum a new signal appears (α_Z, β_Z, Σ_Z, ω_Z) at a lower chemical shift (Fig 11b). As explained for **1** earlier, the appearance of a new set of NMR peaks for protons in close vicinity of the azobenzene group undergoing switching upon irradiation seems more intuitive than for the protons further away from the azobenzene group. The finding that the switching of azobenzene units affects even the remotest protons in the alkyl chains seems to suggest an interaction of some sort between the alkyl chains. As proposed for **1** (*vide supra*), the alkyl chains of **2** could also interact with one another in an intramolecular or intermolecular manner rendering themselves sensitive to any change in the molecular geometry which would in turn alter the interactions between the chains and therefore the chemical shifts of all the protons present in the chain as well. A simple model showing a possibility of an intramolecular and intermolecular interaction between the alkyl chains if proposed in Fig 12. In an all–*E* molecule of **2** (Fig 12a) the adjacent alkyl chains are not within each other's reach to form intramolecular van der Waals interactions so the chains may only interact with the conjugated system of the molecule (phenyl rings, N=N groups). Switching the azobenzene units to the *Z*–state, however, brings the adjacent alkyl chains close enough to engage in intramolecular van der Waals interactions (Fig 12a). The two different environments of the alkyl chains could explain the different chemical shifts for all the aliphatic protons as observed in the NMR spectra upon irradiation. Fig 12b shows a possible intermolecular interaction between the molecules of **2** through van der Waals interactions between the alkyl chains. Switching the configuration of the azobenzene units upon irradiation would undoubtedly also change the distances and interactions between the chains and therefore also the chemical shifts in the NMR spectra. The aggregation through intermolecular interactions is entropically more favourable and therefore also more likely than the occurrence of intramolecular interactions. Such an aggregation phenomenon of **2** would however be expected to be concentration dependent. A systematic dilution experiment should therefore be conducted to check for the concentration dependence of the spectra at the photostationary state. This might reveal whether the origin of the different chemical shifts (upon irradiation) for all the aliphatic protons in **2** is of intramolecular or intermolecular origin.

a

b
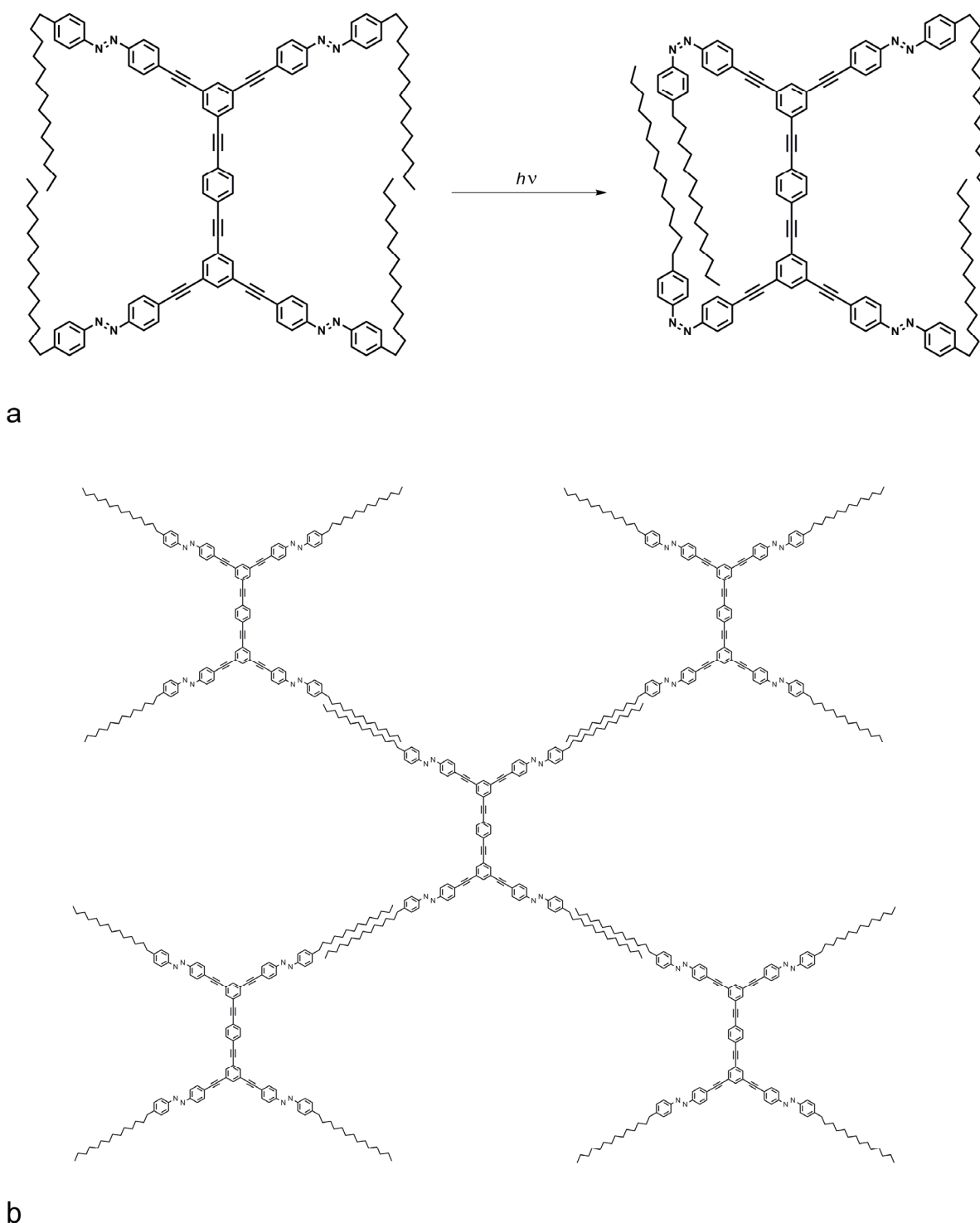
Figure 12. A model by which the alkyl chains of **2** could come into interaction with each other
a: intramolecularly, **b:** intermolecularly.

Similar to what was discussed for **1** earlier, the photostationary state of **2**, after irradiation with light at 365 nm, contains about 72 % of the *Z*–configured azobenzene groups as evidenced by NMR. Since a molecule of **2** contains a total of four equivalent azobenzene groups, the question of the distribution of *E*– and *Z*–configured azobenzene groups arises. Is there 72 % of the molecules that have all four azobenzene groups *Z*–configured and 28 % of the all–*E*–molecules or is

there a mixture of (*E,E,E,E*), (*E,E,E,Z*), (*E,E,Z,Z*), (*E,Z,Z,Z*) and (*Z,Z,Z,Z*) molecules with a total of 72 % of all the azobenzene groups *Z*–configured and 28 % *E*–configured? The aromatic region of the ^{1}H–NMR spectrum of **2** (Fig 10), is more complicated than that of **1** (Fig 6), due to the presence of a total of three singlet peaks (at 7.53, 7.70 and 7.71 ppm) corresponding to the non-azobenzene aromatic protons in **2** as opposed to only one (at 7.75 ppm) in **1**. The spectrum becomes even more complicated once all the new peaks appear upon irradiation with light at 365 nm (Fig 10). As a result thereof it is impossible to assign all the (overlapping) peaks in the spectrum and therefore also understand which species are present in the mixture at a certain degree of photoconversion. From the sheer complexity of the spectra, however, it seems like there are more than two species present in the mixture at any given moment (after irradiation). This would indicate that upon irradiation a mixture of all possible isomers of **2** is formed and not a mixture of all–*E* and all–*Z* isomers of **2** which is in agreement with our findings for **1**.

As was the case with **1**, the four switching groups in a molecule of **2** do not "feel" one another in the sense that they switch independently of one another and they always exhibit the same NMR pattern (either the *E*–pattern or the *Z*–pattern) regardless of the configuration of the other azobenzene groups present in the molecule. These conclusions are also supported by the UV–Vis spectroscopic study of the switching phenomenon of **2** which shows the same switching pattern in the spectrum as a typical monoazobenzene molecule[7] (Fig 9). This conclusion is in accord with a computational result for a similar four-legged molecule, "the molecular arachnoid" that predicts the four legs to behave as independent units[26].

Kinetics of the thermal isomerization

As already observed by both UV–Vis and NMR spectroscopic techniques, the *Z*–isomer may be isomerized to the *E*–isomer photochemically (irradiation with either UV light at 312 nm or visible light) or thermally. The thermal step is driven by the relative instability of the *Z*–isomer[7,47]. This means that, if kept in the absence of light, the less stable *Z*–isomer will spontaneously isomerize to the more stable *E*–isomer with the rate of the process depending on temperature[7]. Temperature dependent UV–Vis spectroscopy was used to follow the kinetics of the *Z* to *E* thermal isomerization process in **2** (Fig 13).
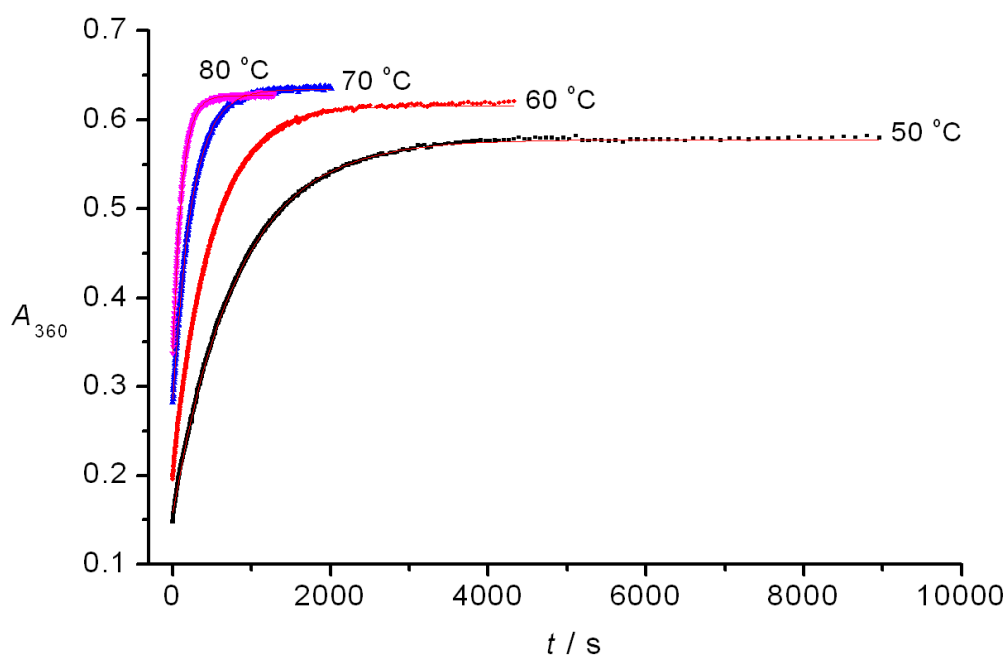
Figure 13. The data points collected by following the absorbance at 360 nm of a sample of **2** over time at different temperatures, c = $5.0 \cdot 10^{-6}$ mol dm^{-3} in *n*-heptane, and the calculated values ($-$) as obtained by nonlinear regression analyses.

A sample of a solution of **2** in *n*-heptane was irradiated with light at 365 nm to the photostationary state and the absorbance was followed at maximum absorption (λ_{max} = 360 nm) over time in the temperature range 50–80 °C. The collected data were fitted to the exponential function assuming first-order kinetics for the thermal step[50]. The collected data as well the fits are shown in Fig 13 and the parameters from the fits are given in Table 2. Good fits to the monoexponential function, like the ones shown in Fig 13 and described in Table 2, suggest that all the *Z*–azobenzene groups in **2** exhibit the same kinetics in the process of isomerization regardless of the configuration of the adjacent azobenzene units in the molecule. As in the case of **1**, this suggests independent switching behaviour of the azobenzene switching units in **2**.

Table 2. The half-lives, $t_{1/2}$, at different temperatures as obtained from the regression analyses of the data in Fig 13.

Θ / °C	$t_{1/2}$ / min	R^2
50	9.4	0.99980
60	5.6	0.99985
70	2.8	0.99974
80	1.3	0.99940

From Table 2 it can be seen that the half-life for the thermal isomerization, $t_{1/2}$, ranges from 9.4 min at 50 °C to 1.3 min at 80 °C which seems to agree with the values obtained for **1**.

The data from Table 2 can be analyzed according to the Eyring equation to obtain the activation parameters, $\Delta^{\ddagger}H$ and $\Delta^{\ddagger}S$ (Fig 14).
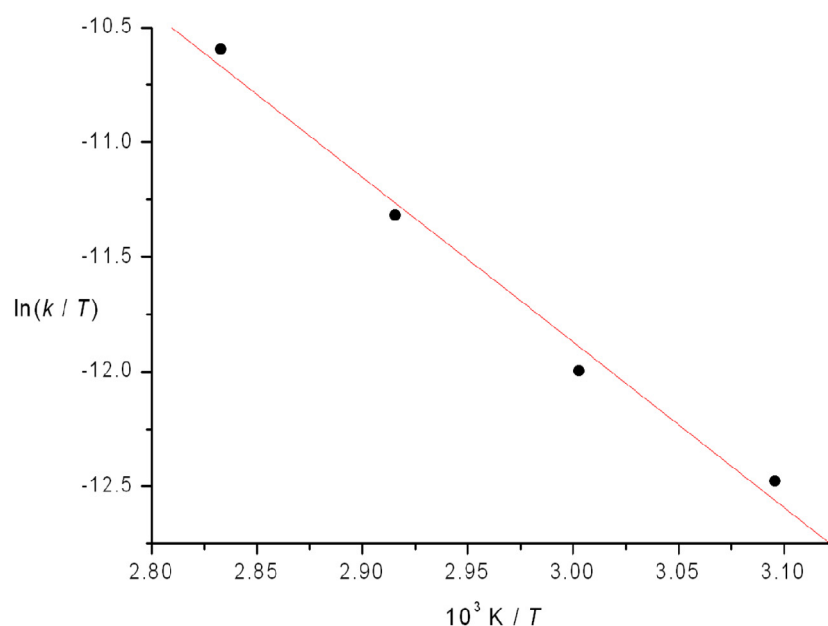
Figure 14. The data points from Table 2 analyzed according to the Eyring equation and the calculated values (–) as obtained by linear regression analysis.

From the analysis in Fig 14 the following activation parameters were obtained: $\Delta^{\ddagger}H = (60 \pm 5)$ kJ mol^{-1}, $\Delta^{\ddagger}S = (-117 \pm 15)$ J K^{-1} mol^{-1}. Previously reported values for these parameters for different azobenzene systems are roughly in the range 35 – 100 kJ mol^{-1} and $-200 - 50$ J K^{-1} mol^{-1}, respectively, depending on the exact

structure of the azobenzene compounds as well as the solvent used during the measurements[51,52,53,54]. Our values for **2** are well within that range and they agree very well with the values obtained for **1**. The activation parameters allow for the calculation of the half-life for the thermal isomerization at 25 °C, $t_{1/2}$ = 72 min. Furthermore, these parameters can give some information about the mechanism of the thermal isomerization and this will be discussed in the next section.

The fact that the half-lives measured in the temperature range 50–80 °C as well as the Eyring activation parameters for **1** and **2** agree very well is further evidence that the azobenzene groups in **1** and **2** act independently. It seems as though we actually measured the kinetics of the azobenzene unit of molecules **1** and **2** (Fig 4c, 11c) irrespective of the structure of the molecule as a whole. This has also been observed for some azobenzene-containing dendrimers[25].

Proposed mechanism of the thermal isomerization

The photoisomerization and the thermal isomerization of azobenzenes are thought to proceed via one of the two mechanisms; the rotation mechanism or the inversion mechanism[7,55]. As depicted in Fig 15, the former mechanism involves rotation about the N–N bond weakened by electronic excitation whereas the latter one involves a rehybridization of the N–atom from an sp^2 state to an sp^1 state with only minor change in the azo π bond order.
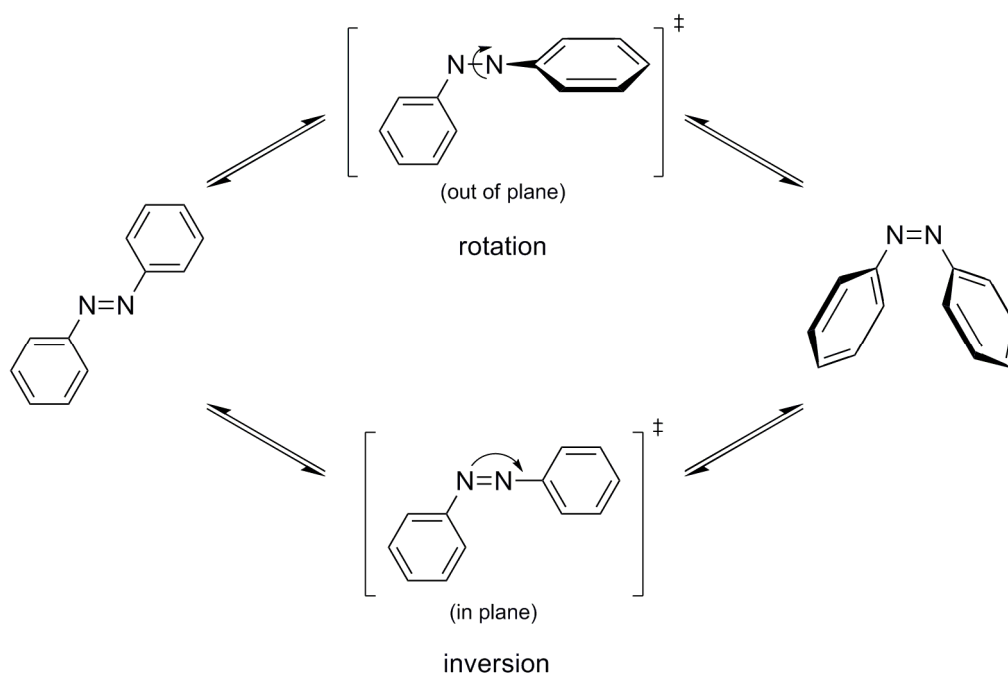
Figure 15. Two mechanisms for the isomerization of azobenzene; rotation and inversion.

Since the photoisomerization process is extremely rapid it can only be followed experimentally by ultrafast spectroscopic techniques or studied computationally[56].

The thermal isomerization is most often much slower and therefore also easier to study[7,57]. The mechanisms of the thermal isomerization of a series of azobenzenes in various solvents have been studied and a compensation relationship between $\Delta^{\ddagger}H$ and $\Delta^{\ddagger}S$ has been established, such that a plot of $\Delta^{\ddagger}H$ versus $\Delta^{\ddagger}S$ is linear[52,57], as shown in Fig 16. All the azobenzenes undergoing the thermal isomerization via the inversion mechanism gave collinear data points in such a plot. The azobenzene compounds undergoing the thermal isomerization via the rotation mechanism, however, gave data points that exhibited collinearity within their own series but were not collinear with the data points from the former series of azobenzenes. These isokinetic plots are therefore used to distinguish between the two mechanisms of the thermal isomerization of novel azobenzenes or of the existing ones in new solvents[57,58].

For most azobenzene compounds the thermal *Z*–to–*E* isomerization proceeds via the inversion mechanism[58]. Push-pull substituted azobenzenes, however, undergo this reaction via the rotational pathway. Azobenzenes with a *p*–NO_2 group can isomerize via both mechanisms, depending on the solvent[52,57].

The plot shown in Fig 16 is taken from the literature[57]; the data points used to make the plots are simple azobenzene compounds studied previously[52,57,58]. As can be seen from the plot, some data points deviate significantly from the linearity predicted by the model; the data points found between the two lines are assumed to indicate an intermediate mechanism having both the rotation- and inversion-character.
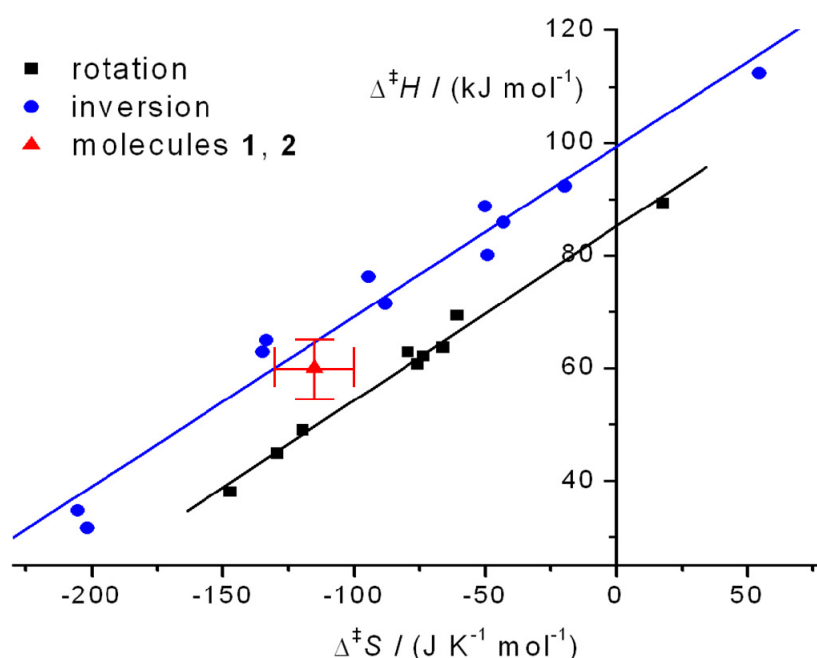
Figure 16. Isokinetic plots for the thermal isomerization of azobenzene derivatives; the data points used to make the plots are given and further referenced in the study by Wazzan[57]. The data point obtained for compounds **1** and **2** is highlighted in red.

As can be seen from Fig 16, the data point describing the azobenzene compounds **1** and **2** studied here (data point given in red; only one data point is given since the values obtained for **1** and **2** are virtually the same) is found between the two lines. With the uncertainty of the measurements, it is impossible to determine its exact position in the plot. The data point is however located closer to the straight line fitted to the points corresponding to azobenzene compounds that follow the inversion pathway during the thermal isomerization step (it is collinear with the other data points with R^2 = 0.9643). This indicates a mechanism between the rotation and inversion mechanisms but probably with higher inversion-character than rotation. The data point from Fig 16 should however be determined more accurately to draw any further conclusions.

The mechanism of isomerization may prove to be of upmost importance for the development of azobenzene-equipped molecules for propulsion on a surface. If the photoinduced *E*–to–*Z* isomerization of an azobenzene group proceeds via a rotation pathway while the thermal *Z*–to–*E* isomerization follows an inversion pathway[59], the combination of the two processes may lead to the switching motion accompanied by translational motion. This could provide the driving force for the movement of such molecules on a surface[22]. Care should be taken, however, in designing molecules for surface-related purposes as molecular properties may prove to be quite different on a surface than in solution; it has already been shown for azobenzene compounds that the activation parameters have different values on surfaces than in solution[20,60]. It remains a question, however, if isomerization processes will follow the same mechanism on a surface as in solution[61]. Studying the kinetics of the thermal isomerization of **1** and **2** on a surface might therefore prove rather insightful.

*Preliminary surface studies of molecules **1** and **2***

Molecules **1** and **2** were separately dissolved in 1-phenyloctane (*c* = 1 mmol dm^{-3}) and the solutions were dropcast onto freshly cleaved HOPG surface. The solid/liquid interface was examined by scanning tunneling microscopy (STM) in the dark. The HOPG surface could be observed with atomic resolution, as shown in Fig 17. Molecules of **1** or **2** could, however, not be observed under the conditions used. Further surface studies at the solid-liquid interface are ongoing as well as investigation of single molecules under ultrahigh vacuum conditions.
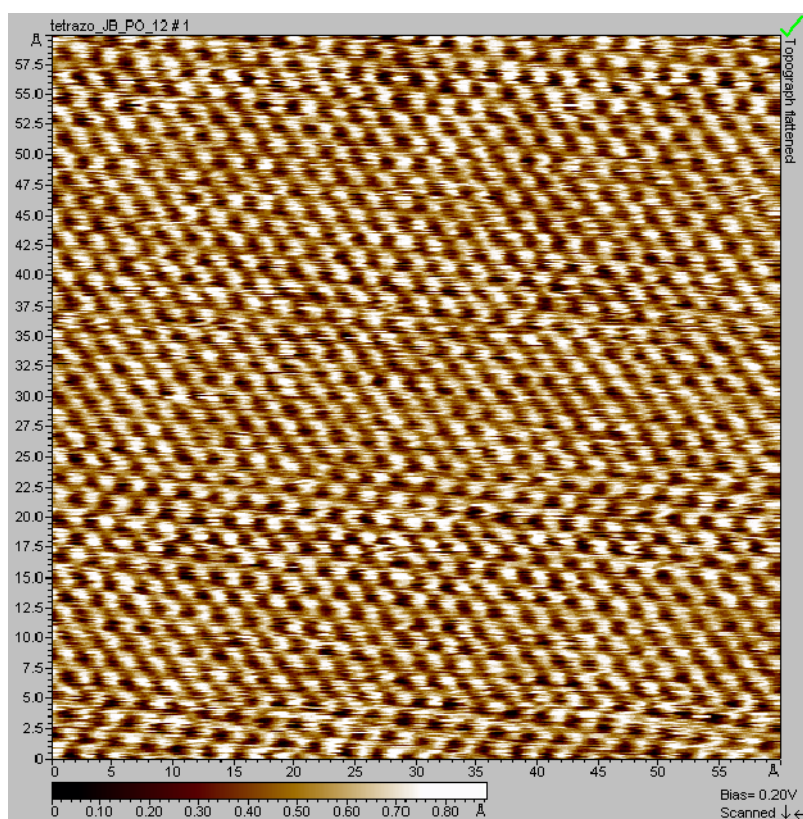
Figure 17. A typical STM image recorded during the investigation of the solid/liquid interface after dropcasting a solution of molecules of **1** in 1-phenyloctane (c = 1 mmol dm^{-3}) on the HOPG surface. Imaging conditions for the resolution of graphite lattice: 0.1 nA, 0.2 V, 6 x 6 nm.

Conclusions

With the goal of studying molecules with multiple switching groups on surfaces, two new molecules have successfully been designed, synthesized and characterized; molecule **1** bearing three azobenzene switching units and molecule **2** bearing four of them. Due to their high symmetry the molecules were prepared through a convergent synthetic route. The photochemical properties of both **1** and **2** were extensively studied in solution by UV−Vis and NMR spectroscopic techniques. They exhibit typical azobenzene switching behaviour; the azobenzene group may be photoisomerized between the $E-$ and $Z-$isomeric forms and the $Z-$azobenzene group may also be thermally isomerized to the more stable $E-$isomer. For both molecules **1** and **2** up to about 75 % of the $Z-$isomer can be obtained by irradiation. The kinetics of the thermal isomerization process were studied at different temperatures and the half-life of 70 min at room temperature was determined for the process for both molecules. The activation parameters were also obtained from the kinetic study but, due to the uncertainty of the measurements, they did not reveal the dominant mechanism for the thermal isomerization process.

It is worth noting that molecules **1** and **2** act in the same way with respect to their photochemical properties. The kinetic parameters obtained for the two

molecules are also in excellent agreement with each other. It appears that every azobenzene group switches independently of the rest of the molecule.

There is evidence however that the long alkyl chains of **1** (and those of **2** just as well) interact with one another. The nature of this interaction is not clear at this point but it might indicate an aggregation phenomenon. This possible tendency towards aggregation might favour the formation of self-assembled monolayers at the solid-liquid interface. Furthermore, the photostationary state is quite rich in the *Z*–isomer which would be beneficial for the study of the switching process on a surface. The half-life of 70 min (at room temperature) for the thermal isomerization would allow enough time to observe the *Z*–configured groups on the surface and would not be too long to observe the thermal isomerization to the *E*–isomer either. All these properties combined make molecules **1** and **2** very good candidates for surface switching studies.

Preliminary surface studies on molecules **1** and **2** were conducted at the solid-liquid interface but no molecules have been observed up to now. Further investigations are ongoing.

Acknowledgements

Experimental section

Synthesis, characterization and physico–chemical measurements

General remarks

Chemicals were purchased from Sigma–Aldrich and used as received, solvents were reagent grade, distilled and dried before use according to standard procedures. For physicochemical measurements Uvasol-grade solvents from Merck were used. Reactions were performed under nitrogen atmosphere unless specified otherwise. Analytical TLC was performed with Merck silica gel 60 F254 plates and visualization was accomplished by UV light. Column chromatography was performed on silica gel (Aldrich 60, 230–400 mesh). ^{1}H–NMR spectra were recorded on a Varian AMX-500 (500 MHz), a Varian AMX400 (400 MHz) or a Varian AMX300 (300 MHz). ^{13}C–NMR spectra were recorded on a Varian AMX-500 (125 MHz), a Varian AMX400 (100 MHz) or a Varian AMX300 (75 MHz). Chemical shifts are denoted in δ–unit (ppm) relative to CDCl$_3$ (for ^{1}H detection δ = 7.26 ppm, for ^{13}C detection δ = 77.16 ppm), CD$_2$Cl$_2$ (for ^{1}H detection δ = 5.32 ppm, for ^{13}C detection

δ = 53.50 ppm), DMSO-d_6 (for ^{1}H detection δ = 2.50 ppm), toluene-d_8 (for ^{1}H detection δ = 2.09 ppm) or CD$_3$OD (for ^{1}H detection δ = 4.87ppm, for ^{13}C detection δ = 49.00 ppm). For ^{1}H–NMR spectroscopy the splitting pattern of peaks is designated as follows: s (singlet), d (doublet), t (triplet), q (quartet), m (multiplet), br (broad), dd (doublet of doublets). HRMS spectra were obtained on LTQ Orbitrap XL mass spectrometer (Thermo Fisher Scientific) with ESI, APCI or APPI ionization. MALDI–TOF spectra were recorded on a 4800 Proteomics Analyzer MALDI–TOF/TOF instrument (Applied Biosystems) in the *m/z* range 400–5000. Data acquisition was performed in positive ion mode. The samples were dissolved in THF (γ = 1 mg cm^{-3}) and mixed in 1:1 (v:v) ratio with a solution of the MALDI–TOF matrix (2,5-dihydroxybenzoic acid, *c* = 0.2 mol dm^{-3} in THF). Melting points were taken on a Büchi Melting Point B–545 apparatus. UV–Vis measurements were performed using a Hewlett-Packard HP 8453 FT spectrophotometer. Samples were measured in a quartz cuvette of 1 cm path length. Irradiation experiments with UV light were performed using a Spectroline model ENB-280C/FE lamp with λ = (312 ± 30) nm and λ = (365 ± 30) nm. Irradiation experiments with visible light were performed using a Thor Labs OSL1-EC Fiber Illuminator fitted with suitable cut-off filters. In irradiation experiments where the process was followed by NMR, the sample was irradiated in an NMR tube at 4 °C. STM measurements were conducted on a PicoSPM instrument (Molecular imaging, Scientec). The STM tips were mechanically cut from Pt/Ir wire (80:20, diameter 0.25 mm, Goodfellow). Prior to STM imaging, the sample was dissolved in 1-phenyloctane (*c* = 1 mmol dm^{-3}) and the solution was dropcast onto freshly cleaved HOPG surface, then the STM tip was immersed into the solution.

1-nitroso-4-tetradecylbenzene 4: A solution of 4-tetradecylaniline **3** (2.58 g, 8.9 mmol) in dichloromethane (75 ml) was mixed with an aqueous solution of oxone (2 KHSO$_5$ · KHSO$_4$ · K$_2$SO$_4$) (17.2 g, 28 mmol in 75 ml of distilled water) at room temperature and under a nitrogen atmosphere. The reaction mixture was stirred vigorously overnight. The layers were separated and the aqueous layer was extracted with dichloromethane (75 ml). The combined organic layers were washed with hydrochloric acid (aq, *c* = 1 mol dm^{-3}, 50 ml), saturated aqueous NaHCO$_3$ solution (50 ml) followed by washing with a saturated aqueous NaCl solution (50 ml). The organic layer was dried on anhydrous MgSO$_4$, the salt was removed by filtration and the solvent was evaporated. The crude product was purified by column chromatography with petroleum ether 40–60 / dichloromethane 3:1 as eluent. Upon evaporation of the solvent the product was stored at −18 °C which afforded pale yellow crystals (0.90 g) in 33 % yield.

^{1}H NMR (500 MHz, CDCl$_3$): δ 7.82 (d, *J* = 8.3 Hz, 2H), 7.39 (d, *J* = 8.5 Hz, 2H), 2.69 (t, *J* = 7.6 Hz, 2H), 1.66 (m, 2H), 1.44–1.15 (br, 22H), 0.88 (t, *J* = 6.9 Hz, 3H). ^{13}C NMR (125 MHz, CDCl$_3$): δ 165.89, 152.25, 129.24, 121.61, 36.41, 32.07, 31.02, 29.84, 29.82, 29.80 (2C), 29.77, 29.67, 29.57, 29.51, 29.41, 22.85, 14.28.

HRMS (ESI): *m/z* calculated for $C_{20}H_{34}NO^+$: 304.26404 [M+H]$^+$, found 304.26264 [M+H]$^+$.

(*E*)-1-(4-iodophenyl)-2-(4-tetradecylphenyl)diazene 5: Compound **4** (0.60 g, 1.9 mmol) was dissolved along with 4-iodoaniline (0.83 g, 3.8 mmol) in glacial acetic acid (20 ml) at room temperature and under an argon atmosphere. The reaction mixture was stirred overnight at room temperature. Water (50 ml) was added and the solution was extracted with diethylether (100 ml). The organic extracts were washed with a saturated aqueous NaCl solution (50 ml) and dried on anhydrous $MgSO_4$. The salt was removed by filtration and the solvent was evaporated. The crude product was purified by column chromatography using petroleum ether 40–60 / dichloromethane 2:1 as eluent. Evaporation of solvent afforded product **5** as an orange solid (0.9 g) in 90 % yield. Product **5** was kept in the absence of light.

^{1}H NMR (500 MHz, CDCl$_3$): δ 7.83–7.91 (m, 2H), 7.67 (d, *J* = 8.5 Hz, 2H), 7.34 (d, *J* = 8.2 Hz, 2H), 2.71 (t, *J* = 7.7 Hz, 2H), 1.69 (m, 2H), 1.51–1.23 (br, 22H), 0.95 (t, *J* = 6.9 Hz, 3H). ^{13}C NMR (125 MHz, CD$_2$Cl$_2$): δ 152.08, 150.80, 147.03, 138.34, 129.20, 124.49, 123.15, 97.35, 36.07, 32.10, 31.39, 29.89, 29.87, 29.86, 29.84 (2C), 29.77, 29.67, 29.55, 29.46, 22.86, 14.32. HRMS (APCI): *m/z* calculated for $C_{26}H_{38}IN_2^+$: 505.20797 [M+H]$^+$, found 505.20830 [M+H]$^+$.

1,3,5-tris((4-((*E*)-(4-tetradecylphenyl)diazenyl)phenyl)ethynyl)benzene 1: Compound **5** (260 mg, 0.52 mmol) was dissolved along with 1,3,5-triethynylbenzene (25 mg, 0.17 mmol) in a mixture of *i*-Pr$_2$NH (20 ml), THF (7 ml) and toluene (7 ml) under an argon atmosphere. To this solution CuI (3 mg, 0.017 mmol) and Pd(PPh$_3$)$_4$ (30 mg, 0.026 mmol) were added. The progress of the reaction could be followed by TLC with *n*-pentane/AcOEt 60:1 as eluent. The reaction mixture was stirred overnight at room temperature. Upon completion of the reaction the solvent was evaporated and the crude was suspended in dichloromethane (30 ml) and filtered through a plug of silica. The filtrate was subsequently evaporated. The crude product was purified by column chromatography on SiO$_2$ with *n*-pentane/toluene 18:5 as eluent affording product **1** as an orange solid (77 mg) in 36 % yield; mp 87.6–89.9 °C. Product **1** was kept in the absence of light.

^{1}H NMR (400 MHz, CD$_2$Cl$_2$): δ 7.93 (d, *J* = 7.7 Hz, 6H), 7.87 (d, *J* = 7.6 Hz, 6H), 7.76 (s, 3H), 7.72 (d, *J* = 7.9 Hz, 6H), 7.36 (d, *J* = 7.8 Hz, 6H), 2.70 (t, *J* = 7.5 Hz, 6H), 1.66 (m, 6H), 1.41–1.22 (br, 66H), 0.88 (t, *J* = 6.4 Hz, 9H). ^{13}C NMR (100 MHz, CDCl$_3$): δ 152.31, 151.08, 147.17, 134.50, 132.67, 129.29, 125.13, 124.11, 123.17, 123.03, 90.73, 90.08, 36.10, 32.09, 31.43, 29.86, 29.83 (2C), 29.82 (2C), 29.75, 29.66, 29.52, 29.46, 22.85, 14.29. HRMS (ESI): *m/z* calculated for $C_{90}H_{115}N_6^+$: 1279.91832 [M+H]$^+$, found 1279.91827 [M+H]$^+$.

1-bromo-3,5-diethynylbenzene 9: 1-bromo-3,5-diiodobenzene **7** (1.0 g, 2.5 mmol) was suspended in Et$_3$N (17.5 ml) (the solvent was degassed with argon) with the addition of triisopropylsilylacetylene (1.1 ml, 5.0 mmol), PdCl$_2$(PPh$_3$)$_2$ (40 mg, 0.057

mmol) and CuI (36 mg, 0.19 mmol). The suspension was stirred under argon at room temperature for 3 days. The progress of the reaction could be followed by reverse phase TLC with MeOH as eluent. Upon completion of the reaction the reaction mixture was diluted with diethylether (50 ml), washed with water (50 ml) and dried on anhydrous Na_2SO_4. The salt was removed by filtration and the solvent was evaporated. The residue was quickly passed through a column of normal phase silica with *n*-pentane and collected as crude **8** (1.3 g) without further purification.

The crude product **8** (1.3 g) was dissolved in THF (56 ml) and water (1.4 ml) with the addition of the THF solution of tetra-*n*-butylammonium fluoride (5.3 ml, *c* = 1.0 mol dm^{-3}). The solution was stirred for 3 h at room temperature. The solvent was evaporated and diethylether was added (60 ml). The solution was washed with water (50 ml), dried on anhydrous Na_2SO_4, filtered and evaporated. The crude product was purified by column chromatography (on normal phase silica) using *n*-pentane as eluent affording product **9** (345 mg) as a pale yellow solid in a total yield of 70 % over two steps.

^{1}H NMR (500 MHz, CD_2Cl_2): δ 7.62 (d, *J* = 1.3 Hz, 2H), 7.54 (t, *J* = 1.3 Hz, 1H), 3.22 (s, 2H). ^{13}C NMR (125 MHz, CD_2Cl_2): δ 135.66, 134.72, 124.68, 122.32, 81.42, 79.77.

1-bromo-3,5-bis((4-((*E*)-(4-tetradecylphenyl)diazenyl)phenyl)ethynyl)benzene 10: Compounds **9** (15 mg, 0.074 mmol) and **5** (80 mg, 0.16 mmol) were dissolved in a mixture of *i*-Pr$_2$NH (6 ml), THF (2 ml) and toluene (2 ml) under an argon atmosphere. The resulting solution was degassed with argon. To this solution CuI (1 mg, 0.005 mmol) and Pd(PPh$_3$)$_4$ (8.6 mg, 0.007 mmol) were added and the solution was stirred overnight at room temperature. The progress of the reaction could be followed by TLC with *n*-pentane / AcOEt 60:1 as eluent. The solvent was evaporated and the crude was purified by column chromatography using *n*-pentane / AcOEt 86:1 as eluent. The isolated solid was suspended in MeOH and the solution was decanted off. This procedure was repeated 2 or 3 times until the isolated solid was pure by NMR analysis. Product **10** (39 mg) was obtained as a dark red solid in 55 % yield. An alternative method of purification of **10** is column chromatography using *n*-pentane / dichloromethane / toluene 10:1:1 as eluent.

^{1}H NMR (500 MHz, CD_2Cl_2): δ 7.92 (d, *J* = 8.5 Hz, 4H), 7.86 (d, *J* = 8.3 Hz, 4H), 7.73–7.69 (m, 7H), 7.36 (d, *J* = 8.3 Hz, 4H), 2.70 (t, *J* = 7.6 Hz, 4H), 1.66 (m, 4H), 1.40–1.21 (br, 44H), 0.88 (t, *J* = 6.9 Hz, 6H). ^{13}C NMR (125 MHz, CDCl$_3$): δ 152.49, 151.07, 147.27, 134.37, 133.44, 132.75, 129.33, 125.31, 124.84, 123.17, 123.03, 122.21, 91.28, 89.36, 36.10, 32.08, 31.44, 29.85, 29.83, 29.82, 29.81 (2C), 29.73, 29.65, 29.52, 29.44, 22.85, 14.29. HRMS (APCI): *m/z* calculated for $C_{62}H_{78}BrN_4^+$: 957.54099 [M+H]$^+$, found 957.53958 [M+H]$^+$.

1,4-bis((3,5-bis((4-((*E*)-(4-tetradecylphenyl)diazenyl)phenyl)ethynyl)phenyl)ethynyl)benzene   2:
Compound **10** (52 mg, 0.052 mmol) and 1,4-diethynylbenzene (4.9 mg, 0.038 mmol) were dissolved in a mixture of *i*-Pr$_2$NH (4 ml), THF (1 ml) and toluene (1 ml) under an argon atmosphere. To this solution CuI (2 mg, 0.011 mmol) and Pd(PPh$_3$)$_4$ (8.1 mg, 0.007 mmol) were added and the reaction mixture was stirred at reflux for 5 h. The solvent was evaporated and the crude product was purified by column chromatography using *n*-pentane / dichloromethane / toluene 10:1:1 as eluent. This afforded product **2** as an orange solid (30 mg) in a 42 % yield.

^{1}H NMR (500 MHz, CDCl$_3$): δ 7.91 (d, *J* = 8.3 Hz, 8H), 7.85 (d, *J* = 8.1 Hz, 8H), 7.72 (s, 2H), 7.70 (s, 4H), 7.67 (d, *J* = 8.3 Hz, 8H), 7.53 (s, 4H), 7.33 (d, *J* = 8.2 Hz, 8H), 2.67 (t, *J* = 7.4 Hz, 8H), 1.62 (m, 8H), 1.37–1.17 (br, 88H), 0.86 (t, *J* = 6.8 Hz, 12H). ^{13}C NMR (125 MHz, CDCl$_3$): δ 152.33, 151.07, 147.20, 134.47 (2C), 132.68, 131.87, 129.31, 125.12, 125.08, 124.11, 124.08, 123.16, 123.03, 90.71, 90.48, 90.06, 89.91, 36.10, 32.08, 31.44, 29.86, 29.84, 29.83, 29.81 (2C), 29.74, 29.65, 29.52, 29.45, 22.85, 14.29. HRMS (MALDI; matrix: 2,5–dihydroxybenzoic acid): *m/z* calculated for C$_{134}$H$_{159}$N$_8{}^+$: 1881.27213 [M+H]$^+$, found 1881.0406 [M+H]$^+$.

References

1. W. R. Browne, B. L. Feringa *Nature Nanotechnol.* **2006**, *1*, 25–35.

2. E. R. Kay, D. A. Leigh, F. Zerbetto *Angew. Chem. Int. Ed.* **2007**, *46*, 72–191.

3. V. Balzani, A. Credi, M. Venturi, *Molecular Devices and Machines – A Journey into the Nano World*, Wiley–VCH, Weinheim, Germany **2003**.

4. *Molecular Switches* (Ed: B. L. Feringa and W. R. Browne), Wiley–VCH, 2nd edition, Weinheim, Germany **2011**.

5. G. Vives, J. M. Tour *Acc. Chem. Res.* **2009**, *42*, 473–487.

6. T. Kudernac, N. Ruangsupapichat, M. Parschau, B. Maciá, N. Katsonis, S. R. Harutyunyan, K.–H. Ernst, B. L. Feringa *Nature* **2011**, *479*, 208–211.

7. E. Merino, M. Ribagorda *Beilstein J. Org. Chem.* **2012**, *8*, 1071–1090.

8. T. Muraoka, K. Kinbara, Y. Kobayashi, T. Aida *J. Am. Chem. Soc.* **2003**, *125*, 5612–5613.

9. H. W. Kim, J. Jung, M. Han, S. Lim, K. Tamada, M. Hara, M. Kawai, Y. Kim, Y. Kuk *J. Am. Chem. Soc.* **2011**, *133*, 9236–9238.

10. T. Hugel, N. B. Holland, A. Cattani, L. Moroder, M. Seitz, H. E. Gaub *Science* **2002**, *296*, 1103–1106.

11. M. Elbing, A. Błaszczyk, C. von Hänisch, M. Mayor, V. Ferri, C. Grave, M. A. Rampi, G. Pace, P. Samorì, A. Shaporenko, M. Zharnikov *Adv. Funct. Mater.* **2008**, *18*, 2972–2983.

12. G. Pace, V. Ferri, C. Grave, M. Elbing, C. von Hänisch, M. Zharnikov, M. Mayor, M. A. Rampi, P. Samorì *PNAS* **2007**, *104*, 9937–9942.

13. V. Ferri, M. Elbing, G. Pace, M. D. Dickey, M. Zharnikov, P. Samorì, M. Mayor, M. A. Rampi *Angew. Chem. Int. Ed.* **2008**, *47*, 3407–3409.

14. A. S. Kumar, T. Ye, T. Takami, B.−C. Yu, A. K. Flatt, J. M. Tour, P. S. Weiss *Nano Lett* **2008**, *8*, 1644−1648.

15. M. Alemani, M. V. Peters, S. Hecht, K.−H. Rieder, F. Moresco, L. Grill *J. Am. Chem. Soc.* **2006**, *128*, 14446−14447.

16. M. Alemani, S. Selvanathan, F. Ample, M. V. Peters, K.-H. Rieder, F. Moresco, C. Joachim, S. Hecht, L. Grill *J. Phys. Chem. C* **2008**, *112*, 10509−10514.

17. B.-Y. Choi, S.−J. Kahng, S. Kim, H. Kim, H. W. Kim, Y. J. Song, J. Ihm, Y. Kuk *Phys. Rev. Lett.* **2006**, *96*, 156106.

18. J. Henzl, M. Mehlhorn, H. Gawronski, K.−H. Rieder, K. Morgenstern *Angew. Chem. Int. Ed.* **2006**, *45*, 603−606.

19. M. J. Comstock, N. Levy, A. Kirakosian, J. Cho, F. Lauterwasser, J. H. Harvey, D. A. Strubbe, J. M. J. Fréchet, D. Trauner, S. G. Louie, M. F. Crommie *Phys. Rev. Lett.* **2007**, *99*, 038301.

20. M. Wolf, P. Tegeder *Surf. Sci.* **2009**, *603*, 1506−1517.

21. D. Bléger, A. Ciesielski, P. Samorì, S. Hecht *Chem. Eur. J.* **2010**, *16*, 14256−14260.

22. T. Sasaki, J. M. Tour *Org. Lett.* **2008**, *10*, 897−900.

23. E. M. Purcell *Proc. Natl. Acad. Sci. USA* **1997**, *94*, 11307−11311.

24. O. Villavicencio, D. V. McGrath in *Advances in Dendritic Macromolecules* (Ed: G. R. Newkome), Elsevier Science Ltd., Oxford, United Kingdom **2002**, *5*, p. 1−44.

25. R. Deloncle, A.-M. Caminade *J. Photochem. Photobiol. C* **2010**, *11*, 25−45.

26. J. Zeitouny, A. Belbakra, A. Llanes-Pallas, A. Barbieri, N. Armaroli, D. Bonifazi *Chem. Comm.* **2011**, *47*, 451−453.

27. T. Takahashi, T. Tanino, H. Ando, H. Nakano, Y. Shirota *Mol. Cryst. Liq. Cryst.* **2005**, *430*, 9−14.

28. J. Bahrenburg, C. M. Sievers, J. Boyke Schönborn, B. Hartke, F. Renth, F. Temps, C. Näther, F. D. Sönnichsen *Photochem. Photobiol. Sci.* **2013**.

29. P. Wolfer, H. Audorff, K. Kreger, L. Kador, H.-W. Schmidt, N. Stingelin, P. Smith *J. Mater. Chem.* **2011**, *21*, 4339−4345.

30. J. Robertus, S. F. Reker, T. C. Pijper, A. Deuzeman, W. R. Browne, B. L. Feringa *Phys. Chem. Chem. Phys.* **2012**, *14*, 4374−4382.

31. J. Mielke, S. Selvanathan, M. Peters, J. Schwarz, S. Hecht, L. Grill *J. Phys.: Condens. Matter* **2012**, *24*, 394013.

32. U. H. F. Bunz *Chem. Rev.* **2000**, *100*, 1605−1644.

33. Y. Shirai, T. Sasaki, J. M. Guerrero, B.−C. Yu, P. Hodge, J. M. Tour *ACS Nano* **2008**, *2*, 97−106.

34. N. Katsonis, A. Marchenko, D. Fichou *J. Am. Chem. Soc.* **2003**, *125*, 13682−13683.

35. P. Wu, G. Deng, S. Xu, Q. Fan, L. Wan, C. Wang, C. Bai *Chinese Science Bulletin* **2002**, *47*, 1514−1517.

36. S. Duhm, Q. Xin, N. Koch, N. Ueno, S. Kera *Org. Electron.* **2011**, *12*, 903−910.

37. K. G. Nath, O. Ivasenko, J. A. Miwa, H. Dang, J. D. Wuest, A. Nanci, D. F. Perepichka, F. Rosei *J. Am. Chem. Soc.* **2006**, *128*, 4212−4213.

38. J. Jiang, T. D. Krauss, L. E. Brus *J. Phys. Chem. B* **2000**, 104, 11936−11941.

39. D. Rajwar, X. Sun, S. J. Cho, A. C. Grimsdale, D. Fichou *CrystEngComm* **2012**, *14*, 5182−5187.

40. L. Askadskaya, C. Boeffel, J. P. Rabe *Ber. Bunsenges. Phy. Chem.* **1993**, *97*, 517−521.

41. A. L. Kanibolotsky, I. F. Perepichka, P. J. Skabara *Chem. Soc. Rev.* **2010**, *39*, 2695−2728.

42. K. S. Mali, J. Adisoejoso, E. Ghijsens, I. de Cat, S. de Feyter *Acc. Chem. Res.* **2012**, *45*, 1309–1320.

43. F. A. Garlichs–Zschoche, K. H. Dötz *Organometallics* **2007**, *26*, 4535–4540.

44. H. Kai, S. Nara, K. Kinbara, T. Aida *J. Am. Chem. Soc.* **2008**, *130*, 6725–6727.

45. P. N. W. Baxter *Chem. Eur. J.* **2003**, *9*, 5011–5022.

46. J. G. Rodríguez, T. Laparra *Tetrahedron* **2009**, *65*, 2551–2555.

47. J. Griffiths *Chem. Soc. Rev.* **1972**, *1*, 481–493.

48. P. Bortolus, S. Monti *J. Phys. Chem.* **1979**, *83*, 648–652.

49. F. Serra, E. M. Terentjev *Macromolecules* **2008**, *41*, 981–986.

50. H. Rau *Photochemistry and Photophysics* (Ed: J. F. Rabek); CRC Press, Inc.; Boca Raton, FL, **1990**, *Vol. 2*, p.119.

51. P. D. Wildes, J. G. Pacifici, G. Irick Jr., D. G. Whitten *J. Am. Chem. Soc.* **1971**, *93*, 2004–2008.

52. T. Asano, T. Okada, S. Shinkai, K. Shigematsu, Y. Kusano, O. Manabe *J. Am. Chem. Soc.* **1981**, *103*, 5161–5165.

53. N. Nishimura, T. Sueyoshi, H. Yamanaka, E. Imai, S. Yamamoto, S. Hasegawa *Bull. Chem. Soc. Jpn.* **1976**, *49*, 1381–1387.

54. K. Matczyszyn, W. Bartkowiak, J. Leszczynski *J. Mol. Struct.* **2001**, *565–566*, 53–57.

55. J. García–Amorós, D. Velasco *Beilstein J. Org. Chem.* **2012**, *8*, 1003–1017.

56. C. R. Crecca, A. E. Roitberg *J. Phys. Chem. A* **2006**, *110*, 8188–8203.

57. N. Wazzan (2009) *Cis–Trans Isomerisation of Azobenzenes Studied by NMR Spectroscopy with In situ Laser Irradiation and DFT Calculations* PhD Thesis, University of Edinburgh, UK.

58. J. P. Otruba III, R. G. Weiss *J. Org. Chem.* **1983**, *48*, 3448–3453.

59. G. R. Mitchell, N. R. King *Macromol. Symp.* **1999**, *137*, 155–165.

60. S. Hagen, P. Kate, M. Peters, S. Hecht, M. Wolf, P. Tegeder *Appl. Phys. A* **2008**, *93*, 253–260.

61. M. J. Comstock, D. A. Strubbe, L. Berbil–Bautista, N. Levy, J. Cho, D. Poulsen, J. M. J. Fréchet, S. G. Louie, M. F. Crommie *Phys. Rev. Lett.* **2010**, *104*, 178301.

Chapter 3

Molecular Switches on Wheels

This chapter deals with the design, preparation and solution-study of novel light-driven molecular vehicles. The molecules are equipped with an azobenzene unit and two wheels; a new design of the molecular wheel is introduced. The molecules are designed for surface studies with the aim of investigating their surface-traversing properties.

Introduction

In the attempt of bringing molecular motion under control, studies in nanotechnology have put considerable effort into the investigation of surface-bound systems[1,2,3,4]. Immobilization of molecular systems onto a surface eliminates or reduces Brownian motion that is otherwise present in solution and strongly interferes with the artificially induced motion of molecules. Surpassing the mere study of switching behaviour on surfaces[5,6,7,8,9,10,11,12,13,14,15,16], recent advances have led to the attempts to mimic the motion from the macroscopic world right down to the molecular level[3,17,18,19,20,21,22].

A report of a triptycene molecular wheel (Fig 1a), that could be moved across the surface by rolling rather than by hopping or sliding paved the way for future developments[23]. One after another, reports of various nanovehicles began appearing[3,17,18]. Nanocars and nanotrucks equipped with fullerene wheels (Fig 1b), underwent directional thermal motion or were successfully pulled by the STM tip with a directional preference[24,25]. Although not autonomous, the movement was shown to proceed by rolling of the wheels[26]. By careful design of the nanovehicles, both translational and pivoting motion could be demonstrated. In an attempt to achieve autonomous motion the next generation of molecules was equipped with an engine. The first design was the „nanoworm" equipped with an azobenzene unit[27] (Fig 1c). Undergoing photoisomerization and thermal isomerization via two different pathways, the switching motion was envisaged to be accompanied by a translational component propelling the "nanoworm". No surface studies were reported however. Another design of a nanocar came equipped with a unidirectional light-driven rotary molecular motor[4] that was supposed to propel the vehicle in a paddlewheel-like motion[28,29] (Fig 1d). Although the first motorized nanovehicle, it has not been reported to undergo any autonomous movement on a surface. Fullerene wheels were eventually found to quench photochemical processes. For that reason as well as for synthetic and solubility reasons, fullerene wheels were replaced for carborane or adamantane wheels[30,31,32,33]. In order to benefit from an alternative technique for following molecules on surfaces, the newest generation of nanovehicles is equipped with a fluorophore that allows for the imaging of single-molecules by the use of fluorescence microscopy[32,34,35,36] (Fig 1e). An alternative means of fuelling the propulsion of nanovehicles has also been proposed; active Hoveyda–Grubbs catalyst nanocars are envisaged to engage in surface-initiated ring-opening metathesis polymerization (ROMP) triggering polymer chain growth which should in turn propel the nanovehicle[37]. Norbornene would be used to fuel these nanocars. No surface studies of these chemically fuelled nanovehicles have been reported up to date however.
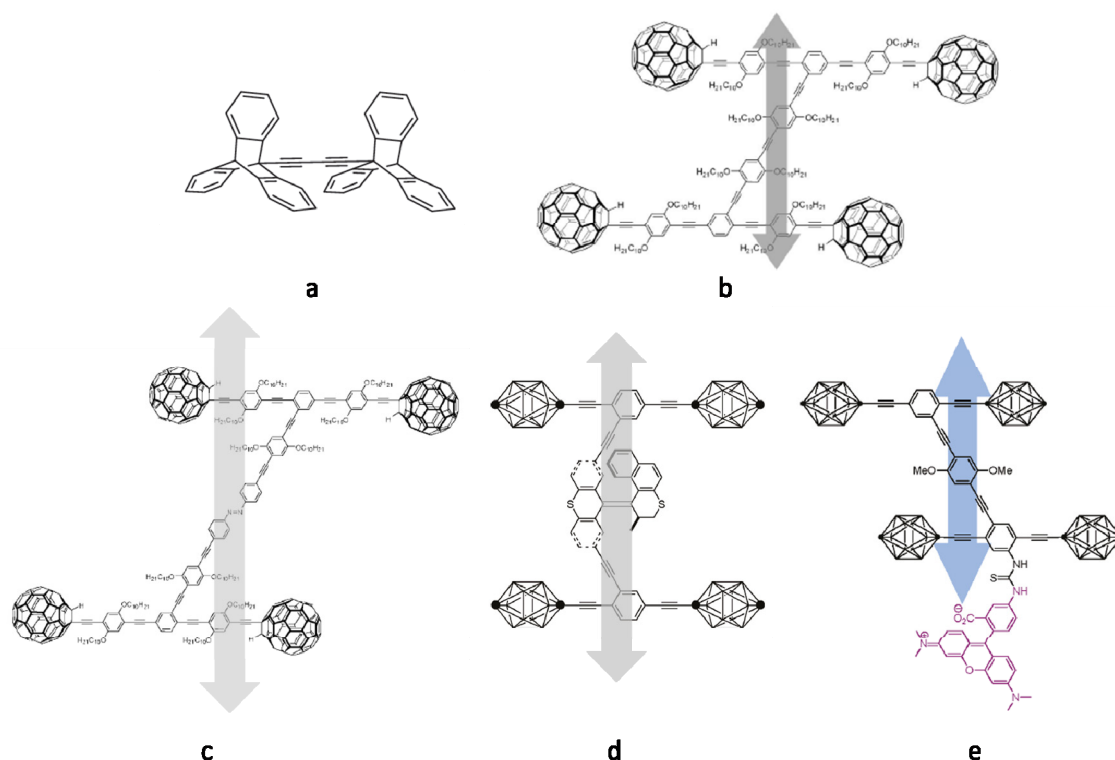
Figure 1. Recent progress on the development of nanovehicles; **a:** triptycene molecular wheels, **b:** nanocar equipped with fullerene wheels, **c:** "nanoworm" equipped with fullerene wheels and a central azobenzene group, **d:** nanocar equipped with carborane wheels and a rotary motor, **e:** nanocar equipped with carborane wheels and a fluorescent tag.

The newest design of a nanocar from our laboratories appeared in the literature recently[38]. It is a molecule equipped with four functional units – unidirectional rotary motors[2,4] (Fig 2a). These units serve multiple purpose in the molecular design; through continuous and well-defined conformational and configurational changes they act as molecular wheels as well as the engine of the nanovehicle. These structural changes arise through sequential electronic and vibrational excitation. The molecule is propelled across the surface in a unidirectional fashion through a paddlewheel type motion (Fig 2b). By tuning of the chirality of the individual motor units the system may be adapted to follow either linear or random surface trajectories or to remain stationary.
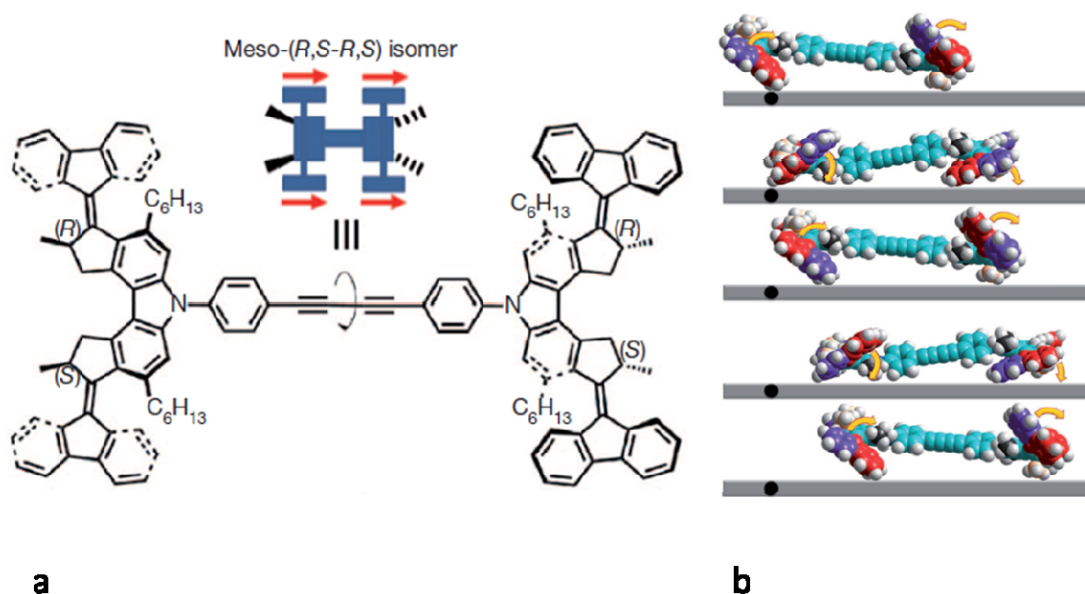
Figure 2. Electrically driven nanocar; **a:** molecular structure, **b:** paddlewheel type motion[38].

Although directional movement on a surface has been realized with the design depicted in Fig 2, there is still ample room for improvement[3]. Despite being equipped with light-driven rotary motors, the current nanocar is driven electrically *i.e.* by pulsing it with an STM tip. Light, however, is still considered as the ultimate fuel for severals reasons: it can be switched on and off quite easily and rapidly, the system can be operated from a distance, lasers allow for working in a very small space and very short time domains, photons can be useful to „read" the state of the system and control the operation of the machine in addition to supplying energy for work[1]. The idea of a light-driven nanovehicle is therefore still highly appealing. Furthermore, future application of these devices will require them to be more efficient which undoubtedly requires more research in this area[2].

In an alternative approach we have designed molecules **1a** and **1b** which are depicted in Fig 3.

1a   **1b**
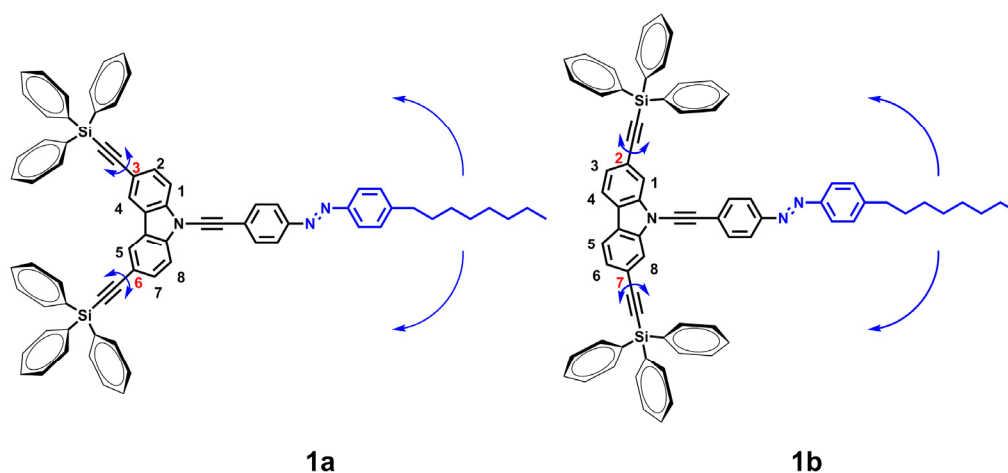
Figure 3. Design of molecules **1a** and **1b** as well as the anticipated mode of motion (highlighted in blue).

Molecules **1a** and **1b** both have a rigid carbazole core that is equipped with two triphenylsilylethynyl groups. The only difference between the two molecules is the position of these groups; in **1** they are attached to positions 3 and 6 in the carbazole whereas in **1b** they are attached to positions 2 and 7 in the carbazole. The triphenylsilyl group has been chosen as a new design of a molecular wheel. A comparison of the triphenylsilyl wheel to the original triptycene wheel (Fig 4), reveals the same symmetry as well as a certain structural similarity. The main difference, however, is a less rigid scaffold in the new design due to the absence of the polycyclic core of the wheel. It should be interesting to see how the new, more flexible wheels behave on the surface compared to those reported in the literature[3,17,23,32]. Another difference is a silicon atom in the new design as opposed to a carbon atom in the triptycene wheel. The C–Si bond (0.189 nm) is longer than the C–C bond (0.153 nm)[39] which makes the triphenylsilyl wheel slightly bigger than the triptycene wheel. The C–Si bond (290 kJ mol^{-1}) is, however, weaker than the C–C bond (356 kJ mol^{-1})[39] which might render the wheels sensitive to elevated temperatures (for example, in the process of transferring the molecules onto a surface). The triphenylsilyl wheels are, however, synthetically more accessible than the triptycene wheels. Both carbazole units are further derivatized with an azobenzene group that bears a C$_8$-alkyl chain. The azobenzene group should convert light into mechanical energy through the switching process and the alkyl chain should increase the solubility of the molecule and help the molecule adsorb onto the surface if studied on *n*-pentacontane-modified highly ordered pyrolytic graphite (HOPG).
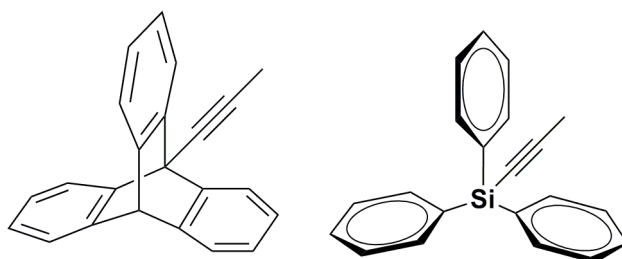
Figure 4. Comparison of the triptycene and the triphenylsilyl wheel.

Fig 3 also shows the envisaged mode of motion of molecules **1a** and **1b** on a surface (highlighted in blue); repeated switching of the azobenzene units should cause a swim-like motion of the „tail" propelling the molecule in a forward or backward direction via rolling of the molecular wheels.

Our primary objectives are to synthesize and characterize compounds **1a** and **1b**, and study their switching properties in solution. This should allow us to compare the behaviour of these novel molecules to simple azobenzene molecules but also to molecules discussed in Chapter 2. The results should already give an indication about their utility for any surface studies. Ultimately, we would like to study these molecules on a surface. The first step would be imaging of individual molecules by STM. The next step would be to follow the process of photoisomerization on the

surface by STM. Comparing the switching process on the surface to the same process in solution is of utmost importance for understanding the differences between the behaviour of molecules in solution and on the surface. It should also be investigated if the switching on the surface can be performed reversibly and repeatedly. If so, the next step would be to study if the continuous isomerization process provides enough work to affect the position of the molecule on the surface. If, upon continuous switching, any change in the position of the molecule were to be observed, detailed studies should be carried out to learn more about the mechanism of the motion. Does the molecule move by rolling of the triphenylsilyl wheels rather than by hopping or sliding across the surface? This would also evaluate the new design of molecular wheels. Comparing the surface behaviour of molecules **1a** and **1b**, differing only in the position of the wheels, is also highly interesting. Is one position of the wheels superior to the other? In a macroscopic way of looking at things, it may seem intuitive that the design in **1b** will give better functioning (rolling) wheels. We need to keep in mind, however, that the nanoworld is not a mere miniature of the macroscopic world and that the major effects and parameters playing a role might be different at the nanoscale than in the macroscopic world[1,2]. The comparison of molecules **1a** and **1b** on a surface would therefore be most insightful. Furthermore, comparing these monoazobenzene molecules to the multiazobenzene molecules prepared in Chapter 2 might give a hint on what the future generations of nanovehicles should look like. Should they be equipped with a single engine or with multiple engines? Should they be flat or should the wheels lift the molecule above the surface? How strong should the interaction between the molecules and the surface be in order to achieve controlled motion over the surface? The investigations described above should address some of these questions and evaluate our new design of molecular wheels as well as of nanovehicles in general and bring us one step closer to an autonomously moving nanovehicle[3].

Results and discussion

Synthesis and characterization

Molecules **1a** and **1b** were synthesized according to Scheme 1. The syntheses were carried out in a convergent manner. Since the two molecules differ only in the position of the triphenylsilylethynyl groups, their syntheses were for the most part analogous. The azobenzene group, once synthesized, could be used for the preparation of both molecules.
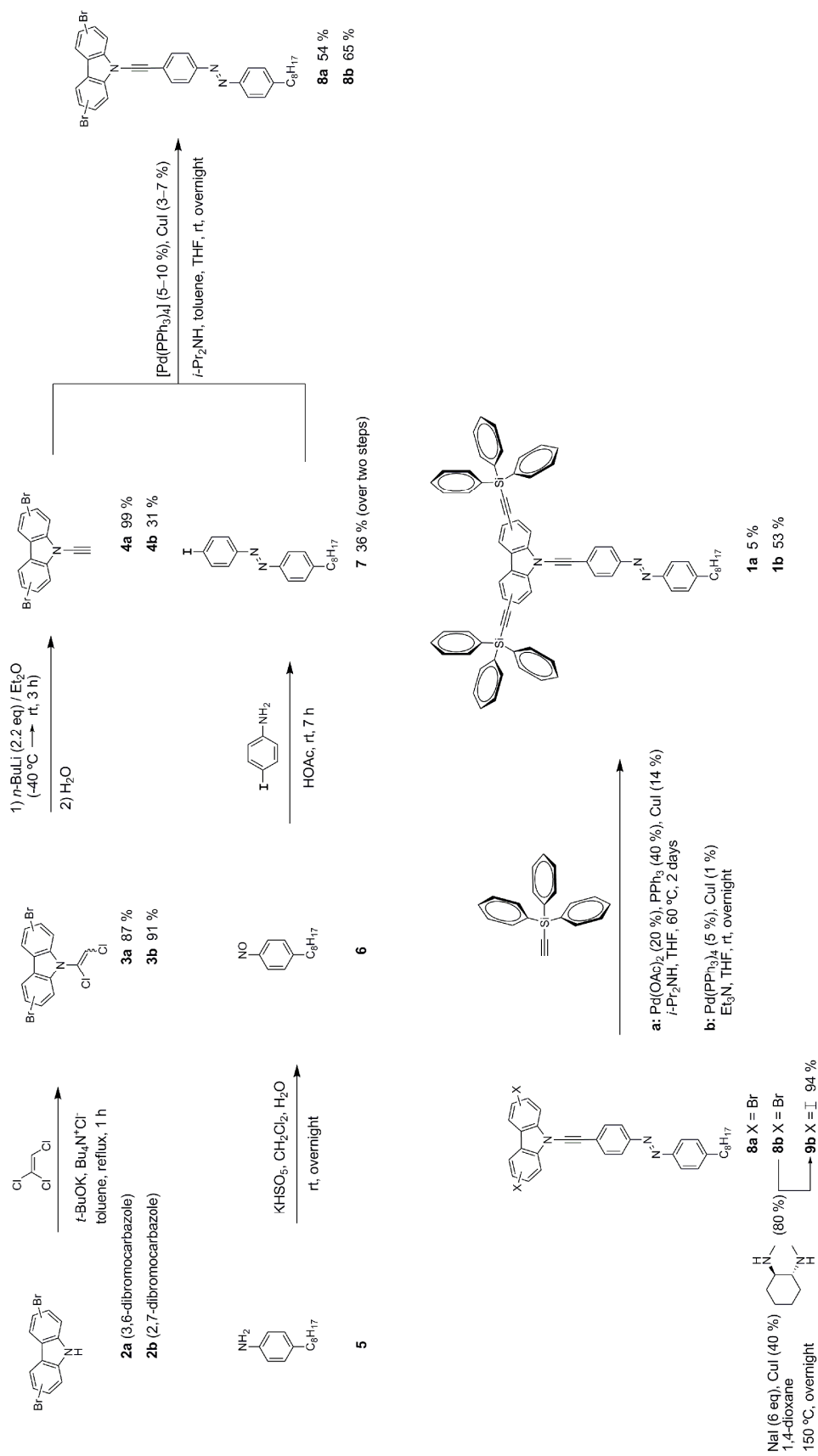
Scheme 1. Syntheses of molecules **1a** and **1b**; the **a**–series corresponds to the 3,6-carbazole derivatives and the **b**–series to the 2,7-carbazole derivatives.

The unsymmetrically substituted azobenzene unit **7** was prepared in a 36 % overall yield by the coupling of the corresponding nitroso compound **6** with 4-iodoaniline following a literature procedure for an analogous azobenzene derivative differing from **7** only in the alkyl chain length[40]. 1-Nitroso-4-octylbenzene **6** was prepared by the oxidation of 4-octylaniline **5** with oxone (2 KHSO$_5$ · KHSO$_4$ · K$_2$SO$_4$) and was in turn coupled to 4-iodoaniline in acetic acid. This reaction afforded the iodo-functionalized azobenzene molecule **7** which was used as a building block in the syntheses of both target molecules **1a** and **1b**.

The syntheses of the carbazole cores of molecules **1a** and **1b** both started from dibromocarbazole derivatives. 3,6–Dibromocarbazole was purchased from Sigma–Aldrich and 2,7–dibromocarbazole was prepared according to a literature procedure[41]. The dibromocarbazole was first functionalized with a 1,2-dichlorovinyl group which was in turn converted into an ethynyl group using *n*-BuLi. These two synthetic procedures were adapted from literature procedures describing analogous reactions on carbazole[42,43]. Due to the lithiation of the bromine atoms in **3a** and **3b** as a possible side reaction, the reaction of *n*-BuLi on the 2,3-dichlorovinyl group was carried out at lower temperature than originally described for the carbazole analogue[43]. The *N*-ethynyl group appeared unstable under the conditions of column chromatography on silica. Purification of compound **4b** by means of column chromatography resulted in degradation of a substantial amount of the material lowering the isolated yield accordingly. Compound **4a**, however, did not require purification by chromatography, as evidenced by NMR, and thus the yield was significantly higher than for the isomeric compound **4b** (Scheme 1).

Carbazole ynamides **4a** and **4b** were coupled to the iodo-functionalized azobenzene compound **7** in a Sonogashira reaction adapting the conditions from a literature procedure describing Sonogashira coupling reactions on ynamides[44]. The conjugates **8a** and **8b** were obtained in moderate to good yields.

The last step of the synthesis is the attachment of two triphenylsilylethynyl groups to molecules **8a** and **8b**. Product **1a** was isolated in a poor 5 % yield after a Sonogashira coupling reaction of **8a** and triphenylsilylacetylene using Pd(OAc)$_2$ as a catalyst source. The coupling reaction proceeded rather sluggishly even at elevated temperature and the addition of the fresh catalyst was required during the course of the reaction to push the reaction forward. After purification of the crude product by means of chromatography, a number of crystallization steps was still necessary to achieve the desired purity of the product rendering the yield rather poor. In an attempt to prepare **1b** in a higher yielding reaction, we opted to first convert the dibromo-functionalized **8b** into the diiodo-functionalized **9b** as it is known that iodo-compounds tend to be more reactive in Sonogashira coupling reactions than bromo-compounds[45]. The exchange of the bromine atoms in **8b** for iodine atoms was carried out in high yield following an adapted literature procedure[46]. Sonogashira coupling of the diiodo-functionalized **9b** with triphenylsilylacetylene was carried out with Pd(PPh$_3$)$_4$ as a catalyst source at room temperature affording the product **1b** in

53 % yield. Much like with **1a**, both column chromatography as well as repeated crystallizations were necessary to achieve the desired purity of the product. Despite the same tedious purification process, **1b** was obtained from the final step in a considerably higher yield than **1a** which points to different reactivities of **8a** and **9b** in the final reaction step. Furthermore, the reaction was completed in 18 h at room temperature in the case of **9b** whereas it took 68 h at reflux and adding fresh catalyst for **8a** to be converted to the product. As anticipated[45], the iodo-functionalized **9b** is more reactive in a Sonogashira coupling reaction than the corresponding bromo-functionalized **8a**.

All the synthetic intermediates were characterized by [1]H−NMR and APT NMR spectroscopic techniques as well as by high resolution mass spectrometry. The target molecules **1a** and **1b**, however, could not be characterized by mass spectrometry (ESI, APCI, APPI, MALDI). The correct molecular ion or one derived from it could not be detected. The molecules have been characterized by [1]H−NMR and APT NMR spectroscopic techniques which supports the suggested structures. The [1]H−NMR spectra show additional protons in the aromatic region when compared to the spectra of **8a**, **8b** and **9b** as well as the shifting of the peaks corresponding to the protons of the carbazole unit. In addition to the signals corresponding to the triphenylsilyl groups, the APT spectra show four signals in the region 87−111 ppm which correspond to the C−atoms belonging to C≡C bonds. Furthermore, two of the signals show double the intensity of the remaining two indicating the presence of two magnetically different C≡C bonds in 2:1 ratio. This again is in strong support of the structures of target molecules **1a** and **1b**. It is at this point unclear why the target molecules could not be detected by HRMS. It is possible that the triphenylsilylethynyl group degrades upon ionization or that the target molecules do not get ionized under the conditions tried.

Photochemical characterization

Molecule 1a

UV−Vis spectroscopic study

The photochemical properties of switch **1a** were examined in solution (*n*-heptane) by means of UV−Vis spectroscopy (Fig 5). The UV−Vis spectrum of **1a** shows a strong absorption band with λ_{max} = 360 nm (Fig 5a). Upon irradiation of the sample with light at λ = 365 nm, the band drops in intensity and a weak new band appears simultaneously in the region around 325 nm. Subsequent irradiation with light at λ = 312 nm or an increase in temperature causes the newly formed band to reduce in intensity again and the original band with λ_{max} = 360 nm to reappear in its original intensity. This behaviour is typical of azobenzene compounds[47,48]. The UV−Vis spectral changes upon irradiation with 365 nm, however, do not completely resemble a typical azobenzene compound; no new band is observed in the visible region and the increased absorption around 325 nm is weaker than usual. The

reason for these observations is probably the extended conjugated system in **1a**; **1a** absorbs rather strongly both in the region around 325 nm as well as above 400 nm causing an overlap with the newly formed azobenzene bands upon irradiation at 365 nm. When the sample at the 365 nm photostationary state was irradiated with visible light at $\lambda > 420$ nm, no changes in the spectrum were observed.
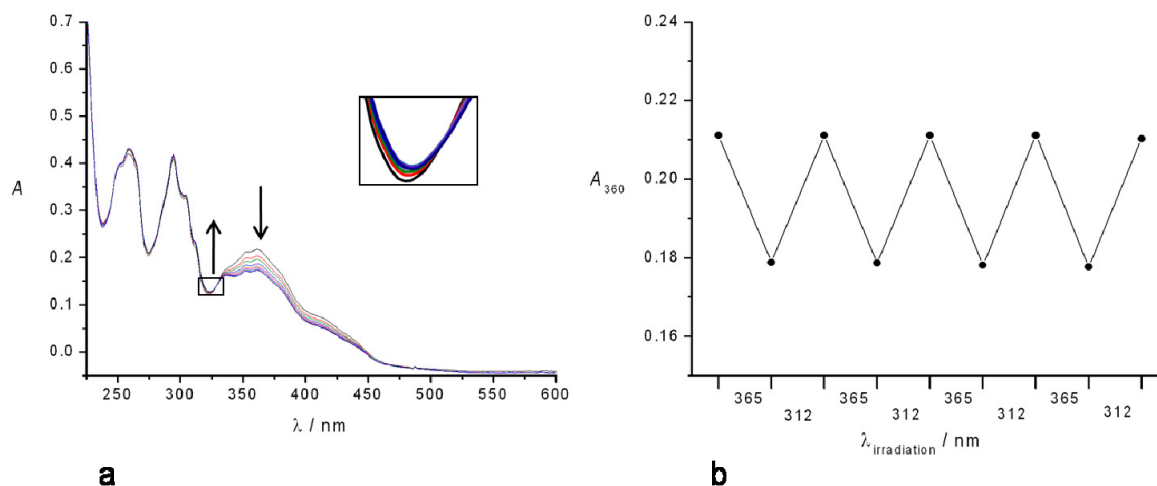
Figure 5. a: UV–Vis Spectra of switch **1a**. Irradiation with light at 365 nm and 312 nm **b:** Monitoring of the absorbance at 360 nm upon irradiation with light of alternating wavelength, 5 min each step. Solution of **1a** in *n*-heptane, $c = 1.4 \cdot 10^{-5}$ mol dm^{-3}, -10 °C.

The change in absorbance was followed at $\lambda_{max} = 360$ nm during repeated irradiation of alternating wavelength (365 nm and 312 nm) and this resulted in a graph that is depicted in Fig 5b. It is clearly shown that the photochemical switching process may be reproduced several times without any noticeable fatigue.

Irradiation of the sample kept in the dark (*E*–isomer) with light at 365 nm establishes a photoequilibrium between the *E*–isomer and the *Z*–isomer of the azobenzene (Scheme 2). The change in the composition of the solute (the ratio of the *E*– and *Z*–isomer) is reflected in the UV–Vis spectrum of the solution; the spectrum changes during irradiation until a photoequilibrium has been reached. The exact photostationary state composition of the solute cannot be estimated at this point but will be addressed at a later stage. Irradiation with light at $\lambda = 312$ nm causes a new photoequilibrium to be established which is again reflected in the UV–Vis spectra of the solution. Since the spectrum taken at photoequilibrium appears identical to the one of the *E*–isomer it can be concluded that the photostationary state (at $\lambda = 312$ nm) consists predominately of the *E*–isomer. The observation that the sample at the 365 nm photostationary state cannot be irradiated back to the *E*–form by using visible light suggests that the difference in the absorption of visible light by the *Z* and *E*–isomer is cancelled out by the difference in quantum yields for the photoisomerization between the two isomers by visible light.
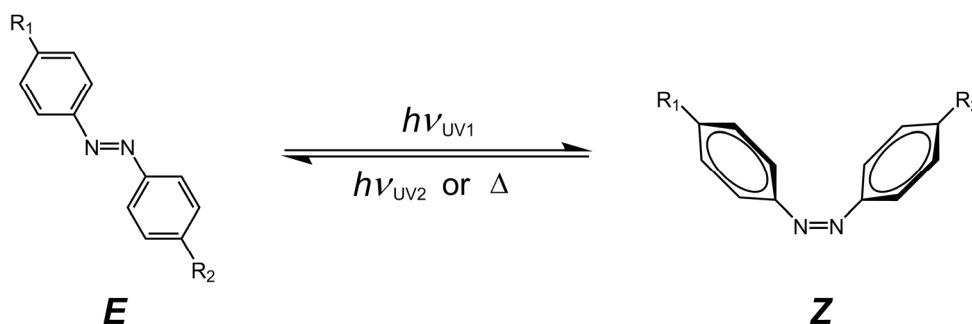
Scheme 2. Typical switching behaviour of azobenzenes.

After the photostationary state has been reached by irradiation of the *E*–isomer with light at 365 nm, the change can also be reversed thermally *i.e.* by warming up the sample. The spectrum of the pure *E*–isomer was once again recovered. This complete thermal reversal of the changes brought about by irradiation with light at 365 nm makes sense since the less stable *Z*–isomer is well known to thermally convert to the more stable *E*–isomer[47,48], Scheme 2. The time it takes for the full recovery of the original spectrum of the *E*–isomer will depend on the temperature of the system. This phenomenon will be studied in more detail at a later stage.

^{1}H–NMR spectroscopic study

The switching behaviour of molecule **1a** was also studied in CDCl$_3$ by means of ^{1}H–NMR spectroscopy (Fig 6). Irradiation of the solution containing only the *E*–isomer of **1a** with light at 365 nm was accompanied by the appearance of new signals in both the aromatic as well as in the aliphatic region of the spectrum. It was proceeded with the irradiation until no further changes could be observed in the spectrum (Fig 6b). The photostationary state had been reached at that point and the solute contained 44 % of the newly formed species. Subsequent irradiation of the sample at the photostationary state with light at 312 nm resulted in the gradual decrease in the intensity of the new signals (Fig 6c). The sample could be irradiated with light at 365 nm again until a photostationary state was reached (Fig 6d). Warming up the sample to 40 °C resulted in the disappearance of newly formed signals (Fig 6e).
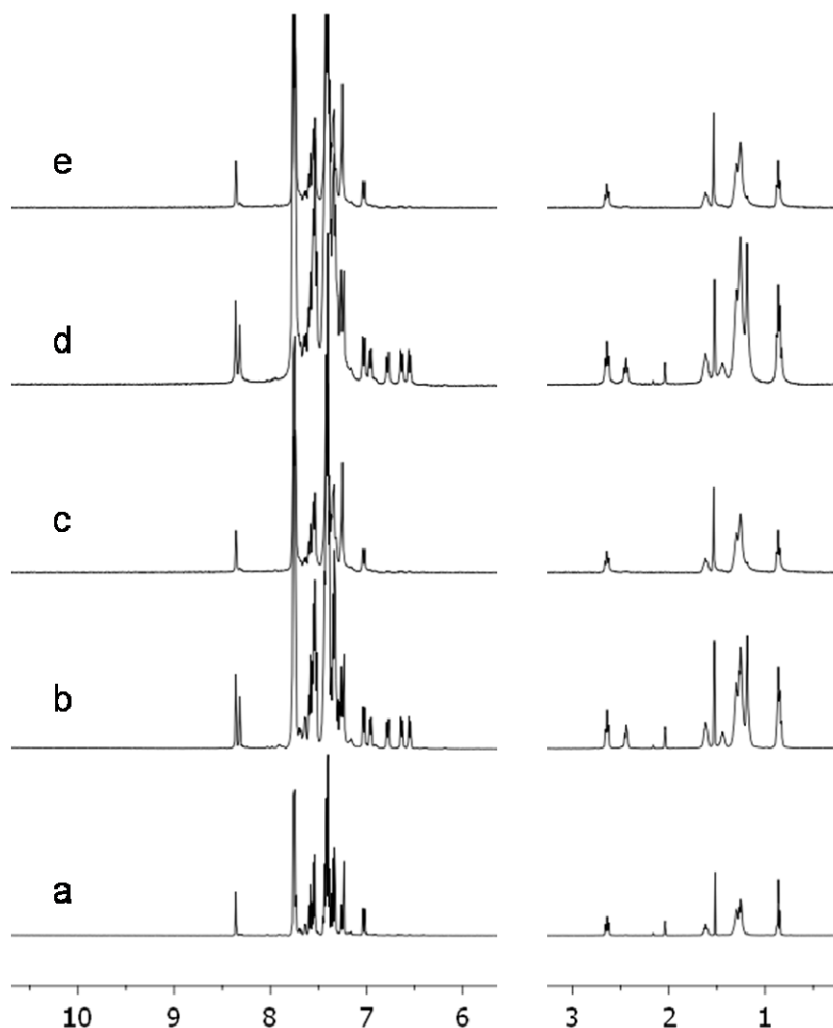
Figure 6. ^{1}H–NMR spectra of switch **1a**, in CDCl$_3$, at −10 °C **a:** in the dark, **b:** sample from **a** irradiated at 365 nm for 7 h, **c:** sample from **b** irradiated at 312 nm for 3 h, **d:** sample from **c** irradiated at 365 nm for 3 h, **e:** sample from **d** warmed up to 40 °C for 2 h.

It should be noted that the NMR experiments were performed in CDCl$_3$ whereas the UV–Vis experiments were conducted in *n*-heptane. The same trends were observed, however, by both spectroscopic methods. The observed behaviour is in accordance with reported behaviour of azobenzene compounds[47].

The NMR signals that shift (most) upon irradiation are those corresponding to the protons that are in immediate vicinity of the azobenzene unit that undergoes the isomerization process. As seen in Fig 6, the aromatic signals undergoing most change upon irradiation are the ones corresponding to the aromatic protons of the azobenzene unit (4 new doublets appearing under 7 ppm). The singlet at 8.36 ppm (corresponding to a proton in the carbazole unit) also shifts, although quite moderately. There are also some changes in the aliphatic region of the spectrum however (Fig 6). Much like it was the case with the molecules discussed in Chapter 2, all of the protons in the alkyl chain appear to shift in the spectrum upon irradiation; the closer they are to the azobenzene unit, the more they shift. The C$_8$-

alkyl chain here being considerably shorter than the C_{14}-alkyl chain in molecules described in Chapter 2, the changes in chemical shifts observed for **1a** for the protons throughout the whole chain do not appear as counterintuitive as they did in Chapter 2.

Kinetics of the thermal isomerization

As already mentioned, the *Z*–isomer may be isomerized to the *E*–isomer photochemically (irradiation with UV light at 312 nm) or thermally. The driving force for the latter process comes from the relative instability of the *Z*–isomer[47,48]; if kept in the absence of light the less stable *Z*–isomer will spontaneously isomerize to the more stable *E*–isomer. The rate at which it undergoes the thermal process depends on the temperature but is always much lower than the rate of the photochemical isomerization[47]. In order to gain more insight into the behavior of **1a**, we opted to follow the kinetics of the thermal isomerization step.

UV–Vis spectroscopic study

Temperature dependent UV–Vis spectroscopy was used to follow the *Z*–to–*E* isomerization process in time (Fig 7).
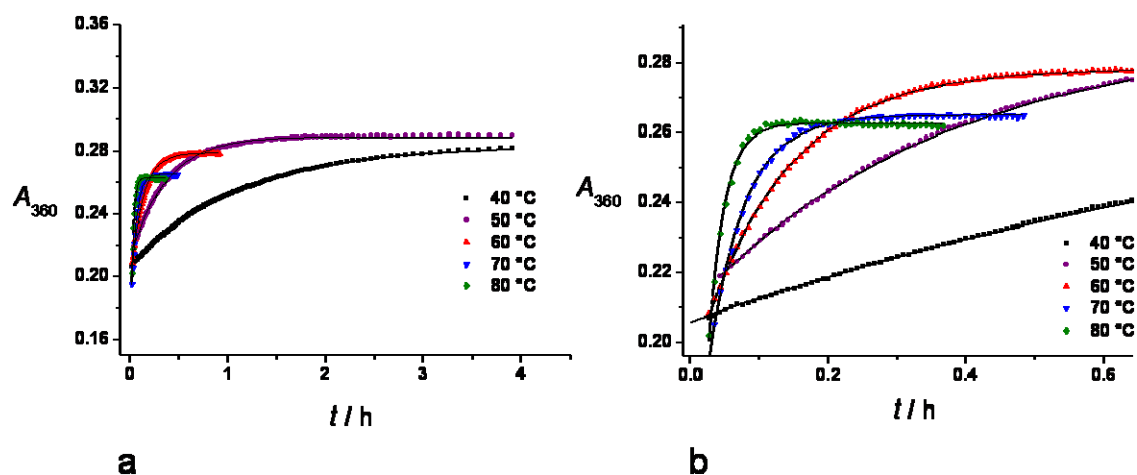
Figure 7. The data points collected by following the absorbance at 360 nm of a sample of **1a** over time at different temperatures, *c* = 1.4·10^{-5} mol dm^{-3} in *n*-heptane, and the calculated values (–) as obtained by nonlinear regression analyses. **a:** all the collected data points, **b:** a blow-up of the graph for the first 0.6 h.

A sample of a solution of **1a** in *n*-heptane was irradiated with light at 365 nm to the photostationary state and the absorbance was followed in the region of maximum absorption (λ_{max} = 360 nm) over time in the temperature range 40–80 °C. The collected data were fitted to the exponential function assuming first-order kinetics for the thermal step[49]. The collected data as well the fits are shown in Fig 7 and the parameters from the fits are given in Table 1.

Table 1. The half-lives of the thermal isomerization of **1a**, $t_{1/2}$, at different temperatures as obtained from the regression analyses of the data in Fig 7.

Θ / °C	$t_{1/2}$ / min	R^2
40	46	0.999
50	15	0.999
60	5.2	0.999
70	2.2	0.999
80	1.0	0.996

From Table 1 it can be seen that the half-life for the thermal isomerization of **1a**, $t_{1/2}$, ranges from 46 min at 40 °C to 1.0 min at 80 °C. This does not differ much from what was observed for molecules discussed in Chapter 2.

The data from Table 1 can be analyzed according to the Eyring equation to obtain the activation parameters, $\Delta^{\ddagger}H$ and $\Delta^{\ddagger}S$ (Fig 8).
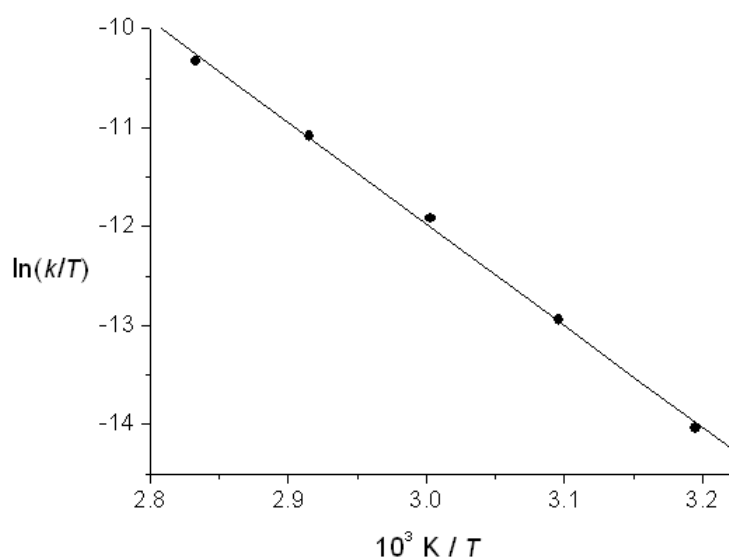
Figure 8. The data points from Table 1 (thermal isomerization of **1a**) analyzed according to the Eyring equation and the calculated values (–) as obtained by linear regression analysis.

From the analysis in Fig 8 the following activation parameters were obtained: $\Delta^{\ddagger}H = (85 \pm 2)$ kJ mol^{-1}, $\Delta^{\ddagger}S = - (41 \pm 7)$ J K^{-1} mol^{-1}. Previously reported values for these parameters for different azobenzene systems are roughly in the range 35 – 100 kJ mol^{-1} and –200 – 50 J K^{-1} mol^{-1}, respectively, depending on the exact

structure of the azobenzene compounds as well as the solvent used during the measurements[50,51,52,53]. Our values for **1a** are well within that range. The activation parameters allow for the calculation of the half-life for the thermal isomerization at 25 °C, $t_{1/2}$ = 3.4 h. This value is of the same order of magnitude as the one determined for molecules **1** and **2** in Chapter 2 (1.2 h found for both **1** and **2**). The activation parameters can give some information about the mechanism of the thermal isomerization as well but this will be discussed at a later stage.

NMR spectroscopic study

The kinetics of the thermal isomerization was also followed by ^{1}H–NMR spectroscopy. The sample of **1a** in CD_2Cl_2 was irradiated at 365 nm at 4 °C until the photostationary state was reached. An ^{1}H–NMR spectrum was taken every 15 min at different temperatures in the range 5 – 35 °C. The spectra obtained at 33.6 °C as a function of time are depicted in Fig 9.
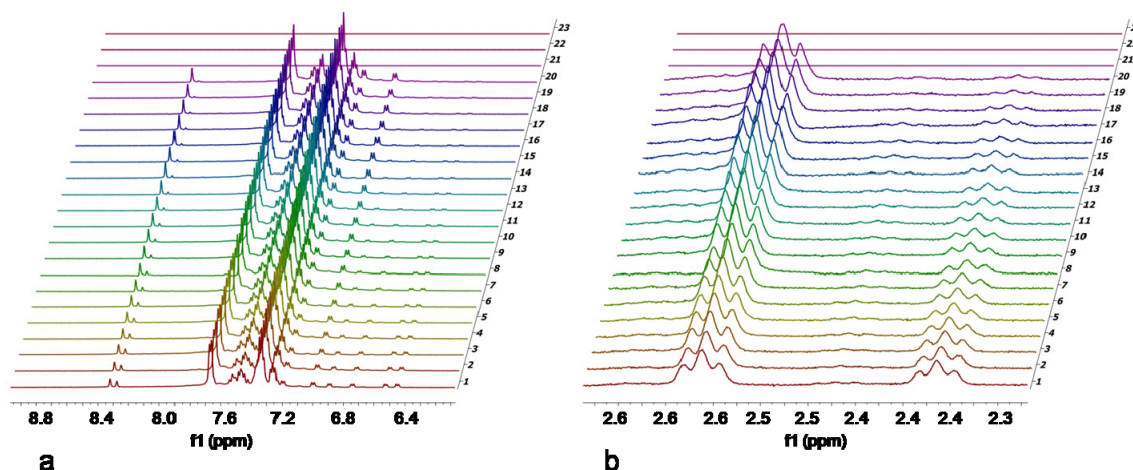
Figure 9. Arrayed ^{1}H–NMR spectra (CD_2Cl_2, 33.6 °C) of a sample of **1a** over time. The sample is obtained by irradiating the solution at λ = (365 ± 20) nm. A spectrum was taken every 15 min (the numbers on the y-axis are experiment numbers). **a:** Aromatic region, **b:** Part of the aliphatic region.

From every spectrum a ratio of the molar concentrations of *E*– and *Z*–molecules, *r*, is obtained by integration of the signals in the aliphatic region (Fig 9b).

$$r = \frac{[E]}{[Z]}$$ (1)

The first-order rate law may be applied to describe the conversion of the *Z*–isomer to the *E*–isomer[49] (eq 2):

$$[Z] = [Z]_0 \, e^{-kt}$$ (2)

where [*Z*] describes the molar concentration of the *Z*–isomer at time *t*, [*Z*]$_0$ is the molar concentration of the *Z*–isomer at time *t* = 0 and *k* is the reaction rate constant.

It also needs to be emphasized that the sum of the molar concentrations of the *Z*–isomer and the *E*–isomer is always constant (eq 3) as they are the only two chemical species interconverting.

$$[Z] + [E] = [Z]_0 + [E]_0 \tag{3}$$

Combining the definition of *r* (eq 1) with the first order rate law describing the conversion of the *Z*–isomer to the *E*–isomer (eq 2) and keeping in mind that equation 3 holds at any given time, one can obtain equation 4:

$$\frac{r+1}{r_0+1} = e^{kt} \tag{4}$$

which can be linearized to give equation 5.

$$\ln\frac{r+1}{r_0+1} = kt \tag{5}$$

Equation 5 is used to fit the data obtained from the arrayed NMR spectra (like those shown in Fig 9) at different temperatures in the range 5 – 35 °C.

The data points along with the fitted lines are given in Fig 10.
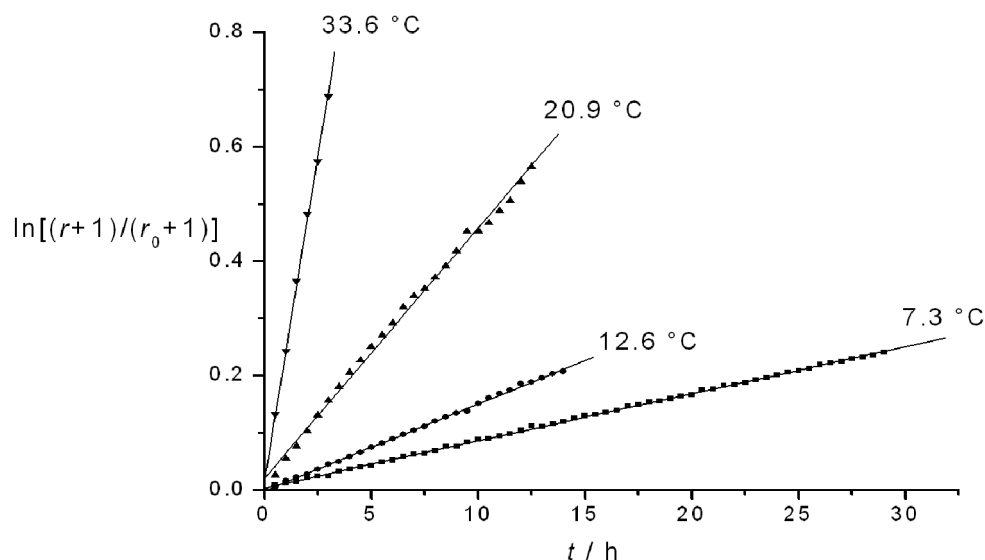
Figure 10. Monitoring the ratio of molar concentrations of *E*–**1a** and *Z*–**1a**, *r*, over time by ^{1}H–NMR, in CD$_2$Cl$_2$, at different temperatures, after irradiating the solution at λ = (365 ± 20) nm. The data points are taken from the arrayed NMR spectra like the one depicted in Fig 9. (–) Calculated by linear regression according to eq 5.

As evident from eq 5, the slope of a straight line in Fig 10 is equal to the rate constant, *k*, at that temperature. The rate constants, converted into half-lives, $t_{1/2}$, are given in Table 2.

Table 2. The half-lives, $t_{1/2}$, at different temperatures as obtained from the regression analyses of the data in Fig 10.

| Θ / °C	$t_{1/2}$ / h	R^2
7.3	83	0.999
12.6	47	0.999
20.9	16	0.996
33.6	3	0.998

As shown in Table 2, the half-lives for the thermal isomerization of *Z*−**1a** to *E*−**1a** are in the range from 83 to 3 h in the temperature range 5 – 35 °C (as compared to 46 – 1 min in the temperature range 40 – 80 °C, Table 1).

The data from Table 2 may be further analyzed according to the Eyring equation in order to obtain the activation parameters, $\Delta^{\ddagger}H$ and $\Delta^{\ddagger}S$ (Fig 11).
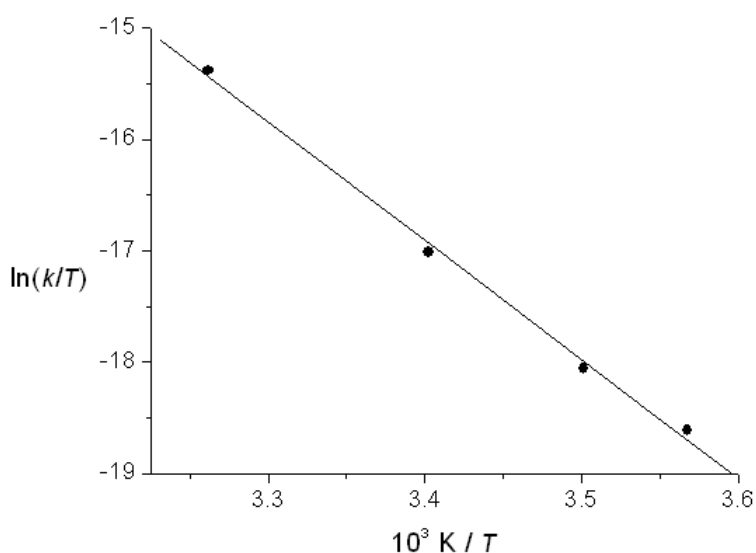
Figure 11. The data points from Table 2 analyzed according to the Eyring equation and the calculated values (−) as obtained by linear regression analysis.

From the analysis in Fig 11 the following activation parameters were obtained: $\Delta^{\ddagger}H$ = (88 ± 4) kJ mol^{-1}, $\Delta^{\ddagger}S$ = − (38 ± 13) J K^{-1} mol^{-1}. This agrees well with the values obtained from the UV−Vis spectroscopic study; (85 ± 2) kJ mol^{-1} and − (41 ± 7) J K^{-1}

mol^{-1}, respectively, especially considering that the measurements in the UV−Vis spectroscopic study were performed in *n*-heptane whereas the measurements in the NMR study were carried out in CD$_2$Cl$_2$. The activation parameters were used to calculate the half-life at 25 °C obtaining the values of 8.0 h in CD$_2$Cl$_2$ and 3.4 h in *n*-heptane.

Molecule 1b

UV−Vis spectroscopic study

Photochemical properties of molecule **1b** were examined in solution (*n*-heptane) by means of UV−Vis spectroscopy (Fig 12). The UV−Vis spectrum of **1b** shows a strong absorption band with λ_{max} = 330 nm (Fig 12a). Upon irradiation of the sample with light at λ = 365 nm, a drop in intensity is seen in the region between 350 and 440 nm and there is a small increase in absorbance in the region around 280 nm. Subsequent irradiation with light at λ = 312 nm or an increase in temperature cause those changes to revert. Compound **1b** appears to behave similarly to compound **1a** and such behaviour is typical of azobenzene compounds[47,48]. The changes in the spectrum upon irradiation are not as pronounced as with simple azobenzene compounds though. That probably has to do with extensive overlap of bands in the UV−Vis of **1b** due to the presence of an extended conjugated system in addition to the azobenzene chromophore. If the sample at the 365 nm photostationary state is irradiated with visible light at λ > 420 nm, no changes in the spectrum are observed.
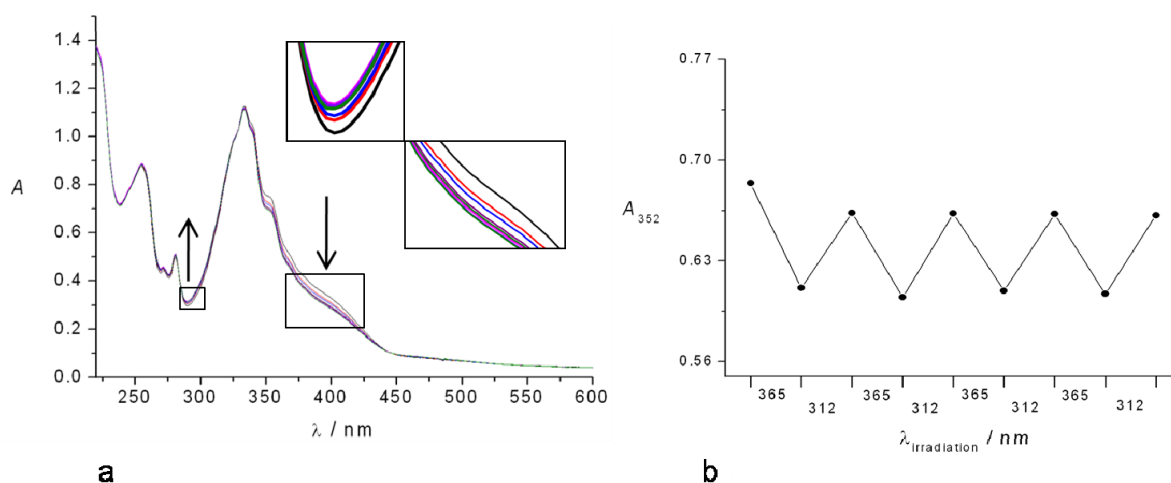
Figure 12. a: UV−Vis Spectra of switch **1b**. Irradiation with light at 365 nm and 312 nm **b:** Monitoring of the absorbance at 352 nm upon irradiation with light of alternating wavelength, 5 min each step. Solution of **1b** in *n*-heptane, *c* = 1.4 · 10^{-5} mol dm^{-3}, −10 °C.

The absorbance was followed in the region of maximum change (λ = 352 nm) during repeated irradiation at alternating wavelength (365 nm and 312 nm) and this resulted in modulated absorption depicted in Fig 12b. The graph shows that the photochemical switching process may be repeated several times with only little fatigue.

Just like with compound **1a**, irradiation of the sample of **1b** kept in the dark (*E*–isomer) with light at 365 nm establishes a photoequilibrium between the *E*–isomer and the *Z*–isomer of the azobenzene (Scheme 2). The change in the composition of the solute (the ratio of the *E*– and *Z*–isomer) is reflected in the UV–Vis spectrum of the solution; the spectrum changes during irradiation until a photoequilibrium has been reached. Irradiation at λ = 312 nm causes a new photoequilibrium to be established which is again reflected in the UV–Vis spectra of the solution. The spectrum taken at photoequilibrium is almost identical to the one of the *E*–isomer so it can be concluded that the photostationary state (at λ = 312 nm) consists predominately of the *E*–isomer. The observation that the sample at the 365 nm photostationary state cannot be irradiated back to the *E*–form by using visible light suggests that the difference in the absorption of visible light by the *Z* and *E*–isomer is cancelled out by the difference in quantum yields for the photoisomerization between the two isomers by visible light.

After the photostationary state has been reached by irradiation of the *E*–isomer with light at 365 nm, the change can also be reversed thermally *i.e.* by warming up the sample. The spectrum of the pure *E*–isomer will once again be recovered as the less stable *Z*–isomer thermally converts to the more stable *E*–isomer[47,48] (Scheme 2). The kinetics of the thermal isomerization step will be discussed later.

^1H–NMR spectroscopic study

The switching behaviour of molecule **1b** was also studied in CDCl$_3$ by means of ^{1}H–NMR spectroscopy (Fig 13). Irradiation of the solution containing only the *E*–isomer of **1b** at 365 nm was accompanied by the appearance of new signals in both the aromatic as well as in the aliphatic region of the spectrum. It was proceeded with the irradiation until no further changes could be observed in the spectrum (Fig 13b,d). The photostationary state had been reached at that point and the solute contained 33 % of the newly formed species. Irradiation of the sample now at the photostationary state with light at 312 nm resulted in the gradual decrease in the intensity of the new peaks (Fig 13c). The sample could be irradiated with the light at 365 nm again until a photostationary state was reached (Fig 13d). Warming up the sample to 40 °C or leaving it in the dark overnight resulted in the disappearance of newly formed peaks and the restoration of the original spectrum (Fig 13e).
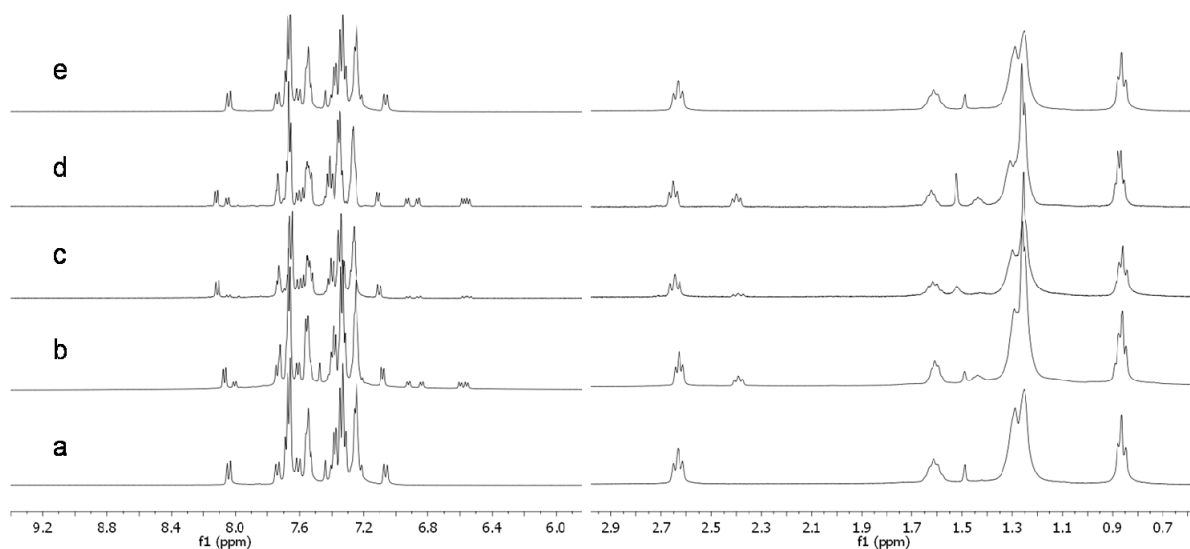
Figure 13. ^{1}H–NMR spectra of switch **1b**, in CDCl$_3$, at –10 °C (irradiation was performed at 4 °C); **a:** in the dark, **b:** sample from **a** irradiated at 365 nm overnight, **c:** sample from **b** irradiated at 312 nm for 2 h, **d:** sample from **c** irradiated at 365 nm for 3 h, **e:** sample from **d** left in the dark at room temperature overnight.

It should be noted that the NMR experiments were performed in CDCl$_3$ whereas the UV–Vis experiments were conducted in *n*-heptane. The same trends in isomerization behaviour were observed, however, by means of both spectroscopic methods and are in accordance with those of other azobenzene compounds[47,48].

The NMR signals that shift (most) upon irradiation are those corresponding to the protons that are in immediate vicinity of the azobenzene unit that undergoes the isomerization process. As seen in Fig 13, the new aromatic signals appearing upon irradiation are the five doublets at 8.05, 6.93, 6.86, 6.58 and 6.55 ppm. The doublet at 8.05 ppm corresponds to a proton in the carbazole unit which shifts only moderately from its parent signal (8.12 ppm) upon irradiation. The other four newly formed doublet signals correspond to the aromatic signals of the *Z*–azobenzene unit; although the corresponding signals of the *E*–azobenzene unit could not be identified due to overlap with other aromatic signals, it is obvious from Fig 13 that they shift to a higher extent upon irradiation (compared to the doublet at 8.12 ppm) which is expected since they are in the immediate vicinity of the N=N group undergoing isomerization. There are also some changes in the aliphatic region of the spectrum however (Fig 13). Much like it was the case with **1a** as well as with molecules **1** and **2** discussed in Chapter 2, all of the protons in the alkyl chain in **1b** undergo change upon irradiation; the closer they are to the azobenzene unit, the more they change (the signal at 2.65 ppm corresponding to methylene group attached directly to the azobenzene group shifts to 2.40 ppm, the one at 1.62 ppm corresponding to the adjacent methylene group shifts to 1.44 ppm, the signal at 0.88 ppm corresponding to the terminal methyl group shifts to 0.87 ppm).

Kinetics of the thermal isomerization

As already observed by both UV−Vis and NMR spectroscopic techniques, the *Z*−isomer may be isomerized to the *E*−isomer photochemically (irradiation with UV light at 312 nm) or thermally. The thermal step is driven by the relative instability of the *Z*−isomer[47,48]. This means that, if kept in the absence of light, the less stable *Z*−isomer will spontaneously isomerize to the more stable *E*−isomer. The rate of the thermal process depends on temperature[48].

UV−Vis spectroscopic study

Temperature dependent UV−Vis spectroscopy was used to follow the kinetics of the *Z* to *E* thermal isomerization process in **1b** (Fig 14).
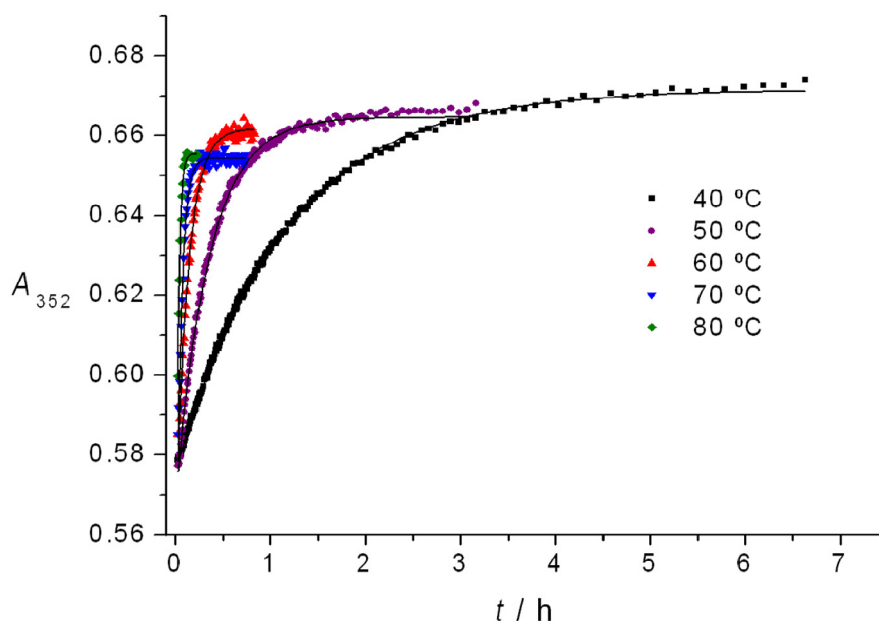
Figure 14. The data points collected by following the absorbance at 352 nm of a sample of **1b** over time at different temperatures, c = 1.4·10^{-5} mol dm^{-3} in *n*-heptane, and the calculated values (−) as obtained by nonlinear regression analyses.

A sample of a solution of **1b** in *n*-heptane was irradiated with light at 365 nm to the photostationary state and the absorbance was followed over time in the region of maximum change (λ = 352 nm) in the temperature range 40 − 80 °C. The collected data were fitted to the exponential function assuming first-order kinetics for the thermal step[49]. The collected data as well the fits are shown in Fig 14 and the parameters from the fits are given in Table 3.

Table 3. The half-lives of the thermal isomerization of **1b**, $t_{1/2}$, at different temperatures as obtained from the regression analyses of the data in Fig 14.

Θ / °C	$t_{1/2}$ / min	R^2
40	48	0.999
50	15	0.998
60	5.3	0.995
70	2.2	0.992
80	1.1	0.994

From Table 3 it can be seen that the half-life for the thermal isomerization of **1b**, $t_{1/2}$, ranges from 48 min at 40 °C to 1.1 min at 80 °C which seems to agree well with the values obtained for **1a**.

The data from Table 3 can be further analyzed according to the Eyring equation to obtain the activation parameters, $\Delta^{\ddagger}H$ and $\Delta^{\ddagger}S$ (Fig 15).
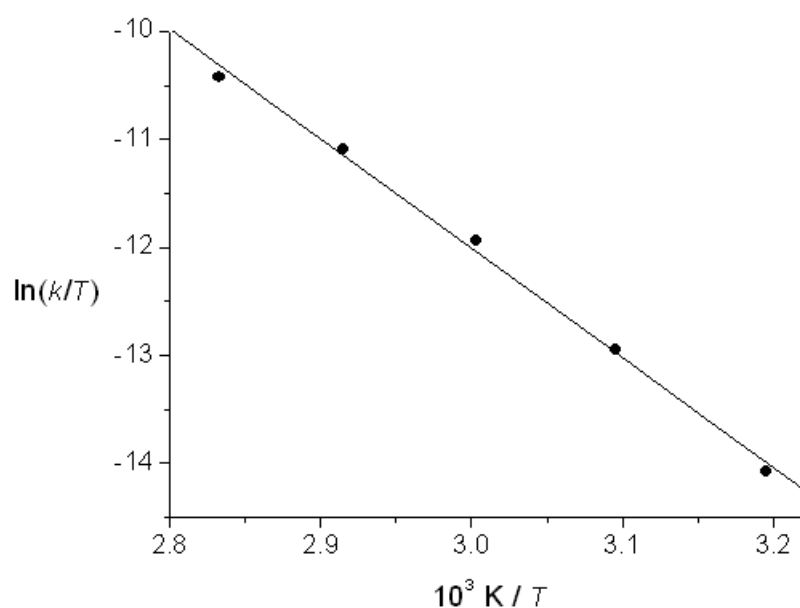
Figure 15. The data points from Table 3 (thermal isomerization of **1b**) analyzed according to the Eyring equation and the calculated values (–) as obtained by linear regression analysis.

From the analysis in Fig 15 the following activation parameters were obtained for **1b**: $\Delta^{\ddagger}H = (85 \pm 3)$ kJ mol^{-1}, $\Delta^{\ddagger}S = - (43 \pm 10)$ J K^{-1} mol^{-1}. The values obtained here are in good agreement with the values obtained for **1a** ($\Delta^{\ddagger}H = (85 \pm 2)$ kJ mol^{-1},

$\Delta^{\ddagger}S = -(41 \pm 7)$ J K^{-1} mol^{-1}). It appears that the different position of the wheels does not significantly influence the kinetics of the thermal isomerization. The activation parameters allow for the calculation of the half-life for the thermal isomerization at 25 °C, $t_{1/2} = 4.3$ h which is also not much different than the half-life for **1a** (3.4 h, as calculated for 25 °C).

NMR spectroscopic study

The kinetics of the thermal isomerization was also followed by ^{1}H–NMR spectroscopy. The sample of **1b** in CD$_2$Cl$_2$ was irradiated at 365 nm at 4 °C until the photostationary state was reached. An ^{1}H–NMR spectrum was taken every 15 min at different temperatures in the range 5 – 35 °C. The spectra obtained at 23.0 °C as a function of time are depicted in Fig 16.

a   **b**
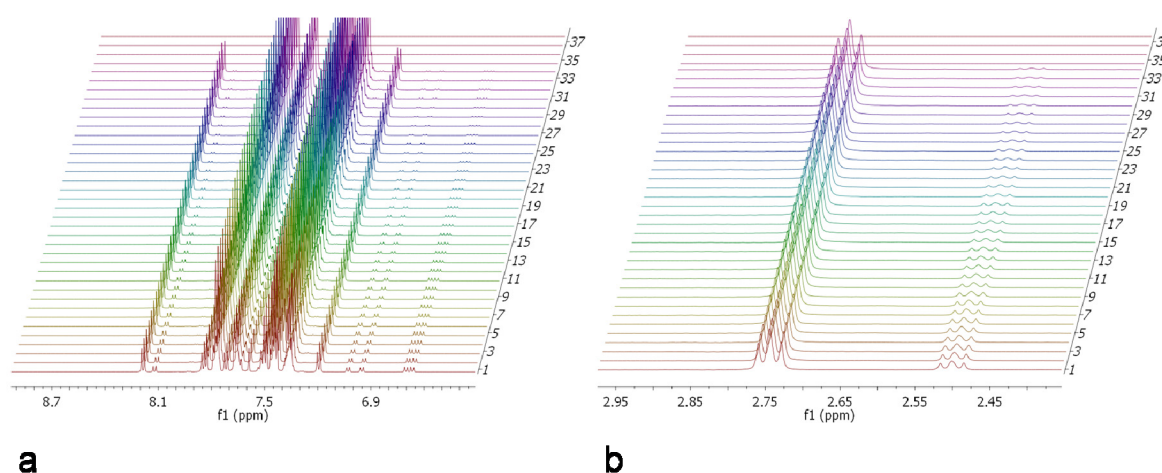
Figure 16. Arrayed ^{1}H–NMR spectra (CD$_2$Cl$_2$, 23.0 °C) of a sample of **1b** over time. The sample is obtained by irradiating the solution at $\lambda = (365 \pm 20)$ nm. A spectrum was taken every 15 min (the numbers on the y-axis are experiment numbers). **a:** Aromatic region, **b:** Part of the aliphatic region.

The arrayed spectra, shown in Fig 16, and similar arrayed spectra at other temperatures, were used to obtain the ratio of the molar concentrations of *E*-**1b** and *Z*-**1b**, *r*, at different points in time. The data obtained at different temperatures in the range 0 – 35 °C were analyzed according to equation 5 and shown along with the fitted lines in Fig 17.
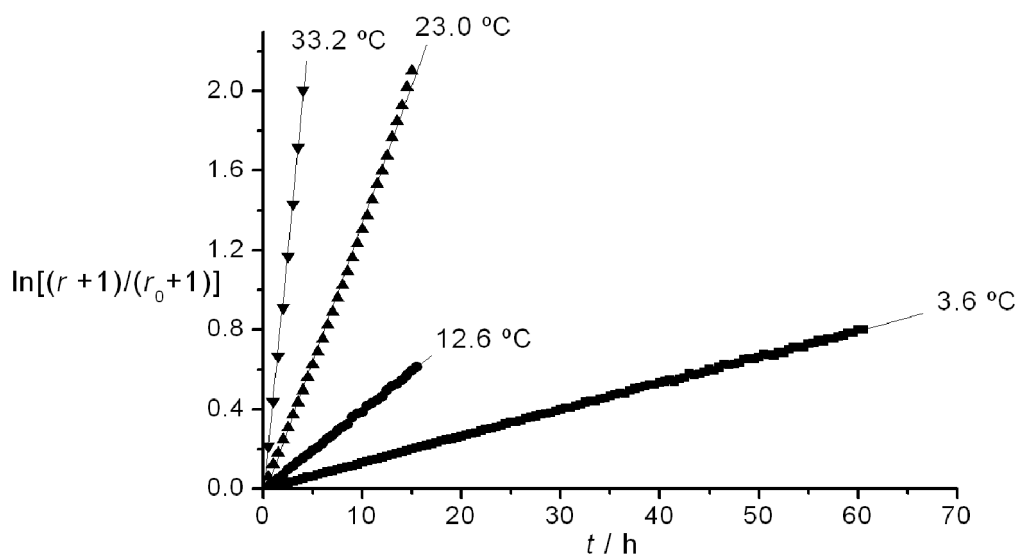
Figure 17. Monitoring the ratio of molar concentrations of *E*–**1b** and *Z*–**1b**, *r*, over time by ^{1}H–NMR, in CD_2Cl_2, at different temperatures, after irradiating the solution at $\lambda = (365 \pm 20)$ nm. The data points are taken from the arrayed NMR spectra like the one depicted in Fig 16. (–) Calculated by linear regression according to eq 5.

According to equation 5 the slope of a straight line in Fig 17 is equal to the rate constant, *k*, at that temperature. The rate constants, converted into half-lives, $t_{1/2}$, are given in Table 4.

Table 4. The half-lives, $t_{1/2}$, at different temperatures as obtained from the regression analyses of the data in Fig 17.

Θ / °C	$t_{1/2}$ / h	R^2
3.6	52	0.999
12.6	17	0.999
23.0	5	0.998
33.2	1.4	0.997

As shown in Table 4, the half-lives for the thermal isomerization of *Z*–**1b** to *E*–**1b** in CD_2Cl_2 are in the range from 52 to 1.4 h in the temperature range 0 – 35 °C (as compared to 48 – 1 min in the temperature range 40 – 80 °C, Table 3).

The data from Table 4 may be further analyzed according to the Eyring equation in order to obtain the activation parameters, $\Delta^{\ddagger}H$ and $\Delta^{\ddagger}S$ (Fig 18).
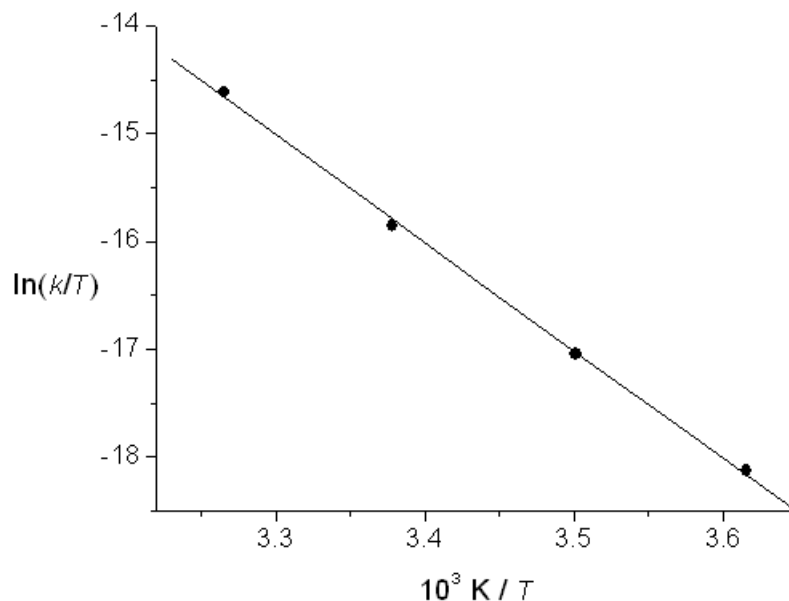
Figure 18. The data points from Table 4 analyzed according to the Eyring equation and the calculated values (–) as obtained by linear regression analysis.

From the analysis in Fig 18 the following activation parameters were obtained: $\Delta^{\ddagger}H$ = (83 ± 2) kJ mol^{-1}, $\Delta^{\ddagger}S$ = – (48 ± 8) J K^{-1} mol^{-1}. These data agree well with the values obtained from the UV–Vis spectroscopic study; $\Delta^{\ddagger}H$ = (85 ± 3) kJ mol^{-1}, $\Delta^{\ddagger}S$ = – (43 ± 10) J K^{-1} mol^{-1}, especially considering that the measurements in the UV–Vis spectroscopic study were performed in *n*-heptane whereas the measurements in the NMR study were carried out in CD$_2$Cl$_2$. The activation parameters were used to calculate the half-life at 25 °C obtaining the values of 4.2 h in CD$_2$Cl$_2$ and 4.3 h in *n*-heptane.

The values obtained by the two spectroscopic techniques agree well for both **1a** and **1b**. This means that the kinetics of the thermal isomerization are not much affected by the solvent. Furthermore, molecules **1a** and **1b** appear to exhibit the same kinetic behaviour with practically the same values for activation parameters and half-lives. This shows that the position of the wheels on the carbazole core has little influence on the behaviour of the azobenzene group in the thermal isomerization process, as expected from the design (Fig 3). The photostationary state after irradiation at 365 nm, however, appears to be richer in the *Z*–isomer for **1a** than for **1b** (44 % *vs* 33 %). Also, the photostationary states of **1a** and **1b** contain less of the *Z*–isomer than the multiazobenzene molecules studied in Chapter 2 (around 70 %). The photostationary states (30 – 40 % of the *Z*–isomer) agree with those reported for oligo(phenylene ethynylene)-based azobenzene compounds[31].

Proposed mechanism of the thermal isomerization

The photoisomerization and the thermal isomerization of azobenzenes are thought to proceed via one of the two mechanisms; the rotation mechanism or the inversion mechanism[47,54]. As depicted in Fig 19, the former mechanism involves rotation about the N–N bond weakened by electronic excitation whereas the latter one involves a rehybridization of the N–atom from an sp^2 state to an sp^1 state with only minor change in the azo π bond order.
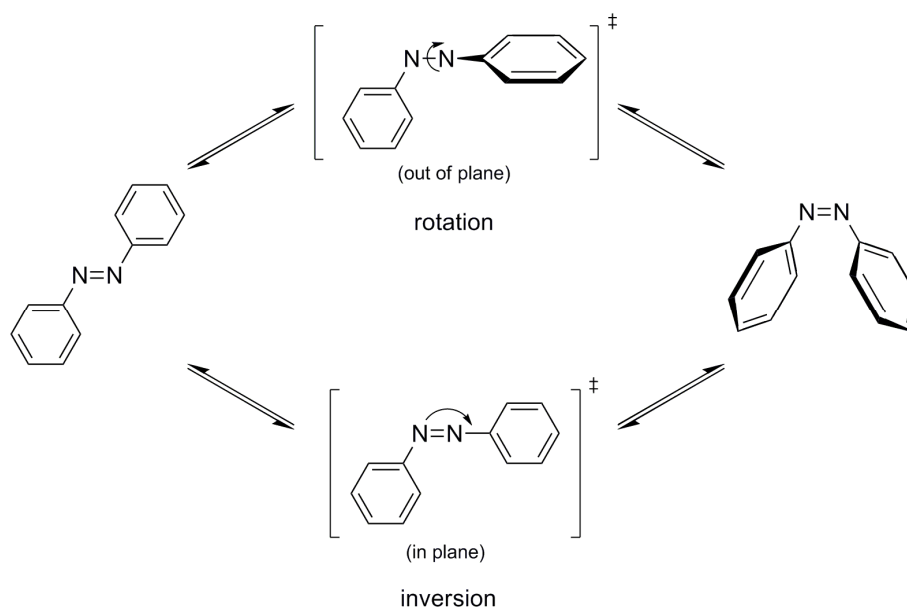
Figure 19. Two mechanisms for the isomerization of azobenzene; rotation and inversion.

This is covered more elaborately in Chapter 2. The isokinetic plots, like the ones in Fig 20, are normally used to determine the mechanism of the thermal isomerization process[55,56,57]. The plot from Fig 20 is taken from the literature[56]; the data points used to make the plots are simple azobenzene compounds studied previously[50,55,56].
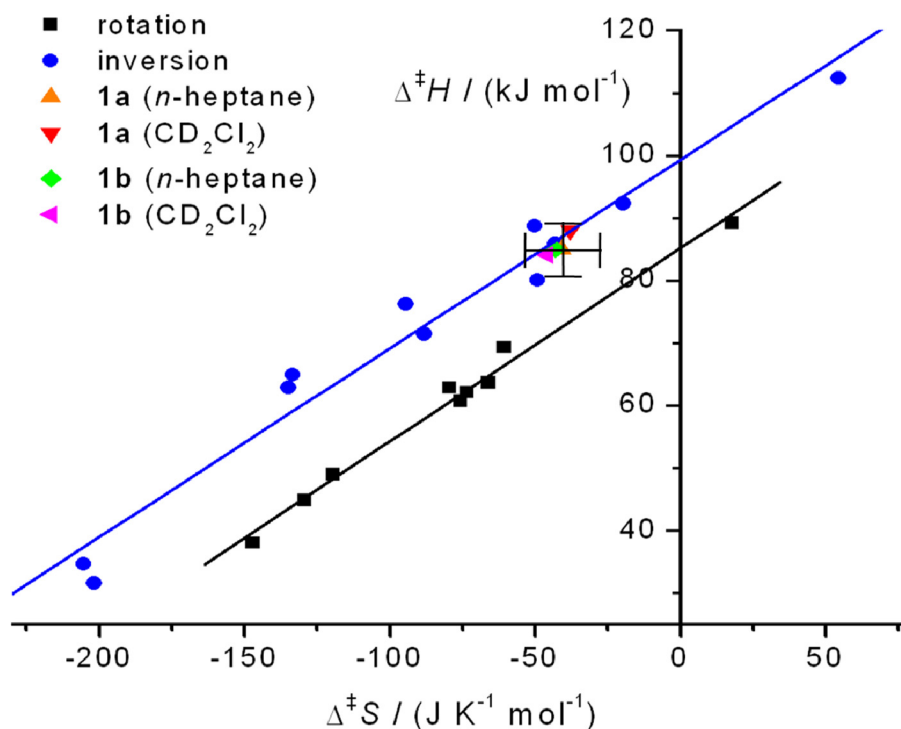
Figure 20. Isokinetic plots for the thermal isomerization of azobenzene derivatives; the data points used to make the plots are given and further referenced in the study by Wazzan[56]. The data points obtained for compounds **1a** and **1b** are highlighted in orange, red, green and pink and the uncertainty highlighted in black corresponds to the measurement with the highest determined uncertainty.

As can be seen from Fig 20, the azobenzene compounds **1a** and **1b** studied here (both in *n*-heptane and CD_2Cl_2) are collinear with the points corresponding to azobenzene compounds that follow the inversion pathway during the thermal isomerization step. This is not surprising since the two molecules do not bear any strongly electron−donating or electron−withdrawing groups which seems to be a prerequisite for the process to proceed via the rotation mechanism[51,56]. It is interesting to note, however, that the extended conjugation of the azobenzene groups in **1a** and **1b** does not appear to have any influence on the mechanism of the thermal isomerization of this switching group.

The mechanism of isomerization may prove to be of outmost importance for the development of azobenzene-equipped molecules for propulsion on a surface. If the photoinduced *E*−to−*Z* isomerization of an azobenzene group proceeds via a rotation pathway while the thermal *Z*−to−*E* isomerization follows an inversion pathway[58], the combination of the two processes may lead to the switching motion accompanied by translational motion. This could provide the driving force for the movement of such molecules on a surface[27]. Care should be taken, however, in designing molecules for surface-related purposes as molecular properties may prove to be quite different

on a surface than in solution; it has already been shown for azobenzene compounds that the activation parameters have different values on surfaces than in solution[59,60]. It remains a question, however, whether isomerization processes will follow the same mechanism on a surface as in solution[61]. The study of the kinetics of the thermal isomerization of **1a** and **1b** on a surface might therefore prove rather insightful; molecules **1a** and **1b** might show different behaviour on a surface than in solution (different mechanism of thermal isomerization with different half-lives). More understanding of the differences between the solution- and surface-behaviour of molecules will therefore be highly beneficial for the design of new generations of nanovehicles.

*Preliminary surface studies of molecules **1a** and **1b***

Molecule **1a** was dissolved in 1-phenyloctane (c = 1 mmol dm^{-3}) and the solution was dropcast on freshly cleaved HOPG surface. The solid/liquid interface was examined by scanning tunneling microscopy (STM). The HOPG surface could be observed with atomic resolution. Molecules of **1a** could, however, not be observed under the conditions used. Further surface studies of **1a** and **1b** at the solid/liquid interface are ongoing as well as investigation of single molecules under ultrahigh vacuum conditions.

Conclusions

In an attempt to contribute to the development of light-propelled nanovehicles, we have designed two new molecules. They consist of a carbazole core, an azobenzene switching group and two triphenylsilyl wheels; the two molecules differ in the position of the wheels on the carbazole unit. With this design we wish to test the utility of the new molecular wheel as well as of the azobenzene group for the development of surface-traversing molecules. The molecules were successfully prepared through a convergent synthetic route. The photochemical properties of both molecules were extensively studied in solution by UV−Vis and NMR spectroscopic techniques. They exhibit typical azobenzene switching behaviour; the azobenzene group can be photoisomerized between the *E*− and *Z*−isomeric forms and the *Z*−azobenzene group can also be thermally isomerized to the more stable *E*−isomer. For both molecules up to 30 − 40 % of the *Z*−isomer was observed upon irradiation at 365 nm. The kinetics of the thermal isomerization process at different temperatures were studied in two different solvents by two different spectroscopic techniques and the half-lives in the range 3 − 8 h at room temperature were obtained. The activation parameters could also be obtained from the kinetic study revealing the inversion mechanism as the dominant pathway for the thermal isomerization of these molecules in solution. The parameters were found to be solvent-independent. It is worth noting that the two new molecules have very similar photochemical properties (photostationary states, half-lives and activation parameters for the thermal isomerization, etc). As expected, it appears that the

azobenzene group is not severely influenced by the position of the wheels on the carbazole unit.

The two molecules have retained the basic azobenzene properties. The half-life of several hours (at room temperature) for the thermal isomerization would allow the isomerization process to be followed on the surface. All these properties combined make the new molecules very good candidates for surface studies.

Preliminary surface studies on one of the molecules were conducted at the solid/liquid interface but no molecules have been observed up to now. Further investigations are ongoing, both at the solid/liquid interface as well as under ultrahigh vacuum.

Acknowledgements

The preliminary STM measurements of **1a** described in this chapter were carried out by Xiaoyan Zhang and Arjen Cnossen who are acknowledged for their contributions.

Experimental section

Synthesis, characterization and physico–chemical measurements

General remarks

The experiments were performed as described in the section *General Remarks* in Chapter 2.

3,6-dibromo-9-(1,2-dichlorovinyl)-9*H*-carbazole 3a: A suspension of 3,6-dibromocarbazole **2a** (3.0 g, 9.2 mmol), n-Bu$_4$N$^+$Cl$^-$ (256 mg, 0.9 mmol), t-BuOK (3.1 g, 28 mmol) and trichloroethylene (2.5 ml, 28 mmol) in toluene (300 ml) was vigorously stirred at reflux and under a nitrogen atmosphere. The progress of the reaction could be followed by TLC (n-pentane/AcOEt 30:1). The reaction was typically complete after 1-1.5 h. The solvent was evaporated and the residue was suspended in dichloromethane (200 ml) and filtered through a plug of silica. The solvent was evaporated affording **3a** (3.3 g) in 87 % yield. The product may be additionally purified for analytical purposes by means of column chromatography on silica using n-pentane/AcOEt 30:1 as eluent.

^{1}H NMR (500 MHz, CDCl$_3$): δ 8.05 (s, 2H), 7.54 (d, J = 8.4 Hz, 2H), 7.22 (d, J = 8.4 Hz, 2H), 6.75 (s, 1H). ^{13}C NMR (125 MHz, CDCl$_3$): δ 137.40, 130.07, 126.28, 124.97, 123.59, 118.27, 115.09, 112.66. HRMS (APCI): m/z calculated for C$_{14}$H$_8$Br$_2$Cl$_2$N$^+$: 419.83801 [M+H]$^+$, found 419.82697 [M+H]$^+$.

2,7-dibromo-9-(1,2-dichlorovinyl)-9*H*-carbazole 3b: A suspension of 2,7-dibromocarbazole **2b** (1.5 g, 4.6 mmol), n-Bu$_4$N$^+$Cl$^-$ (128 mg, 0.5 mmol), t-BuOK (1.6 g, 14 mmol) and trichloroethylene (1.25 ml, 14 mmol) in toluene (400 ml) was

vigorously stirred at reflux and under a nitrogen atmosphere. The progress of the reaction could be followed by TLC (silica, *n*-pentane/AcOEt 30:1). The reaction was complete after 2 h. The solvent was evaporated and the residue was suspended in AcOEt (100 ml) and filtered through a plug of silica. The solvent was evaporated affording **3b** (1.8 g) in 91 % crude yield. The crude material was used directly in the following step.

^{1}H NMR (400 MHz, CDCl$_3$): δ 7.87 (d, *J* = 8.2 Hz, 2H), 7.54 (s, 2H), 7.46 (d, *J* = 8.3 Hz, 2H), 6.86 (s, 1H).

3,6-dibromo-9-ethynyl-9*H*-carbazole 4a: Compound **3a** (1.7 g, 4.0 mmol) was dissolved in dry Et$_2$O (170 ml) with stirring, at −40 °C and under an argon atmosphere. A solution of *n*-BuLi in hexanes (*c* = 1.6 mol dm^{-3}; 5.5 ml, 8.8 mmol) was slowly added. The temperature was slowly raised to 0 °C and the reaction mixture was stirred for 3 h at that temperature. The temperature was then lowered to −20 °C and the reaction was quenched by adding a saturated aqueous solution of NaCl (50 ml). To this AcOEt (100 ml) was added and the layers were separated. The organic extracts were dried on anhydrous Na$_2$SO$_4$, the salt was removed by filtration and the solvent was evaporated affording **4a** as a brown solid (1.4 g) in 99 % yield.

^{1}H NMR (500 MHz, CDCl$_3$): δ 8.05 (d, *J* = 1.6 Hz, 2H), 7.61 (dd, *J* = 8.6, 1.4 Hz, 2H), 7.48 (d, *J* = 8.6 Hz, 2H), 3.45 (s, 1H). ^{13}C NMR (75 MHz, CDCl$_3$): δ 139.48, 130.45, 124.06, 123.55, 115.61, 112.99, 63.74, 63.60. HRMS (APCI): *m/z* calculated for C$_{14}$H$_8$Br$_2$N$^+$: 349.90030 [M+H]$^+$, found 349.89986 [M+H]$^+$; *m/z* calculated for C$_{28}$H$_{15}$Br$_4$N$_2$$^+$: 698.79278 [2M+H]$^+$, found 698.79237 [2M+H]$^+$.

2,7-dibromo-9-ethynyl-9*H*-carbazole 4b: Compound **3b** (1.75 g, 4.20 mmol) was dissolved in dry Et$_2$O (175 ml) with stirring, at −40 °C and under an argon atmosphere. A solution of *n*-BuLi in hexanes (*c* = 1.6 mol dm^{-3}; 5.8 ml, 9.2 mmol) was slowly added. The temperature was slowly raised to 0 °C and the reaction mixture was stirred for 2.5 h at that temperature. The temperature was then lowered to −20 °C and the reaction was quenched by adding a saturated aqueous solution of NaCl (50 ml). To this AcOEt (100 ml) was added and the layers were separated. The organic extracts were dried on anhydrous Na$_2$SO$_4$, the salt was removed by filtration and the solvent was evaporated. The crude product was purified by column chromatography using *n*-pentane/AcOEt 60:1 as eluent to afford an off-white solid (461 mg) in a 31 % yield. Product **4b** appears to undergo degradation during column chromatography so this purification step should be omitted if possible.

^{1}H NMR (400 MHz, CDCl$_3$): δ 7.84–7.70 (m, 4H), 7.45 (d, *J* = 8.3 Hz, 2H), 3.46 (s, 1H). ^{13}C NMR (100 MHz, CDCl$_3$): δ 141.24, 126.04, 121.83, 121.60, 120.88, 114.75, 63.90 (2C). HRMS (APCI positive mode): *m/z* calculated for C$_{14}$H$_8$Br$_2$N$^+$: 349.90030 [M+H]$^+$, found 349.89889 [M+H]$^+$; (negative mode) *m/z* calculated for C$_{14}$H$_6$Br$_2$N$^-$: 347.88465 [M-H]$^-$, found 347.88239 [M-H]$^-$.

1-nitroso-4-octylbenzene 6: A solution of 4-octylaniline **5** (2.0 g, 9.8 mmol) in dichloromethane (130 ml) was mixed with an aqueous solution of oxone (2 KHSO$_5$ · KHSO$_4$ · K$_2$SO$_4$) (12.0 g, 19.6 mmol in 130 ml of distilled water) at room temperature and under an argon atmosphere. The reaction mixture was stirred vigorously overnight. The layers were separated and the aqueous layer was extracted with dichloromethane (100 ml). The combined organic layers were washed with hydrochloric acid (aq, c = 2 mol dm^{-3}, 100 ml) and a saturated aqueous NaHCO$_3$ solution (100 ml). The organic layer was dried on anhydrous Na$_2$SO$_4$, the salt was removed by filtration and the solvent was evaporated. The crude product (1.1 g) consisted of **6** and **5** in an approximate 2:1 ratio and was used directly in the next step. For analytical purposes the crude product could be purified by column chromatography on silica with petroleum ether 40–60 / dichloromethane 1:1 as eluent. Upon evaporation of the solvent the product was isolated as a green liquid.

^{1}H NMR (300 MHz, CDCl$_3$): δ 7.83 (d, J = 8.3 Hz, 2H), 7.39 (d, J = 8.3 Hz, 2H), 2.69 (t, J = 7.5 Hz, 2H), 1.65 (m, 2H), 1.42–1.17 (br, 10H), 0.88 (t, J = 6.6 Hz, 3H).

(*E*)-1-(4-iodophenyl)-2-(4-octylphenyl)diazene 7: Crude compound **6** (1.1 g with **6** to **5** ratio 2.3:1; 3.5 mmol **6**) was dissolved along with 4-iodoaniline (7.0 g, 32 mmol) in glacial acetic acid (120 ml) at room temperature and under an argon atmosphere. The reaction mixture was stirred for 7 h at room temperature. The acetic acid was evaporated and hydrochloric acid (aq, c = 2 mol dm^{-3}, 200 ml) and dichloromethane (200 ml) were added to the residue. The layers were separated and the organic extract were dried on anhydrous Na$_2$SO$_4$. The salt was removed by filtration and the solvent was evaporated. The crude product (2.9 g) was suspended in *n*-pentane and filtered. The filtrate was evaporated affording the product (1.47 g) in 36 % yield over two steps. For analytical purposes the product can be purified further by column chromatography using *n*-pentane as eluent. Product **7** was kept in the absence of light.

^{1}H NMR (400 MHz, CDCl$_3$): δ 7.85 (d, J = 8.4 Hz, 4H), 7.65 (d, J = 8.0 Hz, 2H), 7.32 (d, J = 7.9 Hz, 2H), 2.69 (t, J = 7.6 Hz, 2H), 1.66 (m, 2H), 1.43–1.19 (br, 10H), 0.90 (t, J = 6.4 Hz, 3H). ^{13}C NMR (100 MHz, CDCl$_3$): δ 152.17, 150.93, 147.15, 138.41, 129.28, 124.51, 123.14, 97.33, 36.09, 32.03, 31.42, 29.62, 29.45, 29.42, 22.83, 14.27. HRMS (APCI): *m*/*z* calculated for C$_{20}$H$_{26}$IN$_2$$^+$: 421.11407 [M+H]$^+$, found 421.11093 [M+H]$^+$.

(*E*)-3,6-dibromo-9-((4-((4-octylphenyl)diazenyl)phenyl)ethynyl)-9*H*-carbazole 8a: Compound **4a** (166 mg, 0.48 mmol) and **7** (200 mg, 0.48 mmol) were dissolved in a mixture of *i*-Pr$_2$NH (20 ml), THF (8.0 ml) and toluene (8.0 ml) under an argon atmosphere. To this solution CuI (6 mg, 0.033 mmol) and Pd(PPh$_3$)$_4$ (55 mg, 0.048 mmol) were added and the reaction mixture was stirred at room temperature overnight. The progress of the reaction could be followed by TLC using *n*-pentane/AcOEt 30:1 as eluent. An orange precipitate was collected by filtration and washed with cold *n*-heptane affording **8a** (116 mg). The filtrate was collected,

evaporated and crystallized from cold *n*-heptane affording a precipitate that was subsequently washed with cold *n*-heptane to afford more of **8a** (50 mg). The product was obtained in 54 % overall yield.

^{1}H NMR (500 MHz, CDCl$_3$): δ 8.12 (s, 2H), 7.95 (d, *J* = 8.1 Hz, 2H), 7.87 (d, *J* = 7.9 Hz, 2H), 7.73 (d, *J* = 8.1 Hz, 2H), 7.67 (d, *J* = 8.6 Hz, 2H), 7.61 (d, *J* = 8.6 Hz, 2H), 7.34 (d, *J* = 7.9 Hz, 2H), 2.70 (t, *J* = 7.6 Hz, 2H), 1.66 (m, 2H), 1.42–1.14 (br, 10H), 0.89 (t, *J* = 6.5 Hz, 3H). ^{13}C NMR (75 MHz, CDCl$_3$): δ 152.11, 151.10, 147.21, 139.51, 132.14, 130.52, 129.34, 124.70, 124.37, 123.70, 123.18, 123.15, 115.72, 113.16, 79.98, 75.71, 36.11, 32.04, 31.43, 29.62, 29.45, 29.41, 22.83, 14.26. HRMS (APCI): *m/z* calculated for C$_{34}$H$_{32}$Br$_2$N$_3^+$: 640.09630 [M+H]$^+$, found 640.09567 [M+H]$^+$; *m/z* calculated for C$_{68}$H$_{63}$Br$_4$N$_6^+$: 1283.18068 [2M+H]$^+$, found 1283.18014 [2M+H]$^+$.

(*E*)-2,7-dibromo-9-((4-((4-octylphenyl)diazenyl)phenyl)ethynyl)-9*H*-carbazole 8b: Compound **4b** (100 mg, 0.29 mmol) and **7** (120 mg, 0.29 mmol) were dissolved in a mixture of *i*-Pr$_2$NH (12 ml), THF (4.5 ml) and toluene (4.5 ml) under an argon atmosphere. To this solution CuI (2 mg, 0.010 mmol) and Pd(PPh$_3$)$_4$ (16 mg, 0.014 mmol) were added and the reaction mixture was stirred at room temperature overnight. The progress of the reaction could be followed by TLC using *n*-pentane/AcOEt 30:1 as eluent. The solvent was evaporated and the residue was suspended in hot *n*-heptane and filtered. The product was crystallized from *n*-heptane several times until a desired purity was achieved. Product **8b** was obtained as a waxy red solid in 65 % yield (119 mg).

^{1}H NMR (400 MHz, CDCl$_3$): δ 7.96 (d, *J* = 8.3 Hz, 2H), 7.88 (d, *J* = 8.1 Hz, 2H), 7.83 (s, 2H), 7.80 (d, *J* = 8.3 Hz, 2H), 7.74 (d, *J* = 8.3 Hz, 2H), 7.47 (d, *J* = 8.3 Hz, 2H), 7.34 (d, *J* = 8.1 Hz, 2H), 2.70 (t, *J* = 7.7 Hz, 2H), 1.67 (m, 2H), 1.42–1.17 (br, 10H), 0.89 (m, 3H). ^{13}C NMR (100 MHz, CDCl$_3$): δ 152.12, 151.08, 147.16, 141.18, 132.22, 129.31, 126.08, 124.52, 123.16 (2C), 122.05, 121.67, 120.91, 114.78, 79.47, 75.81, 36.11, 32.04, 31.45, 29.63, 29.47, 29.42, 22.85, 14.28. HRMS (APCI): *m/z* calculated for C$_{34}$H$_{32}$Br$_2$N$_3^+$: 642.09425 [M+H]$^+$, found 642.09316 [M+H]$^+$; *m/z* calculated for C$_{68}$H$_{63}$Br$_4$N$_6^+$: 1283.18068 [2M+H]$^+$, found 1283.17863 [2M+H]$^+$.

(*E*)-2,7-diiodo-9-((4-((4-octylphenyl)diazenyl)phenyl)ethynyl)-9*H*-carbazole 9b: Compound **8b** (223 mg, 0.35 mmol) was dissolved in 1,4-dioxane (23 ml) in a high-pressure tube and under an argon atmosphere. To this solution CuI (27 mg, 0.14 mmol), NaI (315 mg, 2.1 mmol) and *trans*−*N,N'*−dimethylcyclohexane−1,2-diamine (45 μl, 0.28 mmol) were added and the reaction mixture was stirred vigorously in a sealed high-pressure tube at 150 °C overnight. The reaction mixture was then filtered through a plug of silica (and flushed with dichloromethane) and the solvent was evaporated affording **9b** (242 mg) in 94 % crude yield. The crude product was used directly in the next reaction without further purification.

^{1}H NMR (300 MHz, CDCl$_3$): δ 8.03 (s, 2H), 7.97 (d, *J* = 8.5 Hz, 2H), 7.88 (d, *J* = 8.3 Hz, 2H), 7.80−7.63 (m, 14H), 7.34 (d, *J* = 8.3 Hz, 2H), 2.70 (t, *J* = 7.4 Hz, 2H), 1.66 (m, 2H), 1.43−1.19 (br, 10H), 0.89 (t, *J* = 6.6 Hz, 3H). ^{13}C NMR (75 MHz, CDCl$_3$): δ 152.09, 151.09, 147.11, 140.84, 132.22, 131.37, 129.29, 124.56, 123.16 (2C), 122.59, 121.86, 120.54, 91.82, 80.33, 75.77, 36.10, 32.02, 31.42, 29.61, 29.46, 29.41, 22.82, 14.26. HRMS (APCI): *m/z* calculated for C$_{34}$H$_{32}$I$_2$N$_3^+$: 736.06856 [M+H]$^+$, found 736.06744 [M+H]$^+$.

(*E*)-9-((4-((4-octylphenyl)diazenyl)phenyl)ethynyl)-3,6-bis((triphenylsilyl)ethynyl)-9*H*-carbazole 1a: Compound **8a** (110 mg, 0.17 mmol) and triphenylsilylacetylene (151 mg, 0.51 mmol) were dissolved in a mixture of *i*-Pr$_2$NH (8.3 ml) and THF (16.0 ml) under an argon atmosphere. To this solution CuI (5 mg, 0.024 mmol), Pd(OAc)$_2$ (8 mg, 0.034 mmol) and PPh$_3$ (18 mg, 0.068 mmol) were added and the reaction mixture was stirred at 60 °C for 68 hours. The progress of the reaction could be followed by TLC using *n*-pentane/AcOEt 12:1 as eluent. The solvent was evaporated and the crude product was purified by column chromatography using *n*-pentane/AcOEt 12:1 as eluent followed by repeated crystallizations from *n*-heptane affording the desired product (9 mg) in 5 % yield.

^{1}H NMR (500 MHz, CDCl$_3$): δ 8.38 (s, 2H), 7.80−7.75 (m, 10H), 7.64−7.54 (m, 8H), 7.49−7.33 (m, 20H), 7.28 (d, *J* = 8.4 Hz, 2H), 7.05 (d, *J* = 8.6 Hz, 2H), 2.66 (t, *J* = 7.6 Hz, 2H), 1.63 (m, 2H), 1.38−1.22 (br, 10H), 0.88 (t, *J* = 6.8 Hz, 3H). ^{13}C NMR (125 MHz, CDCl$_3$): δ 152.62, 151.02, 147.20, 139.17, 135.78, 135.69, 133.97, 132.67, 130.31, 130.01, 129.23, 128.20, 128.12, 125.12, 123.80, 123.25, 123.13, 116.77, 115.52, 111.78, 110.61, 105.69, 93.18, 87.82, 36.06, 32.01, 31.39, 29.58, 29.42, 29.38, 22.81, 14.26.

(*E*)-9-((4-((4-octylphenyl)diazenyl)phenyl)ethynyl)-2,7-bis((triphenylsilyl)ethynyl)-9*H*-carbazole 1b: Compound **9b** (233 mg, 0.317 mmol) and triphenylsilylacetylene (270 mg, 0.951 mmol) were dissolved in a mixture of Et$_3$N (10.0 ml) and THF (5.0 ml) under an argon atmosphere. To this solution CuI (0.6 mg, 0.0032 mmol) and Pd(PPh$_3$)$_4$ (18 mg, 0.016 mmol) were added and the reaction mixture was stirred at room temperature overnight (18 hours). The progress of the reaction could be followed by TLC using *n*-pentane/AcOEt 12:1 as eluent. The solvent was evaporated and the crude product was purified by column chromatography using *n*-pentane/AcOEt 7.5:1 as eluent followed by repeated crystallizations from *n*-heptane affording the desired product as a dark red solid (175 mg) in 53 % yield.

^{1}H NMR (400 MHz, CDCl$_3$): δ 8.04 (d, *J* = 8.0 Hz, 2H), 7.74 (d, *J* = 7.6 Hz, 2H), 7.67 (m, 12H), 7.61 (d, *J* = 7.9 Hz, 2H), 7.55 (m, 8H), 7.44 (s, 2H), 7.41−7.21 (m, 14H), 7.06 (d, *J* = 8.1 Hz, 2H), 2.66 (t, *J* = 7.6 Hz, 2H), 1.63 (m, 2H), 1.38−1.22 (br, 10H), 0.88 (t, *J* = 6.8 Hz, 3H). ^{13}C NMR (125 MHz, CDCl$_3$): δ 152.62, 151.03, 147.09, 139.12, 137.07, 135.76, 135.62, 133.69, 132.71, 130.18, 130.00, 129.21, 128.21,

128.10, 125.53, 124.47, 123.26, 123.11, 120.86, 120.74, 116.73, 115.23, 110.44, 105.87, 92.81, 89.43, 36.05, 32.01, 31.40, 29.59, 29.41, 29.38, 22.81, 14.26.

References

1. V. Balzani, A. Credi, M. Venturi *Molecular Devices and Machines – A Journey into the Nano World*, Wiley–VCH, Weinheim, Germany **2003**.

2. W. R. Browne, B. L. Feringa *Nature Nanotechnol.* **2006**, *1*, 25–35.

3. C. Joachim, G. Rapenne *ACS Nano* **2013**, *7*, 11–14.

4. B. L. Feringa *J. Org. Chem.* **2007**, *72*, 6635–6652.

5. D. Dulić, S. J. van der Molen, T. Kudernac, H. T. Jonkman, J. J. D. de Jong, T. N. Bowden, J. van Esch, B. L. Feringa, B. J. van Wees *Phys. Rev. Lett.* **2003**, *91*, 207402.

6. N. Katsonis, T. Kudernac, M. Walko, S. J. van der Molen, B. I. van Wees, B. L. Feringa *Adv. Mater.* **2006**, *18*, 1397–1400.

7. T. Kudernac, S. J. van der Molen, B. J. van Wees, B. L. Feringa *Chem. Commun.* **2006**, 3597–3599.

8. W. R. Browne, T. Kudernac, N. Katsonis, J. Areephong, J. Hjelm, B. L. Feringa J. *Phys. Chem. C* **2008**, *112*, 1183–1190.

9. M. Elbing, A. Błaszczyk, C. von Hänisch, M. Mayor, V. Ferri, C. Grave, M. A. Rampi, G. Pace, P. Samorì, A. Shaporenko, M. Zharnikov *Adv. Funct. Mater.* **2008**, *18*, 2972–2983.

10. G. Pace, V. Ferri, C. Grave, M. Elbing, C. von Hänisch, M. Zharnikov, M. Mayor, M. A. Rampi, P. Samorì *PNAS* **2007**, *104*, 9937–9942.

11. V. Ferri, M. Elbing, G. Pace, M. D. Dickey, M. Zharnikov, P. Samorì, M. Mayor, M. A. Rampi *Angew. Chem. Int. Ed.* **2008**, *47*, 3407–3409.

12. A. S. Kumar, T. Ye, T. Takami, B.–C. Yu, A. K. Flatt, J. M. Tour, P. S. Weiss *Nano Lett.* **2008**, *8*, 1644–1648.

13. M. Alemani, M. V. Peters, S. Hecht, K.–H. Rieder, F. Moresco, L. Grill *J. Am. Chem. Soc.* **2006**, *128*, 14446–14447.

14. B.-Y. Choi, S.–J. Kahng, S. Kim, H. Kim, H. W. Kim, Y. J. Song, J. Ihm, Y. Kuk *Phys. Rev. Lett.* **2006**, *96*, 156106.

15. J. Henzl, M. Mehlhorn, H. Gawronski, K.–H. Rieder, K. Morgenstern *Angew. Chem. Int. Ed.* **2006**, *45*, 603–606.

16. M. J. Comstock, N. Levy, A. Kirakosian, J. Cho, F. Lauterwasser, J. H. Harvey, D. A. Strubbe, J. M. J. Fréchet, D. Trauner, S. G. Louie, M. F. Crommie *Phys. Rev. Lett.* **2007**, *99*, 038301.

17. Y. Shirai, J.-F. Morin, T. Sasaki, J. M. Guerrero, J. M. Tour *Chem. Soc. Rev.* **2006**, *35*, 1043–1055.

18. G. Vives, J. M. Tour *Acc. Chem. Res.* **2009**, *42*, 473–487.

19. J. K. Gimzewski, C. Joachim *Science* **1999**, *283*, 1683–1688.

20. F. Chiaravalloti, L. Gross, K.–H. Rieder, S. M. Stojkovic, A. Gourdon, C. Joachim, F. Moresco *Nature Mater.* **2007**, *6*, 30–33.

21. K. L. Wong, G. Pawin, K.–Y. Kwon, X. Lin, T. Jiao, U. Solanki, R. H. J. Fawcett, L. Bartels, S. Stolbov, T. S. Rahman *Science* **2007**, *315*, 1391–1393.

22. L. Gross, K.–H. Rieder, F. Moresco, S. M. Stojkovic, A. Gourdon, C. Joachim *Nature Mater.* **2005**, *4*, 892–895.

23. L. Grill, K.–H. Rieder, F. Moresco, G. Rapenne, S. Stojkovic, X. Bouju, C. Joachim *Nature Nanotechnol.* **2007**, *2*, 95–98.

24. Y. Shirai, A. J. Osgood, Y. Zhao, K. F. Kelly, J. M. Tour *Nano Lett.* **2005**, *5*, 2330–2334.

25. A. V. Akimov, A. V. Nemukhin, A. A. Moskovsky, A. B. Kolomeisky, J. M. Tour *J. Chem. Theory Comput.* **2008**, *4*, 652–656.

26. Y. Shirai, A. J. Osgood, Y. Zhao, Y. Yao, Lionel Saudan, H. Yang, C. Yu-Hung, L. B. Alemany, T. Sasaki, J.–F. Morin, J. M. Guerrero, K. F. Kelly, J. M. Tour *J. Am. Chem. Soc.* **2006**, 128, 4854–4864.

27. T. Sasaki, J. M. Tour *Org. Lett.* **2008**, *10*, 897–900.

28. J.–F. Morin, Y. Shirai, J. M. Tour *Org. Lett.* **2006**, *8*, 1713–1716.

29. P.–T. Chiang, J. Mielke, J. Godoy, J. M. Guerrero, L. B. Alemany, C. J. Villagómez, A. Saywell, L. Grill, J. M. Tour *ACS Nano* **2012**, *6*, 592–597.

30. J.–F. Morin, T. Sasaki, Y. Shirai, J. M. Guerrero, J. M. Tour *J. Org. Chem.* **2007**, *72*, 9481–9490.

31. Y. Shirai, T. Sasaki, J. M. Guerrero, B.–C. Yu, P. Hodge, J. M. Tour *ACS Nano* **2008**, *2*, 97–106.

32. P.–L. E. Chu, L.–Y. Wang, S. Khatua, A. B. Kolomeisky, S. Link, J. M. Tour *ACS Nano* **2013**, *7*, 35–41.

33. G. Vives, J. H. Kang, J. F. Kelly, J. M. Tour *Org. Lett.* **2009**, *11*, 5602–5605.

34. J. Godoy, G. Vives, J. M. Tour *Org. Lett.* **2010**, *12*, 1464–1467.

35. K. Claytor, S. Khatua, J. M. Guerrero, A. Tcherniak, J. M. Tour, S. Link *J. Chem. Phys.* **2009**, *130*, 164710.

36. G. Vives, J. M. Guerrero, J. Godoy, S. Khatua, Y.-P. Wang, J. L. Kiappes, S. Link, J. M. Tour *J. Org. Chem.* **2010**, *75*, 6631–6643.

37. J. Godoy, G. Vives, J. M. Tour *ACS Nano* **2011**, *5*, 59–90.

38. T. Kudernac, N. Ruangsupapichat, M. Parschau, B. Maciá, N. Katsonis, S. R. Harutyunyan, K.–H. Ernst, B. L. Feringa *Nature* **2011**, *479*, 208–211.

39. J. Clayden, N. Greeves, S. Warren *Organic Chemistry* Oxford University Press, 2nd Ed., Oxford, UK, **2012**.

40. F. A. Garlichs–Zschoche, K. H. Dötz *Organometallics* **2007**, *26*, 4535–4540.

41. M. Sonntag, P. Strohriegl *Chem. Mater.* **2004**, *16*, 4736–4742.

42. J. Pielichowski, P. Czub *Synth. Comm.* **1995**, *25*, 3647–3654.

43. C. Cuniberti, G. Dellepiane, P. Piaggio, R. Franco, G. F. Musso, C. Dell'Erba, G. Garbarino *Chem. Mater.* **1996**, *8*, 708–713.

44. M. R. Tracey, Y. Zhang, M. O. Frederick, J. A. Mulder, R. P. Hsung *Org. Lett.* **2004**, *6*, 2209–2212.

45. R. Chinchilla, C. Nájera *Chem. Rev.* **2007**, *107*, 874–922.

46. A. Klapars, S. L. Buchwald *J. Am. Chem. Soc.* **2002**, *124*, 14844–14845.

47. E. Merino, M. Ribagorda *Beilstein J. Org. Chem.* **2012**, *8*, 1071–1090.

48. J. Griffiths *Chem. Soc. Rev.* **1972**, *1*, 481–493.

49. H. Rau *Photochemistry and Photophysics* (Ed: J. F. Rabek); CRC Press, Inc.; Boca Raton, FL, **1990**, *Vol. 2*, p.119.

50. P. D. Wildes, J. G. Pacifici, G. Irick Jr., D. G. Whitten *J. Am. Chem. Soc.* **1971**, *93*, 2004–2008.

51. T. Asano, T. Okada, S. Shinkai, K. Shigematsu, Y. Kusano, O. Manabe *J. Am. Chem. Soc.* **1981**, *103*, 5161–5165.

52. N. Nishimura, T. Sueyoshi, H. Yamanaka, E. Imai, S. Yamamoto, S. Hasegawa *Bull. Chem. Soc. Jpn.* **1976**, *49*, 1381–1387.

53. K. Matczyszyn, W. Bartkowiak, J. Leszczynski *J. Mol. Struct.* **2001**, *565–566*, 53–57.

54. J. García–Amorós, D. Velasco *Beilstein J. Org. Chem.* **2012**, *8*, 1003–1017.

55. C. R. Crecca, A. E. Roitberg *J. Phys. Chem. A* **2006**, *110*, 8188–8203.

56. N. Wazzan (2009) *Cis–Trans Isomerisation of Azobenzenes Studied by NMR Spectroscopy with In situ Laser Irradiation and DFT Calculations* PhD Thesis, University of Edinburgh, UK.

57. J. P. Otruba III, R. G. Weiss *J. Org. Chem.* **1983**, *48*, 3448–3453.

58. G. R. Mitchell, N. R. King *Macromol. Symp.* **1999**, *137*, 155–165.

59. M. Wolf, P. Tegeder *Surf. Sci.* **2009**, *603*, 1506–1517.

60. S. Hagen, P. Kate, M. Peters, S. Hecht, M. Wolf, P. Tegeder *Appl. Phys. A* **2008**, *93*, 253–260.

61. M. J. Comstock, D. A. Strubbe, L. Berbil–Bautista, N. Levy, J. Cho, D. Poulsen, J. M. J. Fréchet, S. G. Louie, M. F. Crommie *Phys. Rev. Lett.* **2010**, *104*, 178301.

Chapter 4

Molecular Multiswitches on Wheels

*This chapter describes a new design of a light-driven surface-traversing molecule. The molecule features two wheels and two azobenzene switching units. As the azobenzene switches are known for their ability to act in concert and provide work, the newly designed molecule, equipped with two switching units, is envisaged to display different surface-behaviour than the molecules discussed in Chapter 3.*

Introduction

In the course of the development of surface-traversing nanovehicles, azobenzene compounds have also been envisaged to provide the means of propelling these molecules[1,2,3]. The unique switching behaviour between the *E*– and *Z*–isomers of these groups is accompanied by a severe geometric change as well as a significant change in the dipole moment of the azobenzene moiety[4]. Furthermore, the photochemical and thermal isomerization normally proceed via different pathways and a combination of the two processes may lead to a switching motion accompanied by translational motion[2,5]. For these reasons azobenzene groups have been considered good candidates for providing the driving force for the movement of such azobenzene-equipped molecules as well as for building other dynamic molecular devices[4].

It has been demonstrated that the collective nature of the azobenzene isomerization may be harnessed to provide measurable work[6,7]. This means that multiple azobenzene units may act in concert. It might therefore prove beneficial to use multiazobenzene systems to provide the driving force for the propulsion of nanovehicles. This idea of multiple molecular engines has also been used in the design of the first electrically driven nanocar[8]; the nanovehicle is equipped with a total of four molecular motors which provide the driving force for the motion of the molecule on the surface (Fig 1a). For this molecule directional motion has clearly been demonstrated. For a nanovehicle equipped with a single molecular motor (Fig 1b), however, no such observations have been reported[9,10]. The use of the collective nature of four molecular motors in the former design might have been the crucial point that led to its successful propulsion.

a   b
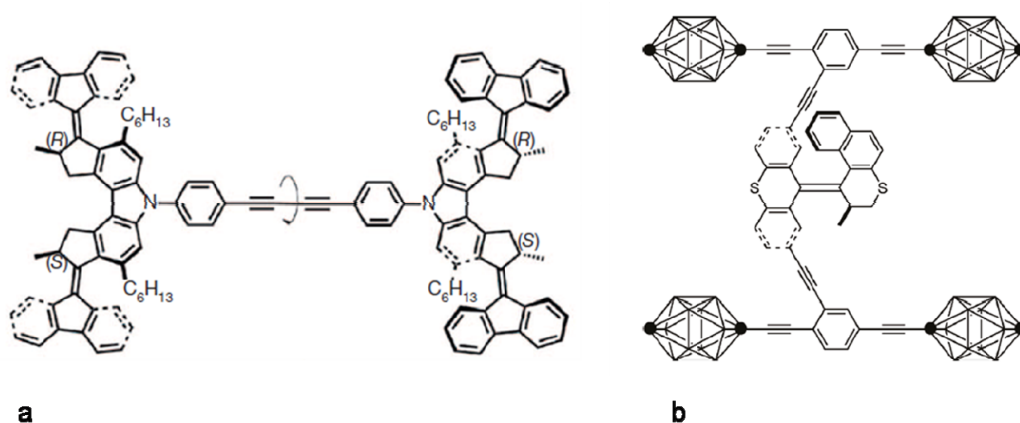
Figure 1. Recent designs of nanovehicles; **a:** nanocar equipped with four molecular motors, **b:** nanocar equipped with four carborane wheels and a single rotary motor.

In order to get more insight into the behaviour of nanovehicles on surfaces and to find out if the collective nature of the azobenzene switching process may be utilized for the movement of these molecules across surfaces, we have designed molecules bearing two azobenzene groups, as shown in Fig 2.

1a (X = O)
1b (X = −)

2
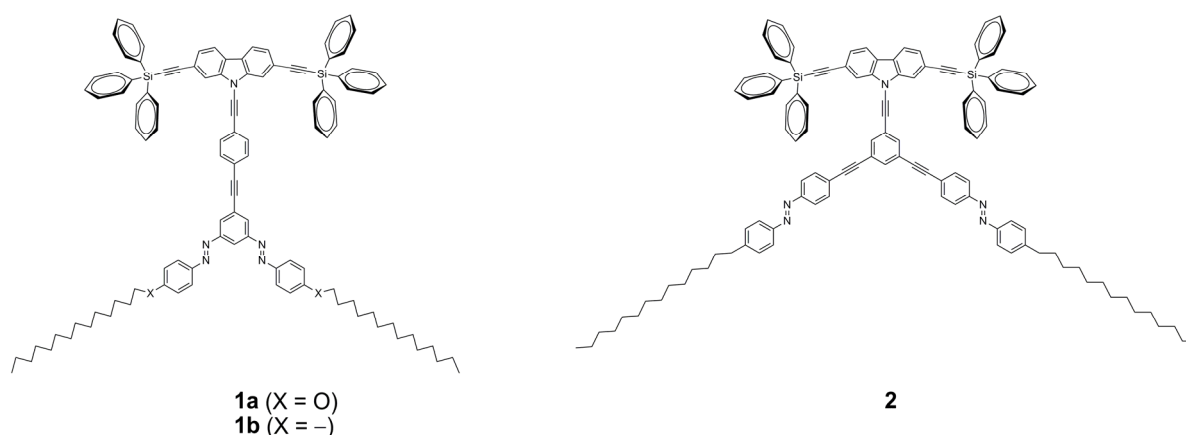
Figure 2. Design of molecules **1a,b** and **2**.

Molecules **1a** and **1b** have a bisazobenzene group; two azobenzene groups sharing a benzene ring. Molecule **2**, on the other hand, has two separate azobenzene groups (Fig 2). The remaining parts of the molecules are taken over from the design we introduced in Chapter 3; a carbazole core bearing two triphenylsilylethynyl groups serving as wheels. We have arbitrarily chosen to make the molecules with the wheels at positions 2 and 7 in the carbazole unit. Making the isomers with the wheels positioned at C−atoms 3 and 6 in the carbazole would be equally interesting and will be considered in the future. At this point, however, we would just like to investigate the molecular design with two azobenzene groups regardless of the position of the wheels.

Figure 3 depicts a possible behaviour of molecules **1a,b** or **2** upon switching on a surface. Once irradiated, one of the two azobenzene units switches causing a slight change in the position of the molecule on the surface. The switching of the second azobenzene unit makes a similar movement. Following this pattern the molecule might move across the surface one step at a time. It should be noted, however, that the motion of molecules is not expected to display any net directionality.
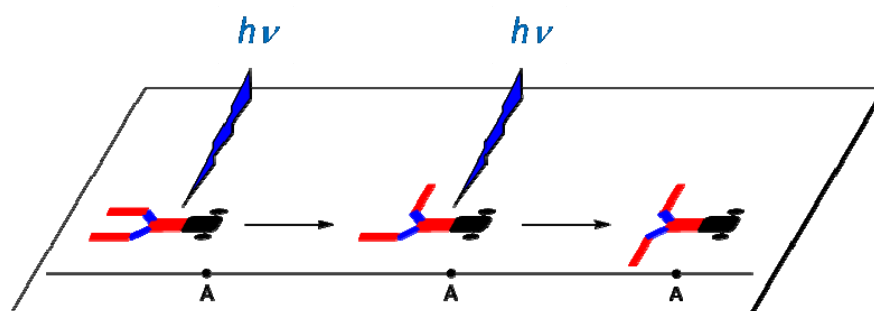
Figure 3. A schematic representation of molecules **1a,b** or **2** moving on a surface as a result of the sequential switching of the azobenzene groups.

It would be interesting to see if different designs of **1a,b** and **2** made a difference in the behaviour of these molecules on a surface; the azobenzene groups in molecules **1a** and **1b** share the central benzene ring whereas molecule **2**

possesses two separate azobenzene groups. In **1a**,**b** the group undergoing structural perturbation upon irradiation is located more centrally in the molecule than is the case in **2**. Would this make it easier to transfer the structural change of the switching unit onto the wheels and the rest of the molecule? Or would two separate switching units located on the sides of molecule **2** do a better job pushing the molecule forward (or backward)? Most importantly we would like to address the question of having multiple switching units in the molecule as opposed to having a single one; will multiple units benefit propulsion? To this end we would like to compare surface−behaviour of molecules **1a**,**b** and **2** to the behaviour of those discussed in Chapter 3.

Before any surface-studies are underway, however, the molecules need to be investigated in solution. Apart from azobenzene-containing dendrimeric structures[11,12], multiazobenzene compounds have not been studied extensively in solution[13,14,15,16]. Bisazobenzene and trisazobenzene compounds, comprising two or three azobenzene groups with a joint central benzene ring, have been reported but their switching behaviour has only scarcely been investigated[17,18,19,20,21,22,23]. Furthermore, there have been reports of photochemical quenching when multiple azobenzene groups are present in a molecule[24,25,26]. For this reason it is of utmost importance to first study the novel molecules in solution.

Our primary objectives are therefore to synthesize compounds **1a**,**b** and/or **2**, characterize them and study their switching properties in solution. This should allow us to compare the behaviour of these novel molecules to their monoazobenzene analogues discussed in Chapter 3. It will be interesting to see if the photochemical properties change in the presence of an additional azobenzene unit. Ultimately, we would like to study these molecules on a surface and compare their surface−behaviour to monoazobenzene molecules; there is reason to believe that the molecules equipped with multiple switching units are more likely to propel the molecule across the surface[3,6,7,8]. These studies should address some of the key questions in nanotechnology and contribute to the development of autonomous surface-traversing molecules[3].

Results and discussion

Synthesis and characterization

The attempted syntheses of molecules **1a** and **1b** are shown in Schemes 1−3. The synthetic route started with the commercially available 5-iodo-1,3-dinitrobenzene **3** (Scheme 1). Compound **3** was reduced to compound **4** in 94 % yield following a literature procedure[27]. Numerous attempts were made to convert both amino groups into azobenzene units in a single step. Despite the absence of similar double diazotation reactions in the literature, it was attempted to form a double diazonium ion of **4** and then react it with two molecules of phenol following

literature conditions to form a simple monoazobenzene compound[28]. This attempt failed as no product was formed in the reaction. We reason that the anticipated intermediate, a double diazonium ion derived from **4**, bearing two charged diazonium groups on the same benzene group, is too unstable to be formed under the conditions used. The formation of a bisazobenzene group via coupling of a nitroso compound and an amine was also attempted[29]. The coupling reaction of diamine **4** with 4-nitrosophenol to make the intermediate **5** for the synthesis of **1a** did not give any product. A similar coupling reaction between diamine **4** and 4-tetradecylnitrosobenzene (preparation described in Chapter 2) to make the intermediate **6** for the synthesis of **1b** did not work either. Similar coupling reactions between 4-alkylnitrosobenzene and 4-iodoaniline were successfully carried out in Chapters 2 and 3 so it is at this point unclear why this coupling reaction failed. The only difference is in the structure of substrate **4** compared to 4-iodoaniline; it seems that the extra amino group in **4** somehow interferes with the coupling.
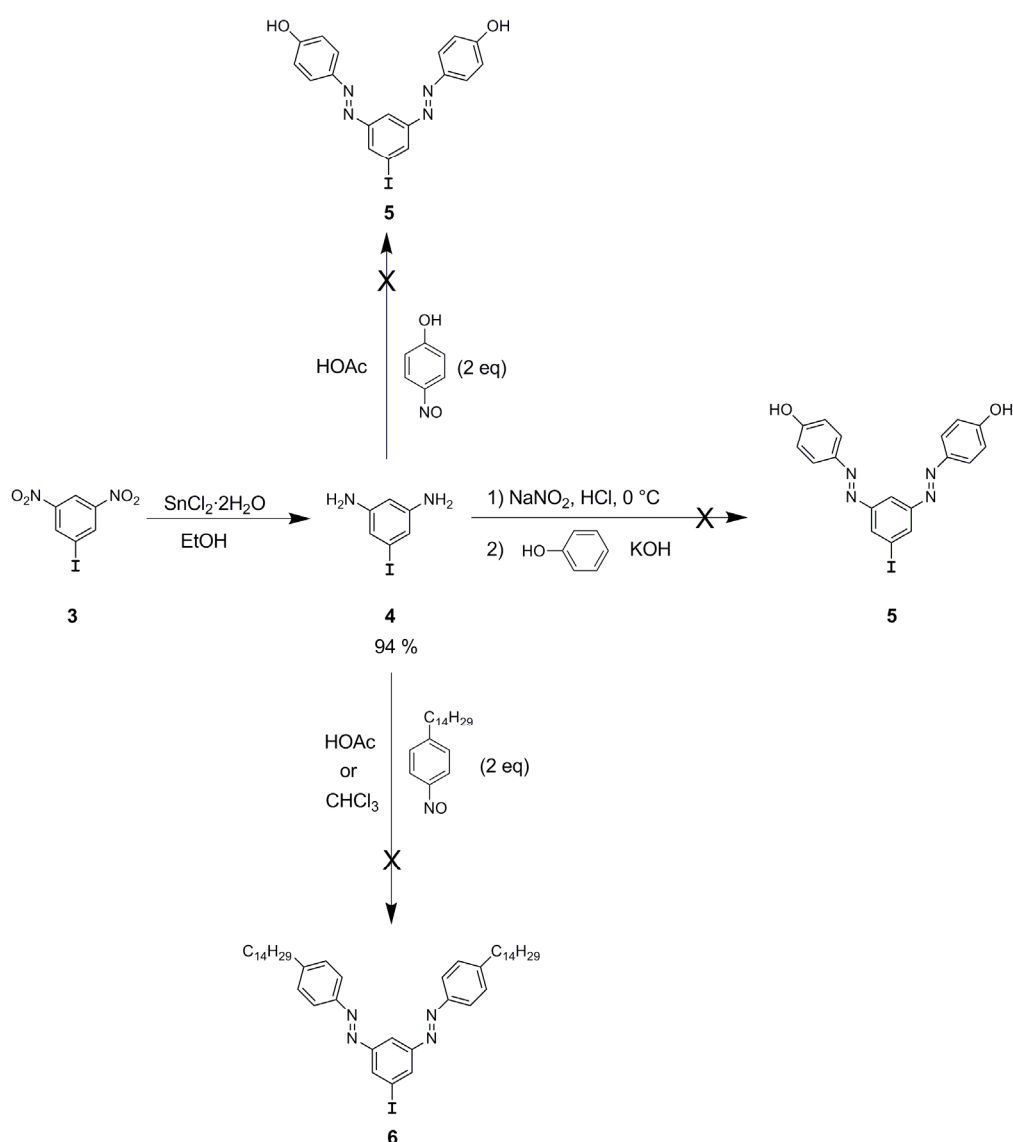
Scheme 1. First attempted synthesis of the intermediates for the preparation of molecules **1a** and **1b**; the diamine **4** is envisaged to react twice to give bisazobenzenes **5** or **6**.

Literature procedures for the preparation of similar bisazobenzene compounds included reactions on the monoprotected amines which would be deprotected after carrying out the diazotation reaction and reacted in a second diazotation reaction[20,30]. In order to use this synthetic strategy we modified an acylation procedure from the literature[31] to monoprotect diamine **4** so as to obtain **7** (Scheme 2). The monoprotection reaction proceeded with moderate yield. Coupling reactions of **7** with nitroso compounds did not afford any product; solvents, reactant ratios and temperature were all varied but no conversion was observed. It is at this point not clear why these coupling reactions failed despite having the second amino group protected. The diazotation coupling was also tried; following a literature procedure[20] product **8** was obtained in 27 % yield whereas the modified conditions from another literature procedure[30] afforded **8** in 57 % yield.
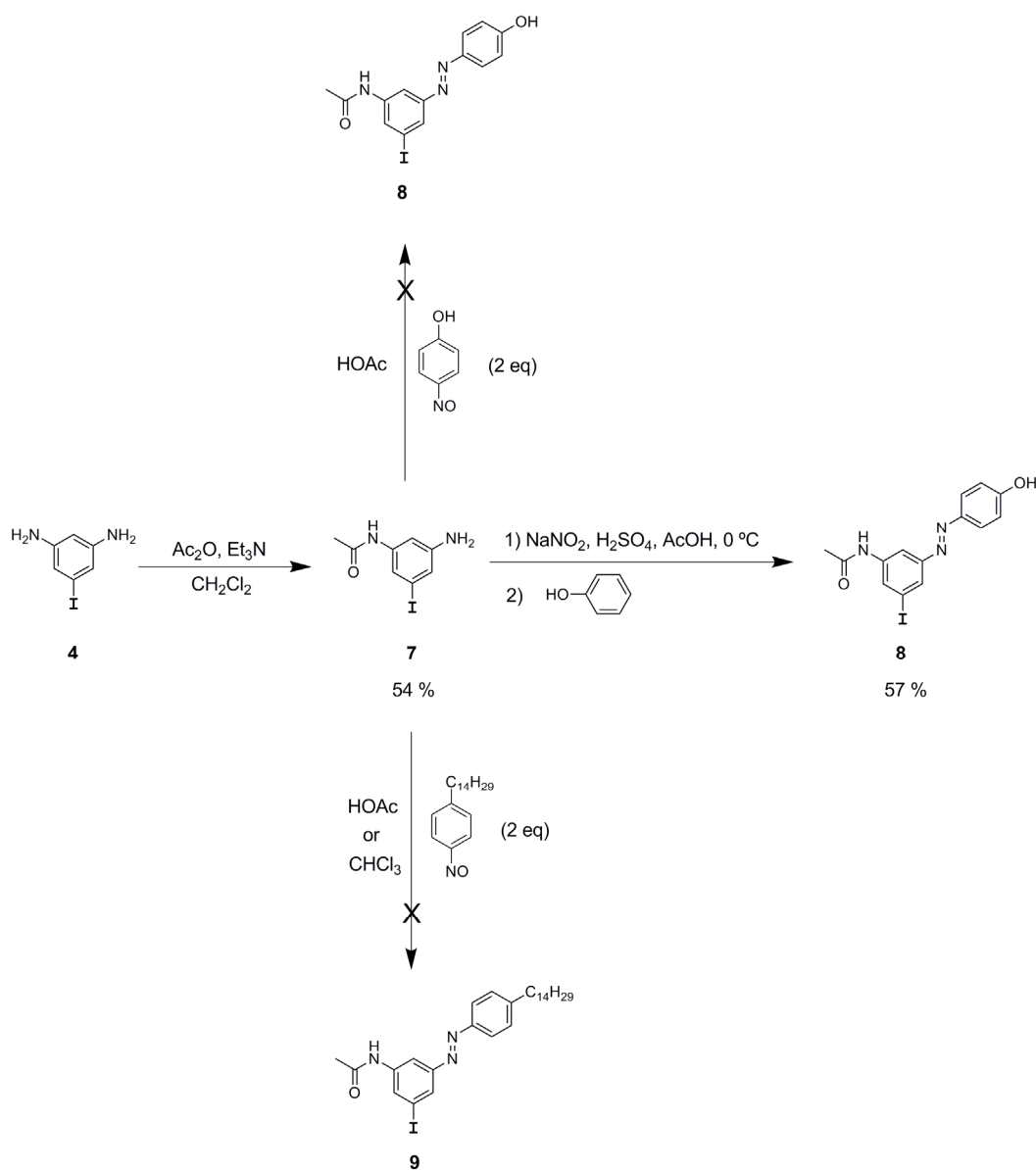
Scheme 2. Attempted synthesis of the intermediates for the preparation of molecules **1a** and **1b**; the synthesis proceeds through the monoprotected diamine **7**.

Deprotection of the protected amino group in **8** proceeded smoothly to afford compound **10** following a literature procedure for a similar compound[20] (Scheme 3). Diazotation of **10**, under the conditions reported[20,30] for the preparation of the analogues of **5** having no iodine atom as well as successfully used on **7** to obtain **8**, did not afford product **5**; the iodine atom appears to affect the reactivity of the second amino group towards the diazotation reaction.
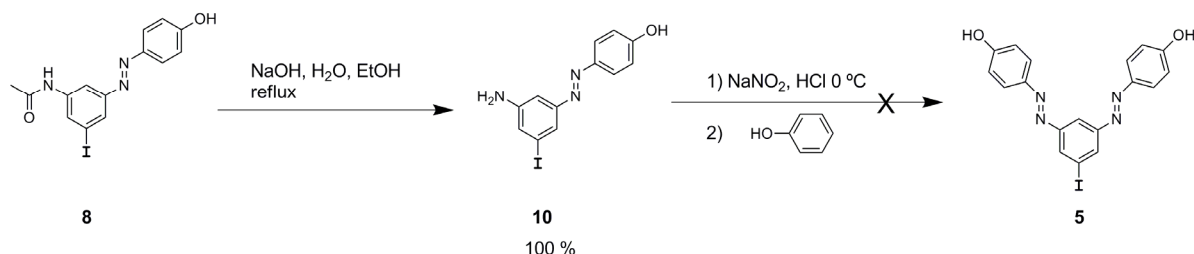
Scheme 3. Attempted synthesis of the intermediate **5** for the preparation of **1a**; the formation of the second azobenzene group.

The synthetic route towards compounds **1a** and **1b** (Schemes 1–3), was at this point abandoned and our efforts were directed towards the synthesis of compound **2** (Scheme 4).

The synthesis of **2** started with compound **11**, cointaining two azobenzene groups and a bromine atom where the molecule could be further functionalized. The synthesis of compound **11** was described in Chapter 2. Compound **11** was transformed into its iodo-analogue[32] in order to make it more reactive in the Sonogashira coupling reaction[33] with compound **13** (the preparation of **13** was described in Chapter 3). The coupling between **12** and **13** proceeded in 48 % yield to give compound **14**. The last step in the preparation of **2** was the attachment of triphenylsilyl wheels. This was achieved in a double Sonogashira coupling reaction between compound **14** and triphenylsilylacetylene. The reaction proceeded rather sluggishly but its progress could easily be followed by TLC. In the course of the reaction fresh portions of the acetylene and the catalyst were added in order to push the reaction forward. Product **2** was isolated in 19 % yield.
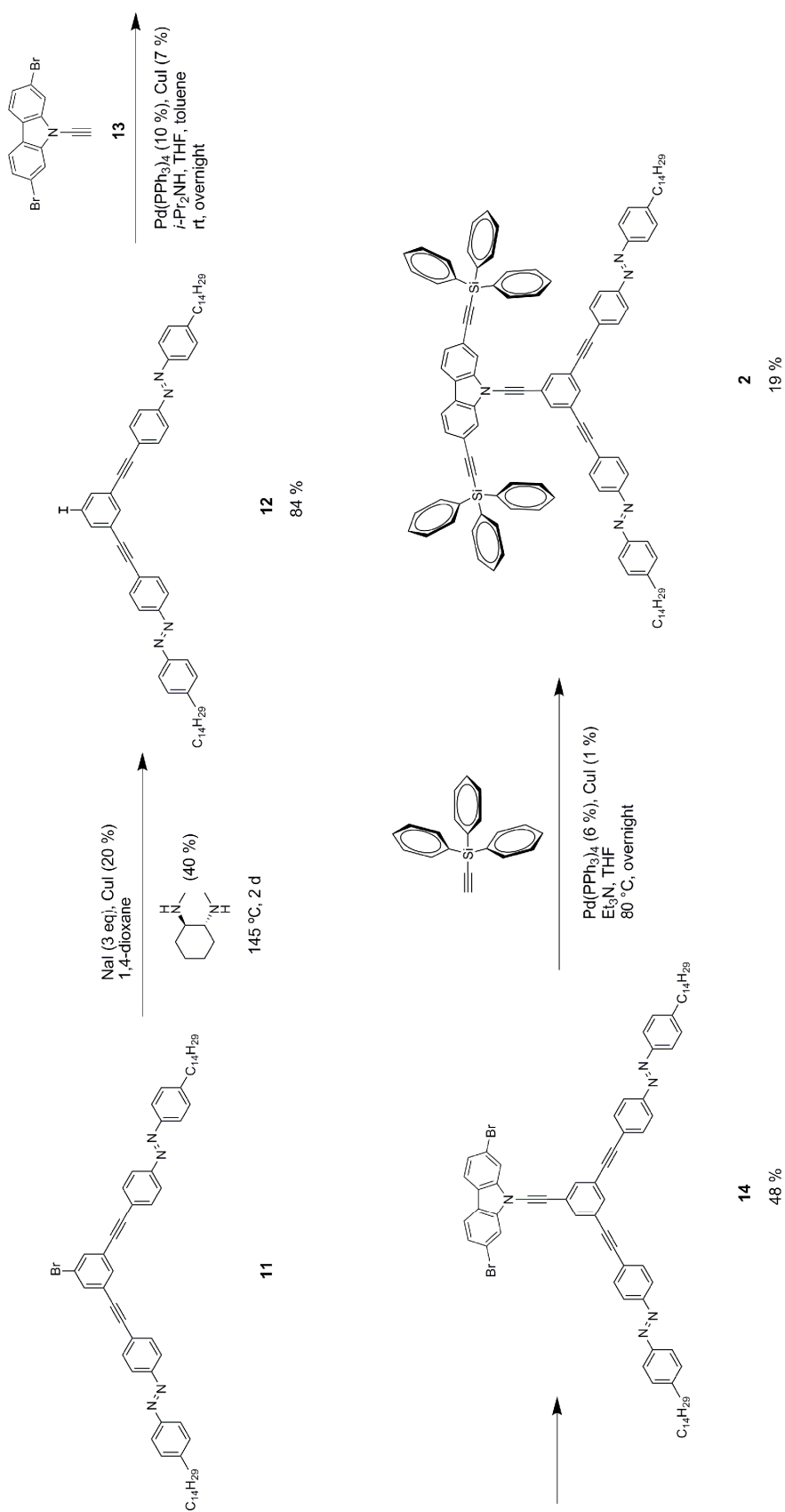
Scheme 4. Synthesis of molecule **2**.

All the synthetic intermediates were characterized by [1]H−NMR and APT NMR spectroscopic techniques as well as by high resolution mass spectrometry. The target molecule **2**, however, could not be characterized by mass spectrometry (ESI, APCI, APPI, MALDI) as the masses obtained could not be rationalized in terms of the chemical structure. We reported similar behaviour of the final molecules in Chapter 3, also bearing triphenysilyl wheels; the correct molecular ion or one derived from it could not be detected. Molecule **2** has been characterized by [1]H−NMR and APT NMR spectroscopic techniques which supports the suggested structure. The [1]H−NMR spectrum shows additional protons in the aromatic region when compared to the spectrum of **14** as well as the shifting of the doublet signal corresponding to the protons in the carbazole unit. In addition to the signals corresponding to the triphenylsilyl groups, the APT spectrum shows six signals in the region 89−111 ppm which correspond to the C−atoms belonging to C≡C bonds. Furthermore, two of the signals show half the intensity of the remaining four indicating the presence of three magnetically different C≡C bonds in 2:2:1 ratio. The chemical shifts belonging to C−atoms associated with C≡C bonds are in excellent agreement with the chemical shifts observed for these three different types of C≡C bonds in molecules already discussed in Chapters 2 and 3. Together these data strongly support the structure of target molecule **2**. As already mentioned in Chapter 3, it is at this point unclear why the target molecules containing triphenylsilylethynyl groups could not be detected by mass spectrometry.

Photochemical characterization

Molecule 2

UV−Vis spectroscopic study

Photochemical properties of molecule **2** were examined in solution (*n*-heptane) by means of UV−Vis spectroscopy (Fig 4). The UV−Vis spectrum of **2** shows a strong absorption band with λ_{max} = 335 nm. Upon irradiation of the sample with light at λ = 365 nm, the band drops in intensity and a weak new band appears simultaneously in the region around 300 nm. A weak new band appears in the visible region as well, λ_{max} = 450 nm. Subsequent irradiation with light at λ = 312 nm, λ > 420 nm or an increase in temperature will cause the newly formed bands to decrease in intensity again and the original band with λ_{max} = 335 nm to reappear in its original intensity. This behaviour is typical of azobenzene compounds[4]. It is worth noting, however, that the UV−Vis spectral changes of **2** upon irradiation with 365 nm show some differences from the monoazobenzene analogues studied in Chapter 3; molecules from Chapter 3 did not form a new band in the visible region nor could they be isomerized back using visible light.
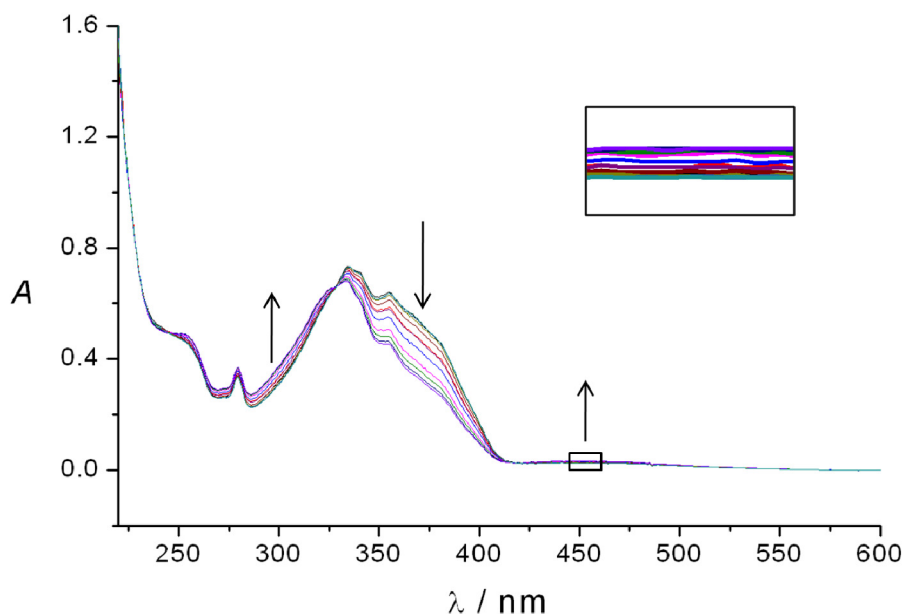
Figure 4. UV–Vis spectra of **2** in *n*-heptane, *c* = 1.2 · 10^{-5} mol dm^{-3}, 0 °C, under Ar, upon switching back and forth (repeatedly) with 365 nm, 312 nm, λ > 420 nm and Δ (to 50 °C and then back to 0 °C).

Irradiation of the sample kept in the dark (*E*–isomer) with light at 365 nm establishes a photoequilibrium between the *E*–isomer and the *Z*–isomer of the azobenzene[4] (Scheme 5). The change in the composition of the solute (the ratio of the *E*– and *Z*–isomer) is reflected in the UV–Vis spectrum of the solution; the spectrum changes during irradiation until a photoequilibrium has been reached. The exact composition of the solute at the photoequilibrium cannot be estimated at this point but will be addressed at a later stage. Irradiation with light at λ = 312 nm or λ > 420 nm causes a new photoequilibrium to be established which is again reflected in the UV–Vis spectra of the solution. Since the spectra after irradiation with light at λ = 312 nm or λ > 420 nm appear identical to the one of the *E*–isomer it can be concluded that the photostationary states (PSSs) for the *Z*–to–*E* photoisomerization consist predominately of the *E*–isomer.
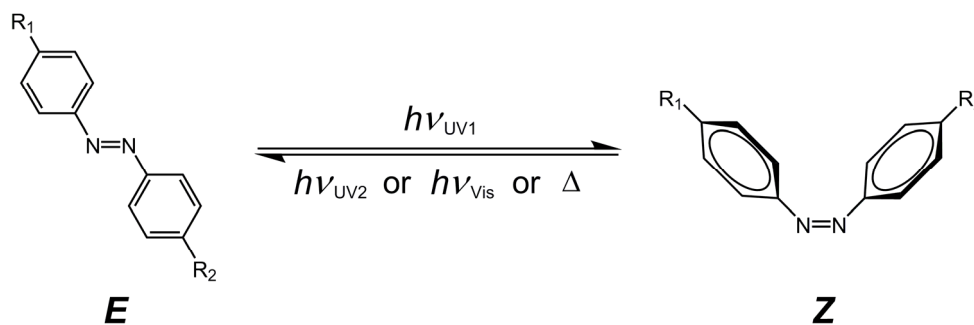

Scheme 5. Typical switching behaviour of azobenzenes.

After the PSS (*Z*) has been reached by irradiation of the *E*–isomer with light at 365 nm, the change can also be reversed thermally *i.e.* by warming up the sample to 50 °C. The spectrum of the pure *E*–isomer was once again recovered. This complete thermal reversal of the changes brought about by irradiation with light at 365 nm makes sense since the less stable *Z*–isomer is well known to thermally convert to the more stable *E*–isomer[4] (Scheme 2). The time it takes for the full recovery of the original spectrum of the *E*–isomer will depend on the temperature of the system. This phenomenon will be studied in more detail at a later stage.

^{1}H–NMR spectroscopic study

The switching behaviour of molecule **2** was also studied in CD_2Cl_2 by means of ^{1}H–NMR spectroscopy (Fig 5). Irradiation of the solution containing only the *E*–isomer of **2** with light at 365 nm was accompanied by the appearance of new signals in both the aromatic as well as in the aliphatic region of the spectrum. It was proceeded with the irradiation until no further changes could be observed in the spectrum (Fig 5b). The photostationary state had been reached at that point and the solute contained around 50 % of the newly formed species. Irradiation of the sample now at the photostationary state with light at 312 nm resulted in the gradual decrease in the intensity of the new peaks (Fig 5c). Some minor signals, however, remained after the irradiation or after heating the sample to 40 °C for 30 min.
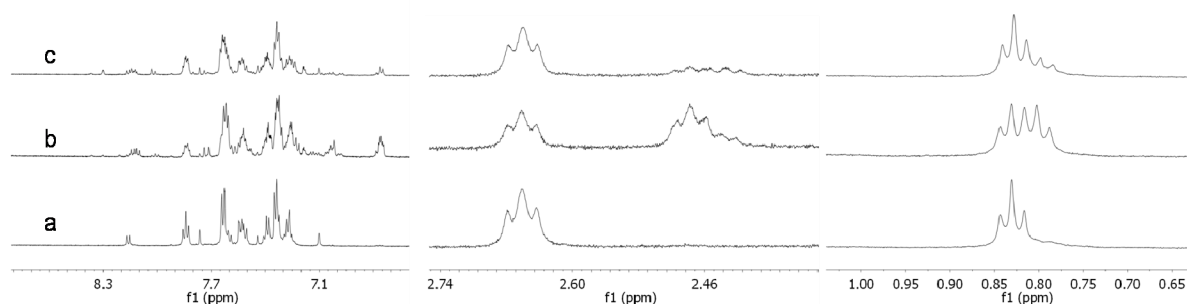
Figure 5. ^{1}H–NMR spectra of switch **2**, in CD_2Cl_2, under Ar, at 0 °C **a:** in the dark, **b:** sample from **a** irradiated at 365 nm for 1 h, **c:** sample from **a** irradiated at 312 nm for 1.3 h.

The NMR signals that shift (most) upon irradiation are those corresponding to the protons that are in immediate vicinity of the azobenzene unit that undergoes the isomerization process; this was discussed in detail in Chapters 2 and 3. Much like is the case with the molecules studied in Chapters 2 and 3, it appears that even the most remote protons in the alkyl chains experience a change upon the switching of the azobenzene unit. This is evidenced by the shifting of the signal at 0.88 ppm upon switching (Fig 5) belonging to the terminal methyl group in the alkyl chain of **2**. As discussed in Chapter 2, this indicates an interaction between the long alkyl chains of **2**, be it of inter- or intramolecular nature.

The most intense peaks appearing upon irradiation at 365 nm correspond to the *Z*–isomer of the azobenzene groups (Fig 5b). These peaks disappear upon

irradiation with light at 312 nm or by warming up the sample; this corresponds to the isomerization of the *Z*–isomer back to the *E*–isomer (Fig 5c). This is in complete agreement with what we observed for azobenzene molecules in Chapters 2 and 3. Some signals of lower intensity, however, remain after irradiation with light at 312 nm or heating (Fig 5c). This suggests that these peaks correspond to protons belonging to a chemical entity formed during irradiation with light at 365 nm and not undergoing reversible isomerization. This is a sign of a photochemical side reaction forming an undesired product. The sample was degassed with argon prior to the experiments to ensure the exclusion of oxygen, a common cause of photochemical side reactions[34]. This, however, did not lead to the subsidence of the side reaction.

It appears that the long irradiation times (up to 1.5 h) may not be the only cause of the side product being formed as it has also been observed after working with solutions of **2** for a prolonged time in the absence of UV light (for example during purification of **2** by repeated crystallizations). This side reaction has never been observed for the multiazobenzene compounds discussed in Chapter 2. It has, however, been observed for the monoazobenzene analogues of **2** discussed in Chapter 3 but only after being exposed to air for longer periods of time.

There are two possibilities that could lead to the side reaction; compound **2** might be inherently prone to degradation under certain conditions (possibly a photooxidative degradation[35,36]) or there is an impurity present in the sample of **2** that enhances its degradation under certain conditions. In any case, it appears that the degradation is significantly more pronounced in **2** than in other molecules studied so far (Chapters 2 and 3).

Kinetics of the thermal isomerization

As already mentioned, the *Z*–isomer may be isomerized to the *E*–isomer photochemically (irradiation with either UV light at 312 nm or visible light at wavelength higher than 420 nm) or thermally. The driving force for the latter process comes from the relative instability of the *Z*–isomer[4]; if kept in the absence of light the less stable *Z*–isomer will spontaneously isomerize to the more stable *E*–isomer. The rate at which it undergoes the thermal process depends on the temperature but is always much slower than the photochemical isomerization[4].

No degradation has been observed by UV–Vis spectroscopy (possibly due to much lower concentrations of the analyte and shorter irradiation times than in the NMR investigations) so we decided to use this technique to study the kinetics of the thermal isomerization of **2**. Given the possibility, however, that there is still a side reaction taking place which is not observed by UV–Vis spectroscopy, the results obtained from this study should be taken with care. The results should nevertheless give an indication of the thermal isomerization rate of **2**.

Temperature dependent UV–Vis spectroscopy was therefore used to follow the process in time (Fig 6).
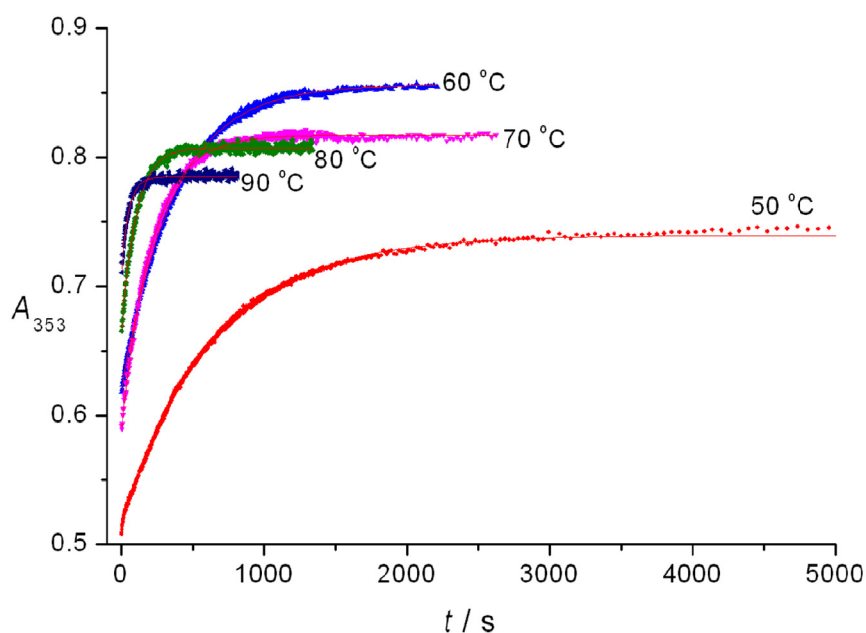
Figure 6. The data points collected by following the absorbance at 353 nm of a sample of **2** over time at different temperatures, c = 1.2·10^{-5} mol dm^{-3} in *n*-heptane, under Ar, and the calculated values (−) as obtained by nonlinear regression analyses.

A sample of a solution of **2** in *n*-heptane was irradiated with light at 365 nm to the photostationary state and the absorbance was followed in the region of the maximum change in absorption (λ = 353 nm) (Fig 4) over time in the temperature range 50–90 °C. The collected data were fitted to the exponential function assuming first-order kinetics for the thermal step[37]. The collected data as well the fits are shown in Fig 6 and the parameters from the fits are given in Table 1.

Table 1. The half-lives, $t_{1/2}$, at different temperatures as obtained from the regression analyses of the data in Fig 6.

Θ / °C	$t_{1/2}$ / min	R^2
50	7.4	0.99916
60	4.2	0.99944
70	2.5	0.99889
80	1.2	0.99382
90	0.6	0.96961

From Table 1 it can be seen that the half-life for the thermal isomerization, $t_{1/2}$, ranges from 7.4 min at 50 °C to 0.6 min at 90 °C. This does not differ much from the half-lives observed for molecules discussed in Chapters 2 and 3.

The data from Table 1 can be analyzed according to the Eyring equation to obtain the activation parameters, $\Delta^{\ddagger}H$ and $\Delta^{\ddagger}S$ (Fig 7).
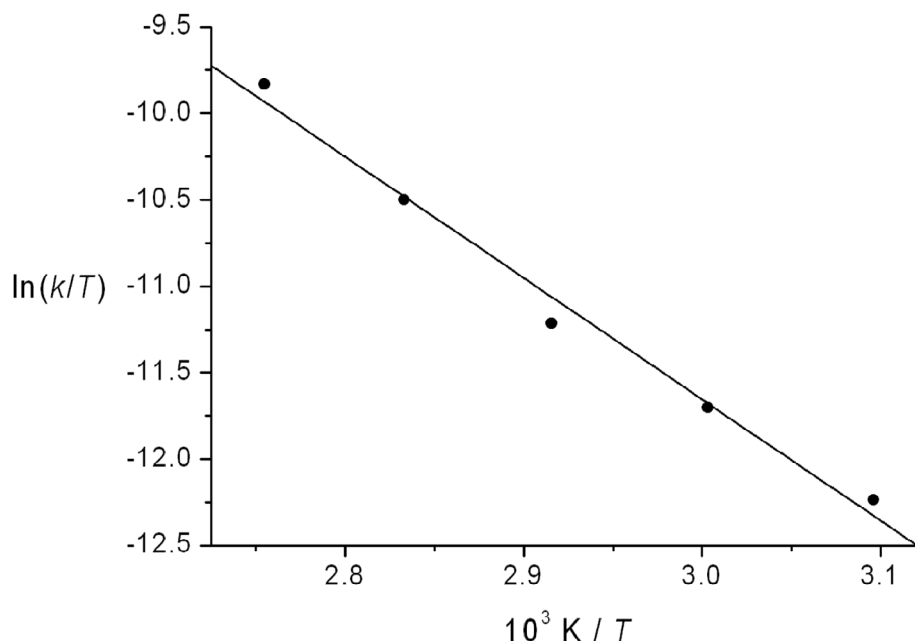
Figure 7. The data points from Table 1 analyzed according to the Eyring equation and the calculated values (–) as obtained by linear regression analysis.

From the analysis in Fig 7 the following activation parameters were obtained: $\Delta^{\ddagger}H$ = (58 ± 4) kJ mol^{-1}, $\Delta^{\ddagger}S$ = – (120 ± 10) J K^{-1} mol^{-1}. Previously reported values for these parameters for different azobenzene systems are roughly in the range 35 – 100 kJ mol^{-1} and –200 – 50 J K^{-1} mol^{-1}, respectively, depending on the exact structure of the azobenzene compounds as well as the solvent used during the measurements[38,39,40,41]. The values for **2** determined here are well within that range and also in good agreement with the values obtained for multiazobenzene molecules discussed in Chapter 2. The activation parameters for **2** are however quite different from those obtained for the monoazobenzene analogues from Chapter 3 ($\Delta^{\ddagger}H$ = 85 kJ mol^{-1}, $\Delta^{\ddagger}S$ = – 41 J K^{-1} mol^{-1}). It appears that, in terms of photochemical behaviour, molecule **2** resembles the multiazobenzene molecules from Chapter 2 more than it resembles the monoazobenzene molecules from Chapter 3 (bearing the same wheels). Both **2** and the two molecules in Chapter 2 have two or three azobenzene groups connected to a central benzene ring whereas the molecules in Chapter 3 have a single azobenzene unit connected to the N-atom of the carbazole unit. It seems that the structural aspect of the (multi)azobenzene unit is what is most important for its photochemical behaviour; a similar design of

the switching unit will cause similar photochemical behaviour regardless of the remainder of the molecule (although part of the same conjugated system). This is an important finding that is going to be beneficial for designing future azobenzene molecules.

The activation parameters allow for the calculation of the half-life for the thermal isomerization at 25 °C, $t_{1/2}$ = 55 min (0.92 h). This value does not differ much from the values determined for multiazobenzene molecules discussed in Chapter 2 (70 min) but appears to be somewhat smaller than the values obtained for monoazobenzene molecules in Chapter 3 (3–4 h); this again confirms the structure–photochemical property relationship discussed in the previous paragraph. The activation parameters can also give some information about the mechanism of the thermal isomerization as well and this will be discussed in the next section.

The abovementioned similarities in behaviour between **2** and multiazobenzene molecules discussed in Chapter 2 would indicate that a solution of **2** at the photostationary state reached by irradiation with light at 365 nm contains a distribution of the molecules (*E*,*E*)–**2**, (*E*,*Z*)–**2** and (*Z*,*Z*)–**2** (as determined by the ^{1}H–NMR study, the sample of **2** at PSS contains about 50 % of *Z*–azobenzene moieties). A detailed discussion on the distribution of isomeric molecules at the PSS can be found in Chapter 2. The presence of side products at the PSS of **2**, however, makes it impossible to account for all the isomers of **2** in the ^{1}H–NMR spectra in order to confirm this hypothesis.

Proposed mechanism of the thermal isomerization

As already discussed in Chapters 2 and 3, the photoisomerization and the thermal isomerization of azobenzenes are thought to proceed via one of the two mechanisms; the rotation mechanism or the inversion mechanism[4,42]. This is discussed more elaborately in Chapter 2.

The isokinetic plots, like the ones in Fig 8, are normally used to determine the mechanism of the thermal isomerization process[43,44,45]. The plot in Fig 8 is taken from the literature[44]; the data points used to make the isokinetic plots are simple azobenzene compounds studied previously[38,43,44].
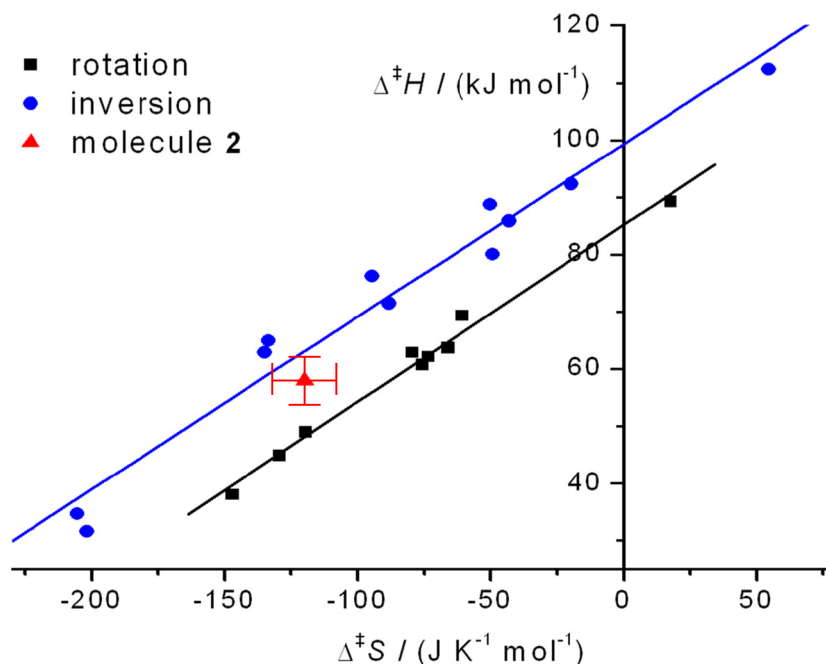
Figure 8. Isokinetic plots for the thermal isomerization of azobenzene derivatives; the data points used to make the plots are given and further referenced in the study by Wazzan[44]. The data point obtained for compound **2** is highlighted in red.

As can be seen from Fig 8, the data point describing molecule **2** studied here in *n*-heptane is found between the two lines. This could indicate a mechanism between the rotation and inversion mechanisms. The position of the data point could also simply be explained by imperfect correlation like for many of the other „inversion" points (Fig 8). The possible degradation process during the measurements might also be involved but, on the other hand, the data point for the molecules in Chapter 2 was similarly positioned in the isokinetic plot and no degradation was observed for those molecules. The position in the isokinetic plots seems to be yet another property of **2** in common with the multiazobenzene molecules from Chapter 2.

Conclusions

In an attempt to contribute to the development of nanovehicles, we have designed new molecules consisting of a carbazole core, two azobenzene switching groups and two triphenylsilyl wheels. Molecules **1a** and **1b** have a bisazobenzene group with a central benzene ring shared by the two azobenzene groups whereas molecule **2** has two separate azobenzene groups. With the new design we would like to investigate the advantages of having more than a single switching unit in the molecule. More specifically, this would address the question whether the extra azobenzene group would help propel the molecule across the surface.

Molecules **1a** and **1b** could not be synthesized so far as the preparation of the key bisazobenzene group failed; two different methods for the preparation of the azobenzene groups were tried without success. Molecule **2** was prepared through a convergent synthetic route. The photochemical properties of **2** were studied in solution by UV−Vis and NMR spectroscopic techniques. The UV−Vis study showed a typical azobenzene switching behaviour; the azobenzene groups may be photoisomerized between the *E*− and *Z*−isomeric forms and the *Z*−azobenzene group may also be thermally isomerized to the more stable *E*−isomer. The kinetics of the thermal isomerization process were studied at different temperatures and the half-life was determined to be 55 min at room temperature. The activation parameters could also be obtained from the kinetic study indicating a mechanism between the rotation and inversion mechanisms for the thermal isomerization of these molecules in solution. The kinetic parameters obtained agreed well with those determined for multiazobenzene molecules in Chapter 2 but not so much with those determined for monoazobenzene molecules in Chapter 3. It appears that the higher degree of structural similarity between the switching units and not between the supporting parts of the molecules is responsible for the similar photochemical properties of the studied molecules. The photochemical behaviour of **2** was also investigated by NMR spectroscopy revealing the typical azobenzene switching behaviour as well as an irreversible side reaction. Unlike the monoazobenzene molecules presented in Chapter 3, it appears that **2** is susceptible to a degradation process which might limit its applicability as a surface-traversing molecule.

Acknowledgements

Experimental section

Synthesis, characterization and physico−chemical measurements

General remarks

The experiments were performed as described in the section *General Remarks* in Chapter 2.

***N*-(3-amino-5-iodophenyl)acetamide 7**: 5-Iodobenzene-1,3-diamine **4** (309 mg, 1.32 mmol) was dissolved in CH_2Cl_2 (15.0 ml) and to that solution Et_3N (240 μl, 1.72 mmol) was added. The solution was stirred in an ice/water bath at 0 − 5 °C and to the cooled solution Ac_2O (165 μl, 1.72 mmol) was added dropwise. After all of the Ac_2O had been added, the mixture was stirred for another 10 min at 0 − 5 °C and then the temperature was raised to room temperature. The progress of the reaction could be followed by TLC (SiO_2, AcOEt/*n*-pentane 2:1). After a few hours a precipitate is formed. The reaction was quenched after 6 h. The suspension was filtered and the filtrate was washed with a saturated aqueous NaCl solution (50 ml)

containing 10 % of the saturated aqueous $NaHCO_3$ solution. The organic layer was then washed further with a saturated aqueous NaCl solution (50 ml), dried on anhydrous Na_2SO_4, filtered and the solvent evaporated. This afforded the product as a white solid (197 mg) in 54 % yield. The product may be additionally purified for analytical purposes by means of column chromatography on SiO_2 using *n*-pentane/AcOEt 1:1 as eluent.

^{1}H NMR (400 MHz, CD_3OD): δ 7.22 (t, *J* = 1.6 Hz, 1H), 6.95 (t, *J* = 1.9 Hz, 1H), 6.82 (t, *J* = 1.7 Hz, 1H), 2.09 (s, 3H). ^{13}C NMR (100 MHz, CD_3OD): δ 171.50, 150.77, 141.38, 120.67, 119.08, 106.86, 94.97, 23.93. HRMS (ESI): *m/z* calculated for $C_8H_{10}IN_2O^+$: 276.98378 $[M+H]^+$, found 276.9829. $[M+H]^+$.

(*E*)-*N*-(3-((4-hydroxyphenyl)diazenyl)-5-iodophenyl)acetamide 8: Compound **7** (300 mg, 1.1 mmol) was dissolved in glacial HOAc (10.0 ml) and the solution was cooled on ice. This solution was added dropwise to a cooled solution of $NaNO_2$ (74 mg, 1.1 mmol) in H_2SO_4 (aq, conc) (3.0 ml). The solution was stirred at 0 °C for 10 min. Next a solution of phenol (102 mg, 1.1 mmol) in glacial HOAc (4.0 ml) was added. The mixture was stirred for 10 min at room temperature and then the pH was set to pH = 7 by the addition of an aqueous solution of NaOH (*c* = 1 mol dm^{-3}). The mixture was extracted with AcOEt (50 ml), the organic extracts were dried on anhydrous Na_2SO_4, the salt was removed by filtration and the solvent was evaporated. This afforded the crude product (440 mg), which was purified by means of column chromatography on SiO_2 using *n*-pentane/AcOEt 1:1 as eluent (during the course of chromatography a gradient is applied up to *n*-pentane/AcOEt 1:4). This afforded the product as an orange solid (239 mg) in 57 % yield.

^{1}H NMR (400 MHz, CD_3OD): δ 8.07 (t, *J* = 1.7 Hz, 1H), 8.00 (t, *J* = 1.8 Hz, 1H), 7.84 (t, *J* = 1.6 Hz, 1H), 7.80 (d, *J* = 8.8 Hz, 2H), 6.91 (d, *J* = 8.8 Hz, 2H), 2.14 (s, 3H). ^{13}C NMR (50 MHz, CD_3OD): δ 171.83, 162.81, 155.13, 147.13, 141.86, 130.50, 126.79, 126.36, 116.82, 115.19, 94.70, 23.95. HRMS (ESI): *m/z* calculated for $C_{14}H_{12}IN_3O_2Na^+$: 403.98719 $[M+Na]^+$, found 403.9861. $[M+Na]^+$.

(*E*)-4-((3-amino-5-iodophenyl)diazenyl)phenol 10: Compound **8** (166 mg, 0.44 mmol) was dissolved in a mixture of an aqueous NaOH solution (*w* = 10 %, 30.0 ml) and EtOH (5.0 ml). The solution was stirred at reflux for 2 h. The solution was allowed to cool to room temperature and the pH was set to pH = 7 by the addition of aqueous hydrochloric acid (*c* = 1 mol dm^{-3}). The suspension was extracted with AcOEt (100 ml), dried over anhydrous Na_2SO_4, filtered and the solvent evaporated. This afforded the product as an orange solid (148 mg) in quantitative yield.

^{1}H NMR (500 MHz, CD_3OD): δ 7.78 (d, *J* = 8.7 Hz, 2H), 7.41 (s, 1H), 7.14 (s, 1H), 7.13 (s, 1H), 6.91 (d, *J* = 8.7 Hz, 2H). ^{13}C NMR (125 MHz, CD_3OD): δ 162.34, 155.76, 151.54, 147.24, 126.05, 125.84, 120.67, 116.72, 110.02, 95.44. HRMS (ESI): *m/z* calculated for $C_{12}H_{11}IN_3O^+$: 339.99468 $[M+H]^+$, found 339.9939. $[M+H]^+$.

1-iodo-3,5-bis((4-((*E*)-(4-tetradecylphenyl)diazenyl)phenyl)ethynyl)benzene 12: Compound **11** (41 mg, 0.043 mmol) was dissolved in 1,4-dioxane (14.0 ml) in a high-pressure tube and to this solution NaI (19 mg, 0.13 mmol), CuI (1.6 mg, 0.0086 mmol) and *trans*–*N,N′*–dimethylcyclohexane–1,2-diamine (2.7 μl, 0.017 mmol) were added under a nitrogen atmosphere. The tube was sealed and the mixture was stirred vigorously at 145 °C for two days. The mixture was allowed to cool to room temperature and was filtered through a plug of silica. The solvent was evaporated affording the product as a red solid (36 mg) in 84 % yield. This reaction is best performed on 50 mg scale due to problems with reproducibilty on larger scales.

^{1}H NMR (500 MHz, CDCl$_3$): δ 7.91 (d, *J* = 8.4 Hz, 4H), 7.88 (s, 2H), 7.86 (d, *J* = 8.1 Hz, 4H), 7.70 (s, 1H), 7.66 (d, *J* = 8.4 Hz, 4H), 7.33 (d, *J* = 8.0 Hz, 4H), 2.69 (t, *J* = 7.6 Hz, 4H), 1.65 (m, 4H), 1.40–1.20 (m, 44H), 0.88 (t, *J* = 6.5 Hz, 6H). ^{13}C NMR (125 MHz, CDCl$_3$): δ 152.38, 151.05, 147.24, 140.07, 133.92, 132.66, 129.31, 125.25, 124.88, 123.16, 123.02, 93.42, 91.29, 89.18, 36.09, 32.08, 31.43, 29.85, 29.82 (2C), 29.81 (2C), 29.73, 29.64, 29.52, 29.44, 22.85, 14.28. HRMS (APCI): *m/z* calculated for C$_{62}$H$_{78}$IN$_4$$^+$: 1005.52712 [M+H]$^+$, found 1005.52998. [M+H]$^+$.

9-((3,5-bis((4-((*E*)-(4-tetradecylphenyl)diazenyl)phenyl)ethynyl)phenyl)ethynyl)-2,7-dibromo-9*H*-carbazole 14: Compounds **12** (100 mg, 0.10 mmol) and **13** (52 mg, 0.15 mmol) were dissolved in a mixture of *i*-Pr$_2$NH (9.0 ml), toluene (3.0 ml) and THF (3.0 ml) under an argon atmosphere. To this solution CuI (1.6 mg, 0.007 mmol) and Pd(PPh$_3$)$_4$ (12 mg, 0.01 mmol) were added. The mixture was stirred at room temperature overnight under an argon atmosphere. The progress of the reaction could be followed by TLC using *n*-pentane/CH$_2$Cl$_2$ 4:1 as eluent. Another portion of the catalyst (12 mg) and compound **13** (52 mg) were added and stirring was continued until the depletion of compound **12** was observed by TLC (a few more hours). The solvent was evaporated and the crude product was purified by column chromatography on SiO$_2$ using *n*-pentane/CH$_2$Cl$_2$ 4:1 as eluent. The collected product was suspended in MeOH and the solution was decanted off. This procedure was repeated several times until the product (orange solid, 59 mg, 48 % yield) was obtained pure by NMR.

^{1}H NMR (400 MHz, CDCl$_3$): δ 7.92 (d, *J* = 8.3 Hz, 4H), 7.89–7.73 (m, 11H), 7.70 (d, *J* = 8.3 Hz, 4H), 7.48 (d, *J* = 8.4 Hz, 2H), 7.33 (d, *J* = 8.2 Hz, 4H), 2.69 (t, *J* = 7.6 Hz, 4H), 1.66 (m, 4H), 1.40–1.17 (m, 44H), 0.88 (t, *J* = 6.5 Hz, 6H). ^{13}C NMR (125 MHz, CDCl$_3$): δ 152.31, 151.06, 147.17, 141.11, 134.29, 133.89, 132.70, 129.29, 126.15, 125.07, 124.26, 123.20, 123.16, 123.02, 122.06, 121.68, 120.96, 114.73, 90.91, 90.02, 78.55, 74.45, 36.09, 32.08, 31.43, 29.85, 29.83 (2C), 29.81 (2C), 29.74, 29.65, 29.52, 29.46, 22.85, 14.29. HRMS (ESI): *m/z* calculated for C$_{76}$H$_{84}$Br$_2$N$_5$$^+$: 1226.50730 [M+H]$^+$, found 1226.50622. [M+H]$^+$.

9-((3,5-bis((4-((*E*)-(4-tetradecylphenyl)diazenyl)phenyl)ethynyl)phenyl)ethynyl)-2,7-bis((triphenylsilyl)ethynyl)-9*H*-carbazole 2: Compound **14** (20 mg, 0.016 mmol) and triphenylsilylacetylene (10 mg, 0.035 mmol) were dissolved in a mixture

of Et$_3$N (3.0 ml) and THF (1.6 ml) in a high-pressure tube under an argon atmosphere. To this solution CuI (one grain) and Pd(PPh$_3$)$_4$ (1 mg, 0.0008 mmol) were added. The high-pressure tube was sealed and the reaction mixture was stirred at 80 °C under an argon atmosphere. The progress of the reaction could be followed by TLC using *n*-pentane/CH$_2$Cl$_2$ 3:1 as eluent. Two additional portions of the catalyst (2 mg), CuI (one grain) and triphenylsilylacetylene (12 mg) were added until the reaction proceeded to completion as monitored by TLC. The mixture was stirred overnight and upon depletion of **14**, as evidenced by TLC, the solvent was evaporated and the crude product was purified by column chromatography using *n*-pentane/CH$_2$Cl$_2$ 3:1. The product as an orange solid (5 mg) was obtained in 19 % yield. Alternatively, the product may be purified by column chromatography on SiO$_2$ using *n*-pentane/AcOEt 15:1 as eluent followed by repeated washing with *n*-heptane.

^{1}H NMR (400 MHz, CD$_2$Cl$_2$): δ 8.15 (d, *J* = 8.1 Hz, 2H), 7.85 (dd, *J* = 8.4 Hz, *J* = 2.1 Hz, 6H), 7.76 (s, 2H), 7.68 (dd, *J* = 7.6 Hz, *J* = 1.2 Hz, 8H), 7.62–7.26 (m, 35H), 7.10 (s, 2H), 2.70 (t, *J* = 7.6 Hz, 4H), 1.69 (m, 4H), 1.40–1.21 (m, 44H), 0.88 (t, *J* = 6.8 Hz, 6H). ^{13}C NMR (125 MHz, CDCl$_3$): δ 152.21, 151.09, 147.17, 139.10, 135.77, 135.62, 133.68, 132.63, 132.60, 130.22, 130.02, 129.31, 128.24, 128.13, 125.70, 125.12, 124.59, 124.15, 123.14, 122.90, 120.92, 120.76, 110.43, 105.41, 93.14, 90.48, 90.18, 89.51, 36.10, 32.08, 31.44, 29.85 (2C), 29.81 (3C), 29.74, 29.65, 29.52, 29.44, 22.85, 14.29.

References

1. G. Vives, J. M. Tour *Acc. Chem. Res.* **2009**, *42*, 473–487.

2. T. Sasaki, J. M. Tour *Org. Lett.* **2008**, *10*, 897–900.

3. C. Joachim, G. Rapenne *ACS Nano* **2013**, *7*, 11–14.

4. E. Merino, M. Ribagorda *Beilstein J. Org. Chem.* **2012**, *8*, 1071–1090.

5. G. R. Mitchell, N. R. King *Macromol. Symp.* **1999**, *137*, 155–165.

6. G. Pace, V. Ferri, C. Grave, M. Elbing, C. von Hänisch, M. Zharnikov, M. Mayor, M. A. Rampi, P. Samorì *Proc. Natl. Acad. Sci. U. S. A.* **2007**, *104*, 9937–9942.

7. V. Ferri, M. Elbing, G. Pace, M. D. Dickey, M. Zharnikov, P. Samorì, M. Mayor, M. A. Rampi *Angew. Chem. Int. Ed.* **2008**, *47*, 3407–3409.

8. T. Kudernac, N. Ruangsupapichat, M. Parschau, B. Maciá, N. Katsonis, S. R. Harutyunyan, K.–H. Ernst, B. L. Feringa *Nature* **2011**, *479*, 208–211.

9. J.–F. Morin, Y. Shirai, J. M. Tour *Org. Lett.* **2006**, *8*, 1713–1716.

10. P.–T. Chiang, J. Mielke, J. Godoy, J. M. Guerrero, L. B. Alemany, C. J. Villagómez, A. Saywell, L. Grill, J. M. Tour *ACS Nano* **2012**, *6*, 592–597.

11. O. Villavicencio, D. V. McGrath in *Advances in Dendritic Macromolecules* (Ed: G. R. Newkome), Elsevier Science Ltd., Oxford, United Kingdom **2002**, *5*, p. 1–44.

12. R. Deloncle, A.-M. Caminade *J. Photochem. Photobiol. C* **2010**, *11*, 25–45.

13. J. Zeitouny, A. Belbakra, A. Llanes-Pallas, A. Barbieri, N. Armaroli, D. Bonifazi *Chem. Comm.* **2011**, *47*, 451–453.

14. T. Takahashi, T. Tanino, H. Ando, H. Nakano, Y. Shirota *Mol. Cryst. Liq. Cryst.* **2005**, *430*, 9–14.

15. J. Bahrenburg, C. M. Sievers, J. Boyke Schönborn, B. Hartke, F. Renth, F. Temps, C. Näther, F. D. Sönnichsen *Photochem. Photobiol. Sci.* **2013**.

16. P. Wolfer, H. Audorff, K. Kreger, L. Kador, H.-W. Schmidt, N. Stingelin, P. Smith *J. Mater. Chem.* **2011**, *21*, 4339–4345.

17. Y. Ito, H. Ito, T. Matsuura *Tetrahedron Lett.* **1988**, *29*, 563–566.

18. K. Yoshida, T. Koujiri, T. Horii, Y. Kubo *Bull. Chem. Soc. Jpn.* **1990**, *63*, 1658–1664.

19. H. Dahn, H. v. Castelmur *Helv. Chim. Acta* **1953**, *36*, 638–645.

20. F. Cisnetti, R. Ballardini, A. Credi, M. T. Gandolfi, S. Masiero, F. Negri, S. Pieraccini, G. P. Spada *Chem. Eur. J.* **2004**, *10*, 2011–2021.

21. J. Robertus, S. F. Reker, T. C. Pijper, A. Deuzeman, W. R. Browne, B. L. Feringa *Phys. Chem. Chem. Phys.* **2012**, *14*, 4374–4382.

22. M. V.d. Auweraer, C. Catry, L. Feng Chi, O. Karthaus, W. Knoll, H. H. Ringsdorf, M. Sawodny, C. Urban *Thin Solid Films* **1992**, *210/211*, 39–41.

23. Y.-W. Choi, Y.-K. Lim, S. U. Lee, C.-G. Cho, Y. Lee, D. Sohn *Curr. Appl. Phys.* **2007**, *7*, 513–516.

24. E. D. King, P. Tao, T. T. Sanan, C. M. Hadad, J. R. Parquette *Org. Lett.* **2008**, *10*, 1671–1674.

25. C. Tie, J. C. Gallucci, J. R. Parquette *J. Am. Chem. Soc.* **2006**, *128*, 1162–1171.

26. M. V. Peters, R. Goddard, S. Hecht *J. Org. Chem.* **2006**, *71*, 7846–7847.

27. M.–A. Kakimoto, M. Yoneyama, Y. Imai *J. Polym. Science: Part A: Polymer Chemistry* **2000**, *38*, 3911–3918.

28. K. Lee, F. Pan, G. T. Carroll, N. J. Turro, J. T. Koberstein *Langmuir* **2004**, *20*, 1812–1818.

29. F. A. Garlichs–Zschoche, K. H. Dötz *Organometallics* **2007**, *26*, 4535–4540.

30. A. I. Kiprianov, V. Buryak *Ukrainskii Khimicheskii Zhurnal (Russian Edition)* **1968**, *34*, 1016–1020.

31. R. Björnestedt, G. Zhong, R. A. Lerner, C. F. Barbas III *J. Am. Chem. Soc.* **1996**, *118*, 11720–11724.

32. A. Klapars, S. L. Buchwald *J. Am. Chem. Soc.* **2002**, *124*, 14844–14845.

33. R. Chinchilla, C. Nájera *Chem. Rev.* **2007**, *107*, 874–922.

34. O. M. Anisimova, M. E. Dzhanashvili, G. E. Krichevskii, V. M. Anisimov *Izv. Akad. Nauk SSSR, Ser. Khim.* **1983**, *32*, 846–848.

35. T. Hihara, Y. Okada, Z. Morita *Dyes and Pigments* **2006**, *69*, 151–176.

36. T. Hihara, Y. Okada, Z. Morita *Dyes and Pigments* **2007**, *75*, 225–245.

37. H. Rau *Photochemistry and Photophysics* (Ed: J. F. Rabek); CRC Press, Inc.; Boca Raton, FL, **1990**, *Vol. 2*, p.119.

38. P. D. Wildes, J. G. Pacifici, G. Irick Jr., D. G. Whitten *J. Am. Chem. Soc.* **1971**, *93*, 2004–2008.

39. T. Asano, T. Okada, S. Shinkai, K. Shigematsu, Y. Kusano, O. Manabe *J. Am. Chem. Soc.* **1981**, *103*, 5161–5165.

40. N. Nishimura, T. Sueyoshi, H. Yamanaka, E. Imai, S. Yamamoto, S. Hasegawa *Bull. Chem. Soc. Jpn.* **1976**, *49*, 1381–1387.

41. K. Matczyszyn, W. Bartkowiak, J. Leszczynski *J. Mol. Struct.* **2001**, *565–566*, 53–57.

42. J. García–Amorós, D. Velasco *Beilstein J. Org. Chem.* **2012**, *8*, 1003–1017.

43. C. R. Crecca, A. E. Roitberg *J. Phys. Chem. A* **2006**, *110*, 8188–8203.

44. N. Wazzan (2009) *Cis–Trans Isomerisation of Azobenzenes Studied by NMR Spectroscopy with In situ Laser Irradiation and DFT Calculations* PhD Thesis, University of Edinburgh, UK.

45. J. P. Otruba III, R. G. Weiss *J. Org. Chem.* **1983**, *48*, 3448–3453.

Chapter 5

Tuning the Rotation Rate of Light–Driven Molecular Motors

This chapter deals with unidirectional light-driven rotary molecular motors. The exceptional features of these molecules render them highly useful to a number of applications in nanotechnology. Many of these applications, however, would benefit from higher rotation rates. To this end a new molecular motor is designed, prepared and thoroughly studied.

Introduction

Many naturally occurring processes include nanometer-scale molecular motors. Myosins are a family of motor proteins that act in concert to achieve muscle contraction. Kinesins and dyneins exist in eukaryotic cells where they transport cellular cargo along the microtubule filaments. The bacterial flagellar motor is responsible for the movement of numerous cellular organisms while the F_1-motor of ATP synthase drives the synthesis of ATP in cells. These are but a few examples of the frequent occurrence of molecular motors in essential biological processes. All of them share a common goal however, and that is to harness work[1].

The development of nanotechnology has stimulated great interest to develop artificial molecular motors that would take inspiration from nature in providing work at the molecular level. Such molecular motors could undoubtedly play a fundamental role in the development of future nanodevices and machines[2]. These systems most often include the conversion of energy into controlled motion. Several entirely synthetic molecular motors have been designed and developed to provide controlled linear or rotary motion by making use of chemical energy, light energy or electron-transfer processes[2,3,4,5,6,7,8,9,10,11,12,13,14,15]. Furthermore, recent developments have allowed work to be harnessed from both synthetic linear molecular motors[16,17] as well as rotary molecular motors[3,18,19,20].

A class of the most promising artificial molecular motors is that based on overcrowded alkenes which possess the ability to undergo repetitive light-driven unidirectional rotary motion around the central C=C bond (the rotary axle). The rotation occurs through two fast photochemical isomerization steps and two slow and rate-determining thermal helix inversion steps[21]. These synthetic molecules have been shown to be able to perform work not only at the molecular level[20] but at the microscopic level as well[18,19].

Being able to tune the rotation rate is of utmost importance for the development of new and more complex motor systems as well as for their application[22,23]. Working with a slower motor may be desirable when trying to introduce new concepts as the isomerization processes are often easier to follow and the changes in properties are more readily studied with a slower motor than a fast one[19,24]. Application however will most often favour a faster motor; higher rotation rates of the motor will compete better with the „Brownian storm" of molecular vibrations and collisions[2,22]. Furthermore, it is highly desirable to have a system with a short response time. Yet another advantage of a faster rotating molecular motor is that it will deliver more work per unit time than a slow one (provided they both deliver the same work per rotation). In a rotational system, power is (classically) expressed[25] as the scalar product of the torque, $\vec{\tau}$, and the angular velocity, $\vec{\omega}$; $P = \vec{\tau} \cdot \vec{\omega}$. This means that a faster rotating motor will have higher power!

Our group has designed, prepared and studied a number of molecular motors[3]. Investigating the rate of rotation has always been paramount to their characterization as molecular motors. In course of this research it has been shown that the structures of both the upper and the lower half of the motor have a strong influence on the rotation rate. Many interesting structure–rate trends have arisen (Scheme 1). For example, a five-membered ring in the upper half of the second-generation motor instead of a six-membered ring will increase the rotation rate dramatically[22,26]. The analogous change in ring size in the lower half however has an opposite effect[27]. Changing the naphthyl group of the upper half for a *p*-xylyl[28] or for a benzothiophene group[29] will reduce the steric hindrance in the *fjord* region and also cause faster rotation. Furthermore, increasing the steric bulk of the substituent at the stereogenic centre has been shown to accelerate the rotation[22,30]; larger groups at this position increase the steric hindrance to a higher extent in the unstable form than in the transition state which results in a lower energy barrier.
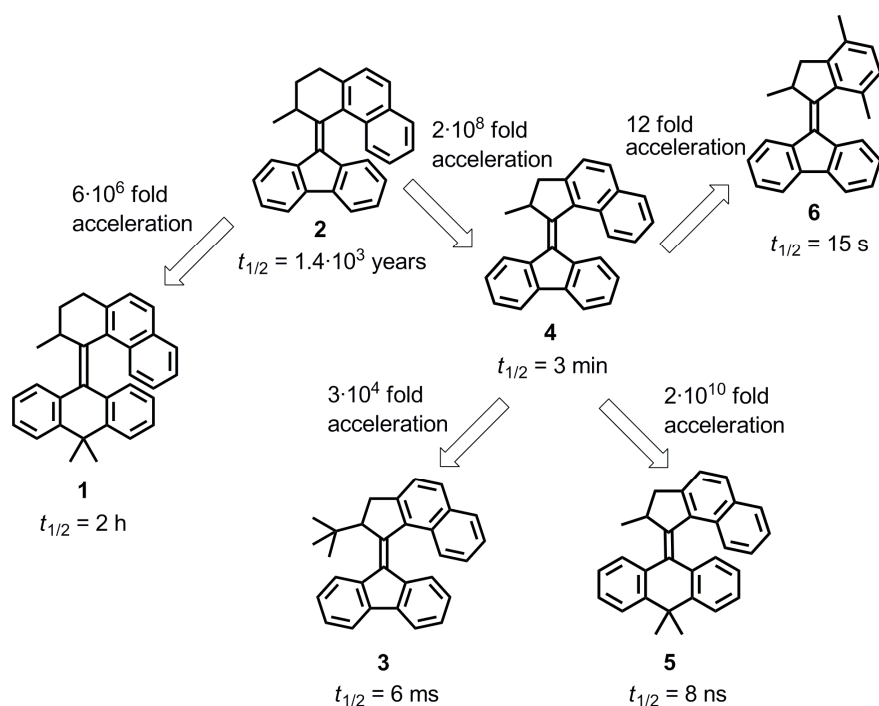
Scheme 1. Representative molecular motors and their rotation rates expressed in terms of the half-life of the thermal step, $t_{1/2}$, at room temperature.

We have been interested in designing faster molecular motors[22,37,38]. Scheme 1 shows a number of structural changes that have been used to achieve this *e.g.* changing the ring sizes or the substituents at the stereogenic centre or the aromatic parts. In our pursuit of faster motors we are interested in learning how many of these structural effects may simultaneously be incorporated into the design and still give a faster motor. As part of the gradual incorporation of the structural features that cause acceleration of the motor we would like to prepare and study molecular motors **7** and **17** as our next design (Fig 1). Motor **4**, as shown in scheme 1, may be accelerated by either replacing its naphthyl moiety by a xylyl moiety (motor **6**) or by

replacing the methyl substituent by a bulkier *tert*-butyl substituent (motor **3**). Motor **7**, our target molecule, may be viewed as having the best of both worlds; both the xylyl moiety and the *tert*-butyl substituent. As shown in Scheme 1, both structural variations seem to accelerate motor **4** individually. With our initial design of motor **7**, we would like to examine how these two „accelerating structural variations" act together. Will the new motor **7** be faster than motor **4**? Will it be faster than motors **3** and **6**? Do the accelerating effects cumulate and does this system retain its unidirectional nature? These are the questions we set out to address.
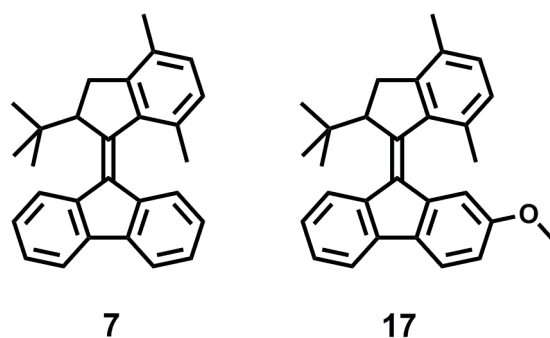

7   **17**

Figure 1. New design of the molecular motor.

Results and discussion

Synthesis and characterization

Overcrowded alkene **7** was synthesized according to Scheme 2. Ketone **9** was prepared by a sequential Friedel-Crafts acylation and alkylation reaction on *p*-xylene following a literature procedure[31,32]. Introducing a *tert*-butyl group in the α-position of ketone **9** required two reaction steps following a procedure for the conversion of cyclopentanone to 2-*tert*-butylcyclopentanone[33]; the ketone was first converted to the TMS-protected enol **10** which was then reacted with *t*-BuCl in the presence of $TiCl_4$ to give the upper-half ketone **11**. Thioketone **12** was prepared by reaction of the ketone with P_4S_{10} and proved to be remarkably stable; thioketones prepared for the synthesis of motors are normally quite unstable and are therefore immediately used in the next step[34]. Thioketone **12** however could be stored for weeks if free of residual P_4S_{10}. We reason that the *t*-Bu and Me group „protect" the thioketo-group rendering it unreactive. Preparing the lower half of the motor was straightforward; fluorenone **13** was converted into hydrazone **14** which was oxidized with MnO_2 to give diazofluorenone **15**. The crucial step of the synthesis was the diazo-thioketone coupling (Barton-Kellogg reaction)[35,36] which provided **16** in moderate yield. The prepared episulfide **16** was desulfurized with $P(C_6H_5\text{-OMe-}p)_3$ to give the overcrowded alkene **7**[35,36]. This more polar phosphine was used instead of the more commonly used PPh_3 due to easier separation of the formed $S=PAr_3$ as well as of the residual PAr_3 from the desired product.
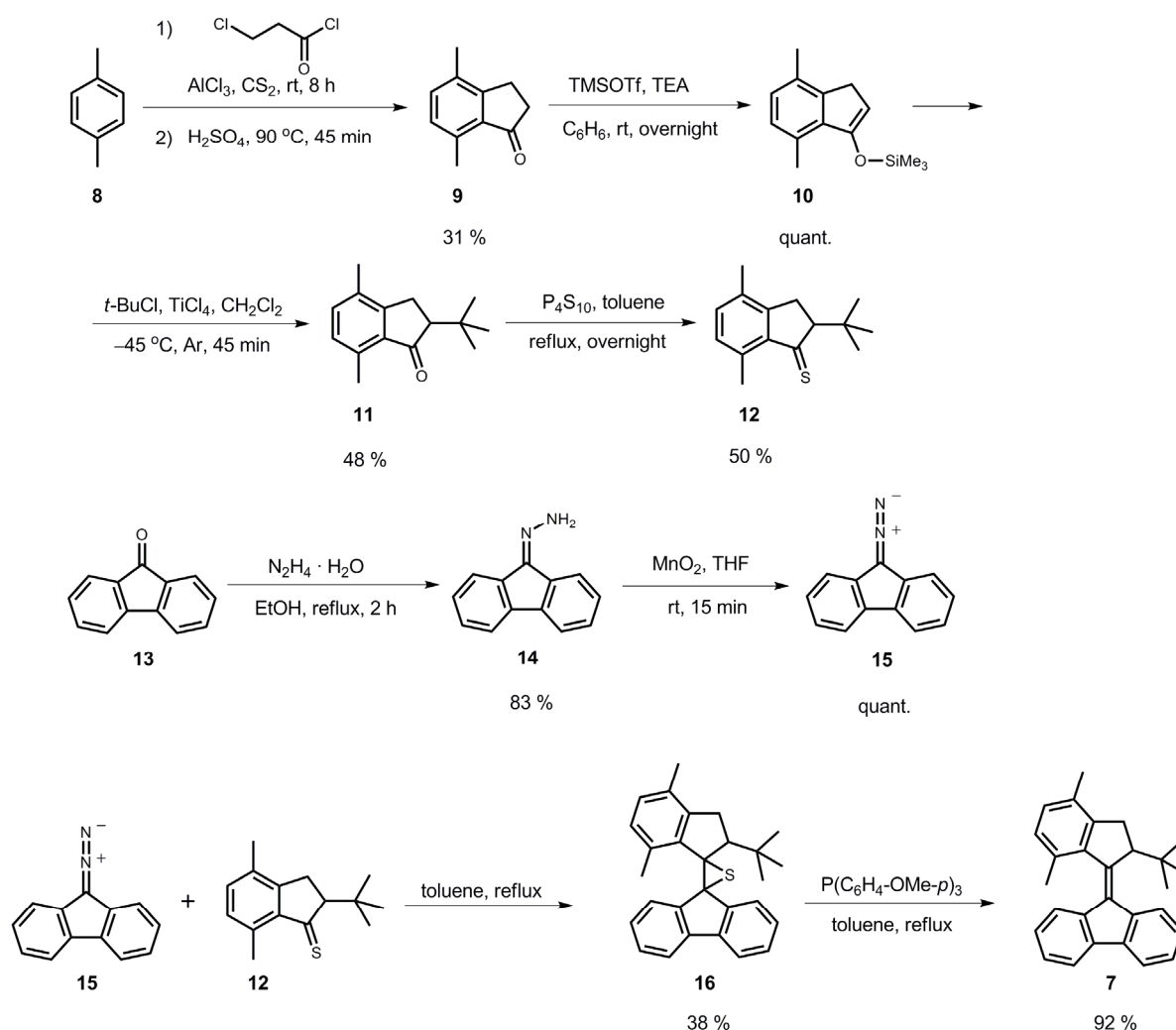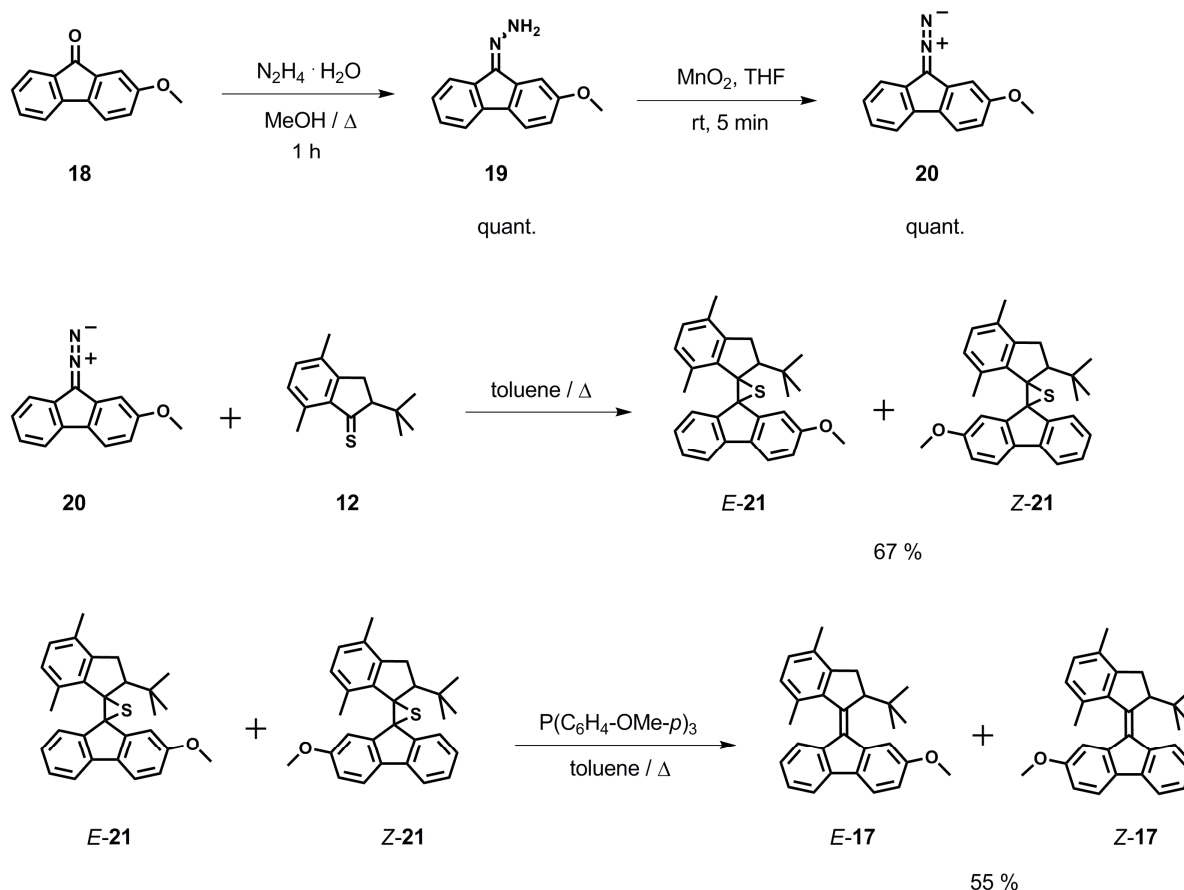
Scheme 2. Synthesis of overcrowded alkene **7**.

All the synthetic intermediates and the target overcrowded alkene **7** were characterized by ^{1}H–NMR and APT NMR spectroscopic techniques as well as by high resolution mass spectrometry (HRMS). In HRMS the final product **7** gives the mass that corresponds to the protonated molecule **7**, $[M+H]^+$. A pattern of three signals from the aliphatic ring protons of the five-membered upper half described earlier for similar overcrowded alkenes[35,36] is also found in the ^{1}H–NMR spectrum of the final product. In addition the signals from the carbon atoms of the central C=C bond are present in the ATP NMR spectrum.

Overcrowded alkene **17** was prepared through an analogous synthetic pathway as motor **7** (Scheme 3). Once more the crucial step in the synthesis was the diazo-thioketone coupling (Barton-Kellogg reaction) which was carried out in good yield. During the purification process of the resulting episulfides it was possible to collect a batch that mostly contained the isomer (*E*)-**21** and another one that mainly contained the other isomer, namely (*Z*)-**21**. These isomers were separately reacted under the desulfurization conditions (in the absence of light) in order to establish if the desulfurization step took place in a stereoselective fashion. Both reactions,

however, gave a mixture of (*E*)-**17** and (*Z*)-**17** in the ratio of 1:1 and are therefore not stereoselective. Molecular motors (*E*)-**17** and (*Z*)-**17** were not separable by column chromatography on silica or by crystallization. The isomers could be separated, however, by preparative HPLC.

Scheme 3. Synthesis of overcrowded alkene **17**.

The product **17** and the synthetic intermediates were characterized by ^{1}H–NMR and APT NMR spectroscopic techniques as well as by high resolution mass spectrometry. The configuration about the central double bond, however, could not be deduced from the ^{1}H–NMR and ^{13}C–NMR spectra of the two isomers of **17**. Both isomers were therefore analyzed by 2D–NOESY NMR techniques. The structures of both isomers of product **17** as well as the crucial NOE contacts are depicted in Fig 2. One isomer shows a NOE contact between the only aromatic proton giving a singlet in the ^{1}H–NMR spectrum (proton *o* in Fig 2) and the proton at the stereogenic centre (proton *f* in Fig 2) as well as with the protons of the *tert*-butyl group (protons *g* in Fig 2). The upper half protons *f* and *g* only come into spatial proximity with the lower half proton *o* in isomer *E*-**17**. The other isomer shows a NOE contact between a lower half aromatic proton that gives a doublet in the ^{1}H–NMR spectrum and proton *f* as well as protons *g* in the upper half. This contact is only possible for the aromatic proton *h* in the lower half (Fig 2) in isomer *Z*-**17**.

E-**17**   *Z*-**17**
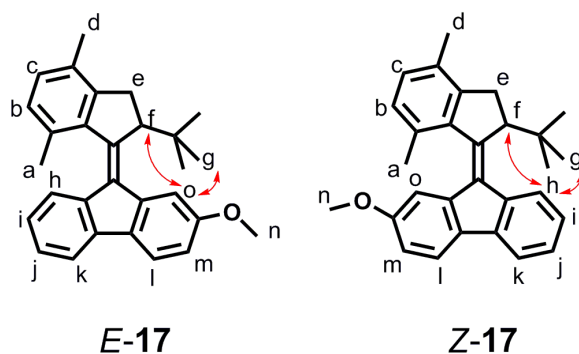
Figure 2. The structures of *E*-**17** and *Z*-**17** and the NOE contacts revealing the configuration about the central C=C bond.

## Photochemical characterization

UV−Vis spectroscopic study

The UV−Vis spectrum of overcrowded alkene **7** in *i*-pentane at −85 °C is shown in Fig 3. In the UV−Vis spectrum, upon irradiation with 365 nm light the band at λ_{max} = 350 nm disappears and at the same time a new band appears at λ_{max} = 430 nm. These changes were not observed at room temperature. The described process is completely reversible if irradiated with visible light (λ > 420 nm) (at −85 °C) or if the temperature is raised to room temperature to allow for the thermal process to take place.
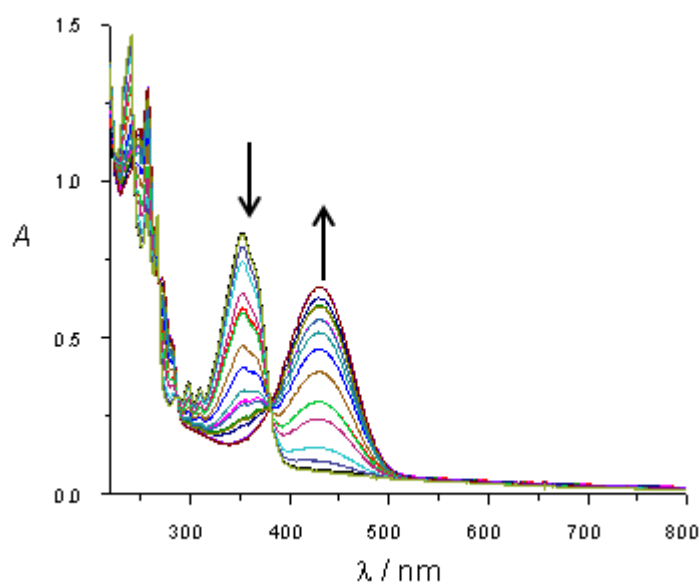
Figure 3. UV−Vis Spectra of motor **7**, c = 2.1·10^{-5} mol dm^{-3}, in *i*-pentane, at −85 °C. Irradiation at λ = (365±30) nm.

These processes correspond to the stable form of motor **7** undergoing photochemical isomerisation to give a mixture of the stable and unstable forms at

the photostationary state and the photochemical or thermal conversion of the unstable form back to the stable form of motor **7** as shown in Scheme 4.
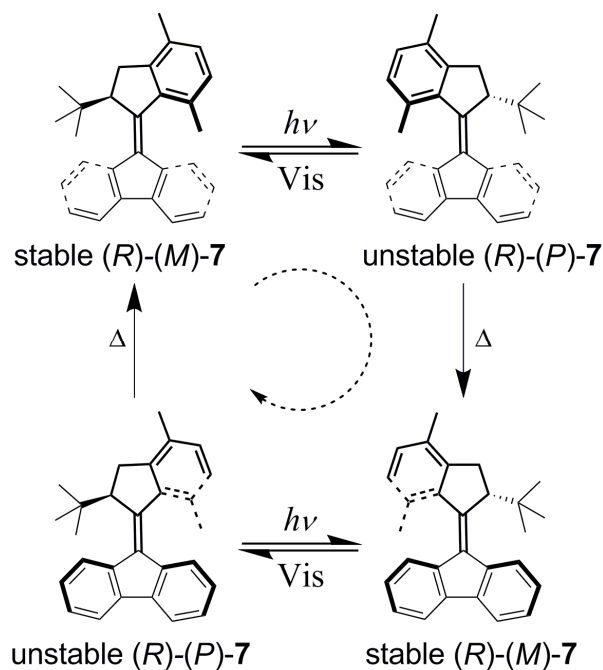
**Scheme 4.** Rotation cycle of motor (*R*)-**7**.

CD spectroscopic study

The same processes may also be followed by CD spectroscopy for which the two enantiomers of motor **7** were resolved. This was achieved by chiral preparative HPLC. As expected the two enantiomers gave CD spectra of opposite sign. Only one enantiomer was chosen for further experiments. In Fig 4 the CD spectrum of the chosen enantiomer of motor **7** was compared to the calculated CD spectrum of the (*R*)-(*M*)-**7** which is the stable form of (*R*)-**7** (*R* defines the absolute configuration at the stereogenic centre in **7**). They agreed well revealing the absolute configuration of the stereogenic centre of the chosen enantiomer of motor **7** as (*R*). Furthermore, the CD spectrum of **7** at the photostationary state reached by irradiation of the chosen enantiomer of motor **7** with 365 nm light at −150 °C compared well with the calculated CD spectrum of (*R*)-(*P*)-**7** which is the unstable form of the (*R*)-motor. The CD spectra were calculated in the gas phase using TD-DFT B3LYP 6-31G(d,p).
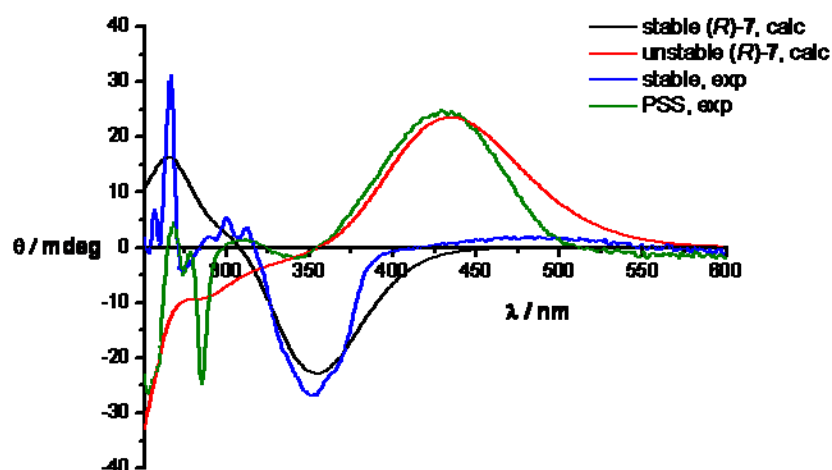
Figure 4. Experimental CD spectra of the chosen enantiomer of motor **7** taken in *i*-pentane, *c* = 2.7 x 10^{-5} mol dm^{-3}. Photostationary state (PSS) reached with 365 nm light. Calculated spectra for (*R*)-**7** obtained using TD-DFT B3LYP 6-31G(d,p).

The switching process of (*R*)-**7** was investigated by CD spectroscopy as depicted in Fig 5. The measurements were performed at −150 °C to prevent any thermal processes at the time scale of the experiments. Irradiation with 365 nm causes the disappearance of the CD signal with λ_{max} = 350 nm and the appearance of a new CD signal with λ_{max} = 430 nm. The positions of the two interconverting CD bands correspond to the positions of the two interconverting UV−Vis bands in terms of wavelength, λ_{max}, Fig 3. The two CD bands are of the opposite sign however, indicating a change in helicity of the motor. This corresponds to reaching the photostationary state upon irradiation with 365 nm. This process can be reversed either photochemically or thermally; irradiation with visible light at λ > 420 nm or warming up to −30 °C restores the original CD spectrum (Fig 5).
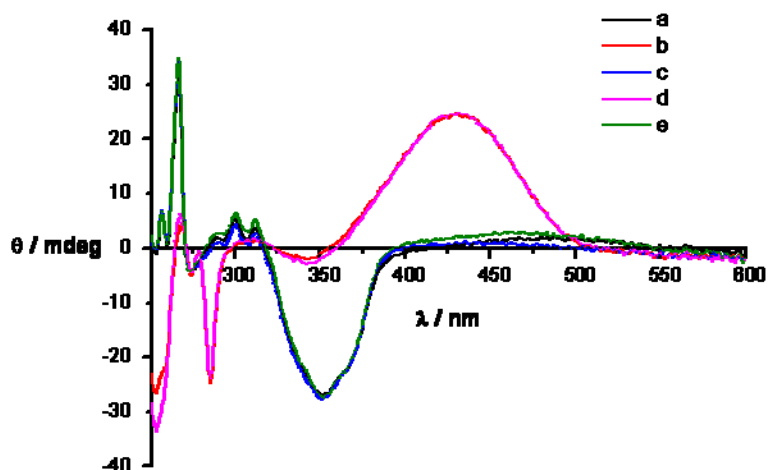
Figure 5. CD spectra of (*R*)-**7** in *i*-pentane, c = 2.7 x 10^{-5} mol dm^{-3}; the photochemical and thermal steps are followed. **a:** sample at 123 K in the absence of light, **b:** sample at 123 K at the PSS (irradiated with UV light at 365 nm for 45 min), **c:** sample in state **b** irradiated with visible light of λ > 420 nm for 1.25 h (123 K), **d:** sample in state **c** irradiated to the PSS (irradiated with UV light at 365 nm for 35 min) at 123 K, **e:** sample in state **d** warmed up to 243 K and then cooled down to 123 K again.

The CD experiments show that the overcrowded alkene **7** changes its helicity in the photochemical as well as in the thermal step (Fig 5) in accordance with the isomerization processes depicted in Scheme 4.

Kinetics of the thermal isomerization

The rotation cycle of a motor comprises two photochemical and two thermal steps. For a motor with a symmetrical lower half, the rotation cycle will have two identical photochemical and two identical thermal steps (Scheme 4). Photochemical steps are fast and thermal steps are slow and therefore rate determining. The rotation rate of motors is thus expressed by the half-life of the thermal step at room temperature. Determining the half-life of the thermal step at room temperature requires either that the reaction kinetics be followed at room temperature or that the kinetic data be extrapolated from the temperatures used. For a fast motor like **7**, following the reaction kinetics at room temperature can prove impossible using standard spectroscopic techniques like UV–Vis, CD or NMR spectroscopy as at room temperature the thermal step is much too fast to be measured by those techniques. A way to come around this, as mentioned above, is to perform the measurements at low temperatures where the reaction is slow enough to be followed by these spectroscopic techniques. The data collected at different (low) temperatures can then be extrapolated to give the half-life at room temperature[37].

We followed the reaction by low-temperature UV–Vis spectroscopy. A solution of motor **7** in *i*-pentane was irradiated with UV light (λ = 365 nm) at −150 °C until the

photostationary state was reached. The rate of thermal isomerization was then followed by UV–Vis spectroscopy at five different temperatures in the range between −75 °C and −100 °C. The data are shown in Fig 6.
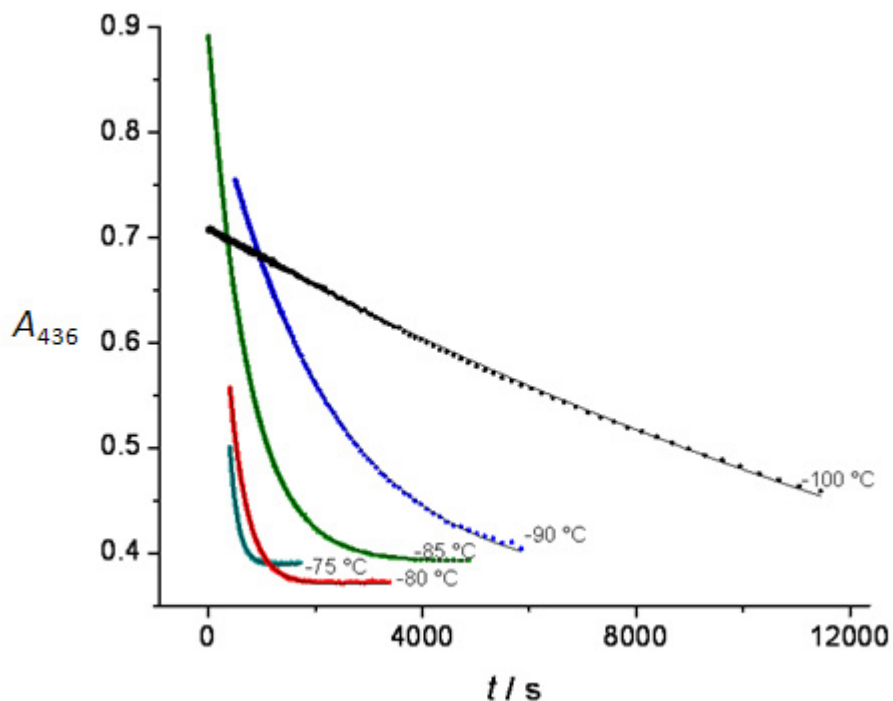
Figure 6. Thermal relaxation of motor **7** in the dark after reaching PSS with irradiation at λ = (365±30) nm, c = 2.1·10^{-5} mol dm^{-3}, in *i*-pentane, followed over time by means of monitoring the absorbance at 436 nm. (·) experimental data, (−) calculated data by means of regression analysis.

The data were fitted to a first-order rate law exponential function by non-linear regression analysis. The resulting half-lives at the measured temperatures are given in Table 1. The values are determined to be between 2 and 250 min in the temperature range between −75 °C and −100 °C.

Table 1. The half-lives, $t_{1/2}$, at different temperatures obtained from the regression analysis of the data in Fig 6.

Θ / °C	$t_{1/2}$ / min	R^2
−75	1.7	0.99955
−80	3.8	0.99977
−85	8.4	0.99992
−90	25	0.99982
−100	250	0.99898

The data in Table 1 can be fitted to the Eyring equation from which the activation enthalpy, $\Delta^{\ddagger}H$ = (55 ± 1.7) kJ mol^{-1}, and entropy, $\Delta^{\ddagger}S$ = (−1.3 ± 9.4) J K^{-1} mol^{-1} can be calculated (Fig 7). These parameters allow for the extrapolation of the data to room temperature. The half-life of the thermal step was in this way determined to be 1 ms at room temperature. These values were derived from the measurements carried out in *i*-pentane.
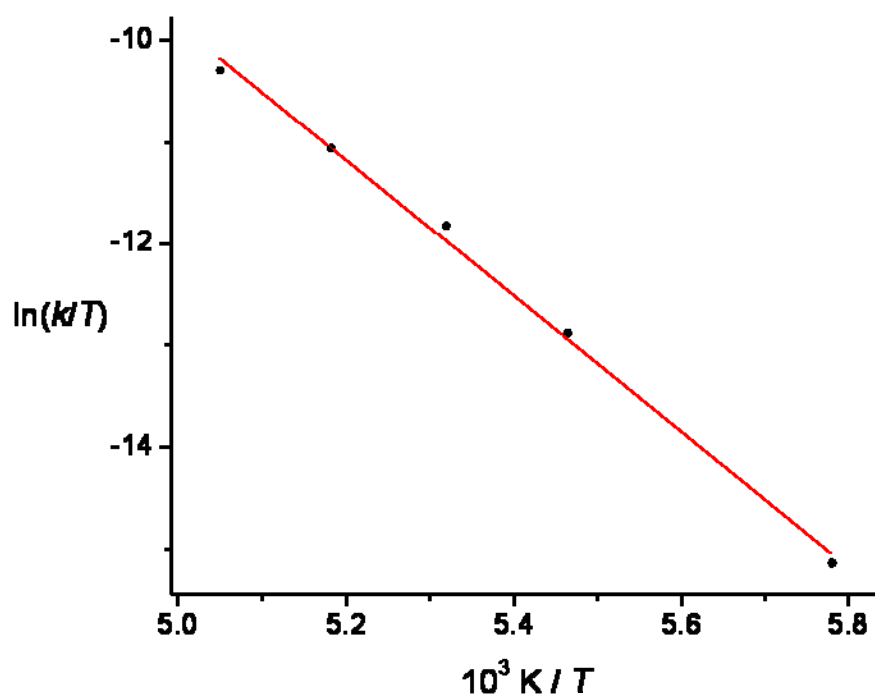
**Figure 7.** The data from Table 1 analyzed by means of the Eyring equation. (·) experimental data, (–) calculated data by means of regression analysis.

This value is obtained by extrapolation over a large temperature range (around 100 K) and the extrapolation is carried out over a logarithmic scale which may introduce a significant error. Furthermore, one cannot exclude the possibility that the

motor exhibits different behavior at low temperatures than at room temperature. For these reasons it is necessary to check the value obtained by the low-temperature kinetic study. The use of a technique that could be used at room temperature would be beneficial; it would allow us to measure the kinetics directly at and around room temperature and it would speed up the experiments as the reaction proceeds much faster at room temperature. We then turned to the use of transient absorption to follow the thermal step around room temperature. This technique is able to record light intensity with high time resolution allowing to follow very fast processes[37,38].

Transient absorption was used to follow the thermal step in *n*-heptane in the temperature range from 15 to 45 °C. A representative transient absorbance trace is shown in Fig 8. The data were fitted to a first-order rate law exponential function to obtain the half-lives at the measured temperatures (Table 2).
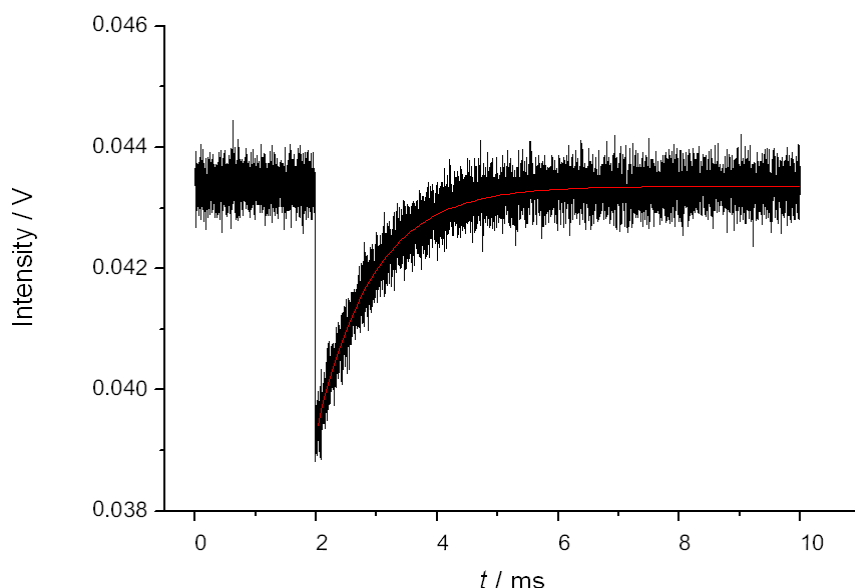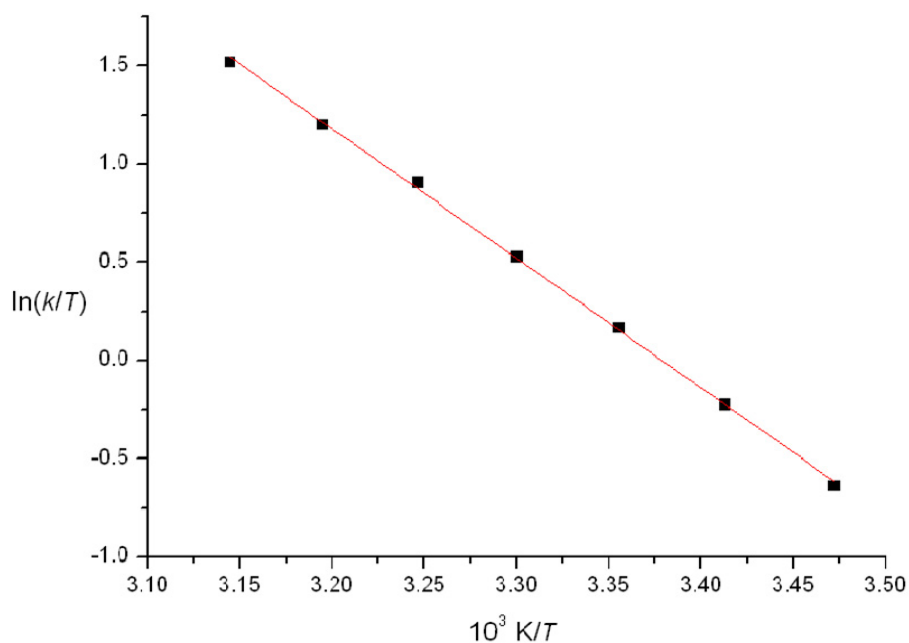

Figure 8. Transient absorption measurements performed on motor **7** in *n*-heptane at 35 °C. PSS reached with 355 nm laser (3 mJ per pulse). Light intensity followed at 430 nm. Experimental data given in black, (–) calculated data by means of regression analysis.

Table 2. The half-lives, $t_{1/2}$, at different temperatures obtained from the regression analysis of the data obtained by transient absorption.

Θ / °C	$t_{1/2}$ / ms
15	4.6
20	2.9
25	2.0
30	1.4
35	0.9
40	0.7
45	0.5

The data obtained were analyzed according to the Eyring equation (Fig 9). From the analysis, the parameters $\Delta^{\ddagger}H$ = (55 ± 1.1) kJ mol^{-1} and $\Delta^{\ddagger}S$ = (−12 ± 4) J K^{-1} mol^{-1} can be calculated. These can be used to calculate the half-life at room temperature, $t_{1/2}$ = 3 ms. These values agree well with those obtained by the UV−Vis spectroscopic study.

Figure 9. The data from the transient absorption measurements analyzed by means of the Eyring equation. (·) experimental data, (−) calculated data by means of regression analysis.

The values of the half-life at room temperature obtained by low-temperature UV−Vis spectroscopy ($t_{1/2}$ = 1 ms, measured in *i*-pentane) and transient absorption ($t_{1/2}$ = 3 ms, measured in *n*-heptane) compare very well. This shows that the kinetics of the thermal step may reliably be followed by any of the two techniques. For fast molecular motors, such as **7**, it is more practical and less time-consuming to follow the process at room temperature by transient absorption spectroscopy.

Furthermore, our result shows that motor **7** exhibits the same behaviour in the thermal step at low temperature as it does at room temperature justifying the process of extrapolation used to obtain the half-life at room temperature from the low-temperature UV−Vis study.

Motor **7** may now be compared to other motors from Scheme 1 on the basis of the half-lives at room temperature (the average of the two experimentally determined values for motor **7** is taken for the comparison). Motor **7** is faster than motor **4** by a factor of 10^5, but also faster 10^4 times than motor **6** and 4 times faster than motor **3**. From this we conclude that adding two „accelerating structural features" to motor **4** makes it indeed faster than adding just any one of them. By simply multiplying the accelerating effects from Scheme 1 (for going from motor **4** to motor **3** and from **4** to **6**) one could roughly predict $4{\times}10^5$ acceleration for going from motor **4** to motor **7**. Such a rough „prediction" actually turns out to be quite close to the acceleration of 10^5 that we observe in reality.

Theoretical investigations (DFTB3LYP6-31G(d,p)) of the unstable and stable forms of motor **7** as well as of the transition state for the thermal process between the two forms were also conducted in the gas phase. The calculated value $\Delta^{\ddagger}G$ = 53 kJ mol^{-1} for the thermal process is in good agreement with the experimentally determined ones ((55 ± 4) and (58 ± 3) kJ mol^{-1} at room temperature, as determined by low-temperature UV−Vis spectroscopy in *i*-pentane and transient absorption spectroscopy in *n*-heptane, respectively). The half-life at room temperature is calculated to be $t_{1/2}$ = 0.4 ms, also in good agreement with the experimentally determined values. The minor differences in the values are most likely due to the solvent effect.

Unidirectionality of rotation

In order to perform continuous work a rotary molecular motor should exhibit unidirectional rotation. The rotary motion of a new motor should therefore be tested for unidirectionality. Motor **7**, however, is not suitable for this because it only has one stable and one unstable form due to its symmetrical lower half so there is no way of telling which direction the rotation adopts on going from the unstable to the stable form. For that reason we have designed molecular motor **17**, bearing a nonsymmetric lower half; this molecule has two distinct stable forms and two distinct unstable forms, as shown in scheme 5. It should now be possible to observe which

unstable form thermally relaxes into which stable form and if the overall rotary process is indeed unidirectional.
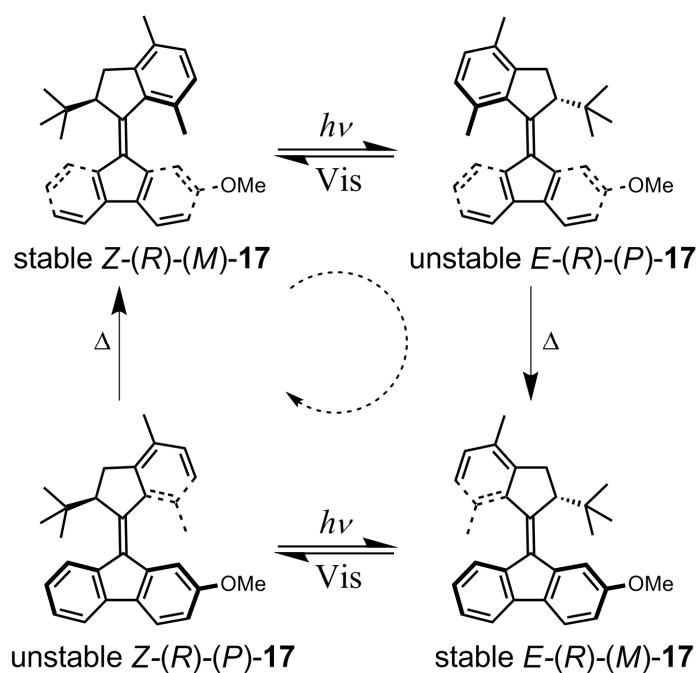

Scheme 5. Rotation cycle of motor (*R*)-**17**.

As mentioned above, in order to confirm unidirectionality of the rotation process one needs to study the directionality of the two thermal steps (Scheme 5). This means one needs to compare the composition of the mixture after each thermal step to the composition of the mixture prior to the thermal step i.e. after the photochemical step (at the photostationary state). The composition of the mixture after the thermal process (ratio of the *E*- and *Z*-stable forms of **17**) can easily be determined by HPLC analysis. The composition of the mixture at the photostationary state (ratio of the unstable form and the stable form of **17**), however, is more difficult to determine because the photostationary state is reached at −150 °C to prevent the unstable form from undergoing the thermal process. Any analysis at that temperature would be extremely difficult to carry out. There is a method developed by Fischer, however, that allows for the estimation of the composition at the photostationary state from UV–Vis spectra by irradiating the sample at two different wavelengths (in two separate experiments)[39]. The method is based on the assumption that the ratio of the quantum yields of the starting and the newly formed species is independent of the wavelength used to reach the photostationary state and therefore allows to calculate the composition at the photostationary state from the difference in the UV–Vis spectra taken at the two photostationary states.

Fig 10 shows the UV–Vis spectra of the stable forms of **17** as well as of the photostationary state mixtures reached by irradiation at two different wavelengths, namely 334 and 365 nm. Using the data from Fig 10 one can apply Fischer's method[39] to estimate the compositions of the mixtures at the photostationary states.

Irradiating *E*-**17** at 334 nm gives the unstable form *Z*-**17** and the stable form *E*-**17** in a 96:4 ratio and irradiating at 365 nm gives the ratio of 97:3. Irradiating *Z*-**17** at 334 nm and 365 nm both give more than 98 % of the unstable form. Motor **17** has a remarkably high content of the unstable form at the photostationary state which is a prerequisite for good working efficiency.
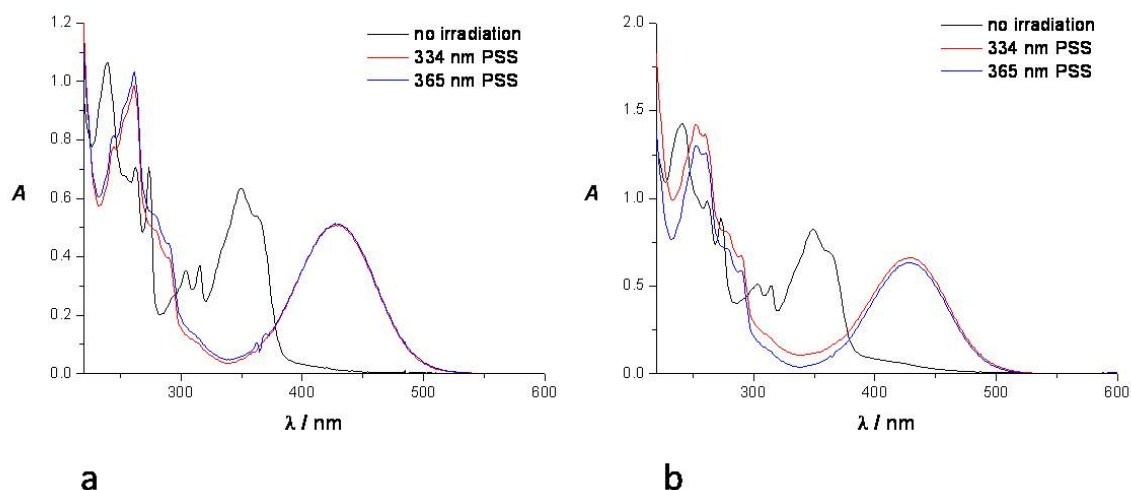
Figure 10. UV–Vis spectra of *Z*-**17** (a) and *E*-**17** (b) taken in *i*-pentane, $c = 2.0 \cdot 10^{-5}$ mol dm^{-3} at −150 °C. Irradiation performed at −150 °C.

The samples irradiated to the photostationary state were then warmed up to room temperature and subsequently analyzed by HPLC to determine the contents of the mixture, namely the ratio of the *E*- and *Z*-stable forms of **17**. The sample of *Z*-**17**, that had been irradiated to the photostationary state with 334 nm light (more than 98 % of the unstable form) and then allowed to warm up, now contained the two stable forms *E*-**17** and *Z*-**17** in a 96:4 ratio. The same result was obtained with 365 nm light. The sample of *E*-**17**, that had been irradiated to the photostationary state with 334 nm light (the unstable *Z*-**17** and stable *E*-**17** form in 96:4 ratio) and then allowed to warm up, now contained the two stable forms *Z*-**17** and *E*-**17** in a ratio of 96:4. The sample of *E*-**17**, that had been irradiated to the photostationary state with 365 nm light (the unstable form *Z*-**17** and the stable form *E*-**17** in a 97:3 ration) and then allowed to warm up, now contained the two stable forms *Z*-**17** and *E*-**17** in a ratio of 93:7. The ratios of the *E*- and *Z*-stable forms of **17** correspond well with the estimated ratios of stable and unstable forms of **17** at the photostationary states. These results show that practically all of the *Z*-unstable form thermally converts to the *Z*-stable form and that the *E*-unstable form thermally converts to the *E*-stable form (Scheme 5). This proves the unidirectionality of the thermal steps and therefore also confirms the unidirectionality of the rotation.

We have shown that the thermal steps are highly efficient (practically all of the unstable form converts to a single stable form) as well as the photochemical steps (very high content of the unstable form). These findings reflect the high efficiency of motor **17** in performing unidirectional rotation.

Conclusions

The elucidation of key structural parameters that govern the rotary speed of light-driven molecular motors is paramount for the design of future systems based on these molecules. To this end we have successfully synthesized a new molecular motor comprising a fluorene lower half and a five-membered ring upper half; the upper half ring is fused to a *p*-xylyl moiety and bears a *tert*-butyl group at the stereogenic centre. The photochemical and thermal behaviour of the motor was studied by low temperature UV−Vis and CD spectroscopic techniques. The kinetics of the thermal isomerization were studied by both low temperature UV−Vis spectroscopy as well as with transient absorption spectroscopy at room temperature and the half-life of the process at room temperature was determined to be 1 and 3 ms, respectively. The values are in very good agreement. In accordance with our predictions the molecular motor shows faster rotation rate (10^4 times) than its analogue bearing a methyl group at the stereogenic centre instead of a *tert*-butyl group. It is also faster (4 times) than the analogue with a naphthyl group fused to the five-membered upper half ring instead of a *p*-xylyl group. This shows that the *tert*-butyl and the *p*-xylyl groups on the five-membered upper half ring may be used simultaneously in the same molecular design to achieve acceleration of the rotation rate of the molecular motor larger than the acceleration obtained by using any one of the two groups individually.

A 2-methoxy-fluorene derivative of the new molecular motor was also synthesized with the purpose of studying the directionality of the motor's rotation. The new molecular motor shows remarkably high photostationary states (above 96 % of the unstable form upon irradiation) as well as unidirectional rotation. These properties make this molecular design highly promising for the use in future applications where molecular motors will be utilized to deliver work.

Acknowledgements

Experimental section

Synthesis, characterization and physico–chemical measurements

General remarks

The experiments were performed as described in the section *General Remarks* in Chapter 2. Cryo–UV–Vis and CD measurements were performed using an Oxford Instruments OptistatDN variable temperature liquid nitrogen cryostat inserted into a Hewlett-Packard HP 8453 FT spectrophotometer or a JASCO J–715 spectropolarimeter. Transient Absorption (TA) experiments were performed using a Nd:YAG Laser: FWHM8 ns, 355/532/1064 nm, up to 600 mW and a Xenon lamp: 250–800 nm, a monochromator 200–2500 nm with an accuracy of 0.2 nm and a PMT 185–900 nm detector. Preparative HPLC purifications were performed on a Shimadzu HPLC system consisting of two LC-20AT pumps, a DGU-20A$_3$ degasser, a SIL-20AC-HT auto-sampler, a CTO-20AC column oven, an SPD-M20A photo diode array detector, an FRC-10A fraction collector and a CBM-20A communication bus module. Irradiation experiments with UV light were performed using a Spectroline model ENB-280C/FE lamp with λ = (312 ± 30) nm and λ = (365 ± 30) nm or a 200 W Oriel Hg–lamp fitted with suitable bandpass filters (typical bandwidth of 10 nm).

The Gaussian 09 program was used for geometry optimizations and the calculation of energies[40]. Initial geometries were optimized using semi-empirical PM3. Geometry optimizations were performed on B3LYP/6-31G(d,p) using tight convergence criteria. To ensure that minima and transition states were reached, frequency analyses of the obtained structures were evaluated; all minima had no imaginary frequencies while all transition states were first-order. Energies reported are SCF energies. CD spectra were calculated using B3LYP/6-31G(d,p).

(4,7-dimethyl-1*H*-inden-3-yloxy)trimethylsilane (10): To a stirred solution of ketone **9**[31,32] (3.0 g, 19 mmol) and Et$_3$N (8.0 ml, 57 mmol) in benzene (60 ml) under a nitrogen atmosphere was added TMSOTf (8.0 ml, 46 mmol) and the resulting mixture was stirred overnight at room temperature. The progress of the reaction was followed by TLC (*n*-pentane/AcOEt 30:1) but care should be taken as the product decomposes on silica. The reaction was quenched by the addition of a saturated aqueous NaHCO$_3$ solution (50 ml). The organic layer was separated and the aqueous layer was washed with *n*-pentane (3 x 20 ml). The combined organic layers were dried on anhydrous Na$_2$SO$_4$. After filtration the solvent was evaporated affording a brown liquid that solidified upon standing. A ^{1}H–NMR spectrum of the crude intermediate **3** showed the complete conversion of ketone **9** into intermediate **10** which was used in the next step without further purification.

^{1}H NMR (400 MHz, CDCl$_3$): δ 7.04 (d, *J* = 7.6 Hz, 2H), 7.00 (d, *J* = 7.6 Hz, 2H), 5.47 (t, *J* = 1.8 Hz, 1H), 3.19 (d, *J* = 1.8 Hz, 2H), 2.65 (s, 3H), 2.38 (s, 3H), 0.40 (s, 9H).

^{13}C NMR (100 MHz, CDCl$_3$): δ 155.67, 141.97, 138.40, 130.37, 129.08, 128.69, 126.46, 105.25, 32.66, 29.95, 18.04, 17.71.

2-*tert*-butyl-4,7-dimethyl-2,3-dihydro-1*H*-inden-1-one (11): Crude compound **10** (obtained from 19 mmol of ketone **9**) was dissolved in dry dichloromethane (24 ml), which was degassed with argon, and 2.4 ml (21 mmol) of *t*-BuCl was added under an argon atmosphere. The solution was cooled down to −50 °C and TiCl$_4$ (2.4 ml, 21 mmol) was added in one portion. The reaction mixture was stirred at that temperature and the progress of the reaction was monitored by TLC (*n*-pentane/AcOEt 30:1). After approximately 1 h the reaction was quenched by adding water (50 ml) and 25 ml of dichloromethane. The layers were separated and the organic layer was washed once more with water and once with diluted aqueous NaHCO$_3$ solution. The organic solution was dried on anhydrous Na$_2$SO$_4$. After filtration the solvent was evaporated affording a brown liquid which was purified by column chromatography on silica using *n*-pentane/AcOEt 30:1 as eluent. This afforded ketone **11** as a waxy off-white solid (2.0 g) in 48 % yield.

^{1}H NMR (400 MHz, CDCl$_3$): δ 7.22 (d, *J* = 7.4 Hz, 1H), 6.99 (d, *J* = 7.4 Hz, 1H), 3.02 (dd, *J* = 17.4, 8.1 Hz, 1H), 2.78 (dd, *J* = 17.4, 3.7 Hz, 1H), 2.58 (s, 3H), 2.44 (dd, *J* = 7.7, 4.4 Hz, 1H), 2.31 (s, 3H). ^{13}C NMR (100 MHz, CDCl$_3$): δ 209.52, 152.93, 135.87, 135.07, 134.30, 132.47, 129.37, 56.91, 33.93, 28.61, 27.84, 18.27, 17.63. HRMS (ESI): *m/z* calculated for C$_{15}$H$_{21}$O$^+$: 217.15924 [M+H]$^+$, found 217.15877 [M+H]$^+$.

2-*tert*-butyl-4,7-dimethyl-2,3-dihydro-1*H*-indene-1-thione (12): Ketone **11** (614 mg, 2.84 mmol) was dissolved in dry toluene (60 ml) and P$_4$S$_{10}$ (14.0 g, 31.5 mmol) was added to the solution. The reaction mixture was heated at reflux with stirring, under a nitrogen atmosphere. After 18 h the reaction mixture was cooled down to room temperature and filtered over a plug of silica (silica flushed with more toluene until all the green component was collected). After removal of the solvent, the crude thioketone was purified by column chromatography on silica using *n*-pentane/toluene 7:1 as eluent. Product **12** was collected as a dark blue liquid (327 mg) in 50 % yield and stored at −24 °C under an argon atmosphere.

^{1}H NMR (400 MHz, CDCl$_3$): δ 7.21 (d, *J* = 7.5 Hz, 1H), 7.01 (d, *J* = 7.5 Hz, 1H), 3.04 (s, 3H), 2.68 (s, 3H), 2.35 (s, 3H), 0.97 (s, 9H). ^{13}C NMR (100 MHz, CDCl$_3$): δ 250.11, 152.94, 145.04, 136.56, 133.47, 132.02, 130.67, 71.17, 35.27, 33.13, 27.97, 21.71, 18.20. HRMS (ESI): *m/z* calculated for C$_{15}$H$_{21}$S$^+$: 233.13640 [M+H]$^+$, found 233.13602 [M+H]$^+$.

Dispiro[9*H*-fluorene-9,2'thiirane-3',1''-(2''-*tert*-butyl-4'',7''-dimethyl-2'',3''-dihydro-1*H*-inden)] (16): Thioketone **12** (50 mg, 0.22 mmol) and diazofluorenone **15** (83 mg, 0.44 mmol) were dissolved in dry toluene (20 ml) under a nitrogen atmosphere and the mixture was stirred at 70 °C for 1 h. The temperature of the solution was slowly increased until reflux. The reaction ran overnight at reflux and

was followed by TLC (*n*-pentane/AcOEt 300:1). Upon depletion of the starting compounds **12** and **15**, solvent was evaporated. The crude product was first purified by column chromatography on silica with *n*-pentane/toluene 11:1 as eluent and then by crystallization from *n*-heptane. Episulfide **16** was obtained as a white solid (32 mg) in 38 % yield.

^{1}H NMR (500 MHz, CDCl$_3$): δ 7.71 (d, *J* = 7.3 Hz, 1H), 7.62 (d, *J* = 7.5 Hz, 1H), 7.52 (d, *J* = 7.6 Hz, 1H), 7.39 (t, *J* = 7.0 Hz, 1H), 7.32 (t, *J* = 7.5 Hz, 1H), 7.18 (t, *J* = 7.2 Hz, 1H), 7.09 (d, *J* = 7.8 Hz, 1H), 6.95 (t, *J* = 7.6 Hz, 1H), 6.81 (d, *J* = 7.7 Hz, 1H), 6.77 (d, *J* = 7.7 Hz, 1H), 2.83 (s, 3H), 2.71 (d, *J* = 6.2 Hz, 1H), 2.42 (d, *J* = 15.7 Hz, 1H), 2.03 (dd, *J* = 15.7, 6.2 Hz, 1H), 1.97 (s, 3H), 0.87 (s, 9H). ^{13}C NMR (125 MHz, CDCl$_3$): δ 145.73, 144.26, 142.40, 141.23, 141.21, 139.09, 132.75, 130.36, 129.61, 128.89, 127.87, 127.55, 126.60, 126.23, 125.97, 124.40, 119.97, 119.61, 60.99, 56.32, 51.59, 34.60, 31.64, 29.28, 20.92, 18.23. HRMS (ESI): *m/z* calculated for C$_{28}$H$_{29}$S$^+$: 397.19900 [M+H]$^+$, found 397.19827 [M+H]$^+$.

9-(2-*tert*-butyl-4,7-dimethyl-2,3-dihydro-1*H*-inden-1-ylidene)-9*H*-fluorene   (7): Episulfide **16** (32 mg, 0.08 mmol) was dissolved along with P(C$_6$H$_5$-OMe-*p*)$_3$ (35 mg, 0.10 mmol) in dry toluene (10 ml) and the stirred mixture was heated at reflux overnight, under a nitrogen atmosphere. The solvent was evaporated and the crude product purified by column chromatography on silica with *n*-pentane/AcOEt 300:1 as eluent. Product **7** was obtained as a white solid (27 mg) in 92 % yield. The enantiomers of **7** were separated by preparative chiral HPLC on an OD−H column with *n*-heptane/propane-2-ol 97:3 as eluent at a flux of 0.5 ml min^{-1}.

^{1}H NMR (500 MHz, CD$_2$Cl$_2$): δ 8.26 (dd, *J* = 5.5, 3.2 Hz, 1H), 7.83 (dd, *J* = 5.5, 3.2 Hz, 1H), 7.76 (d, *J* = 7.5 Hz, 1H), 7.47 (d, *J* = 7.9 Hz, 1H), 7.38 (dd, *J* = 5.7, 3.1 Hz, 2H), 7.30 (t, *J* = 7.4 Hz, 1H), 7.11 (m, 2H), 7.05 (d, *J* = 7.7 Hz, 1H), 4.22 (d, *J* = 5.6 Hz, 1H), 3.03 (dd, *J* = 15.0, 5.5 Hz, 1H), 2.86 (d, *J* = 15.0 Hz, 1H), 2.32 (s, 3H), 2.28 (s, 3H), 0.88 (s, 9H). ^{13}C NMR (125 MHz, CD$_2$Cl$_2$): δ 152.21, 146.29, 142.62, 140.69, 139.77, 139.55, 138.52, 133.29, 130.89, 130.86, 130.38, 128.54, 127.48, 127.24, 126.94, 126.65, 125.38, 124.10, 119.81, 119.22, 58.64, 35.80, 35.46, 29.01, 20.66, 18.26. HRMS (ESI): *m/z* calculated for C$_{28}$H$_{29}$$^+$: 365.22693 [M+H]$^+$, found 365.22620 [M+H]$^+$.

(*E,Z*)-Dispiro[2-methoxy-9*H*-fluorene-9,2'thiirane-3',1''-(2''-*tert*-butyl-4'',7''-dimethyl-2'',3''-dihydro-1*H*-inden)] (21): Thioketone **12** (135 mg, 0.582 mmol) and diazofluorenone **20** (260 mg, 1.17 mmol) were dissolved in dry toluene (55 ml) and heated at reflux under a nitrogen atmosphere overnight. The solvent was evaporated and the crude purified by column chromatography on silica with *n*-pentane/toluene 3:1 as eluent. Two fractions were collected; one containing predominantly one diastereoisomer of **21** (57 mg) and another one containing predominantly the other diastereoisomer of **21** (110 mg). The crude products were immediately used in the next step without further purification. The overall crude yield

of the reaction was 67 %. HRMS (ESI): *m/z* calculated for $C_{29}H_{31}OS^+$: 427.20956 [M+H]$^+$, found 427.20904 [M+H]$^+$.

(*E,Z*)-9-(2-*tert*-butyl-4,7-dimethyl-2,3-dihydro-1*H*-inden-1-ylidene)-2-methoxy-9*H*-fluorene (17): Episulfide **21** (first fraction: 57 mg, 0.13 mmol) and $P(C_6H_5\text{-OMe-}p)_3$ (60 mg, 0.17 mmol) were dissolved in dry toluene (20 ml) and the stirred mixture was heated at reflux overnight, under a nitrogen atmosphere, in the absence of light. The solvent was evaporated and the crude product purified by column chromatography on silica using *n*-pentane/toluene 3:1 as eluent yielding a 1:1 mixture of *E*-**17** and *Z*-**17** (60 mg) as evident from ^{1}H-NMR analysis. The second fraction of episulfide **21** (110 mg, 0.26 mmol) underwent the same reaction yielding a 1:1 mixture of *E*-**17** and *Z*-**17** (95 mg). The two batches of compound **17** were combined (quantitative crude yield). As no separation of the two isomers could be found by TLC, a total of 14.5 mg of *E*-**17** and *Z*-**17** were separated by preparative HPLC on an AD column with *n*-heptane/propane-2-ol 99:1 as eluent at the flux of 1.0 ml min^{-1}. Due to the time consuming process of separation of isomers by HPLC only small amounts of the products *E*-**17** (4 mg) and *Z*-**17** (4 mg) were isolated in 55 % yield. HRMS (ESI): *m/z* calculated for $C_{29}H_{31}O^+$: 395.23749 [M+H]$^+$, found 395.23667 [M+H]$^+$.

Z-**17**: ^{1}H NMR (500 MHz, CD_2Cl_2): δ 8.18 (d, *J* = 7.7 Hz, 1H), 7.68 (d, *J* = 7.3 Hz, 1H), 7.61 (d, *J* = 8.3 Hz, 1H), 7.35–7.22 (m, 2H), 7.09–7.02 (m, 3H), 6.84 (dd, *J* = 8.3, 2.3 Hz, 1H), 4.09 (d, *J* = 5.7 Hz, 1H), 3.53 (s, 3H), 2.92 (dd, *J* = 15.1, 5.5 Hz, 1H), 2.76 (d, *J* = 15.1 Hz, 1H), 2.22 (s, 6H), 0.77 (s, 9H). ^{13}C NMR (125 MHz, CD_2Cl_2): δ 159.56, 152.23, 146.19, 142.48, 140.79, 140.00, 139.55, 133.05, 132.83, 131.07, 130.85, 130.51, 128.22, 127.29, 125.50, 125.21, 119.83, 119.00, 114.04, 109.06, 58.61, 55.42, 35.75, 35.43, 28.99, 20.67, 18.24.

E-**17**: ^{1}H NMR (500 MHz, CD_2Cl_2): δ 7.78 (d, *J* = 1.9 Hz, 1H), 7.68 (d, *J* = 8.3 Hz, 1H), 7.63 (d, *J* = 7.6 Hz, 1H), 7.38 (d, *J* = 8.0 Hz, 1H), 7.23 (t, *J* = 7.4 Hz, 1H), 7.08 (d, *J* = 7.7 Hz, 1H), 7.05–6.97 (m, 2H), 6.93 (dd, *J* = 8.3, 2.0 Hz, 1H), 4.16 (d, *J* = 5.7 Hz, 1H), 3.92 (s, 3H), 3.01(dd, *J* = 14.9, 5.5 Hz, 1H), 2.84 (d, *J* = 15.0 Hz, 1H), 2.30 (s, 3H), 2.25 (s, 3H), 0.86 (s, 9H). ^{13}C NMR (125 MHz, CD_2Cl_2): δ 159.22, 152.51, 146.15, 142.53, 141.21, 139.60, 138.29, 133.90, 133.32, 130.89 (2C), 130.37, 128.51, 127.52, 125.81, 123.91, 120.31, 118.43, 113.34, 111.34, 58.67, 55.98, 35.72, 35.49, 29.05, 20.62, 18.24.

References

1. *Molecular motors* (Ed: M. Schliwa), Wiley–VCH, Weinheim, Germany **2003**.

2. W. R. Browne, B. L. Feringa *Nat. Nanotechnol.* **2006**, *1*, 25–35.

3. J. Michl, E. C. H. Sykes *ACS Nano* **2009**, *3*, 1042–1048.

4. B. L. Feringa *J. Org. Chem.* **2007**, *72*, 6635–6652.

5. T. R. Kelly *Top. Curr. Chem.* **2005**, *262*.

6. A. Credi *Aust. J. Chem.* **2006**, *59*, 157–169.

7. V. Balzani, A. Credi, M. Venturi, *Molecular Devices and Machines – A Journey into the Nano World*, Wiley–VCH, Weinheim, Germany **2003**.

8. A. B. Braunschweig, B. H. Northrop, J. F. Stoddart *J. Mater. Chem.* **2006**, *16*, 32–44.

9. J. F. Stoddart *Acc. Chem. Res.* **2001**, *34*, 410–411.

10. *Molecular Switches* (Ed: B. L. Feringa and W. R. Browne), Wiley–VCH, 2nd edition, Weinheim, Germany **2011**.

11. *Molecular Machines and Motors* (Eds: J.–P. Sauvage, V. Amendola), *Vol. 99*, Springer, Berlin **2001**.

12. T. R. Kelly *Acc. Chem. Res.* **2001**, *34*, 514–522.

13. E. R. Kay, D. A. Leigh, F. Zerbetto *Angew. Chem. Int. Ed.* **2006**, *46*, 72–191.

14. H. L. Tierney, C. J. Murphy, A. D. Jewell, A. E. Baber, E. V. Iski, H. Y. Khodaverdian, A. F. McGuire, N. Klebanov, E. C. H. Sykes *Nat. Nanotechnol.* **2011**, *6*, 625–629.

15. J. S. Seldenthuis, F. Prins, J. M. Thijssen, H. S. J. van der Zant *ACS Nano* **2010**, *4*, 6681–6686.

16. Y. Liu, A. H. Flood, P. A. Bonvallet, S. A. Vignon, B. H. Northrop, H.–R. Tseng, J. O. Jeppesen, T. J. Huang, B. Brough, M. Baller, S. Magonov, S. D. Solares, W. A. Goddard, C.–M. Ho, J. F. Stoddart *J. Am. Chem. Soc.* **2005**, *127*, 9745–9759.

17. J. Berná, D. A. Leigh, M. Lubomska, S. M. Mendoza, E. M. Pérez, P. Rudolf, G. Teobaldi, F. Zerbetto *Nat. Mater.* **2005**, *4*, 704–710.

18. R. Eelkema, M. M. Pollard, J. Vicario, N. Katsonis, B. S. Ramon, C. W. M. Bastiaansen, D. J. Broer, B. L. Feringa *Nature* **2006**, *440*, 163.

19. R. Eelkema, M. M. Pollard, N. Katsonis, J. Vicario, D. J. Broer, B. L. Feringa *J. Am. Chem. Soc.* **2006**, *128*, 14397–14407.

20. T. Kudernac, N. Ruangsupapichat, M. Parschau, B. Maciá, N. Katsonis, S. R. Harutyunyan, K.–H. Ernst, B. L. Feringa *Nature* **2011**, *479*, 208–211.

21. N. Koumura, E. M. Geertsema, A. Meetsma, B. L. Feringa *J. Am. Chem. Soc.* **2000**, *122*, 12005–12006.

22. M. M. Pollard, M. Klok, D. Pijper, B. L. Feringa *Adv. Funct. Mater.* **2007**, *17*, 718–729.

23. M. M. Pollard, P. V. Wesenhagen, D. Pijper, B. L. Feringa *Org. Biomol. Chem.* **2008**, *5*, 1605–1612.

24. A. Cnossen, L. Hou, M. M. Pollard, P. V. Wesenhagen, W. R. Browne, B. L. Feringa *J. Am. Chem. Soc.* **2012**, *134*, 17613–17619.

25. H. Goldstein, C. Poole, J. Safko, *Classical Mechanics*, 3rd ed, Addison–Wesley, San Francisco, USA **2001**.

26. J. Vicario, A. Meetsma, B. L. Feringa *Chem. Commun.* **2005**, 5910–5912.

27. N. Koumura, E. M. Geertsema, M. B. van Gelder, A. Meetsma, B. L. Feringa *J. Am. Chem. Soc.* **2002**, *124*, 5037–5051.

28. M. M. Pollard, A. Meetsma, B. L. Feringa *Org. Biomol. Chem.* **2008**, *6*, 507–512.

29. T. Fernández Landaluce, G. London, M. M. Pollard, P. Rudolf, B. L. Feringa *J. Org. Chem.* **2010**, *75*, 5323–5325.

30. J. Vicario, M. Walko, A. Meetsma, B. L. Feringa *J. Am. Chem. Soc.* **2006**, *128*, 5127–5135.

31. R. T. Hart, R. F. Tebbe *J. Am. Chem. Soc.* **1950**, *72*, 3286–3287.

32. Y. -S. Huang, J. -Q. Liu, L.-J. Zhang, H.-L. Lu *Ind. Eng. Chem. Res.* **2012**, *51*, 1105–1109.

33. P. Garner, Ö. Şeşenoğlu *Org. Lett.* **2004**, *6*, 1217–1219.

34. A. R. Katritzky, O. Meth-Cohn, C. W. Rees, *Comprehensive Organic Functional Group Transformations*; Elsevier Science Ltd.; First Edition **1995**, Cambridge, UK; G. Pattenden Volume 3: *Synthesis: Carbon with One Heteroatom Attached by a Multiple Bond*, p 330–375.

35. M. K. J. ter Wiel, J. Vicario, S. G. Davey, A. Meetsma, B. L. Feringa *Org. Biomol. Chem.* **2005**, *3*, 28–30.

36. J. Vicario, M. Walko, A. Meetsma, B. L. Feringa *J. Am. Chem. Soc.* **2006**, *128*, 5127–5135.

37. M. Klok, N. Boyle, M. T. Pryce, A. Meetsma, W. R. Browne, B. L. Feringa *J. Am. Chem. Soc.* **2008**, *130*, 10484–10485.

38. A. A. Kulago, E. M. Mes, M. Klok, A. Meetsma, A. M. Brouwer, B. L. Feringa *J. Org. Chem.* **2010**, *75*, 666–679.

39. E. Fischer *J. Phys. Chem.* **1967**, *71*, 3704–3706.

40. Gaussian 09, Revision B.01, M. J. Frisch, G. W. Trucks, H. B. Schlegel, G. E. Scuseria, M. A. Robb, J. R. Cheeseman, G. Scalmani, V. Barone, B. Mennucci, G. A. Petersson, H. Nakatsuji, M. Caricato, X. Li, H. P. Hratchian, A. F. Izmaylov, J. Bloino, G. Zheng, J. L. Sonnenberg, M. Hada, M. Ehara, K. Toyota, R. Fukuda, J. Hasegawa, M. Ishida, T. Nakajima, Y. Honda, O. Kitao, H. Nakai, T. Vreven, J. A. Montgomery, Jr., J. E. Peralta, F. Ogliaro, M. Bearpark, J. J. Heyd, E. Brothers, K. N. Kudin, V. N. Staroverov, R. Kobayashi, J. Normand, K. Raghavachari, A. Rendell, J. C. Burant, S. S. Iyengar, J. Tomasi, M. Cossi, N. Rega, J. M. Millam, M. Klene, J. E. Knox, J. B. Cross, V. Bakken, C. Adamo, J. Jaramillo, R. Gomperts, R. E. Stratmann, O. Yazyev, A. J. Austin, R. Cammi, C. Pomelli, J. W. Ochterski, R. L. Martin, K. Morokuma, V. G. Zakrzewski, G. A. Voth, P. Salvador, J. J. Dannenberg, S. Dapprich, A. D. Daniels, Ö. Farkas, J. B. Foresman, J. V. Ortiz, J. Cioslowski, and D. J. Fox, Gaussian, Inc., Wallingford CT, **2009**.

Chapter 6

# Controlling the Rotation Rate of Molecular Rotors

This chapter describes the design, preparation and study of a set of novel binaphthyl-based molecular rotors with the goal of tuning their rotation rate by means of direct steric control as well as by allosteric regulation. The molecules described herein are equipped with multiple rotors rendering them excellent candidates for the study of coupled rotation as well as for exploring the possibilities of selectively addressing only one of the multiple rotors.

Introduction

A *molecular rotor* is a molecular system in which a molecule or part of a molecule rotates against another part of the molecule or against a macroscopic entity such as a surface or a solid[1]. It is common to call the part of the molecule that rotates against the rest the *rotator* and the stationary part of the system with respect to which the rotator turns the *stator*. If the rotor is not mounted on a solid support, it is common to view the part with the larger moment of inertia as stationary (the stator) and the part with the smaller moment of inertia as the rotator. The *axle* is the portion of the molecule that carries the rotator and about which the rotator turns.

Molecular rotors have been studied extensively due to their possible applications in nanotechnology[1,2,3,4,5,6,7]. These promising systems are being investigated for their use in the most recent generations of nanoscale electronics. The construction and operation of nanoscale machines and devices, in which the molecular motion is controlled with the goal of performing a specific function, has been the focus of many research groups. Triggering these devices by external stimuli such as electricity, light or chemical reagents gives rise to various functions including those of diodes, rectifiers, memories, resonant tunnel junctions and single settable molecular switches that can be electronically configured for logic gates[5]. A task of a molecular machine is to perform an action leading to a desired function following the input of a signal with a supply of energy. It is often desirable to have a molecular machine performing mechanical movements under control of appropriate energy inputs[6,7]. Achieving unidirectional motion has been one of the primary objectives of nanotechnology[6] and examples of realizing photochemically driven[6,8], chemically driven[7,9,10,11] and electrically driven[2,12,13] (uni)directional rotary motion have already been reported. This controlled and directional rotary motion has been used to drive a four-wheeled molecule across a surface[14] clearly showing the importance of getting rotary motion under control.

There have been attempts to gain control over the rotation rate in molecular rotors[1,7]. Being able to tune the rotation rate by external stimuli seems highly appealing due to its possible applicability in molecular devices. A design of a molecular brake[7] is shown in Fig 1.
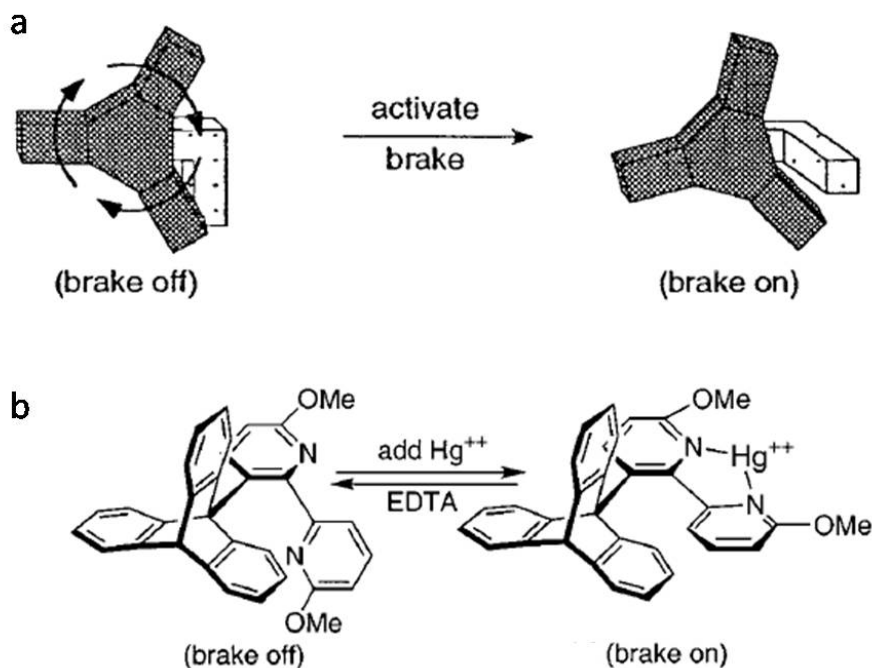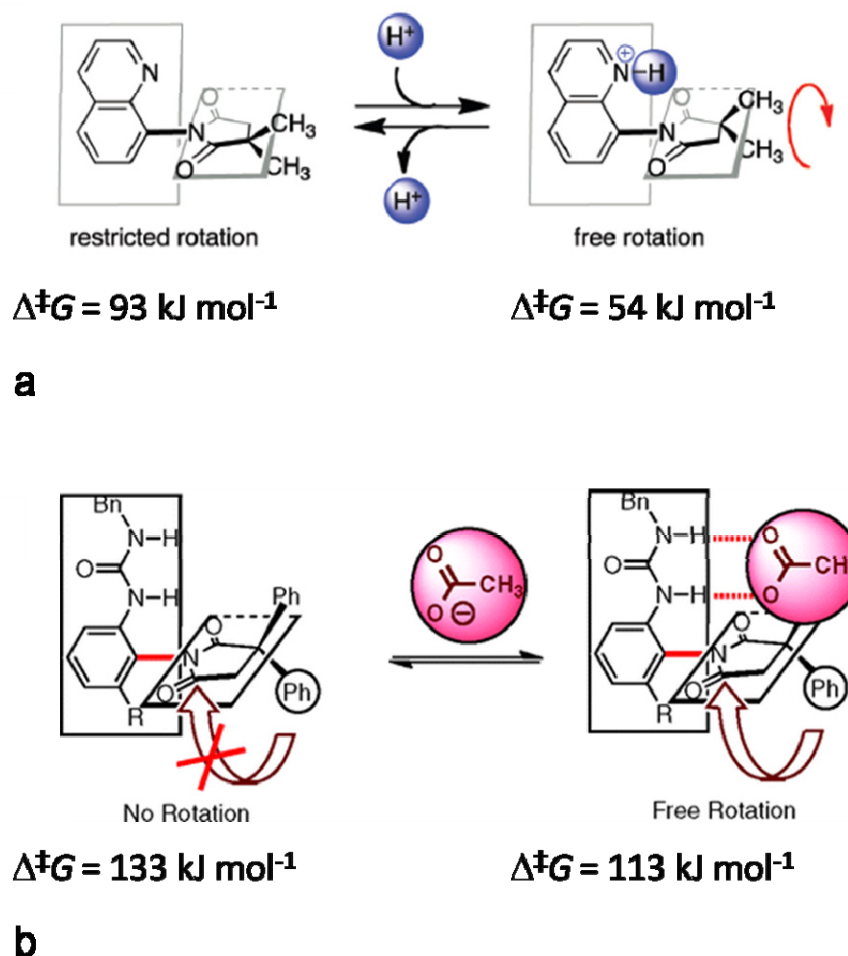
Figure 1. Design of a triptycene rotator with a molecular brake. **a:** a schematic representation of the molecular brake, **b:** the mechanism of action of the molecular brake[7].

The triptycene rotator rotates rapidly in the absence of Hg^{2+} ions. Upon addition of Hg^{2+} ions, the bipyridine moiety coordinates to the Hg^{2+} ion and gets positioned between the two blades of the rotator bringing the triptycene rotator to a halt and therefore acting as a brake. The removal of Hg^{2+} ions restores the rotation.

There have also been examples of the rotation rate of molecular rotors being increased by an additive. Figure 2a shows a rotor whose rotation rate may be increased by seven orders of magnitude upon protonation of the molecule[15]. The protonated quinoline nitrogen forms an intramolecular hydrogen bond with an imide carbonyl stabilizing the planar transition state and therefore accelerating the rotation. The acid catalyzed acceleration can easily be reverted by the increase in pH.

restricted rotation

$\Delta^{\ddagger}G = 93$ kJ mol^{-1}

free rotation

$\Delta^{\ddagger}G = 54$ kJ mol^{-1}

a

No Rotation

$\Delta^{\ddagger}G = 133$ kJ mol^{-1}

Free Rotation

$\Delta^{\ddagger}G = 113$ kJ mol^{-1}

b

Figure 2. Acceleration of a molecular rotor by the addition of **a:** acid[15], **b:** acetate[16].

Another example of regulating the rotation rate of a rotor is shown in Fig 2b. The rotor accelerates upon the addition of acetate[16]. The additive appears to form hydrogen bonds with the rotor and in turn stabilize the planar transition state leading to the lowering of the rotational energy barrier.

There have also been two examples of a rotor function coupled to a separate light-driven rotary motor function[17,18] (Fig 3). The molecular motor[6,8] rotates unidirectionally which can be observed as a sequential interconversion between four isomers. Different isomers of the molecular motor exhibit different rotation rates of the rotor function due to different steric interactions of the rotator with the remainder of the molecule. The rotation rate of the rotor may therefore be tuned by controlling the motor function with light and heat.
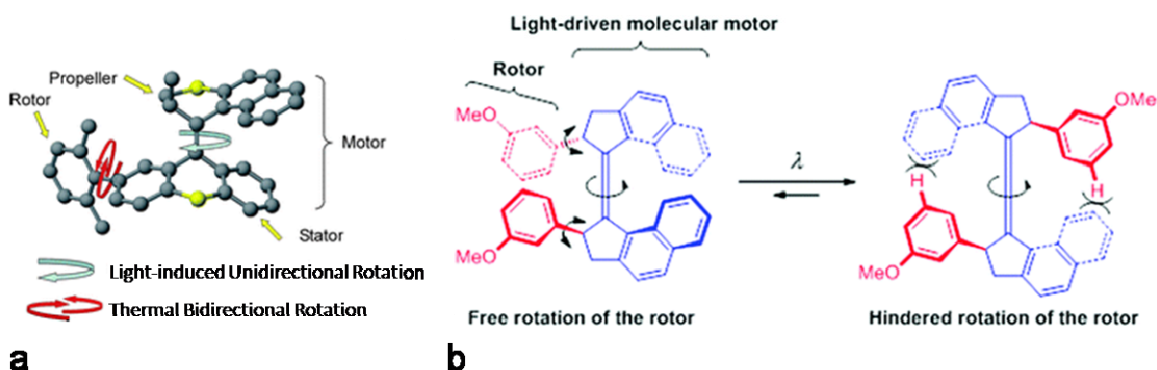
Figure 3. A rotor function coupled to a motor function based on; **a:** a second-generation molecular motor[17], **b:** a first-generation molecular motor[18].

The control of the rotation rate described in the examples above is realized through steric interactions in the immediate vicinity of the rotator; a change in the conformation of the molecule brings about a change in the interactions with the rotator which in turn alters the rotation rate. We have, however, been interested in achieving remote control over the rotation rate of rotors. Is it possible to address a rotor in the region far away from the rotator and still affect its rotation rate? This would allow for better and easier control over molecular machines.

The concept described here is taken from nature where one of the methods cells use to control enzymes and other proteins is through allosteric regulation[19]. In this way the activity of the enzyme is regulated by chemically modifying the enzyme's allosteric site, usually located far away from the enzyme's active site. The changes brought upon the allosteric site are transferred to the active site through conformational changes in the enzyme. The active site is therefore remotely controlled. The process of allosteric regulation is schematically depicted in Fig 4. This method of controlling enzyme activity is quite common in biological systems and long-range allostery is especially important in cell signalling[20].
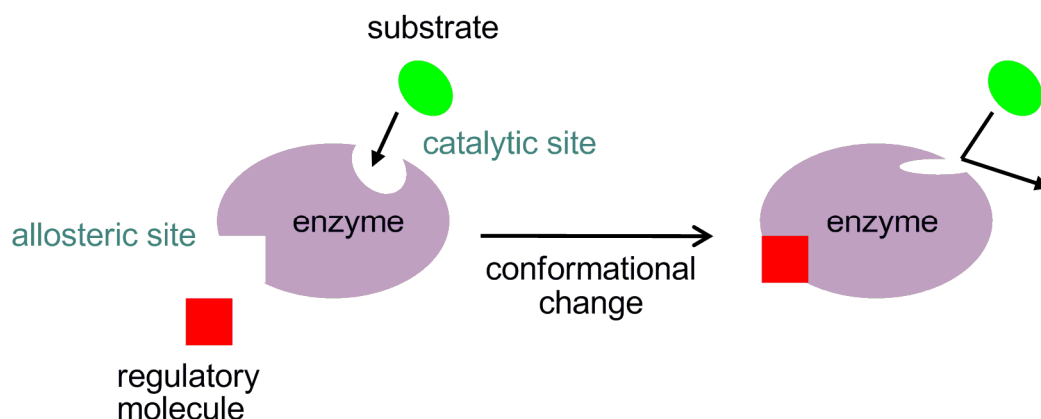

Figure 4. A schematic representation of an allosterically regulated enzyme.

The concept of the transmission of chirality over nanometer distances has not only been investigated in proteins but in smaller molecules as well; the global conformation of a small molecule can be addressed by exploiting inter– and intramolecular interactions and thus provide a simple method for information relay over scales of over 1 nm.[21,22]

In an attempt to mimic nature's effective means of controlling proteins, we have designed molecular rotors that we would like to control in an allosteric fashion. Our novel molecular rotors have a binol core which is equipped with two rotators as shown in Fig 5a,b. Phenyl groups act as rotators (highlighted in blue in Fig 5) and they bear chemically inert groups (methyl or trifluoromethyl groups) for easier detection by NMR spectroscopy. The positioning of these groups is also expected to affect the rotation rate of the rotator[1,23,24,25,26,27]. The molecules have two reactive hydroxyl groups (highlighted in pink in Fig 5) that can easily be modified[28,29]; forming a dialkyl derivative, a phosphoramidite[30], a boronate ester or a metal complex are only some of the possibilities. The primary objective is to investigate if modifying the hydroxyl groups or their derivatives can lead to a change in the rotary behaviour of the rotors incorporated in the molecule. We are interested in the molecules with the rotators positioned on the same side as the chemically modifiable hydroxyl groups as well as in those with the rotators on the opposite side, distant from the hydroxyl groups (Fig 5). This would allow for the direct comparison of the steric and allosteric effects.
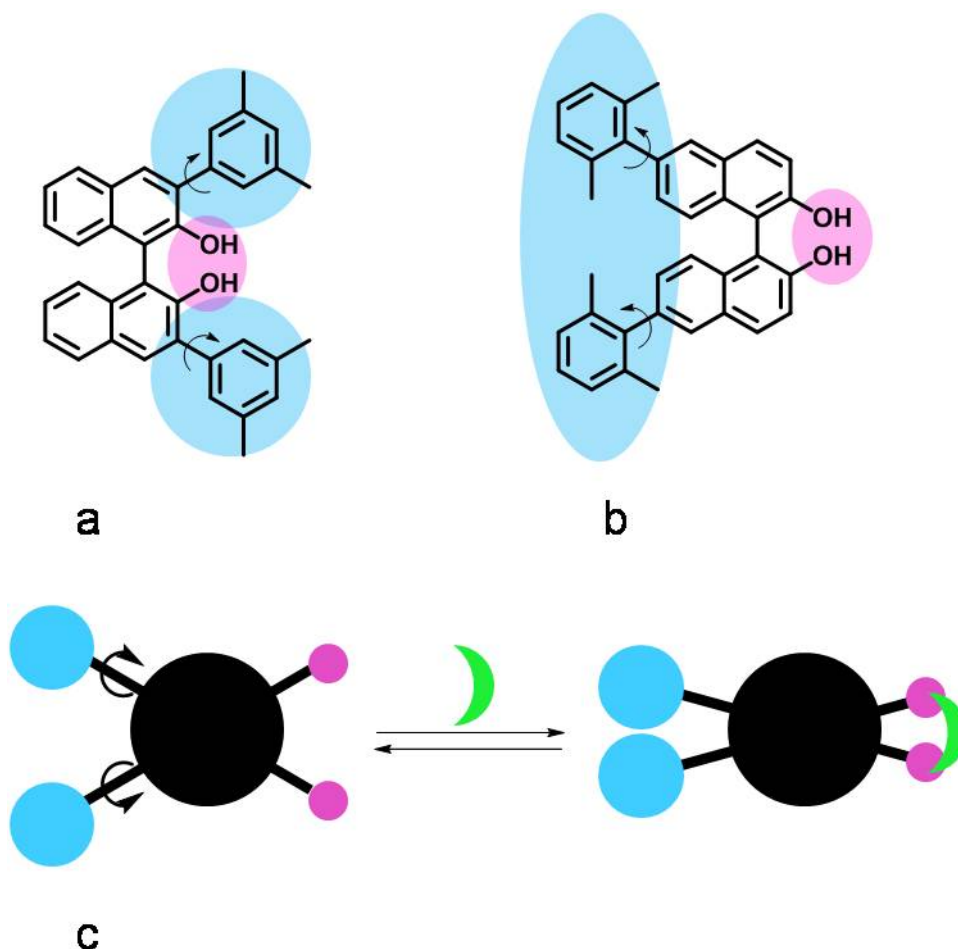
Figure 5. Design of binol–based molecular rotors; highlighted in pink are the areas that can be chemically altered and highlighted in blue are the rotors whose rotation rate may be affected by the chemical change in the pink region. **a:** The pink and the blue regions are on the same side of the binol molecule, **b:** The pink and the blue regions are on the opposite sides of the binol molecule. **c:** Schematic representation of the mechanism of allosteric regulation of the rotor functions depicted in **b**.

The binol core has been chosen for its rigidity and flexibility at the same time. As evident from the structure the binaphthyl system is a molecular rotor as well; the two naphthyl units can rotate with respect to one another[23]. The rotation barrier for binol, however, is rather high (156 kJ mol^{-1} at 195 °C) due to a distortion of the aryl rings when the rings go through the same plane in the transition state[23,31]. This is the reason why the two enantiomers of binol are easily separated and stable at room temperature. Furthermore, stable chiral binaphthyl-based molecules have been used extensively as ligands in enantioselective catalysis[28,29,30,32,33]. Racemization of binol systems only takes place at high temperatures which means our designed molecules should be configurationally stable with respect to the binaphthyl rotor at temperatures not too high (binol shows no sign of racemization on heating at 100 °C for 24 h under neutral conditions)[23]. The presence of the naphthyl–naphthyl biaryl bond will, however, provide a certain degree of flexibility to the molecule allowing the two naphthyl units to adopt different dihedral angles[32]. As schematically depicted in Fig 5c, we anticipate that the changes brought upon the

hydroxyl groups may be transferred to the phenyl rotators through conformational changes of the binaphthyl core mimicking nature's way of controlling proteins through allosteric regulation.

Experimental methods

Dynamic processes have been studied extensively and they are most often followed by means of spectroscopic, chiroptical or chromatographic techniques[23,34]. These methods provide invaluable information about the configurational and conformational stability of (chiral) compounds. They also allow for the kinetics of the process to be followed. The choice of a suitable technique for the study of a dynamic process mainly depends on the reaction rate, the availability of isolated isomers and the capacity of the method to differentiate between interconverting stereoisomers. Chiroptical (polarimetry, circular dichroism, optical rotary dispersion) and chromatographic methods are most often employed in studies of stable compounds; stereoisomers with an interconversion barrier of 100 kJ mol^{-1} or more can often be isolated. The interconversion of stereoisomers exhibiting activation barriers between 20 and 100 kJ mol^{-1} is usually monitored by variable temperature (dynamic) NMR spectroscopy. Fast dynamic processes can be investigated by femtosecond or picosecond pump-probe methods, optical calorimetry measurements, stopped-flow methods and flash photolysis, in conjunction with time-resolved spectroscopy or spectrometry.

Dynamic NMR spectroscopy

Dynamic processes which are slow enough (with an energy barrier between 20 and 100 kJ mol^{-1}) can often be studied by analysis of temperature-dependent NMR spectra of the interconverting species[23,34,35,36]. A particularly simple situation arises when two nuclei (*AB* case) provide sharp signals with equal intensity and undergo chemical exchange resulting in line broadening and coalescence upon heating, as shown in Fig 6.
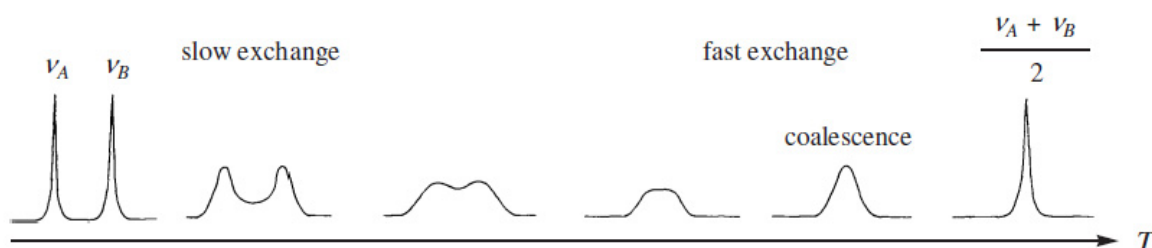
Figure 6. Variable-temperature NMR spectra of an uncoupled dynamic *AB* system[23].

In such a case, one can obtain well resolved signals at low temperatures where the two nuclei do not show measurable exchange. As the temperature is increased, the exchange becomes fast relative to the NMR time scale and only one averaged species is observed due to signal coalescence. In the absence of any coupling, the first-order interconversion rate constant can be calculated according to equation 1:

$$k_{T_c} = \frac{\pi}{\sqrt{2}} \Delta v \qquad (1)$$

where k_{T_c} is the rate constant at the coalescence temperature, T_c, and Δv is the difference in the frequences of the two NMR signals without exchange (at low temperatures, $T \ll T_c$), Fig 6. From equation 1 and the Eyring equation 2 one can obtain equation 3 which can then be used to calculate the free energy of activation for the process, $\Delta^{\ddagger}G$:

$$k_T = \frac{k_B T}{h} e^{-\frac{\Delta^{\ddagger}G}{RT}} \qquad (2)$$

$$\Delta^{\ddagger}G = -RT_c \ln\left(\frac{\pi}{\sqrt{2}} \frac{h}{k_B} \frac{\Delta v}{T_c} \right) \qquad (3)$$

where in equation 2 k_T is the rate constant at temperature T, k_B is the Boltzmann constant, h is Planck's constant and R is the universal gas constant. In equation 3 T_c is the coalescence temperature. The accuracy of the coalescence method is often limited to approximately ± 0.5 to 1.0 kJ mol^{-1} due to difficulties in determination of the exact coalescence temperature[23].

The simplicity of the coalescence method has contributed to its widespread use[23,34,36]. This method, however, is not applicable to interconversions of species with different thermodynamic stability nor to compounds giving complicated NMR spectra with multiple coupling patterns. In these cases, accurate results can be obtained by NMR line shape analysis[23,35]. Variable-temperature NMR spectroscopy has been applied extensively in kinetic studies of stereodynamic processes exhibiting energy barriers between 20 and 130 kJ mol^{-1}. The energy range covered by dynamic NMR is limited by the NMR time scale, signal resolution and the practical NMR temperature range ($-150\ °C$ to $+160\ °C$) which ultimately depends on the melting and boiling points of available deuterated solvents. Since dynamic NMR can be used to study stereolabile compounds that rapidly interconvert at room temperature, it has become a powerful tool for the analysis of rotations about single bonds[23].

Results and discussion

Synthesis and characterization

Our first target molecule was compound **2**, a phenylboronate ester of binol, **1** (Scheme 1). We decided to first try this reaction on the commercially available binol, **1**, before repeating the same reaction on the more precious 3,3'-bis(3,5-dimethylphenyl)-1,1'-binaphthyl-2,2'-diol, shown in Fig 5a. These cyclic boronates

were chosen as targets due to the Lewis-acidic character of the boron atom which would allow for the attachment of a Lewis-basic ligand which would in turn change the geometry of the boron atom from trigonal planar to tetrahedral. We anticipated that this severe geometrical change could be transferred throughout the molecule and affect the rotation properties of the rotors.

The synthesis of the corresponding ester **2** is described in the literature; binol, **1**, and phenylboronic acid should be heated at reflux in toluene in the presence of a water trap[37] (Scheme 1). Despite numerous attempts, however, this procedure did not give any **2** in our hands. It appeared that there was indeed a new compound being formed in the course of the reaction but this compound would always degrade back to the starting compound **1** upon work-up or purification. Furthermore, this compound did not show the same ^{1}H–NMR signals that are reported for **2**. Another procedure reporting the syntheses of similar compounds by simply melting the two components in vacuum was also tried without success[38] (Scheme 1). A different synthetic approach has also been tried; there are reports of the syntheses of similar compounds[39,40] by first deprotonating binol, **1**, and then reacting it with chloro-compounds like dichlorophenylphosphine[40]. The analogous approach using dichlorophenylborane, however, did not result in **2** (Scheme 1).
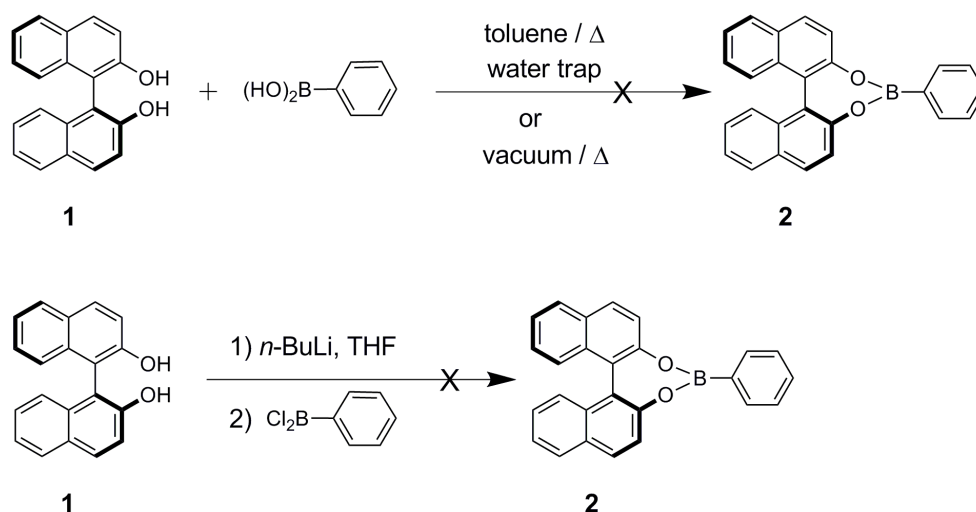

Scheme 1. Synthetic attempts towards compound **2**.

It is not entirely clear why compound **2** is difficult to prepare. Similar seven-membered binol-based cyclic compounds are normally readily prepared and frequently used in asymmetric catalysis[28,29,30,32,33]. Five-membered aromatic and aliphatic cyclic boronates are stable compounds and are widely used as protecting groups for 1,2– and 1,3–diols[41,42,43]. Chiral cyclic boronates are also known for their use in asymmetric synthesis[44,45]. Compound **2**, however, has a seven-membered ring with an aromatic diol part and there are only few reports of that type of boron-containing compounds in the literature[37,46,47]. There is one report of a failed isolation of compound **2** due to its moisture sensitivity[46]. It is possible that such a boron-containing seven-membered ring is not overly stable and that compound **2** is prone

to hydrolysis which is not uncommon for boronate esters[42,43]. An excessive susceptibility to hydrolysis is probably the reason for the synthetic difficulties described above[46]. Having failed at the preparation of compound **2**, we decided to abandon boronate esters as target molecules and rather focus on other derivatives.

Compound **4** was prepared in excellent yield in the reaction of compound **3** (absolute configurations of the binaphthyl core and the stereogenic centres in the phosphoramidite ligand are (*S*), (*R*) and (*R*), respectively) with BH_3 (Scheme 2), following a literature procedure for the preparation of BH_3–adducts of simple binol phosphoramidites[48]. The signal in the ^{31}P–NMR spectrum of **4** agrees with those reported for BH_3–adducts. In ref 48 the authors report a crystal structure with BH_3 positioned on the P-atom and not on the N-atom. Furthermore, the signal at –44.41 ppm in the ^{11}B–NMR spectrum of **4** is in agreement with a P-bound BH_3–group and not with an N-bound BH_3–group[49,50]. From the NMR data as well as by analogy with similar compounds we conclude that in compound **4** the BH_3 molecule is indeed mounted on the P-atom.

**3** **4**

quant.
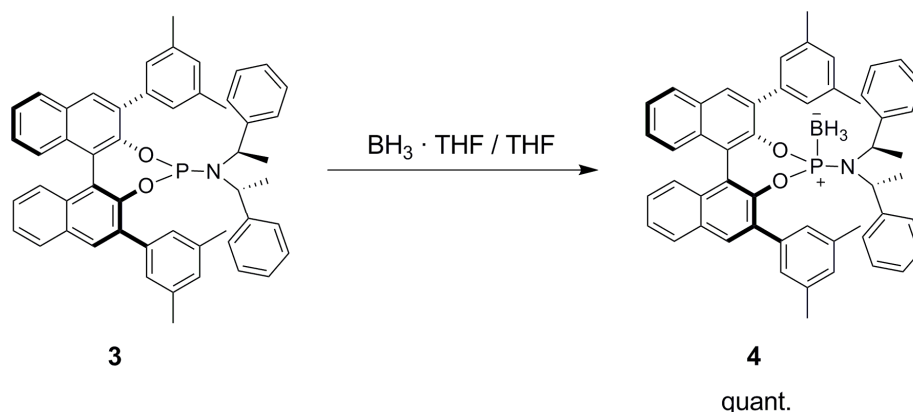
Scheme 2. Synthesis of the borane adduct **4**.

It was also attempted to make analogous adducts of **3** with (*sec*-Bu)$_3$B, Et$_3$B, (MeO)$_3$B, F$_3$B and 9-BBN monomer but without success as these boron compounds appeared to cause decomposition of **3**.

In the preparation of compound **6**, the first step was the bromination of binol which proceeded in excellent yield[51], Scheme 3. The next step was the Suzuki coupling of 6,6'-dibromobinol **5** with 3,5-bis(trifluoromethyl)phenylboronic acid to give product **6**. To avoid protecting and then later deprotecting the hydroxyl groups, we tried a procedure from the literature that performs a Suzuki coupling on a similar unprotected compound[52]. Although formed only in low yield, product **6** was obtained by this method and was characterized by ^{1}H, ^{13}C, ^{19}F–NMR and HRMS.
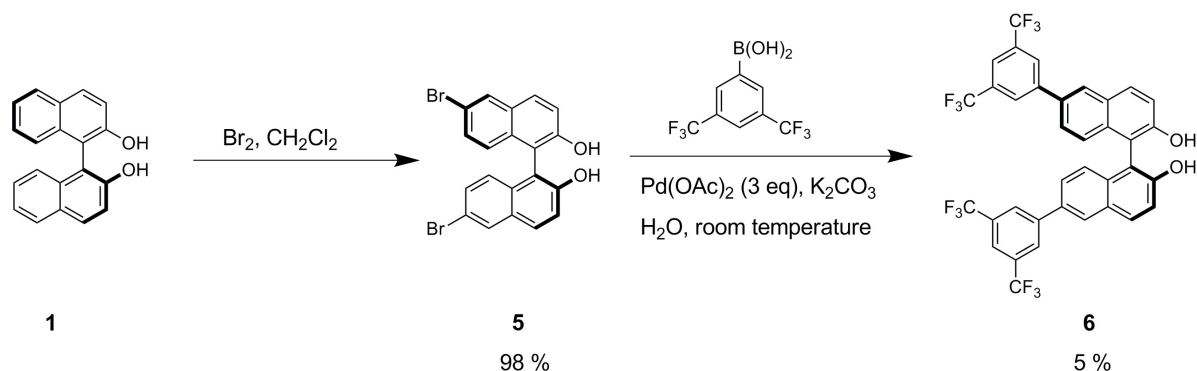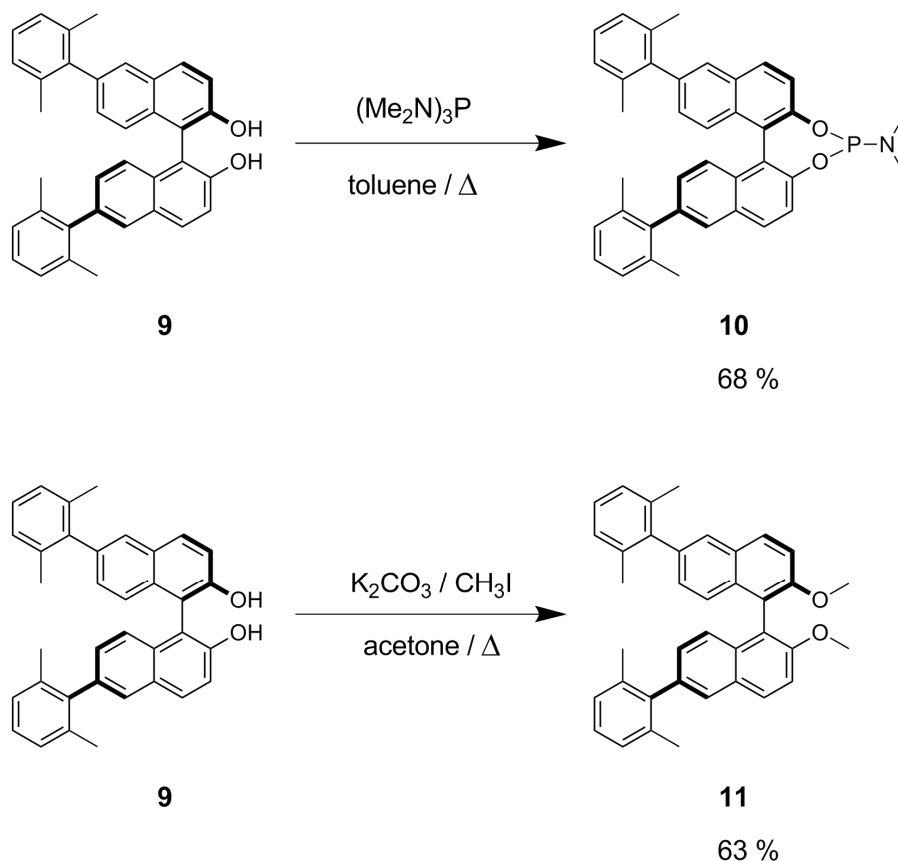
Scheme 3. Synthesis of compound **6**.

The synthesis of compound **9** also starts with 6,6'-dibromobinol **5** (Scheme 4). A Suzuki coupling of **5** with 2,6-dimethylphenylboronic acid, following the conditions used for the preparation of **6**, did not afford the desired product **9**. Compound **9** was then prepared according to a literature procedure; the two hydroxyl groups were first protected in the form of benzyl ethers[53], then the Suzuki coupling was carried out and the protecting groups were removed in a hydrogenolysis reaction affording **9**[54] (Scheme 4). All the reactions proceeded in excellent yields. The ^{1}H–NMR spectrum of **9** was found to be in excellent agreement with the literature spectrum[54].
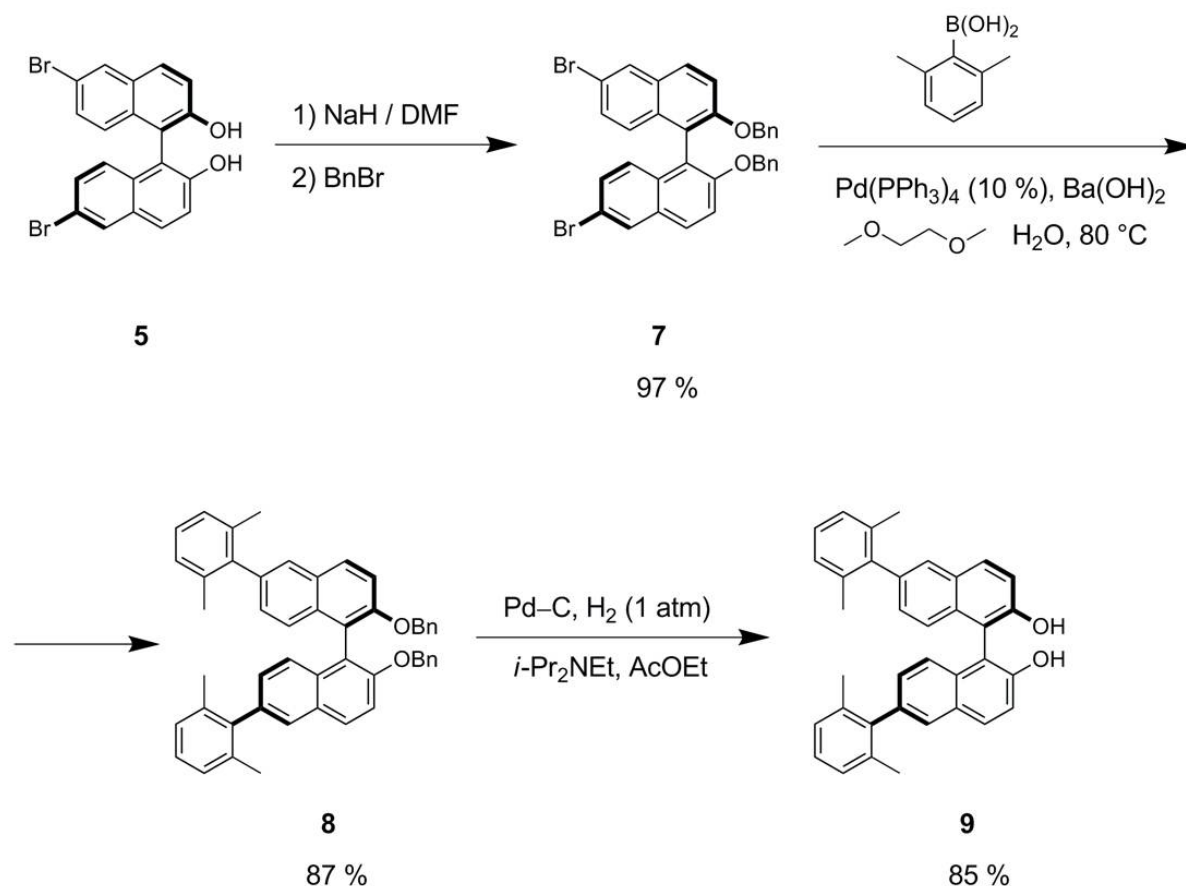
Scheme 4. Synthesis of compound **9**[53,54].

Compounds **10** and **11** were prepared according to Scheme 5. Phosphoramidite **10** was synthesized in good yield by refluxing **9** in the presence of tris(dimethylamino)phosphine following the conditions for the preparation of similar binol-based phosphoramidite compounds[48,55]. Compound **11** was prepared in good yield by methylation of compound **10** with methyl iodide following a literature procedure for the methylation of binol[56].

**Scheme 5.** Syntheses of compounds **10** and **11**.

Both compounds **10** and **11** were characterized by NMR and HRMS.

Rotation rate measurements

Steric effect

3,3'-Bis(3,5-dimethylphenyl)-1,1'-(*S*)-binaphthyl-2,2'-diol 12[57]

The ^{1}H–NMR spectra of compound **12**[57] (Fig 7a), were taken in CDCl$_3$ at 25, –30 and –50 °C (Fig 7b). Apart from a slight change in the chemical shift, no changes in the spectra were observed upon changing the temperature.
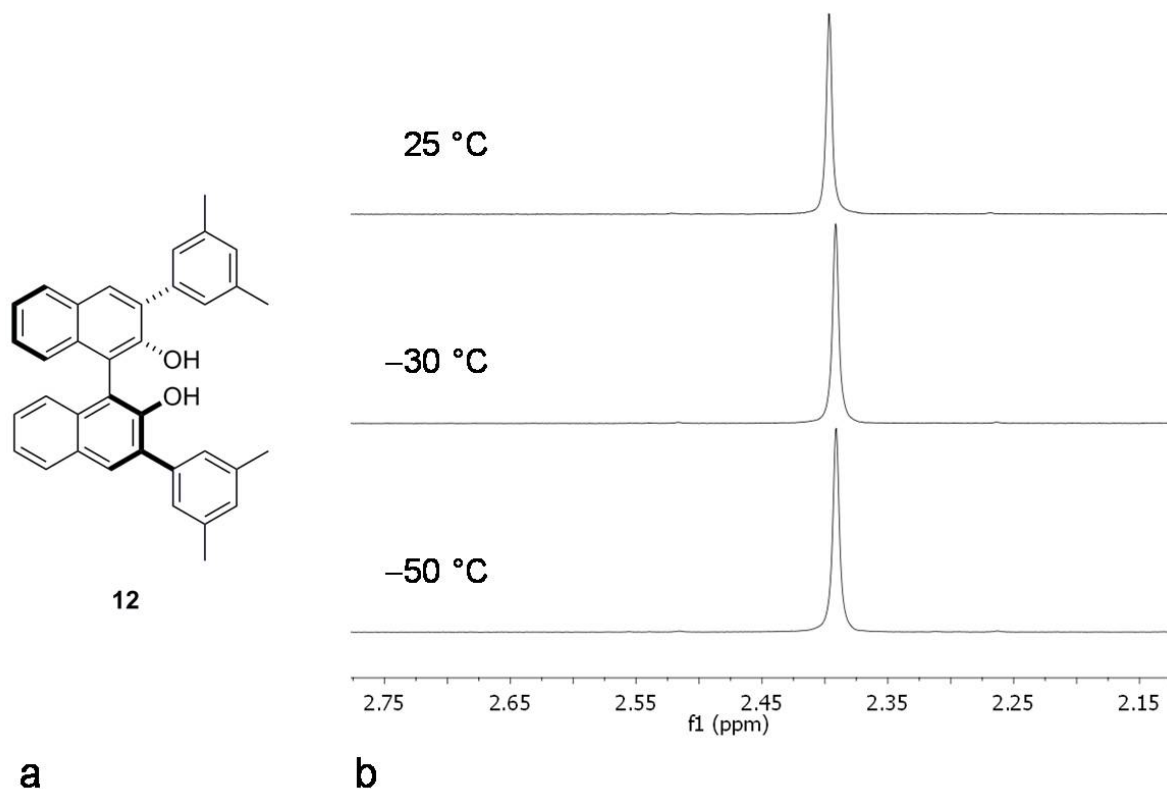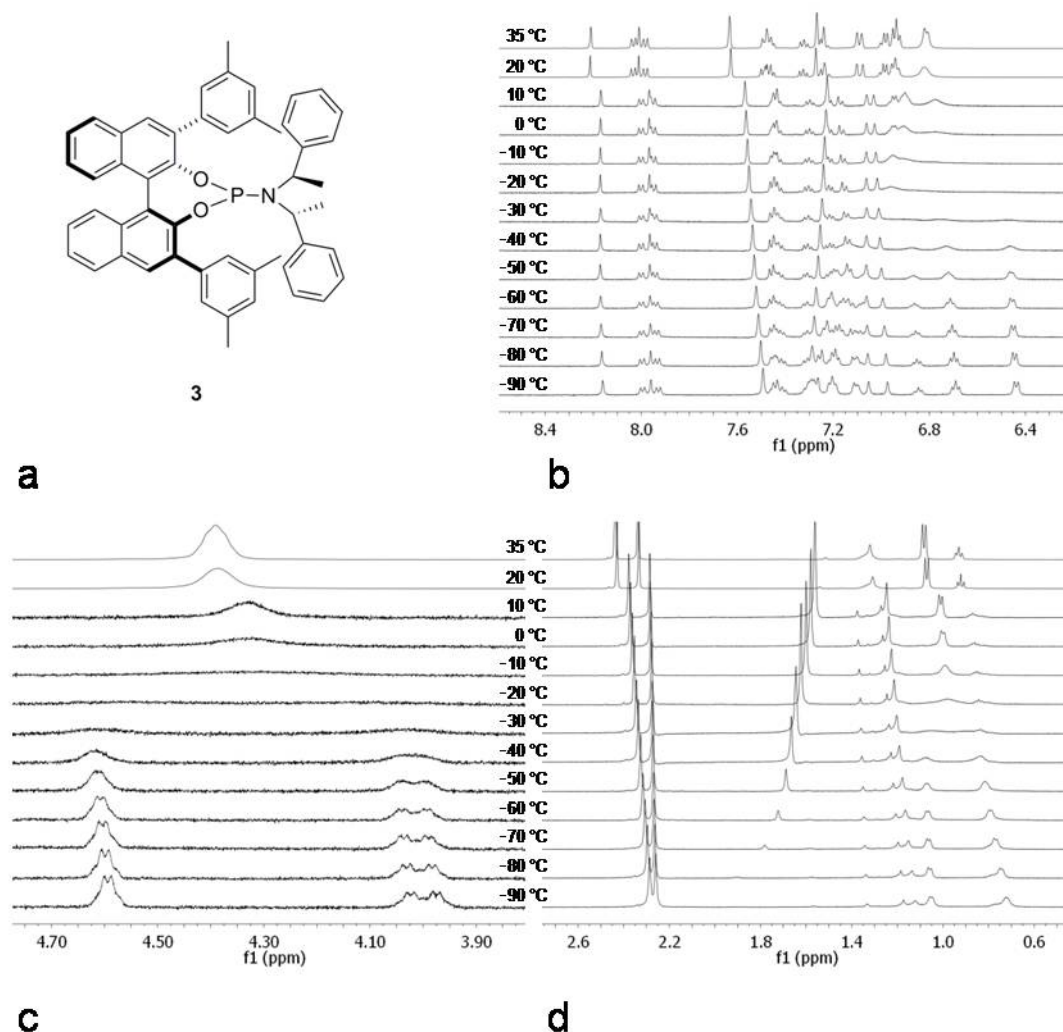
Figure 7. a: Structure of compound **12**, **b:** The aliphatic part of the ^{1}H–NMR spectra of **12** (signal corresponding to the protons in the methyl group) in CDCl$_3$ at different temperatures.

As can be seen from the spectra in Fig 7b, there appears to be only one signal present for all the four methyl groups in **12**. That means that all of the methyl groups are magnetically equivalent indicating fast rotation around the aryl–aryl bond, even at low temperatures. This is not surprising since the biaryl rotor in **12** is mono-*ortho*-substituted by a hydroxyl group and a single *ortho*-substituent does most often not raise the rotation barrier sufficiently to be observed at temperatures not too low[23,24,25,58]. Furthermore, a hydroxyl group is a rather small substituent which will not slow down the rotation significantly like, for example, a *tert*-butyl one. The three *meta*-substituents (two methyl groups and a naphthyl group) are, however, too far away from the axle to make a significant contribution to the rotation barrier[23,58]. Indeed, the DFT calculations have shown that the rotation barrier for the two rotators in **12** in the gas phase is 24 kJ mol^{-1} which is too low to measure with our current NMR setup.

4-(bis((*R*)-1-phenylethyl)amino-2,6-bis(3,5-dimethylphenyl)-(*S*)-dinaphtho[2,1-*d*:1',2'-*f*][1,3,2]dioxaphosphepin-4-ium-4-yl) 3

The ^{1}H–NMR spectra of compound **3** (Fig 8a), were taken in CD$_2$Cl$_2$ at different temperatures in the range from –90 °C to +35 °C (Fig 8b–d). As seen from Fig 8b–d the spectra change upon lowering the temperature, both in the aromatic region (Fig 8b) and the aliphatic region (Fig 8c,d). Some of the peaks in the spectra taken around room temperature are broad. Upon lowering the temperature these peaks

split up into multiple peaks that become sharp at sufficiently low temperatures. In the aromatic region (Fig 8b) this can be seen for the peak at 6.80 ppm and in the aliphatic region this is the case with the broad peak at 4.40 ppm (Fig 8c) and the doublet at 1.00 ppm (Fig 8d). All the multiple peaks present at low temperatures seem to coalesce roughly in the range between −20 and −10 °C. This indicates a dynamic process that can be observed by slowing it down to the NMR time scale with the peaks undergoing changes corresponding to exchanging chemical groups[23,34].


Figure 8. a: Structure of compound **3**, **b:** The aromatic part of the [1]H−NMR spectra of **3** in CD$_2$Cl$_2$, **c:** The aliphatic part (3.90 − 4.70 ppm) of the [1]H−NMR spectra of **3** in CD$_2$Cl$_2$, **d:** The aliphatic part (0.60 − 2.60 ppm) of the [1]H−NMR spectra of **3** in CD$_2$Cl$_2$. The spectra are taken at different temperatures.

The two aliphatic NMR peaks undergoing change, the broad signal at 4.40 ppm and the doublet at 1.00 ppm, correspond to the protons of the CH groups of the amine part in **3** and the CH$_3$ groups of the same part of the molecule, respectively. The aromatic peaks undergoing change correspond to the aromatic protons of the amine part in **3**. These peaks identify the bis(1-phenylethyl)amino group as the

rotator and the P–N bond as the axle. Hindered rotation around the P–N bond is known in the literature[59,60,61,62,63].

The two sharp singlet peaks in the region between 2.20 and 2.50 ppm (Fig 8d) correspond to the methyl groups located on the 3,5-dimethylphenyl rotators in **3** (Fig 8a); one signal corresponds to the two methyl groups on one rotator and the other signal corresponds to the two methyl groups on the other rotator (Fig 8a). This region in the NMR spectrum undergoes some change upon lowering the temperature but that is due to the shifting of one of the signals with temperature and not due to a dynamic process. Down to –90 °C no splitting of either one of the two methyl group signals is observed in the NMR spectra (Fig 8d). This indicates that the rotation around the aryl–aryl bond is so fast that it cannot be observed even at temperatures as low as –90 °C. Much like for compound **12**, such a low rotation barrier is due to a lack of more than a single substituent in the *ortho* position in the biaryl rotor[23,24,25,58]. It may however seem counterintuitive that bridging two hydroxyl groups with a phosphine atom bearing a group as large as a bis(1-phenylethyl)amino group would not increase the rotation barrier of 3,5-dimethylphenyl rotators in **3** compared to **12**. Firstly, the barrier may indeed be affected on going from **12** to **3** but both barriers are too low to be measured by the NMR system at our disposal so the two barriers may not be compared at this point. Secondly, the fact that the attachment of the seemingly large group does not increase the rotation barrier sufficiently for the change to be observed by NMR is not that surprising as there is not much difference in the „steric size" of the *ortho*-substituent between **12** and **3**. What raises the rotation barrier most is the presence of a bulky substituent in the immediate vicinity of the axle as that is what destabilizes the transition state. For example, changing the *ortho*-substituent in simple biphenyl systems from Cl to Br to I changes the rotation barrier only slightly (an increase of 30 % on going from Cl to I) while changing it from Cl to *t*-Bu increases the barrier significantly (200 %)[58]. A significant increase in the barrier will therefore be caused by the placement of a bulky (branched) substituent directly in the *ortho*-position of the biaryl while the mere attachment of a bulky group to the existing *ortho*-substituent (an O-atom in our case) will not affect the barrier significantly as the large group is too far away from the axle to destabilize the transition state for the rotation.

From the experiments shown in Fig 8b–d we conclude that for **3** the rotation of the 3,5-dimethylphenyl rotators is too fast to follow by the NMR system at our disposal. The rotation of the bis(1-phenylethyl)amino group around the P–N bond, however, can be slowed down sufficiently to be studied by NMR. From the spectra shown in Fig 8b–d it can only be concluded that the changeable peaks coalesce somewhere in the temperature range between –20 and –10 °C. In order to determine the coalescence temperature accurately we carried out additional measurements in that temperature range (Fig 9).
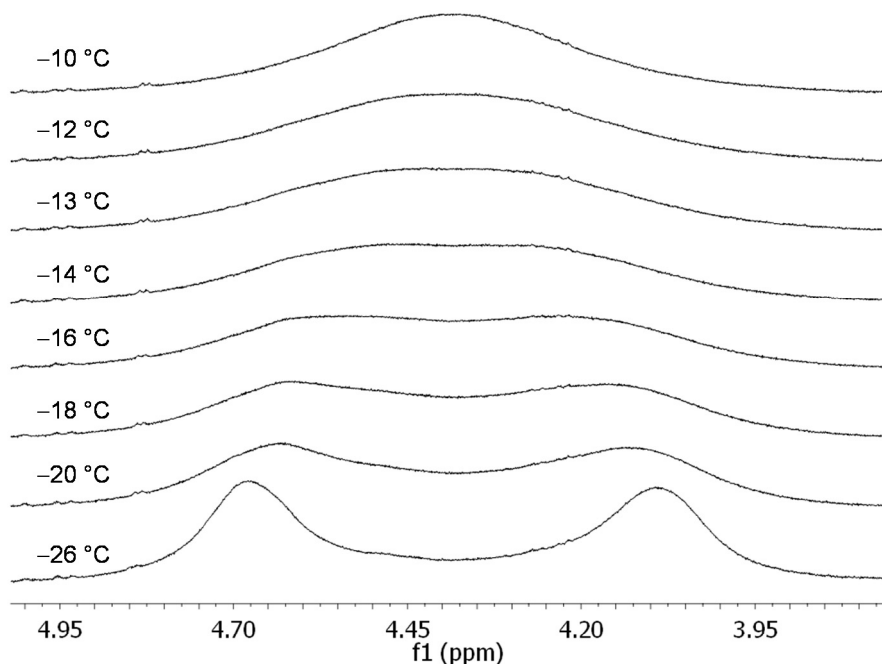
Figure 9. A part of the aliphatic region of the ^{1}H–NMR spectra of **3** in CD_2Cl_2 in the temperature range from −26 °C to −10 °C.

Figure 9 shows the coalescence of the peak at 4.40 ppm, corresponding to the protons of the CH groups in the amine part of **3**. From Fig 9 we determined the coalescence temperature to be −13 °C. From the spectrum taken at −90 °C, Fig 8c (where the two peaks are fully separated), we calculated Δv = 305 Hz. From the coalescence temperature and Δv, and with the help of equation 3, we determined the rotation barrier for the rotation of the bis(1-phenylethyl)amino group around the P–N bond in **3** to be 49 kJ mol^{-1} in CD_2Cl_2. This agrees well with the literature values of around 50 kJ mol^{-1} for rotation around the P–N bond in various compounds[59,60,61,62,63].

The NMR peaks (in CD_2Cl_2) corresponding to exchanging protons (the rotator) in **3** are rather broad around room temperature (Fig 8b–d). In order to check the system at a higher temperature, we also took NMR spectra of **3** in DMSO-d_6 (Fig 10).
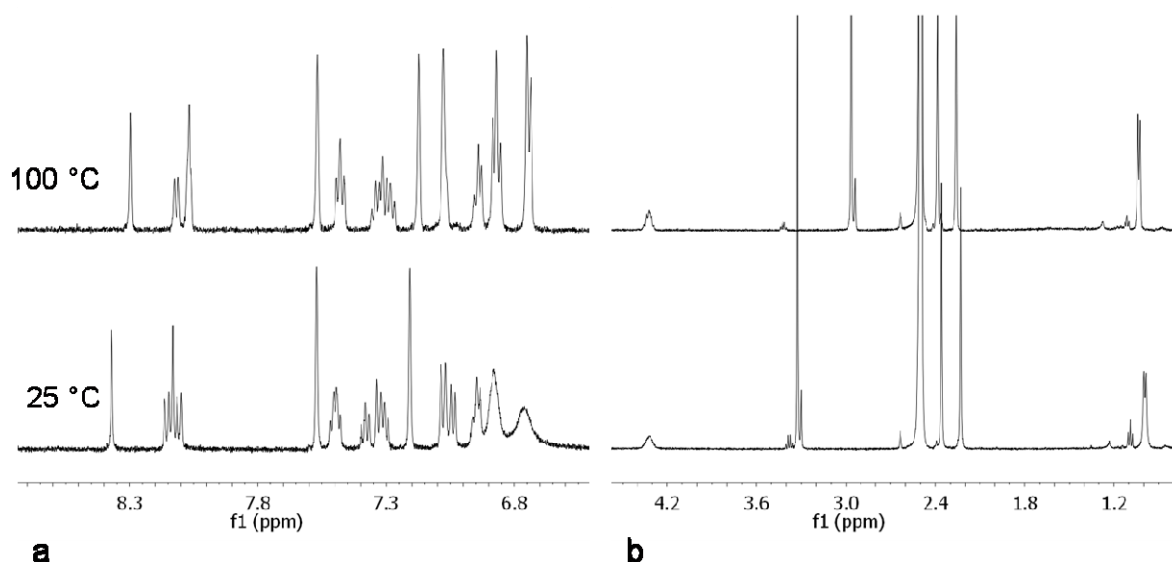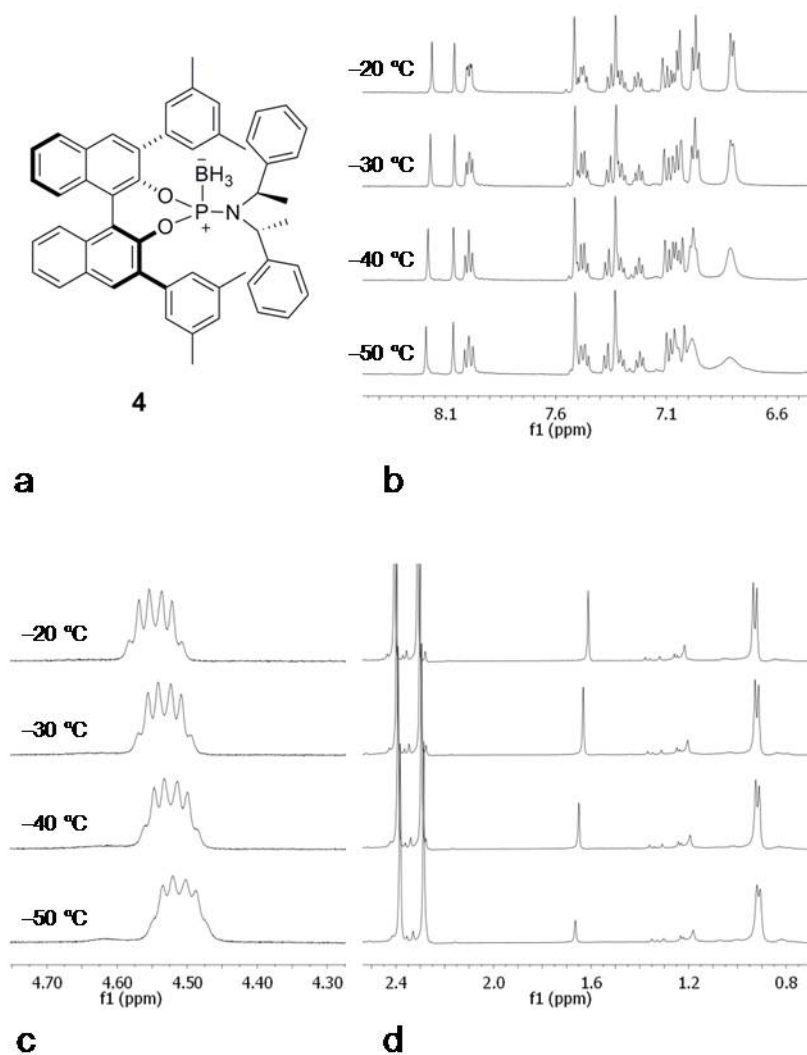
Figure 10. a: The aromatic part of the ^{1}H–NMR spectra of **3** in DMSO-d_6, **b:** The aliphatic part of the ^{1}H–NMR spectra of **3** in DMSO-d_6. The spectra are taken at 25 and 100 °C.

As seen from Fig 10, the NMR peaks corresponding to the protons in the rotator (two peaks between 6.7 and 6.9 ppm, a peak at 4.32 ppm and a peak at 1.0 ppm) still appear somewhat broad at 25 °C. At 100 °C, however, they appear sharp much like the remainder of the NMR peaks. This shows that by warming up the solution of **3** to 100 °C the rotation around the P–N bond is accelerated and is no longer observable on the NMR time scale.

4-(bis((*R*)-1-phenylethyl)amino-2,6-bis(3,5-dimethylphenyl)-(*S*)-dinaphtho[2,1-*d*:1',2'-*f*][1,3,2]dioxaphosphepin-4-ium-4-yl)trihydroborate 4

The ^{1}H–NMR spectra of compound **4**, Fig 11a, were taken in CD$_2$Cl$_2$ at different temperatures in the range from –50 °C to –20 °C (Fig 11b–d). The spectrum undergoes changes upon lowering the temperature; some of the peaks become slightly broader (both in the aromatic and aliphatic region of the spectrum) and those peaks correspond to the protons of the rotator. As the chemical shifts of the NMR signals undergoing change are not much different than for compound **3**, we conclude that it is again the rotation of the bis(1-phenylethyl)amino group around the P–N bond that we observe by NMR. In the study of **3**, the coalescence of the NMR signals corresponding to exchangeable protons was reached at –13 °C and the fully separated peaks were only observable at the temperature of –40 °C or lower. In the case of **4**, the coalescence temperature appears to be well below –50 °C (Fig 11c,d) so the temperature at which the peaks are completely separated (which is needed to obtain $\Delta\nu$ which is in turn needed for the calculation of the rotation barrier) is probably below –90 °C which is not within the reach of the NMR system at our disposal.

Figure 11. a: Structure of compound **4**, **b:** The aromatic part of the ^{1}H–NMR spectra of **4** in CD$_2$Cl$_2$, **c:** The aliphatic part (4.30 – 4.70 ppm) of the ^{1}H–NMR spectra of **4** in CD$_2$Cl$_2$, **d:** The aliphatic part (0.80 – 2.40 ppm) of the ^{1}H–NMR spectra of **4** in CD$_2$Cl$_2$. The spectra are taken at different temperatures.

The significantly lower coalescence temperature for **4** does however indicate a lower rotation barrier in **4** than in **3**. This may seem as an invalid conclusion since T_c and Δv have neither been determined. According to equation 3, however, changes in T_c will affect the barrier to a significantly higher extent than the changes of the same order of magnitude in Δv. This has to do with the fact that the dependence of the barrier on Δv is strictly logarithmic in nature whereas its dependence on T_c is of the type $T_c \ln T_c$. To illustrate this let us consider three hypothetical dynamic systems with parameters as shown in table 1. System A is characterized by T_c = 300 K, which corresponds to +27 °C, and Δv = 300 Hz. Equation 3 gives the barrier of 57 kJ mol^{-1} for system A. If the value for T_c, for another system B, is 200 K (corresponding to –73 °C) which is 2/3 of its value for system A and the value for Δv remains the same (300 Hz), the barrier drops to 38 kJ mol^{-1} which is basically 2/3 of the value for system A. If, for another system C, T_c remains the same as for system

A (300 K) whereas the value for $\Delta\nu$ drops to 200 Hz (which is 2/3 of its value for system A), the energy barrier for system C is calculated to be 58 kJ mol^{-1} which is a change of only 2 % from the value for system A. This simulation shows that the dependence of the rotation barrier on the coalescence temperature is virtually proportional in the range of temperatures of interest for our systems whereas its dependence on the separation of the two coalescing peaks is strictly logarithmic. This means that the value for the barrier is much more sensitive to a change in T_c than to a change in $\Delta\nu$. Furthermore, the change in $\Delta\nu$ is expected to be in the range of 50 – 1000 Hz (which corresponds to a maximum of 2 ppm of difference in chemical shifts on an NMR machine operating at 500 MHz) influencing the rotation barrier by no more than 5 kJ mol^{-1} (when T_c is around 200 K). No expected change in the value of $\Delta\nu$ can therefore override the effect of a significant change in the coalescence temperature (more than 50 K) on the value of the rotation barrier (more than 10 kJ mol^{-1}). In conclusion, this means that a significant change in the coalescence temperature (more than 50 K) may be taken as a significant change in the rotation barrier (5 – 15 kJ mol^{-1}).

Table 1. The parameters for three hypothetical systems and the corresponding free energies of activation as calculated according to equation 3.

system	T_c / K	θ / °C	$\Delta\nu$ / Hz	$\Delta^{\ddagger}G$ / (kJ mol^{-1})
A	300	+27	300	57
B	200	−73	300	38
C	300	+27	200	58

The fact that the value for the barrier is much more sensitive to a change in T_c than to a change in $\Delta\nu$ also implies that the error in the energy barrier will primarily be determined by the uncertainty in T_c and not so much by the uncertainty in $\Delta\nu$, as was mentioned in the description of the experimental method[23].

The attachment of the BH$_3$ molecule to the phophorus atom in **3** to obtain **4** has a significant effect on the rotation rate of the bis(1-phenylethyl)amino group around the P–N bond as evidenced by a significant decrease of the coalescence temperature. A possible explanation for this observation comes from the fact that upon the attachment of BH$_3$ to the phosphorus atom the geometry around the phosphorus atom changes from trigonal pyramidal to tetrahedral allowing for a larger bond angle between the groups attached to the phosphorus[64]. This would in turn allow the rotator, as one of the groups attached to the phosphorus atom, more

space to undergo rotation. A less crowded transition state for the rotation in **4** would have a lower energy than the one in **3** therefore lowering the rotation barrier compared to **3** and increasing the rotation rate.

The rotation rates of both molecules **3** and **4** discussed in this section were measured over a large temperature range in CD_2Cl_2. Since the dependence of the rotation rate on solvent (polarity) is known[65,66,67], care should also be taken about dependence of the permittivity (dielectric constant) of solvents on temperature[68]. This chapter describes temperature dependent measurements in CD_2Cl_2, $CDCl_3$, DMSO-d_6 and toluene-d_8. Upon going from lower to higher temperatures in the relevant temperature ranges the permittivities of the non-deuterated analogues of these solvents decrease by 48 %, 33 %, 11 % and 11 %, respectively[68]. These changes are significant, especially in the case of CD_2Cl_2 and $CDCl_3$. During a measurement over a large temperature range the rotation rate may therefore also be affected by the significant change in the permittivity of the solvent which would in turn influence the values obtained for the rotation barriers. The best way to overcome this issue is to conduct experiments in solvents with less significant changes in the permittivities in the relevant temperature range, like the aforementioned toluene-d_8 or DMSO-d_6. Another convenient solvent would be CCl_4, the permittivity of which changes by a mere 4 % in the relevant temperature range. The disadvantage on many solvents like CCl_4 or DMSO-d_6, however, is a rather narrow temperature range in which they are found in the liquid state. For that and other practical reasons (solubility, overlapping peaks in NMR spectra, etc.) some measurements were nevertheless carried out in CD_2Cl_2 or $CDCl_3$ so the rotation barriers obtained should be used with caution.

As can be seen from Fig 11d, upon lowering the temperature from −20 °C to −50 °C there is no change in the two sharp singlet peaks at 2.4 and 2.3 ppm, corresponding to the methyl groups located on the 3,5-dimethylphenyl rotators in **4** (Fig 11a) (one signal corresponds to the two methyl groups on one rotator and the other signal corresponds to the two methyl groups on the other rotator). This means that the rotation of the 3,5-dimethylphenyl rotators is still too fast to be observed by NMR spectroscopy at the temperature as low as −50 °C. This is not surprising as the biaryl rotors in **4** have but one *ortho*-substituent per rotor and, much like it was the case with **3** and **12**, this does not provide enough steric hindrance in the transition state to raise the rotation barrier significantly[23,24,25,58]. Similarly to what was discussed earlier when comparing **3** and **12**, the addition of the BH_3 group takes place too far away from the axle to make a significant difference on the rotation barrier.

The rotators in **3**, **4** and **12** should be redesigned so as to increase the rotation barrier and achieve a measurable rotation rate. This could be achieved by positioning the methyl groups in the *ortho*-positions in the rotor instead of the *meta*-positions[23]. For such a molecule the DFT calculations indicate an energy barrier of 143 kJ mol^{-1} in the gas phase and 144 kJ mol^{-1} in dichloromethane. A barrier that

high might actually prove too high for practical measurements by means of our current NMR setup. Furthermore, a different choice of solvent would also be necessary. A similar molecule equipped with two 2-methylphenyl rotators, however, might be a good choice as a single *ortho*-positioned methyl group, in combination with the also *ortho*-positioned hydroxyl group, might give an energy barrier most suitable for the study. For the rotation of a 2-methylphenyl rotator in such a molecule there are two transition states; one with the methyl and the hydroxyl group on the same side of the biaryl axle and one with the two groups on opposite sides of the axle. The rotation energy barriers of 83 and 58 kJ mol^{-1} were calculated for the two rotation transition states, respectively. These barriers would indeed allow for the measurement of the rotation rate in the system.

Allosteric effect through covalent modification

(*S*)-6,6'-bis(3,5-bis(trifluoromethyl)phenyl)-1,1'-binaphthyl-2,2'-diol 6

The rotators in **6** were designed with trifluoromethyl groups for two reasons. The first reason was to enable the study of the rotation process by ^{19}F–NMR, which should give clearer NMR spectra. The second reason for the incorporation of trifluoromethyl groups into the rotators in **6** was to render the rotators electron-poor. We are interested in influencing the rotation rate on one side of the molecule by chemically modifying the opposite side (the hydroxyl groups). To this end we would like to investigate whether changing the electron properties on one side of the molecule could have any effect on the rotation rate of the rotators on the other side of the molecule. Furthermore, we would like to investigate if a push–pull system could be designed to influence the rotation rate of the rotators.

The aromatic region of the ^{1}H–NMR spectra of compound **6** (Fig 12a), were taken in CD$_2$Cl$_2$ at 25 °C and –54 °C (Fig 12b). No changes in the spectra were observed upon changing the temperature. That means that the rotation around the aryl–aryl bond is too fast to be observed on the NMR time scale, even at the temperature as low as –54 °C. Since no hindered rotation in **6** was observed by ^{1}H–NMR, no further studies by means of ^{19}F–NMR spectroscopy have been carried out. The fact that the rotation process in **6** is not observed is not surprising since the biaryl rotors in **6** have no substituents in the *ortho*-position to the axle. It is known in the literature that in the absence of any *ortho*-substituents, which would destabilize the transition state and therefore increase the rotation barrier, the rotation in a biaryl rotor proceeds rather fast (rotation barriers in the range 9 – 12 kJ mol^{-1})[23,24,69,70]. DFT calculations were employed to predict the rotation barrier for the two rotors in **6** in the gas phase and a value of 14 kJ mol^{-1} was obtained which agrees with the predictions from the literature as well as with our inability to observe the rotation with the NMR system at our disposal.
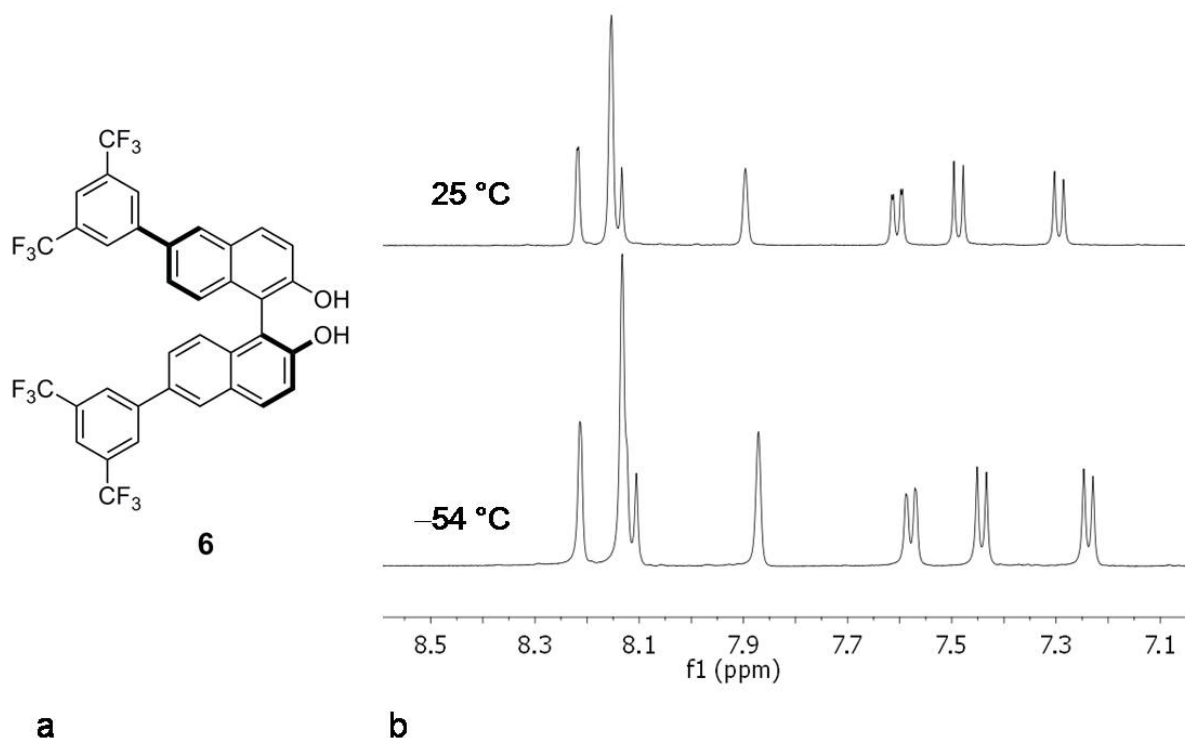
Figure 12. a: Structure of compound **6**, **b:** The aromatic part of the ^{1}H–NMR spectra of **6** in CD_2Cl_2 at 25 °C and –54 °C.

As the rotation of the rotators in **6** appeared to be too fast to be investigated, we did not engage in any derivatization of **6**. The system should rather be redesigned so as to obtain a measurable rotation rate; one of the means of achieving that might be the positioning of the trifluoromethyl groups in the *ortho*-positions in the rotor instead of the *meta*-positions. That would slow down the rotation considerably and a rotation barrier of about 100 kJ mol^{-1} may be expected from the comparison with similar biaryl compounds[23]. The DFT calculations for this molecule predict a barrier of 105 kJ mol^{-1} in the gas phase and 102 and 106 kJ mol^{-1} in toluene and DMSO, respectively.

(*R*)-6,6'-bis(2,6-dimethylphenyl)-1,1'-binaphthyl-2,2'-diol 9

Molecule **9** (Fig 13a) was designed with two 2,6-dimethylphenyl rotators on the opposite side of the hydroxyl groups. The goal is to study the rotation rate of the rotators in **9** before and after chemically modifying the hydroxyl groups and comparing the results to see if modification of the hydroxyl groups located on one side of the molecule has any effect on the rotation rate of the rotators on the other side of the molecule. Not having been able to observe the rotation in **3**, **4**, **6** and **12**, all having rotators with *meta*-substituents, the rotators in **9** have been designed with two methyl groups in the *ortho*-position to the axle (Fig 13a). These groups should provide sufficient destabilization of the transition state and slow down the rotation process allowing it to be investigated by dynamic NMR spectroscopy[23,26]. The DFT

calculations of the energy barrier for the rotation in **9** give 91 kJ mol^{-1} in the gas phase and 87 and 85 kJ mol^{-1} in toluene and DMSO, respectively.

A part of the aliphatic region of the ^{1}H–NMR spectra of compound **9** taken in anhydrous DMSO-d_6 in the temperature range from 20 °C to 90 °C is shown in Fig 13b. Due to considerable overlap of aromatic peaks undergoing change, only the aliphatic region with the peaks corresponding to the methyl groups is given in Fig 13b.
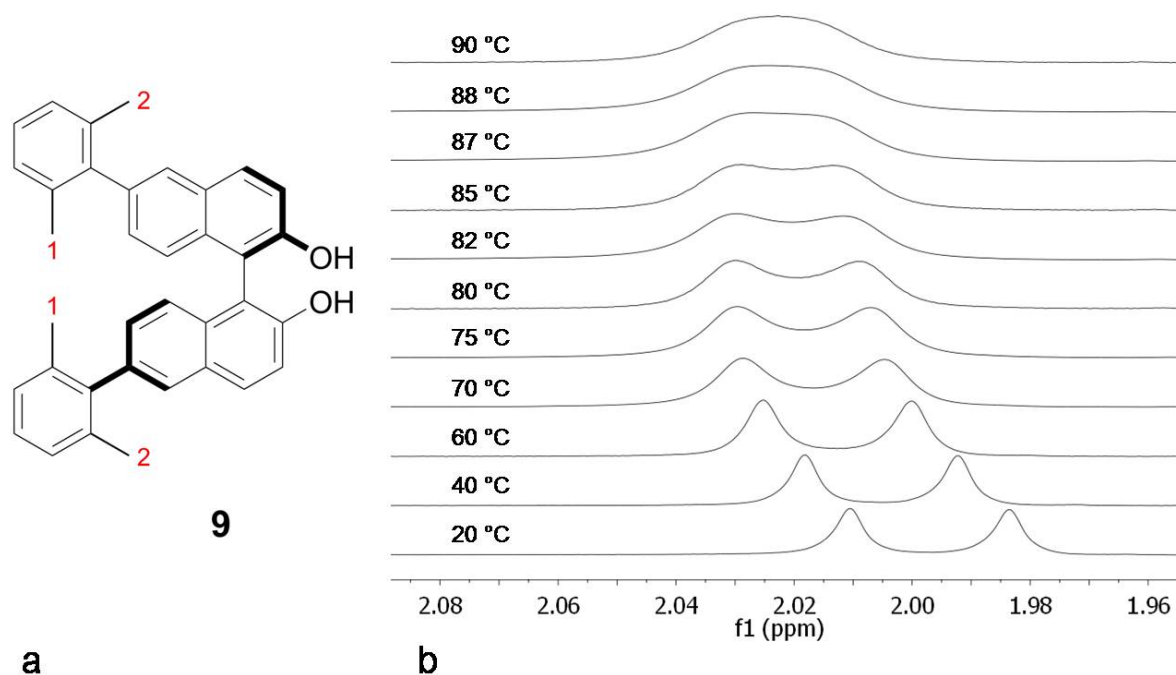

Figure 13. a: Structure of compound **9** with two different positions of methyl groups highlighted with numbers 1 and 2, **b:** The aliphatic part (1.96 – 2.08 ppm) of the ^{1}H–NMR spectra of **9** in anhydrous DMSO-d_6 at different temperatures.

At 20 °C the ^{1}H–NMR spectrum of compound **9** shows two peaks in the aliphatic region, namely a singlet at 1.98 ppm and a singlet at 2.01 ppm (Fig 13b). These signals correspond to the methyl groups in **9**; since the two naphthyl halves of **9** (along with the rotators) are magnetically equivalent, the two signals correspond to two magnetically inequivalent positions in the rotor, namely the methyl group pointing inwards (position 1 in Fig 13a) and the methyl group pointing outwards (position 2 in Fig 13a). As shown in Fig 13b, upon increasing the temperature, the two NMR signals come together and become broader, and eventually coalesce at 88 °C. Above the coalescence temperature there is only one (broad) peak. From the spectrum taken at 20 °C one can determine the separation of the two singlet peaks, Δv = 14 Hz. From the coalescence temperature and Δv, one can use equation 3 to calculate the rotation barrier, $\Delta^{\ddagger}G$ = 79 kJ mol^{-1}. This value agrees well with the literature value of 78 kJ mol^{-1} as determined for 2,2'-dimethylbiphenyl[23] which is also a biaryl rotor with two methyl groups in the *ortho*-positions. It is also in fairly good agreement with the calculated value of 85 kJ mol^{-1}.

In order to investigate a possible effect of water on the rotation barrier of **9**, the measurements described above were repeated in wet DMSO-d_6. However, the very same behaviour with the same coalescence temperature was observed as in anhydrous DMSO-d_6.

Compound **9** was also studied in toluene-d_8 at different temperatues. Due to considerable overlap of aromatic peaks undergoing change, only the part of the aliphatic region with peaks corresponding to methyl groups is given in Fig 14.
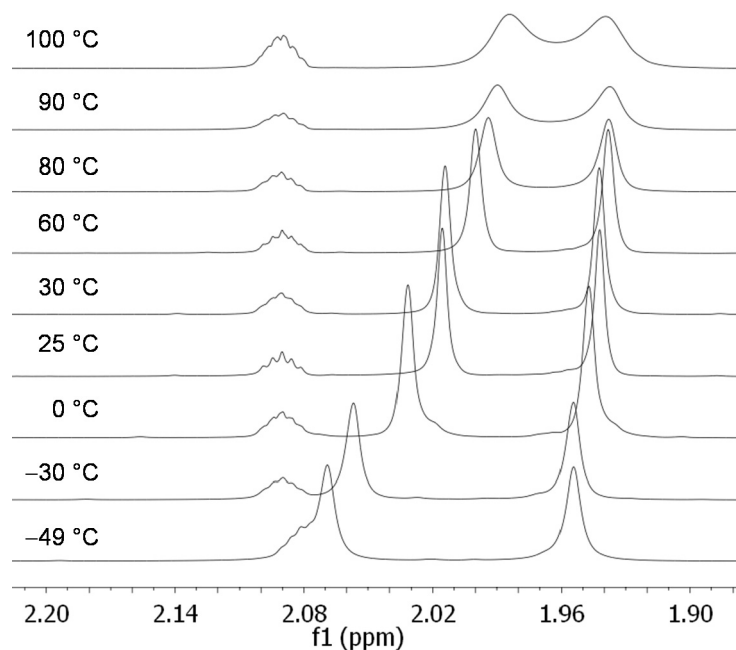

Figure 14. A part of the aliphatic region of the [1]H−NMR spectra of **9** in toluene-d_8 at different temperatures.

As seen from Fig 14, at room temperature and below, there are two singlet peaks present in the spectra, one at 2.02 ppm and one at 1.94 ppm (chemical shifts taken from the spectrum at 25 °C). These signals correspond to the methyl groups in **9** having two different positions in the molecule (positions 1 and 2, Fig 13a). The multiplet at 2.09 ppm comes from the residual incompletely deuterated solvent. As can be seen in Fig 14, upon increasing the temperature, the two singlet peaks come together and become broader. At 100 °C the peaks have not yet merged into a single (broad) peak. Coalescence could not be reached as the maximum operating temperature of the NMR probe used is 100 °C. From the shape of the merging peaks, however, one could make an educated guess that the coalescence would not take place at much higher temperature. From the spectrum taken at 60 °C the separation of the two singlet peaks was estimated, Δv = 31 Hz. The spectrum at 60 °C was chosen for this as that is the highest temperature with the two peaks fully separated. Spectra at temperatures lower than 60 °C were not considered for this purpose due to unequal shifting of the two signals with temperature (Fig 14) as this causes seemingly greater Δv separations. As discussed earlier, however, an error in

Δv is greatly reduced by the logarithmic operation in equation 3 which means that a slightly different estimate of Δv will not give a significantly different value for the barrier. Having estimated Δv and knowing that $T_c > 373$ K (coalescence temperature higher than 100 °C), one can use equation 3 to estimate the energy barrier for the rotation as $\Delta^{\ddagger}G > 79$ kJ mol^{-1}. Since the coalescence of the two peaks has almost been reached at 100 °C, the energy barrier in toluene-d_8 is probably not much higher than 79 kJ mol^{-1} which agrees with the calculated value of 87 kJ mol^{-1}. The barrier is probably also not much different from the barrier determined in DMSO-d_6. For compound **6**, changing the solvent from polar DMSO-d_6 to apolar toluene-d_8 does not appear to make a significant difference in the rotation barrier.

(*R*)-6,6'-bis(2,6-dimethylphenyl)-2,2'-dimethoxy-1,1'-binaphthyl 11

A part of the aliphatic region of the ^{1}H–NMR spectra of compound **11** taken in DMSO-d_6 in the temperature range from 20 °C to 95 °C is shown in Fig 15b. Due to considerable overlap of aromatic peaks undergoing change, only the aliphatic region with the peaks corresponding to the methyl groups is given in Fig 15b.


a   b
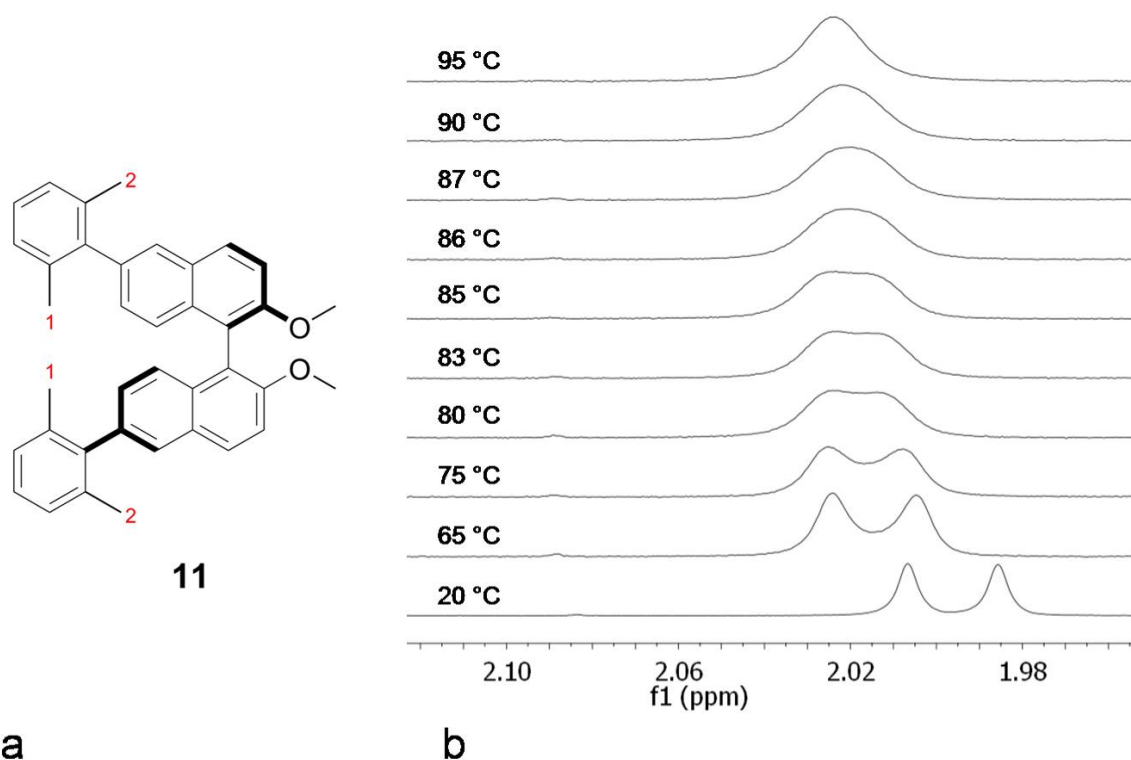
Figure 15. a: Structure of compound **11** with two different positions of methyl groups highlighted with numbers 1 and 2, **b:** The aliphatic part (1.98 – 2.10 ppm) of the ^{1}H–NMR spectra of **11** in DMSO-d_6 at different temperatures.

At 20 °C the ^{1}H–NMR spectrum of compound **11** shows two peaks in the aliphatic region, namely a singlet at 1.99 ppm and a singlet at 2.01 ppm (Fig 15b). These signals correspond to the methyl groups in **11**; one of the signals corresponds to the methyl groups in position 1 and the other signal corresponds to

the methyl groups in position 2, as highlighted in Fig 15a. As shown in Fig 15b, upon increasing the temperature, the two peaks come together and become broader, and eventually coalesce at 86 °C. Above the coalescence temperature there is only one (broad) peak. From the NMR spectrum taken at 20 °C one can determine the separation of the two singlet peaks, Δv = 11 Hz. From the coalescence temperature and Δv, one can use equation 3 to calculate the rotation barrier, $\Delta^{\ddagger}G$ = 79 kJ mol^{-1}. The energy barriers for the rotation in **11** in the gas phase and in DMSO were also calculated by DFT and gave 91 and 83 kJ mol^{-1}, respectively. The latter value is in good agreement with the experimentally determined barrier. The experimental value of 79 kJ mol^{-1} is the same as the value obtained for its non-methylated derivative **9**. This shows that in DMSO-d_6, the rotation barrier of 2,6-dimethylphenyl rotators does not depend on the methyl-protected or unprotected state of the hydroxyl groups.

Compound **11** was also studied in toluene-d_8 at different temperatues. Due to considerable overlap of aromatic peaks undergoing change, only the part of the aliphatic region with peaks corresponding to methyl groups is given in Fig 16.
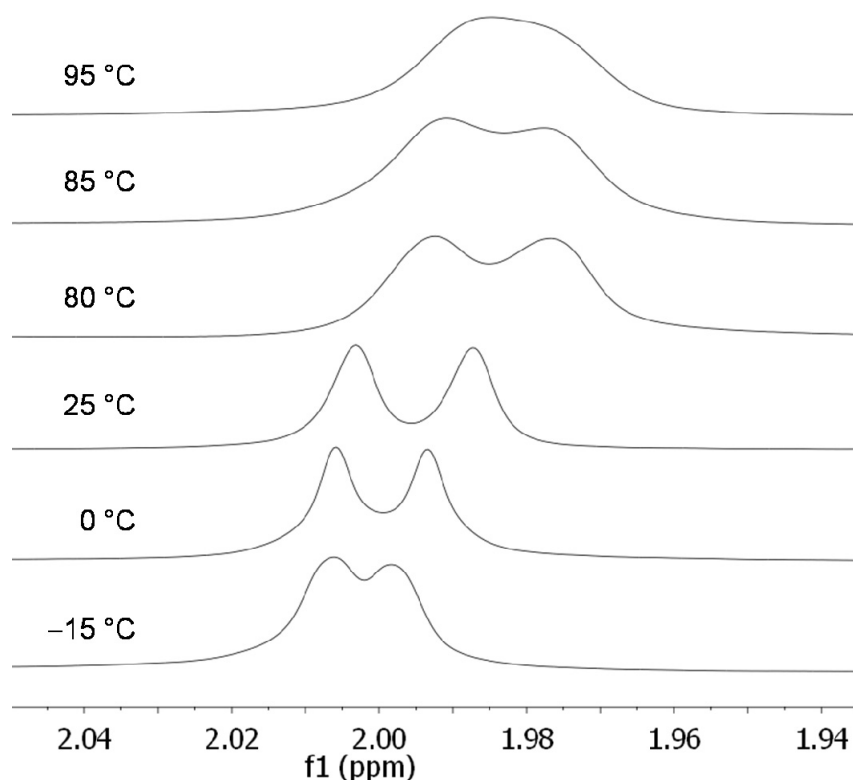
Figure 16. A part of the aliphatic region of the ^{1}H–NMR spectra of **11** in toluene-d_8 at different temperatures.
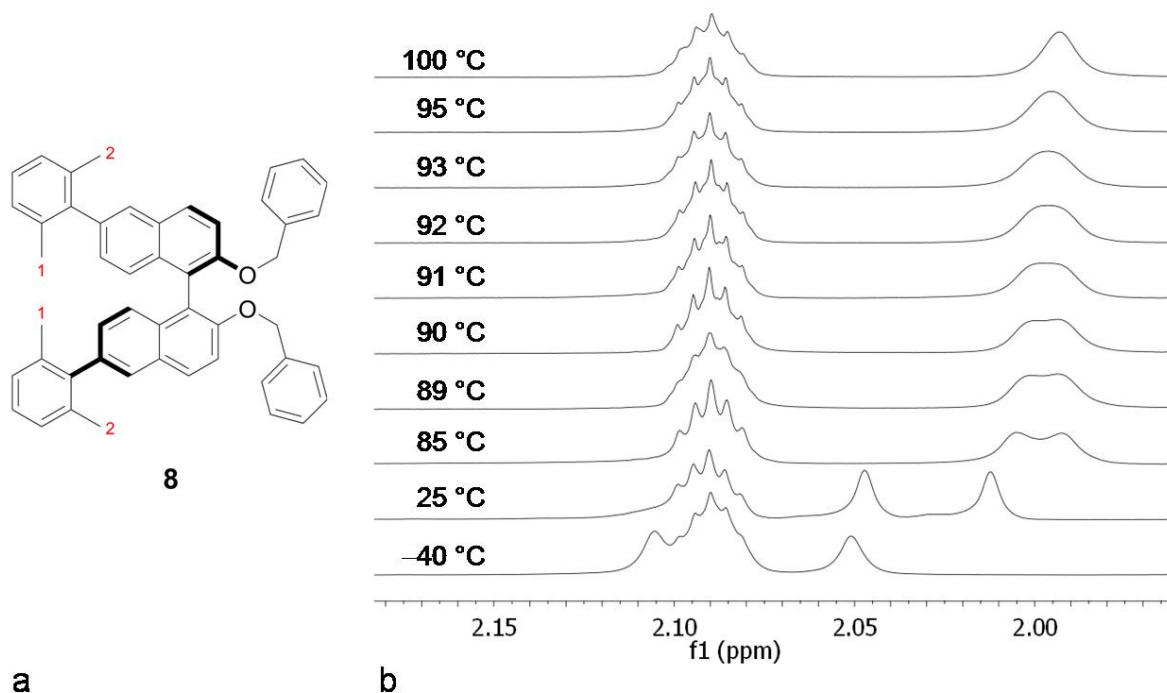
As can be seen from Fig 16 the spectra taken at 0 °C and 25 °C show two peaks in the aliphatic region corresponding to the methyl groups in different positions in the rotors (Fig 15a). Upon increasing the temperature the peaks get closer and become broader, and eventually coalesce at 93 °C. The two peaks

appear to shift to different extents with changing temperature as evidenced by the two peaks getting closer to each other at lower temperatures (see the spectrum taken at −15 °C, Fig 16). This makes the estimation of Δv more difficult. On the other hand, as mentioned earlier, a slightly different estimate of Δv will not give a significantly different value for the barrier. The value for Δv was eventually estimated from the spectrum taken at 25 °C as $\Delta v = 8$ Hz. The rotation barrier was calculated to be $\Delta^{\ddagger}G = 82$ kJ mol^{-1}. This value is in good agreement with the value obtained by DFT calculations of **11** in toluene that gave 86 kJ mol^{-1}. These values are slightly higher than the values determined in DMSO-d_6. The same trend was observed for **9** as well.

(*R*)-6,6'-bis(2,6-dimethylphenyl)-2,2'-dibenzyl-1,1'-binaphthyl 8

Compound **8** (Fig 17a), an intermediate in the synthesis of compound **9** and its derivatives (Scheme 3), was also investigated in toluene-d_8 at different temperatures. Due to considerable overlap of aromatic peaks undergoing change, only the part of the aliphatic region with peaks corresponding to methyl groups is given in Fig 17b.

Figure 17. a: Structure of compound **8** with two different positions of methyl groups highlighted with numbers 1 and 2, **b:** The aliphatic part (1.95 – 2.15 ppm) of the ^{1}H–NMR spectra of **8** in toluene-d_8 at different temperatures.

As can be seen from Fig 17b the spectrum taken at 25 °C shows two peaks in the aliphatic region corresponding to the methyl groups in different positions in the rotors (Fig 17a). Upon increasing the temperature the peaks get closer and become broader, and eventually coalesce at 91 °C. The two peaks appear to shift to different extents with changing temperature as evidenced by the two peaks getting

further away from each other at lower temperatures (see the spectra taken at 25 °C and −40 °C, Fig 17b). This makes the estimation of Δv more difficult. On the other hand, as mentioned earlier, a slightly different estimate of Δv will not give a significantly different value for the barrier. The value for Δv was eventually estimated from the spectrum taken at 85 °C as $\Delta v = 6$ Hz. The two peaks are not fully separated at that temperature but the unequal shifting of the peaks with lowering the temperature is rather severe and the estimation of Δv from a spectrum taken at a temperature where the peaks are fully separated would be erroneous. The rotation barrier was therefore calculated to be $\Delta^{\ddagger}G = 82$ kJ mol^{-1}. This value agrees with the value determined for **11** in toluene-d_8. It appears that the nature of the alkyl groups present on the two hydroxyl groups does not influence the rotation rate of the 2,6-dimethylphenyl rotators. This makes sense as the part of the alkyl group that makes a steric difference between the two alkyl groups is not located in the immediate vicinity of the naphthyl–naphthyl axle and therefore has no influence on the conformation of the binaphthyl system. This in turn explains the absence of any effect on the rotation of the 2,6-dimethylphenyl groups.

9,14-bis(2,6-dimethylphenyl)-*N*,*N*-dimethyl-(*R*)-dinaphtho[2,1-*d*:1',2'-*f*][1,3,2]dioxaphosphepin-4-amine 10

Phosphoramidite **10** was designed for its cyclic structure (Fig 18a) as well as its straightforward preparation from **9** (Scheme 5). The seven-membered ring in **10** might force the molecule into a different conformation (compared to **9** and **11**) through limited rotation around the naphthyl–naphthyl bond which might in turn affect the rotation of the 2,6-dimethylphenyl groups (Fig 5c). The DFT calculations, however, gave energy barriers of 89, 81 and 80 kJ mol^{-1} in the gas phase, DMSO and toluene, respectively.

A part of the aliphatic region of the ^{1}H–NMR spectra of compound **10** taken in DMSO-d_6 in the temperature range from 25 °C to 100 °C is shown in Fig 18b. Due to considerable overlap of aromatic peaks undergoing change, only the aliphatic region with the peaks corresponding to the methyl groups belonging to 2,6-dimethylphenyl rotators is given in Fig 18b.
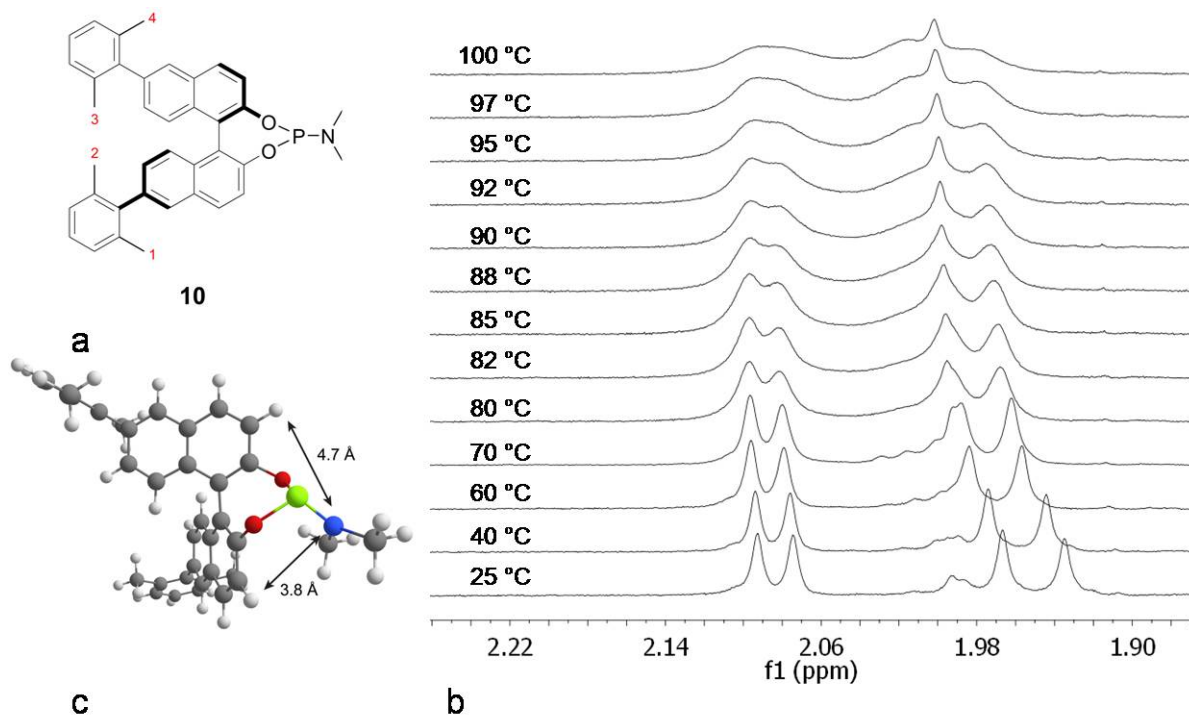
Figure 18. a: Structure of compound **10** with four different positions of methyl groups highlighted with numbers 1 − 4 **b:** The aliphatic part (1.90 − 2.22 ppm) of the ^{1}H−NMR spectra of **10** in DMSO-d_6 at different temperatures. **c:** The calculated structure of **10**; the arrows indicate the N−H distances.

At 25 °C the aliphatic region of the ^{1}H−NMR spectrum of compound **10** in DMSO-d_6 shows four singlet peaks, namely signals at 1.93, 1.97, 2.07 and 2.09 (Fig 18b), and a doublet at 2.54 ppm. The latter corresponds to the two methyl groups on the nitrogen atom (the signal is split into a doublet due to the ^{1}H−^{31}P coupling). Since the chemical shift of the doublet undergoes only a slight change with temperature which is of no importance for the rotational phenomena, this NMR signal will not be discussed further. The four singlet signals, however, correspond to the four methyl groups in the two rotator parts in **10**; this is due to the fact that, unlike molecules **9** or **11**, molecule **10** is not C$_2$ symmetric (Fig 18c) (as part of a seven−membered ring the P−atom and the NMe$_2$ group in **10** are located closer to one naphthyl group than to the other (Fig 18c) making the two naphthyl groups and in turn all the four methyl groups in the rotors magnetically inequivalent; the four different positions of the methyl groups are highlighted by numbers 1−4 in Fig 18a). As shown in Fig 18b, upon increasing the temperature, the two peaks at 1.93 and 1.97 ppm come together and become broader, and eventually coalesce at around 100 °C (for this set of peaks it is not possible to determine the coalescence temperature with high accuracy due to the overlap of the coalescing peak with another peak as well as due to the inability to reach temperatures higher than 100 °C). Similar behaviour is observed for the two peaks at 2.07 and 2.09 ppm, and they coalesce at 100 °C. From the spectra taken at 25 °C one can determine the separations of the peaks, $\Delta\nu$, as 16 and 9 Hz, respectively. From the coalescence temperatures and $\Delta\nu$, one can use equation 3 to calculate the rotation barriers for

the two rotors, $\Delta^{\ddagger}G_1$ = 81 kJ mol^{-1} and $\Delta^{\ddagger}G_2$ = 83 kJ mol^{-1}. Given the difficulty in estimating the coalescence temperature for one set of coalescing peaks, the two values agree within the error margin and are also in very good agreement with 81 kJ mol^{-1} as calculated for both rotors using DFT. This means that the two 2,6-dimethylphenyl groups rotate with the same rates. Furthermore, the values obtained for the rotation barriers in **10** do not appear to be significantly different than the value of 79 kJ mol^{-1} as obtained for **9**. This shows that, in DMSO-d_6, the rotation of 2,6-dimethylphenyl rotators is not significantly influenced by bridging the two hydroxyl groups in form of a phosphoramidite group.

Compound **10** was also studied in toluene-d_8 at different temperatures. Due to considerable overlap of aromatic peaks undergoing change, only the part of the aliphatic region with peaks corresponding to methyl groups is given in Fig 19.
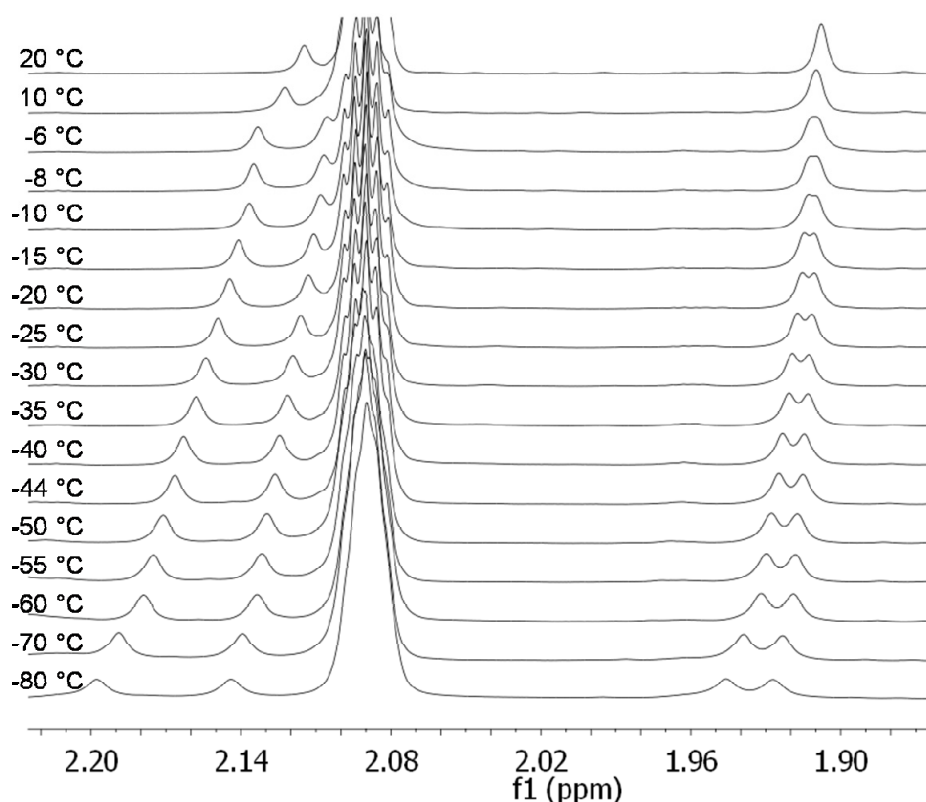
Figure 19. A part of the aliphatic region of the ^{1}H–NMR spectra of **10** in toluene-d_8 at different temperatures.

At −85 °C the ^{1}H–NMR spectrum of compound **10** shows four singlet peaks in the aliphatic region, namely signals at 1.93, 1.95, 2.14 and 2.20 ppm (Fig 19) corresponding to the four methyl groups in the two rotator parts in **10**. As shown in Fig 19, upon increasing the temperature, the two peaks at 1.93 and 1.95 ppm come together and become broader, and eventually coalesce at −6 °C. The value for Δv was estimated to 6 Hz from the spectrum taken at −60 °C and the energy barrier of 59 kJ mol^{-1} was calculated for one of the rotors in **10**. The same changes are observed for the two peaks at 2.14 and 2.20 ppm (Fig 19). The temperature of

coalescence for these two peaks could, however, not be determined due to the shifting of the peaks to lower chemical shifts upon increasing the temperature as this resulted in an overlap of the coalescing peaks with the solvent peak. The energy barrier for the other rotor in **10** could therefore not be determined in toluene-d_8. The value obtained for the rotation barrier for a rotor in **10** in toluene-d_8 appears to be significantly different than the value of 81 or 83 kJ mol^{-1} as obtained in DMSO-d_6. The experimental value of 59 kJ mol^{-1} is also significantly different than the value of 80 kJ mol^{-1} as predicted by DFT calculations. This shows a pronounced solvent effect on the rotation rate of 2,6-dimethylphenyl groups in **10**. It is at this point unclear why this significant solvent effect is only observed for **10** and not for any of the other compounds studied. The disagreement with the theoretical value is also not clear at this point. In order to verify the values reported here it would be wise to use a freshly prepared batch of **10** to repeat the measurements described above. It would also be interesting to investigate **10** in other (similar) solvents in order to determine the rotation barriers of both rotors and see how their values compare. Affecting the two rotors in **10** in different ways and having two rotors in the same molecule operating at different rates would mean a higher degree of control over rotational motion which would undoubtedly pave the way towards the construction and development of more complex artificial rotary systems. These rotary systems will make essential parts in the future design of molecular machinery[1,6].

It is worth noting that, with the exception of compound **10** in toluene-d_8, all the derivatives of **9** (compounds **8**, **9**, **10**, **11**) exhibit the same rotary behaviour with virtually the same energy barriers (79 – 83 kJ mol^{-1}). This means that the chemical changes brought upon the two hydroxyl groups do not have any significant influence on the molecular rotors. It appears that those changes are not severe enough to cause any change in the properties of the binaphthyl core and, in turn, induce a change in the rotors on the other side of the molecule. This was confirmed by DFT optimization of their structures and the calculations of the dihedral angle between the two naphthyl rings; the calculated angles in **9**, **10** and **11** are 89°, 89° and 91 °C, respectively. These values are virtually the same which means that the conformation of the binaphthyl core in those compounds is the same as well which explains the experimentally determined energy barriers. It appears that the seven-membered ring in **10** is large enough to allow the binaphthyl core to attain its most favourable conformation. Attaching a sterically more hindering substituent to the hydroxyl groups, like a *tert*-butyl group for example, might cause a change in the conformation of the binaphthyl core and in turn affect the rotation of the rotors.

Allosteric effect through noncovalent modification

So far we have studied the effect of covalent modification of the two hydroxyl groups in **9** on the rotation behaviour of the two 2,6-dimethylphenyl rotators on the opposite side of the molecule. We would also like to investigate the possibility of

using noncovalent interactions with the hydroxyl groups as a means of affecting the rotors. Biphenol-based compounds are known to form noncovalent complexes with amines through hydrogen bonding[71,72,73,74,75] (Fig 20a). To this end we decided to investigate a mixture of compound **9** (Fig 13a) and 2-amino-3-phenyl-1-propanol **13** as this aminoalcohol had been studied extensively in the presence of biphenols (Fig 20a)[73].

### Complex of (*R*)-9 and (*S*)-2-amino-3-phenyl-1-propanol 13

A mixture of (*R*)-**9** and (*S*)-**13** in a 1:1 molar ratio (Fig 20a) was first studied in toluene-d_8 (this solvent was also used for the study of similar complexes between biphenols and amines[75]) by ^{1}H–NMR spectroscopy. A part of the aliphatic region of the ^{1}H–NMR spectra of the mixture taken in the temperature range from 25 °C to 100 °C is shown in Fig 20b. Due to considerable overlap of aromatic peaks undergoing change, only the aliphatic region with the peaks corresponding to the methyl groups belonging to 2,6-dimethylphenyl rotators is given in Fig 20b.
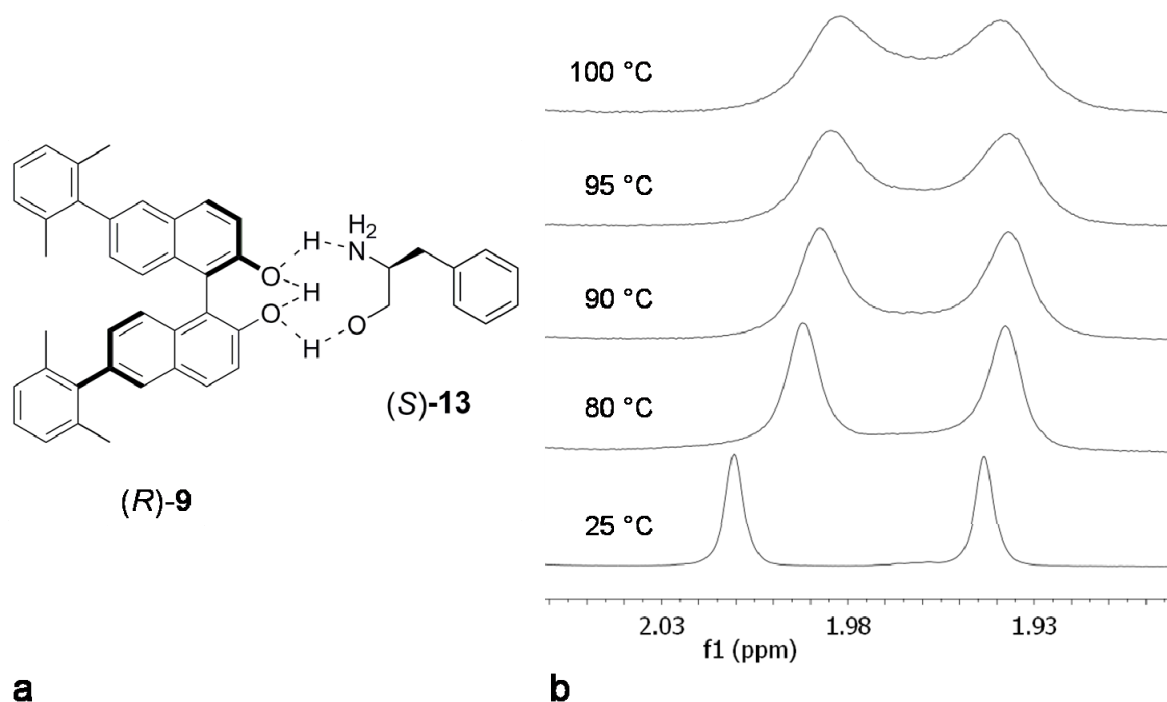
Figure 20. a: Structure of the complex between (*R*)-**9** and (*S*)-**13** as proposed for similar complexes in the literature[73], **b:** The aliphatic part (1.93 – 2.03 ppm) of the ^{1}H–NMR spectra of the mixture of (*R*)-**9** and (*S*)-**13** in toluene-d_8 at different temperatures.

As can be seen from Fig 20b the spectrum taken at 25 °C shows two peaks in the aliphatic region corresponding to the methyl groups in different positions in the rotors (Fig 20a). Upon increasing the temperature the peaks get closer and become broader. Coalescence of the two peaks, however, appears to take place above 100 °C which cannot be investigated further by means of our current NMR setup (a different choice of solvent would also be necessary). The value for $\Delta \nu$ was

estimated from the spectrum taken at 90 °C as $\Delta\nu$ = 25 Hz. With the help of equation 3, one can estimate the rotation barrier as $\Delta^{\ddagger}G$ > 80 kJ mol^{-1}. For pure **9** in toluene-d_8 the barrier was estimated as $\Delta^{\ddagger}G$ > 79 kJ mol^{-1} (Fig 14) which shows that the energy barrier does not decrease upon adding (*S*)-**13**. In Fig 21 we compared the behaviour of (*R*)-**9** in toluene-d_8 in the absence (Fig 21a) and presence of (*S*)-**13** (Fig 21b) at exactly the same temperatures. From the inspection of the coalescing NMR peaks it becomes clear that the two systems behave virtually in the same way. Although the exact energy barriers for the rotation cannot be determined, it can, however, be concluded that the addition of (*S*)-**13** has no influence on the rotary behaviour of (*R*)-**9** in toluene-d_8.
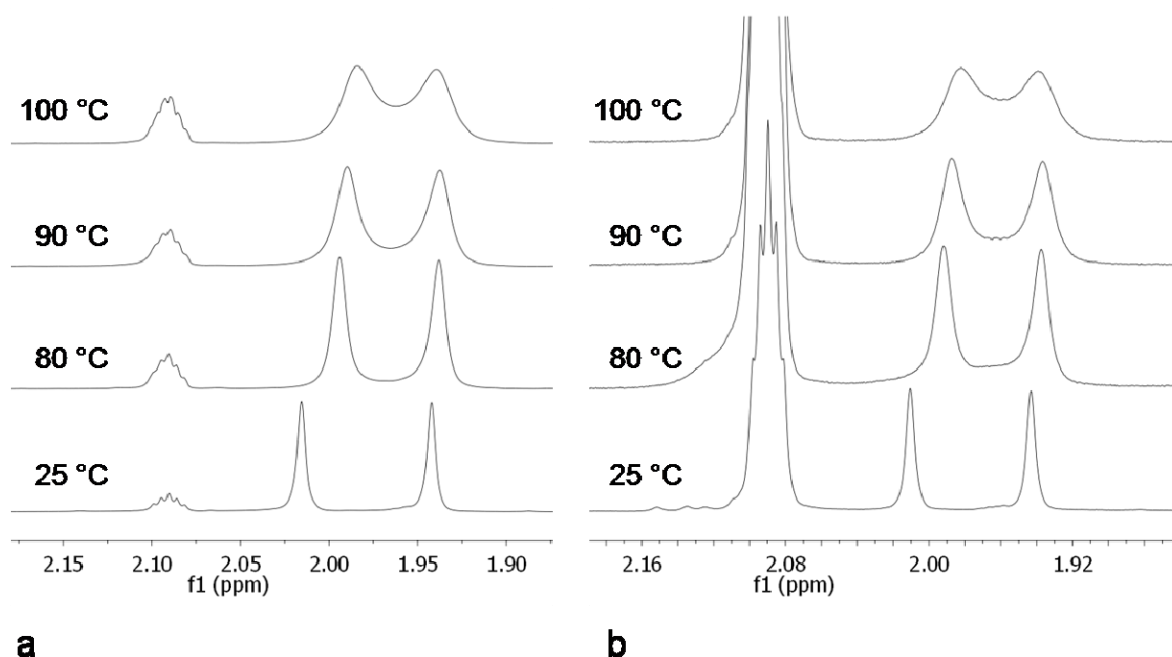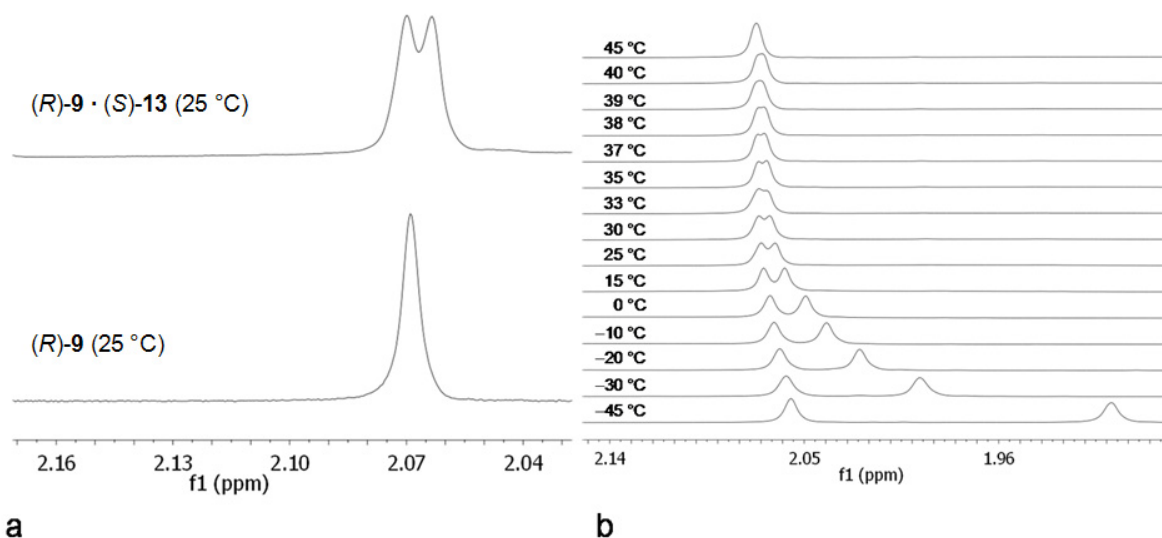

Figure 21. The aliphatic part (1.90 – 2.16 ppm) of the ^{1}H–NMR spectra of (*R*)-**9** in toluene-d_8 at different temperatures **a:** in the absence of (*S*)-**13**, **b:** in a 1:1 mixture with (*S*)-**13**.

A mixture of (*R*)-**9** and (*S*)-**13** in a 1:1 molar ratio (Fig 20a) was also investigated in CDCl$_3$ by ^{1}H–NMR spectroscopy as this was the solvent of choice in the study of the interaction of biphenols with aminoalcohol **13**[73]. Parts of the aliphatic region of spectra of (*R*)-**9** in the absence and in the presence of (*S*)-**13** (a mixture in a 1:1 molar ratio) taken at 25 °C in CDCl$_3$ are shown in Fig 22a. In the absence of (*S*)-**13** compound **9** shows a single singlet peak corresponding to the methyl groups. Spectra containing only **9** in CDCl$_3$ were taken in the temperature range from –45 °C to 25 °C only to give a single peak for the methyl groups at all temperatures (not shown here); it appears that the two peaks corresponding to two differently oriented methyl groups in **9** have the same chemical shift and therefore cannot be distinguished in the ^{1}H–NMR spectra. In a mixture with (*S*)-**13**, compound (*R*)-**9** shows two peaks for the methyl groups (Fig 22a). This could mean two things. The first possibility is that upon complexing (*R*)-**9** with (*S*)-**13** the rotation of the 2,6-dimethylphenyl groups has been slowed down (maybe due to a conformational

change as a result of the interaction) showing two differently oriented methyl groups in each rotor (positions 1 and 2 in Fig 13a). Another possibility is that the rotation of the 2,6-dimethylphenyl groups remains fast rendering the two positions of methyl groups (positions 1 and 2 in Fig 13a) indistinguishable on the NMR time scale. The diastereomeric nature of complex (*R*)-**9** · (*S*)-**13**, however, renders the two rotors diastereotopic causing the two methyl groups of one rotator to appear at a different chemical shift than the two methyl groups of the other rotator. In order to investigate this further we studied the mixture of (*R*)-**9** and (*S*)-**13** in CDCl₃ at different temperatures in the range from –45 °C to 45 °C, as shown in Fig 22b.

Figure 22. a: The aliphatic part (2.04 – 2.16 ppm) of the ¹H–NMR spectra of (*R*)-**9** in CDCl₃ at 25 °C in the absence and in the presence of (*S*)-**13** (1:1 mixture), **b:** The aliphatic part (1.90 – 2.14 ppm) of the ¹H–NMR spectra of a 1:1 mixture of (*R*)-**9** and (*S*)-**13** in CDCl₃ at different temperatures.
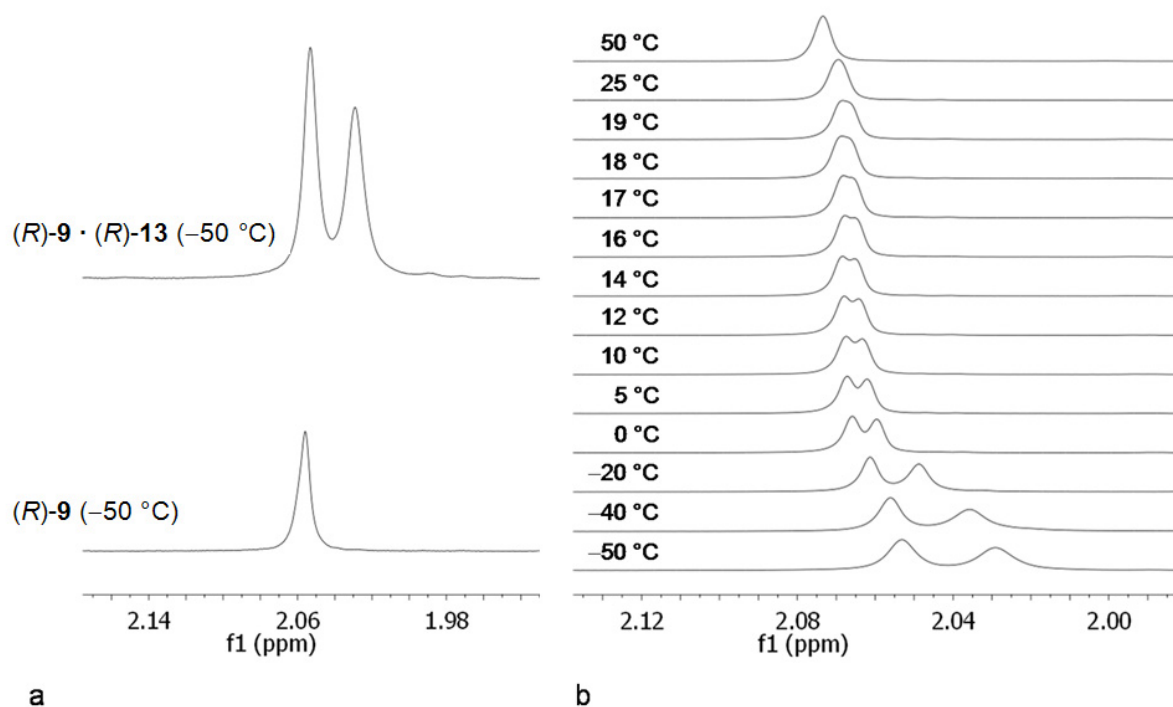
As can be seen from Fig 22b, the spectrum taken at –45 °C shows two peaks widely separated. Upon increasing the temperature the two peaks come together and eventually coalesce at 39 °C. This behaviour is typical of a dynamic process being accelerated at higher temperatures[23,34,35,36] indicating that the two peaks correspond to methyl groups at different positions within each rotor (positions 1 and 2 in Fig 13a). The peak appearing at lower chemical shifts in the spectra in Fig 22b undergoes shifting upon lowering the temperature more severely than the peak appearing at higher chemical shifts making the two peaks shift further apart at lower temperatures. This makes the estimation of the Δv value more difficult. The spectrum taken at 0 °C was chosen for this purpose as the peaks are fairly separated but have not shifted away from each other too much; $\Delta v = 8$ Hz. From equation 3 one can calculate the energy barrier for the rotation as 69 kJ mol⁻¹. This value appears to be much lower than estimated in toluene-d_8 ($\Delta^{\ddagger}G > 80$ kJ mol⁻¹). Since the measurements of (*R*)-**9** in CDCl₃ in the absence of (*S*)-**13** did not afford any parameters, it cannot be concluded at this point whether the lowering of the

rotation barrier is due to the solvent effect (but only visible in the presence of (*S*)-**13**) or due to the presence of (*S*)-**13**, or due to the combination of both. In any case it is highly interesting that the rotation rate of the rotors may be tuned by changing the solvent and/or adding an additive.

Complex of (*R*)-9 and (*R*)-2-amino-3-phenyl-1-propanol 13

A mixture of (*R*)-**9** and (*R*)-**13** in a 1:1 molar ratio was also investigated. Parts of the aliphatic region of spectra of **9** in the absence and in the presence of (*R*)-**13** (a mixture in a 1:1 molar ratio) taken at –50 °C in CDCl$_3$ are shown in Fig 23a. In the absence of (*R*)-**13** compound (*R*)-**9** shows a single singlet peak corresponding to the methyl groups. As mentioned earlier, spectra containing only **9** in CDCl$_3$ were taken in the temperature range from –45 °C to 25 °C only to give a single peak for the methyl groups at all temperatures. In a mixture with (*R*)-**13**, however, compound (*R*)-**9** shows two peaks for the methyl groups (Fig 23a). This is the same behaviour as observed for a mixture of (*R*)-**9** with (*S*)-**13**. In order to investigate this further we studied the mixture of (*R*)-**9** and (*R*)-**13** in CDCl$_3$ at different temperatures in the range from –50 °C to 50 °C, as shown in Fig 23b.

Figure 23. a: The aliphatic part (1.98 – 2.14 ppm) of the ^{1}H–NMR spectra of (*R*)-**9** in CDCl$_3$ at –50 °C in the absence and in the presence of (*R*)-**13** (1:1 mixture), **b:** The aliphatic part (2.00 – 2.12 ppm) of the ^{1}H–NMR spectra of a 1:1 mixture of (*R*)-**9** and (*R*)-**13** in CDCl$_3$ at different temperatures.

As can be seen from Fig 23b, the spectrum taken at –50 °C shows two peaks wide apart. Upon increasing the temperature the two peaks come together and eventually coalesce at 19 °C. This behaviour is typical of a dynamic process being

sped up at higher temperatures[23,34,35,36] indicating that the two peaks correspond to methyl groups at different positions within each rotor (positions 1 and 2 in Fig 13a). The peak appearing at lower chemical shifts in the spectra in Fig 23b undergoes shifting upon lowering the temperature more severely than the peak appearing at higher chemical shifts making the two peaks shift further apart at lower temperatures. This makes the estimation of the Δv value more difficult. The spectrum taken at 5 °C was chosen for this purpose as the peaks are fairly separated but have not shifted away from each other too much; $\Delta v = 2.5$ Hz. From equation 3 one can calculate the energy barrier for the rotation as 67 kJ mol^{-1}. This value appears to be much lower than estimated in toluene-d_8 ($\Delta^{\ddagger}G > 80$ kJ mol^{-1}) in the absence of any additives. The value of 67 kJ mol^{-1} agrees with the value of 69 kJ mol^{-1} as obtained for the mixture of (*R*)-**9** with (*S*)-**13** (within the error margin). This means that the two enantiomeric aminoalcohols **13** influence the rotation rate of (*R*)-**9** in CDCl$_3$ in the same way despite the diastereomeric nature of the complex **9** · **13**. This could be explained by the model of the complex[73] in Fig 20a; although a diastereomeric complex is formed, the stereogenic centre of the aminoalcohol **13** does not appear to be in proximity of the binding site on the binol molecule (according to the model in Fig 20a). It is therefore not surprising that the configuration of the stereogenic centre of the aminoalcohol does not play a significant role in the binding of the aminoalcohol to the chiral binol molecule. As a consequence, the two enantiomeric aminoalcohol molecules affect the rotation rate of rotors in (*R*)-**9** in CDCl$_3$ in the same way.

As discussed earlier in this chapter the rotation barriers obtained in CDCl$_3$ should be taken with caution because the permittivity of the solvent changes significantly (up to 33 %)[68] in the temperature range of the measurements which could in turn also influence the measured rotation rates.

Conclusions

A number of compounds containing molecular rotors have been prepared with the goal of investigating the possibilities of tuning their rotation rate. Compounds **3**, **4** and **12** are binol-based compounds with two 3,5-dimethylphenyl rotators positioned on carbon atoms adjacent (the 3,3' positions on the binol core) to the two hydroxyl groups. We investigated the effect of chemically modifying the two hydroxyl groups, upon going from **12** to **3** and eventually **4**, on the rotation rate of the rotators. The rotation of the 3,5-dimethylphenyl group, however, appeared to have a low energy barrier making the rotation too fast to observe. The rotation of the bis(1-phenylethyl)amino group around the P–N bond in **3** and **4**, however, was slow enough to be studied. Upon going from **3** to **4**, the lowering of the rotation barrier was observed. Molecule **3** is a highly interesting molecule equipped with two very fast rotors and a slow one; the rotation rate of the slow rotor may be increased by converting **3** to **4**. The concept of selectively addressing only one mode of molecular motion is highly interesting for the field of molecular devices and machines.

Compounds **8**–**11** are binol-based compounds with two 2,6-dimethylphenyl rotators positioned on the opposite side of the molecule (the 6,6' positions on the binol core) than the two hydroxyl groups (the 2,2' positions on the binol core). We investigated the effect of chemically modifying the two hydroxyl groups on the rotation rate of the rotors. The rotation was studied in two solvents in order to investigate a possible solvent effect. Although of measurable rate, the rotation of the 2,6-dimethylphenyl groups did not appear to undergo any significant change upon chemically modifying the hydroxyl groups (upon going from **9** to **8**, **10** and **11**) as most of the rotation barriers were found to be in the range 79 – 83 kJ mol^{-1}. The choice of solvent (toluene-d_8 or DMSO-d_6) did not seem to make any difference either, with the exception of compound **10** that exhibited a significantly lower rotation barrier (59 kJ mol^{-1}) in toluene-d_8. The concept of affecting the rotation rate in **10** by a mere change of solvents is rather exciting and requires additional research.

The concept of using noncovalent interaction to remotely affect the rotation rate has also been investigated. Compound (*R*)-**9** was studied in a mixture with (*S*)-2-amino-3-phenyl-1-propanol (*S*)-**13** as this aminoalcohol is known to form hydrogen bonded complexes with biphenols[73]. No effect of (*S*)-**13** on the rotation rate of **9** was found in toluene-d_8 (the barrier was estimated to be higher than 80 kJ mol^{-1}). In CDCl$_3$, however, the barrier in the presence of (*S*)-**13** was found to be significantly lower (69 kJ mol^{-1}). Compound (*R*)-**9** was also investigated in a mixture with (*R*)-**13** in CDCl$_3$. The effect of (*R*)-**13** on the rotation rate of **9** was found to be the same as that of (*S*)-**13** leading to the conclusion that the configuration of the binding aminoalcohol does not have a significant role in affecting the rotation rate of rotors in (*R*)-**9**. The possibility of controlling the rotation rate through the formation of supramolecular complexes, however, is exciting. Moreover, the idea of addressing a molecule on one side and affecting the properties of its rotators on the other side of the molecule is a highly interesting concept. The possibility of remote controlling an artificial system in an allosteric way would undoubtedly pave the way to the development of new systems with molecular machine-like functions.

Acknowledgements

Experimental section

Synthesis, characterization and physico–chemical measurements

General remarks

The experiments were performed as described in the section *General Remarks* in Chapter 2. Temperature-dependent measurements were performed on the Varian AMX-500 (500 MHz); spectra were measured after the reading of the temperature had stabilized (approximately 15 min).

Calculations were performed with Gaussian 09 revision C.01[76]. Geometries were optimized in the gas phase at the B3LYP/6-31G(d,p) level, after which the SCF energy was calculated at the B3LYP/pc-2 level. For the calculation of the thermochemistry, B3LYP/6-31G(d,p) was employed in combination with a hindered rotor analysis[77] which identifies internal rotations and corrects their contribution to the thermochemistry. The energetic contribution of solvation was calculated by a B3LYP/6-31G(d,p) SCF energy + thermochemistry calculation, performed both in the gas phase and in solution using the SMD model[78], after which their difference in Gibbs energy was added to the higher-level gas phase result. For these calculations, the hindered rotor analysis was not applied as it could not be applied successfully in some of the calculations that employed the SMD model.

4-(bis((*R*)-1-phenylethyl)amino-2,6-bis(3,5-dimethylphenyl)-(*S*)-dinaphtho[2,1-*d*:1',2'-*f*][1,3,2]dioxaphosphepin-4-ium-4-yl)trihydroborate 4: Compound **3** (30 mg, 0.04 mmol) was dissolved in THF (750 μl) and a solution of $H_3B \cdot THF$ in THF (133 μl, *c* = 1.0 mol dm^{-3}; 1.32 mmol) was added under a nitrogen atmosphere. The solution was stirred at room temperature for 1.5 h. The progress of the reaction could be followed by TLC (*n*-pentane/CH_2Cl_2 3:1). The solvent was evaporated and the crude product was purified by means of column chromatography using *n*-pentane/CH_2Cl_2 3:1 as eluent. The product (18 mg) was obtained as a white solid in 59 % yield.

^{1}H NMR (400 MHz, CDCl$_3$): δ 8.06 (s, 1H), 8.03 (s, 1H), 7.94 (dd, *J* = 8.1, 3.3 Hz, 2H), 7.53 (s, 2H), 7.46 (m, 2H), 7.35 (br s, 3H), 7.29 (d, *J* = 7.9 Hz, 1H), 7.22 (t, *J* = 7.2 Hz, 1H), 7.14–7.01 (m, 5H), 6.95 (t, *J* = 7.6 Hz, 4H), 6.80 (d, *J* = 7.6 Hz, 4H), 4.62 (dq, *J* = 14.6, 7.1 Hz, 2H), 2.44 (s, 6H), 2.36 (s, 6H), 1.08 (m, 3H), 0.93 (d, *J* = 7.2 Hz, 6H). ^{13}C NMR (125 MHz, CDCl$_3$): δ 146.92, 145.85, 145.80, 138.06, 137.39, 137.28, 136.83, 133.41, 132.74, 132.39, 131.87, 131.27, 131.15, 130.72, 129.60, 129.25, 128.47, 128.37, 128.35, 128.10, 127.83, 127.28, 127.22, 126.98, 126.48, 126.25, 125.75, 125.71, 122.81 (d, *J* = 2.6 Hz), 122.72 (d, *J* = 2.7 Hz), 54.14, 54.09, 21.60, 19.69. ^{31}P NMR (162 MHz, CDCl$_3$): δ 127.80. ^{11}B NMR (128 MHz, acetone): δ −44.41. MS (APCI): *m/z* calculated for $C_{52}H_{50}BNO_2P^+$: 762.36722 [M+H]$^+$, found 762.3667 [M+H]$^+$.

(*S*)-6,6'-bis(3,5-bis(trifluoromethyl)phenyl)-1,1'-binaphthyl-2,2'-diol 6: (*S*)-6,6'-dibromo-1,1'-binaphthyl-2,2'-diol **5** (218 mg, 0.49 mmol) was dissolved in water (50.0 ml) along with K_2CO_3, (837 mg, 5.88 mmol) and $Pd(OAc)_2$ (327 mg, 1.47 mmol) under a nitrogen atmosphere. 3,5-Bis(trifluoromethyl)phenylboronic acid (613 mg, 2.45 mmol) was added portionwise over 3 h as the solution was stirred at room temperature. The progress of the reaction could be followed by TLC using CH_2Cl_2/AcOEt 60:1. The reaction ran overnight. The solvent was evaporated and the residue was purified by means of column chromatography using CH_2Cl_2 as eluent. The purification was carried out twice. The crude product was crystallized from *n*-heptane/CH_2Cl_2 10:1 solution affording a white solid (17.5 mg) in 5 % yield.

^{1}H NMR (500 MHz, CD_2Cl_2): δ 8.22 (s, 2H), 8.15 (s, 4H), 8.14 (d, *J* = 10 Hz, 2H), 7.90 (s, 2H), 7.61 (dd, *J* = 8.7, 1.7 Hz, 2H), 7.49 (d, *J* = 9.0 Hz, 2H), 7.29 (d, *J* = 8.7 Hz, 2H), 5.30 (s, 2H). ^{13}C NMR (125 MHz, CD_2Cl_2): δ 154.25, 143.48, 134.26, 134.07, 132.58, 132.54 (q, *J* = 33 Hz), 130.24, 127.88, 127.75, 126.76, 125.89, 124.09 (q, *J* = 271 Hz), 121.43, 119.48, 116.60. ^{19}F NMR (376 MHz, $CDCl_3$): δ −63.04. MS (ESI): *m/z* calculated for $C_{36}H_{19}F_{12}O_2{}^+$: 711.11934 [M+H]$^+$, found 711.1141 [M+H]$^+$.

9,14-bis(2,6-dimethylphenyl)-*N*,*N*-dimethyl-(*R*)-dinaphtho[2,1-*d*:1',2'-*f*][1,3,2]dioxaphosphepin-4-amine 10: (*R*)-6,6'-bis(2,6-dimethylphenyl)-1,1'-binaphthyl-2,2'-diol **9** (50 mg, 0.10 mmol) was dissolved in toluene (10.0 ml) and $(Me_2N)_3P$ (23 μl, 0.13 mmol) was added under a nitrogen atmosphere. The solution was stirred for 10 min at room temperature and then heated to reflux. The progress of the reaction could be followed by TLC using *n*-pentane/CH_2Cl_2 1:1 or 3:1. The reaction was complete after 2 h. The solvent was evaporated and the residue was purified by means of column chromatography using *n*-pentane/CH_2Cl_2 3:1 as eluent affording the product (39 mg) in 68 % yield.

^{1}H NMR (400 MHz, $CDCl_3$): δ 7.95 (d, *J* = 8.7 Hz, 1H), 7.89 (d, *J* = 8.7 Hz, 1H), 7.70 (dd, *J* = 6.4, 1.2 Hz, 2H), 7.56 (d, *J* = 5.3 Hz, 1H), 7.53 (d, *J* = 5.3 Hz, 1H), 7.50 (d, *J* = 8.7 Hz, 1H), 7.42 (d, *J* = 8.8 Hz, 2H), 7.22–7.07 (m, 8H), 2.63 (d, *J* = 9.0 Hz, 6H), 2.14 (s, 3H), 2.12 (s, 3H), 2.05 (s, 3H), 2.00 (s, 3H). ^{13}C NMR (125 MHz, $CDCl_3$): δ 150.10, 150.06, 149.46, 141.45, 137.62, 137.36, 136.46, 136.41, 136.32, 131.70, 131.68, 131.44, 130.97, 130.40, 130.11, 128.14, 128.08, 127.96, 127.94, 127.51, 127.49 (2C), 127.44, 127.29 (3C), 127.08, 124.12, 124.08, 122.81, 122.34, 122.24. ^{31}P NMR (162 MHz, $CDCl_3$): δ 148.58. HRMS (ESI): *m/z* calculated for $C_{38}H_{35}NO_2P^+$: 568.23999 [M+H]$^+$, found 568.23953 [M+H]$^+$.

(*R*)-6,6'-bis(2,6-dimethylphenyl)-2,2'-dimethoxy-1,1'-binaphthyl 11: (*R*)-6,6'-bis(2,6-dimethylphenyl)-1,1'-binaphthyl-2,2'-diol **9** (30 mg, 0.061 mmol) was dissolved in acetone (6.0 ml) and K_2CO_3 (29 mg, 0.21 mmol) was added under a nitrogen atmosphere. The mixture was heated to reflux, CH_3I (23 μl, 0.37 mmol) was added and the mixture was stirred at reflux for 48 h. The progress of the

reaction was followed by TLC using *n*-pentane/CH_2Cl_2 1:1. The solvent was evaporated and the residue was treated with water (25 ml) and AcOEt (25 ml). The layers were separated and the organic layer was dried on anhydrous Na_2SO_4. The salt was removed by filtration and the solvent was evaporated. The residual material was purified by means of column chromatography using *n*-pentane/CH_2Cl_2 3:2 as eluent. The crude product was suspended in *n*-heptane and the solution was removed by decantation. This procedure was repeated several times affording the product (20 mg) in 63 % yield.

^{1}H NMR (400 MHz, CD_2Cl_2): δ 8.01 (d, *J* = 9.0 Hz, 2H), 7.67 (s, 2H), 7.53 (d, *J* = 9.0 Hz, 2H), 7.24 (d, *J* = 8.6 Hz, 2H), 7.19–7.04 (m, 8H), 3.84 (s, 6H), 2.07 (s, 6H), 2.06 (s, 6H). ^{13}C NMR (125 MHz, $CDCl_3$): δ 155.08, 141.92, 136.62, 136.56, 136.27, 132.97, 129.58, 129.46, 128.26, 127.78, 127.41 (2C), 127.11, 125.60, 119.77, 114.57, 57.17, 21.23, 21.20. HRMS (ESI): *m/z* calculated for $C_{38}H_{35}O_2^+$: 523.26316 [M+H]$^+$, found 523.26255 [M+H]$^+$.

References

1. G. S. Kottas, L. I. Clarke, D. Horinek, J. Michl *Chem. Rev.* **2005**, *105*, 1281–1376.

2. J. Michl, E. C. H. Sykes *ACS Nano* **2009**, *3*, 1042–1048.

3. K. Mislow *Acc. Chem. Res.* **1976**, *9*, 26–33.

4. H. Iwamura, K. Mislow *Acc. Chem. Res.* **1988**, *21*, 175–182.

5. M. Xue, K. L. Wang *Sensors* **2012**, *12*, 11612–11637.

6. W. R. Browne, B. L. Feringa *Nature Nanotechnol.* **2006**, *1*, 25–35.

7. T. R. Kelly *Acc. Chem. Res.* **2001**, *34*, 514–522.

8. B. L. Feringa *J. Org. Chem.* **2007**, *72*, 6635–6652.

9. Y. Lin, B. J. Dahl, B. P. Branchaud *Tetrahedron Lett.* **2005**, *46*, 8359–8362.

10. T. R. Kelly, X. Cai, F. Damkaci, S. B. Panicker, B. Tu, S. M. Bushell, I. Cornella, M. J. Piggott, R. Salives, M. Cavero, Y. Zhao, S. Jasmin *J. Am. Chem. Soc.* **2007**, *129*, 376–386.

11. S. P. Fletcher, F. Dumur, M. M. Pollard, B. L. Feringa *Science* **2005**, *310*, 80–82.

12. H. L. Tierney, C. J. Murphy, A. D. Jewell, A. E. Baber, E. V. Iski, H. Y. Khodaverdian, A. F. McGuire, N. Klebanov, E. C. H. Sykes *Nature Nanotechnol.* **2011**, *6*, 625–629.

13. U. G. E. Perera, F. Ample, H. Kersell, Y. Zhang, G. Vives, J. Echeverria, M. Grisolia, G. Rapenne, C. Joachim, S.-W. Hla *Nature Nanotechnol.* **2013**, *8*, 46–51.

14. T. Kudernac, N. Ruangsupapichat, M. Parschau, B. Maciá, N. Katsonis, S. R. Harutyunyan, K.–H. Ernst, B. L. Feringa *Nature* **2011**, *479*, 208–211.

15. B. E. Dial, P. J. Pellechia, M. D. Smith, K. D. Shimizu *J. Am. Chem. Soc.* **2012**, *134*, 3675–3678.

16. B. E. Dial, R. D. Rasberry, B. N. Bullock, M. D. Smith, P. J. Pellechia, S. Profeta Jr., K. D. Shimizu *Org. Lett.* **2011**, *13*, 244–247.

17. M. K. J. ter Wiel, R. A. van Delden, A. Meetsma, B. L. Feringa *Org. Biomol. Chem.* **2005**, *3*, 4071–4076.

18. A. S. Lubbe, N. Ruangsupapichat, G. Caroli, B. L. Feringa *J. Org. Chem.* **2011**, *76*, 8599–8610.

19. J. M. Berg, J. L. Tymoczko, L. Stryer *Biochemistry* 7th ed; W. H. Freeman Company; New York, USA **2012**.

20. Z. Bu, D. J. E. Callaway *Adv. Protein Chem. Struct. Biol.* **2011**, *83*, 163–221.

21. J. Clayden *Chem. Soc. Rev.* **2009**, *38*, 817–829.

22. J. Clayden in *Molecular Interactions – Bringing Chemistry to Life* , ed. M. G. Hicks and C. Kettner, pub. Beilstein Institut **2007**, ISBN 978–3–8325–1791–5.

23. C. Wolf *Dynamic Stereochemistry of Chiral Compounds: Principles and Applications* 1st ed; Royal Society of Chemistry, Cambridge, UK **2008**.

24. F. Leroux *ChemBioChem* **2004**, *5*, 644–649.

25. F. Grein *J. Phys. Chem. A* **2002**, *106*, 3823–3827.

26. C. Wolf, W. A. König, C. Roussel *Liebigs Ann.* **1995**, 781–786.

27. C. Wolf, D. H. Hochmuth, W. A. König, C. Roussel *Liebigs Ann.* **1996**, 357–363.

28. Y. Chen, S. Yekta, A. K. Yudin *Chem. Rev.* **2003**, *103*, 3155–3211.

29. C. Rosini, L. Franzini, A. Raffaelli, P. Salvadori *Synthesis* **1992**, 503–517.

30. J. F. Teichert, B. L. Feringa *Angew. Chem. Int. Ed.* **2010**, *49*, 2486–2528.

31. L. Meca, D. Řeha, Z. Havlas *J. Org. Chem.* **2003**, *68*, 5677–5680.

32. L. Pu *Chem. Rev.* **1998**, *98*, 2405–2494.

33. P. Kočovský, Š. Vyskočil, M. Smrčina *Chem. Rev.* **2003**, *103*, 3213–3245.

34. F. Gasparrini, L. Lunazzi, D. Misiti, C. Villani *Acc. Chem. Res.* **1995**, *28*, 163–170.

35. F. P. Gasparro, N. H. Kolodny *J. Chem. Educ.* **1977**, *54*, 258–261.

36. B. L. Jensen, R. C. Fort Jr. *J. Chem. Educ.* **2001**, *78*, 538–540.

37. S. Thormeier, B. Carboni, D. E. Kaufmann *J. Organomet. Chem.* **2002**, *657*, 136–145.

38. G. Kaupp, M. R. Naimi–Jamal, V. Stepanenko *Chem. Eur. J.* **2003**, *9*, 4156–4160.

39. T. Iida, N. Yamamoto, H. Sasai, M. Shibasaki *J. Am. Chem. Soc.* **1997**, *119*, 4783–4784.

40. K. Tani, T. Yamagata, K. Nagata *Acta Cryst.* **1994**, *C50*, 1274–1276.

41. J. M. Sugihara, C. M. Bowman *J. Am. Chem. Soc.* **1958**, *80*, 2443–2446.

42. R. J. Ferrier *Adv. Carbohydr. Chem. Biochem.* **1978**, *35*, 31–80.

43. T. W. Greene, P. G. M. Wuts *Protective Groups in Organic Synthesis*, 3rd ed., Wiley, New York **1999**.

44. D. S. Matteson *Acc. Chem. Res.* **1988**, *21*, 294–300.

45. D. S. Matteson *Tetrahedron* **1989**, *45*, 1859–1885.

46. T. Umemoto, K. Adachi *J. Org. Chem.* **1994**, *59*, 5692–5699.

47. D. Balogh, Z. Zhang, A. Cecconello, J. Vavra, L. Severa, F. Teply, I. Willner *Nano Lett.* **2012**, *12*, 5835–5839.

48. K. Li, Z. Zhou, G. Zhao, C. Tang *Heteroatom Chem.* **2003**, *14*, 546–550.

49. E. F. Mooney, B. S. Thornhill *J. Inorg. Nucl. Chem.* **1966**, *28*, 2225–2227.

50. H. Nöth, H. Vahrenkamp *Chem. Ber.* **1966**, *99*, 1049–1067.

51. G. D. Y. Sogah, D. J. Cram *J. Am. Chem. Soc.* **1979**, *101*, 3035–3042.

52. Q. Gu, Z.–Q. Rong, C. Zheng, S.–L. You *J. Am. Chem. Soc.* **2010**, *132*, 4056–4057.

53. T. Hamada, T. Fukuda, H. Imanishi, T. Katsuki *Tetrahedron* **1996**, *52*, 515–530.

54. H. Furuno, T. Hayano, T. Kambara, Y. Sugimoto, T. Hanamoto, Y. Tanaka, Y. Z. Jin, T. Kagawa, J. Inanaga *Tetrahedron* **2003**, *59*, 10509–10523.

55. R. Hulst, N. K. de Vries, B. L. Feringa *Tetrahedron Asymm.* **1994**, *5*, 699–708.

56. M. Hatano, T. Horibe, K. Ishihara *J. Am. Chem. Soc.* **2010**, *132*, 56–57.

57. K. B. Simonsen, K. V. Gothelf, K. A. Jørgensen *J. Org. Chem.* **1998**, *63*, 7536–7538.

58. A. Mazzanti, L. Lunazzi, M. Minzoni, J. E. Anderson *J. Org. Chem.* **2006**, *71*, 5474–5481.

59. A. H. Cowley, M. J. S. Dewar, W. R. Jackson *J. Am. Chem. Soc.* **1968**, *90*, 4185–4186.

60. E. L. Muetterties, P. Meakin, R. Hoffmann *J. Am. Chem. Soc.* **1972**, *94*, 5674–5676.

61. V. Marathias, M. M. Turnbull, R. L. II Abdon, B. O. Coppola *Polyhedron* **1992**, *11*, 2759–2766.

62. D. Dakternieks, R. di Giacomo *Phosphorus and Sulfur* **1985**, *24*, 217–224.

63. D. S. Bader, M. M. Turnbull *Polyhedron* **1990**, *9*, 2619–2623.

64. L. Jones, P. Atkins *Chemistry: Molecules, Matter, and Change* 4th ed; W. H. Freeman, New York, USA **2000**.

65. C. Cox, T. Lectka *J. Org. Chem.* **1998**, *63*, 2426–2427.

66. J. S. Lomas *J. Phys. Org. Chem.* **2007**, *20*, 221–228.

67. A. D. Bain, P. Hazendonk *J. Phys. Chem. A* **1997**, *101*, 7182–7188.

68. D. R. Lide *CRC Handbook of Chemistry and Physics* 85th ed; CRC Press, Boca Raton, USA **2005**.

69. M. P. Johansson, J. Olsen *J. Chem. Theory Comput.* **2008**, *4*, 1460–1471.

70. O. Bastiansen, S. Samdal *J. Mol. Struct.* **1985**, *128*, 115–125.

71. L. Pu *Chem. Rev.* **2004**, *104*, 1687–1716.

72. G. Wojciechowski, Z. Rozwadowski, T. Dziembowska, B. Brzezinski *J. Mol. Struct.* **2001**, *559*, 379–389.

73. R. Eelkema, B. L. Feringa *J. Am. Chem. Soc.* **2005**, *127*, 13480–13481.

74. T. Mizutani, H. Takagi, O. Hara, T. Horiguchi, H. Ogoshi *Tetrahedron Lett.* **1997**, *38*, 1991–1994.

75. H. Takagi, T. Mizutani, T. Horiguchi, S. Kitagawa, H. Ogoshi *Org. Biomol. Chem.* **2005**, *3*, 2091–2094.

76. Gaussian 09, Revision C.01, M. J. Frisch, G. W. Trucks, H. B. Schlegel, G. E. Scuseria, M. A. Robb, J. R. Cheeseman, G. Scalmani, V. Barone, B. Mennucci, G. A. Petersson, H. Nakatsuji, M. Caricato, X. Li, H. P. Hratchian, A. F. Izmaylov, J. Bloino, G. Zheng, J. L. Sonnenberg, M. Hada, M. Ehara, K. Toyota, R. Fukuda, J. Hasegawa, M. Ishida, T. Nakajima, Y. Honda, O. Kitao, H. Nakai, T. Vreven, J. A. Montgomery, Jr., J. E. Peralta, F. Ogliaro, M. Bearpark, J. J. Heyd, E. Brothers, K. N. Kudin, V. N. Staroverov, T. Keith, R. Kobayashi, J. Normand, K. Raghavachari, A. Rendell, J. C. Burant, S. S. Iyengar, J. Tomasi, M. Cossi, N. Rega, J. M. Millam, M. Klene, J. E. Knox, J. B. Cross, V. Bakken, C. Adamo, J. Jaramillo, R. Gomperts, R. E. Stratmann, O. Yazyev, A. J. Austin, R. Cammi, C. Pomelli, J. W. Ochterski, R. L. Martin, K. Morokuma, V. G. Zakrzewski, G. A. Voth, P. Salvador, J. J. Dannenberg, S. Dapprich, A. D. Daniels, O. Farkas, J. B. Foresman, J. V. Ortiz, J. Cioslowski, and D. J. Fox, Gaussian, Inc., Wallingford CT, **2010**.

77. P. Y. Ayala, H. B. Schlegel *J. Chem. Phys.* **1998**, *108*, 2314–2325.

78. A. V. Marenich, C. J. Cramer, D. G. Truhlar *J. Phys. Chem. B*, **2009**, *113*, 6378–6396.

Summary

Despite all the scientific advances over the years, scientists still remain puzzled when it comes to some of the most basic features of biological systems that life is based upon. The way biologically important molecules perform their functions in a highly complex system like a cell still remains to a large extent a mystery. Understanding natural systems at the molecular and even submolecular level is crucial if these systems are to be affected and altered in a controlled way. Interfering with these systems, however, is essential for treating certain diseases and improving the life of many. Getting to understand how biological systems exactly work and manipulating them at the molecular level has proven extremely difficult, not only due to the minuscule size of these highly complex molecules but also due to the prevalence of different physical phenomena at that level.

Nevertheless, one of modern chemistry's main objectives is gaining control over molecular motion. Taking inspiration from nature, scientists have started developing simple artificial systems with the goal of developing controlled motion at the (sub)molecular level. Molecular rotors, motors, shuttles and switches have extensively been used in numerous attempts to bring molecular motion under control. Harnessing molecular motion at the nanoscale paves the road for the realization of another highly important, yet extremely demanding objective in contemporary science and that is to perform work at the molecular level.

The introductory chapter of this thesis aims to give an overview of the numerous attempts by scientists to develop artificial motor systems, the vast majority of which draw inspiration from the remarkable natural dynamic systems. The focus is set on rotary motion and responsive molecules on surfaces. The former describes the development of molecular rotors and the attempts to control them while the latter aims to show how the field progressed from the investigation of small and simple functional molecules to nanovehicles of gradually increasing complexity. As much as has already been done in this field, there is still plenty of room for improvements and further developments. Dynamic systems exhibiting coupled rotary motion have not been studied extensively and selectively addressing only one of multiple rotors within a complex molecular system still remains a challenge. Likewise, although an electrically driven nanocar has been realized, it still fails to use light as fuel for motion despite being equipped with light-driven molecular motors. Moreover, future application of these devices (both molecular rotors and devices operating on surfaces) will require them to be more efficient which undoubtedly requires more research in this area.

The research described in this thesis deals with attempts to control motion at the molecular and submolecular level. The design, preparation and solution-study of new molecules is described with the goal of getting a better understanding of the motion-related behaviour of molecules and molecular devices on surfaces. Furthermore, the

Summary

design, preparation and study of new molecular rotors with the aim of tuning the rotation rate in these systems is also described.

In Chapter 2 of this thesis the design, preparation and characterization of novel multiazobenzene molecules **1** and **2** (Fig 1) are described as well as their properties in solution. The two molecules **1** and **2** are designed to have three or four photoswitching units (Fig 1), respectively, with the goal of studying their surface-behaviour as this type of molecular multiswitches has not been studied extensively and does not appear to be well-understood. Due to their high symmetry the molecules were prepared through convergent synthetic routes. The photochemical properties of both molecules were extensively studied in solution by UV–Vis and NMR spectroscopic techniques. They exhibit typical azobenzene switching behaviour; the azobenzene group may be photoisomerized between the *E*– and *Z*–isomeric forms and the *Z*–azobenzene group may also be thermally isomerized to the more stable *E*–isomer. The kinetics of the thermal isomerization process were investigated at different temperatures and the findings are interpreted in terms of the mechanism for the thermal isomerization process. Both molecules behave in the same way with respect to their photochemical properties and it appears that every azobenzene group switches independently of the rest of the molecule. Based on their solution behaviour the molecules appear to be very good candidates for further investigation on surfaces. Preliminary surface studies are underway.
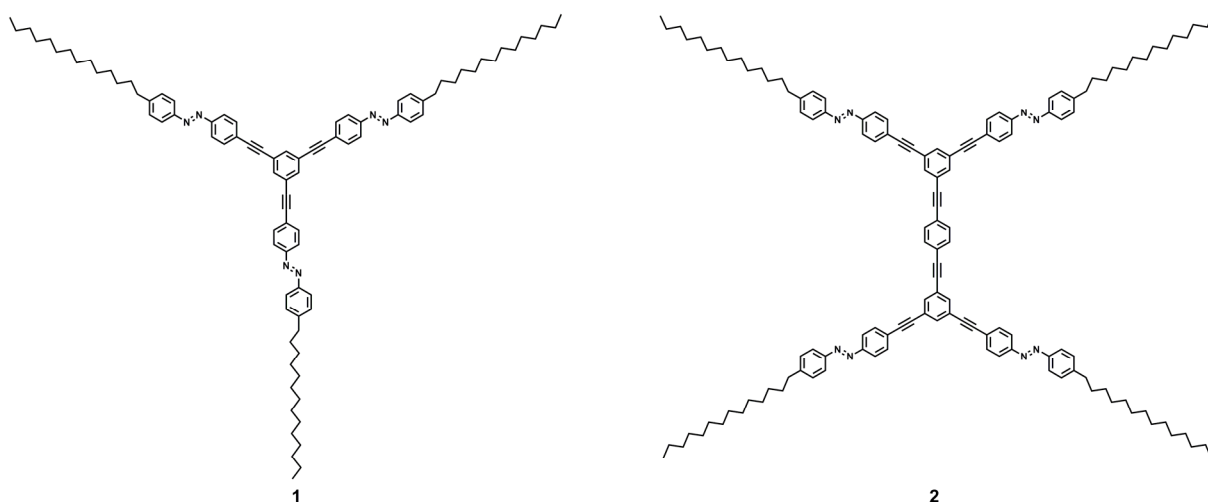
Figure 1. The novel multiazobenzene molecules described in Chapter 2.

Chapters 3 and 4 deal with the design, preparation, characterization and solution-study of novel light-driven molecular vehicles **3a,b** and **4** equipped with two newly designed triphenylsilyl molecular wheels and one or two azobenzene units, respectively (Fig 2). The switching azobenzene units as well as the wheels are connected to a central carbazole unit and, in addition to the number of the switching units, the molecules also differ in the position of the wheels on the carbazole core (Fig 2). The molecules are designed for surface studies with the aim of investigating their surface-traversing properties and contributing to the development of light-

propelled nanovehicles. Due to the known ability of the azobenzene switches to act in concert and provide work, molecule **4** designed in Chapter 4, having two switching units, is envisaged to display different surface-behaviour than the monoazobenzene molecules **3a,b** described in Chapter 3. The molecules were successfully prepared through convergent synthetic routes. The photochemical properties of the new molecules were extensively studied in solution by UV−Vis and NMR spectroscopic techniques. All molecules exhibit typical azobenzene switching behaviour; the azobenzene group can be photoisomerized between the *E*− and *Z*−isomeric forms and the *Z*−azobenzene group can also be thermally isomerized to the more stable *E*−isomer. In case of the bisazobenzene molecule **4**, however, an irreversible side reaction was also observed which might limit its applicability as a surface-traversing molecule. The kinetics of the thermal isomerization process were studied at different temperatures revealing the inversion mechanism as the dominant pathway for the thermal isomerization of monoazobenzene molecules **3a,b** in solution and a mechanism between the rotation and inversion mechanisms in case of bisazobenzene molecule **4** in solution. It is worth noting that the two new monoazobenzene molecules **3a,b**, differing only in the position of the wheels (Fig 2), have very similar photochemical properties. The bisazobenzene molecule **4** discussed in Chapter 4, however, shows more similarity (in terms of behaviour in the thermal isomerization process) with multiazobenzene molecules **1** and **2** described in Chapter 2 (Fig 1) than with monoazobenzene molecules **3a,b** in Chapter 3. It appears that the higher degree of structural similarity between the switching units and not between the supporting parts of the molecules is responsible for the similar photochemical properties of the studied molecules. The two monoazobenzene molecules **3a,b** have fully retained the basic azobenzene properties and make very good candidates for surface studies. Investigations of molecules on surfaces are underway, both at the solid/liquid interface as well as under ultrahigh vacuum.

Summary
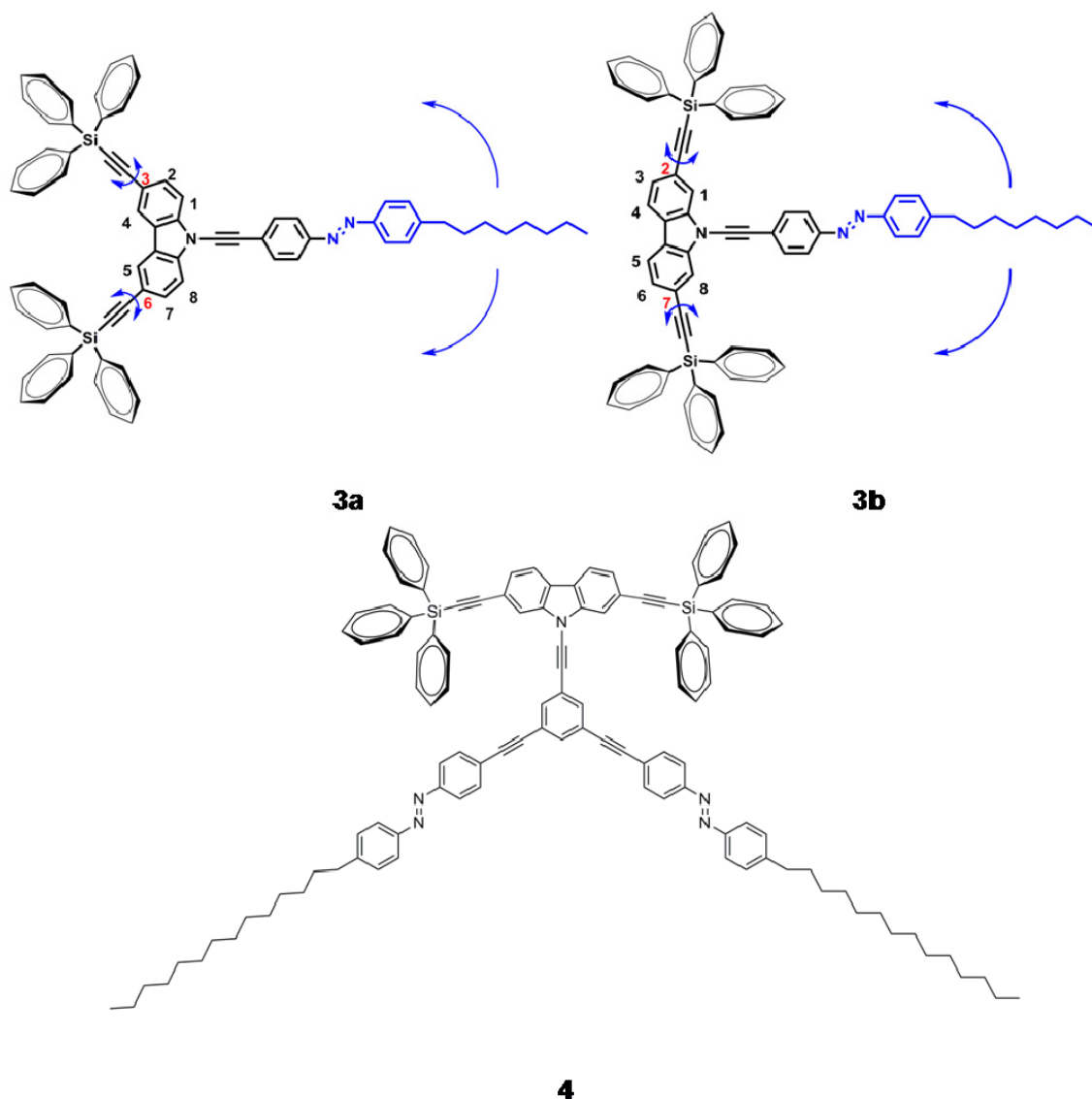
Figure 2. The novel surface-traversing molecules described in Chapters 3 and 4.

Chapter 5 of this thesis deals with unidirectional light-driven rotary molecular motors based on overcrowded alkenes (Fig 3). The exceptional features of these molecules render them highly useful to a number of applications in nanotechnology. Many of these applications, however, would benefit from higher rotation rates. To this end a new molecular motor **5** is designed, prepared and thoroughly studied. As seen from Fig 3, the new motor comprises a fluorene lower half and a five-membered ring upper half; the upper half ring is fused to a *p*-xylyl moiety and bears a *tert*-butyl group at the stereogenic centre. The kinetics of the thermal isomerization were studied by both low temperature UV–Vis spectroscopy as well as by transient absorption spectroscopy at room temperature. These studies revealed that the *tert*-butyl and the *p*-xylyl groups on the five-membered upper half ring may be used simultaneously in the same molecular design to achieve acceleration of the rotation rate of the molecular motor larger than the acceleration obtained by using any one of the two groups individually. Furthermore, the new molecular motor **5** shows remarkably high photostationary states as well as unidirectional rotation.
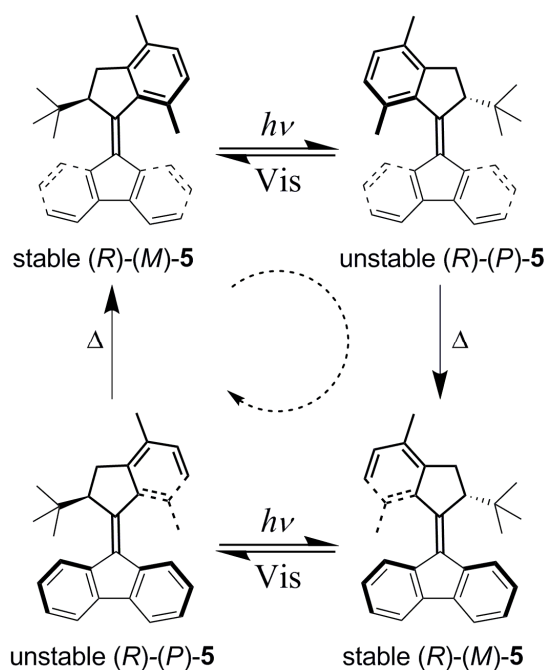
Figure 3. The novel light-driven molecular motor undergoing unidirectional rotation, as discussed in Chapter 5.

Chapter 6 describes the design, preparation and study of a set of novel binaphthyl based molecular rotors with the goal of tuning their rotation rate by means of direct steric control (Fig 4a) as well as by allosteric regulation (Fig 4b,c). The molecules described herein are equipped with multiple rotors rendering them excellent candidates for the study of coupled rotation as well as for exploring the possibilities of selectively addressing only one of the multiple rotors. Several compounds with two 3,5-dimethylphenyl rotators positioned on carbon atoms adjacent (the 3,3' positions on the binol core) to the two hydroxyl groups on binol were prepared and the rotation rates of the rotators investigated before and after chemically modifying the two hydroxyl groups (Fig 4a). The rotation of the 3,5-dimethylphenyl group, however, appeared to have a low energy barrier making the rotation too fast to observe in any of the compounds. The rotation of the bis(1-phenylethyl)amino group around the P–N bond (P-atom bound to the two O-atoms on binol) in one of the compounds studied, however, was slow enough to be studied and showed considerable acceleration upon binding a BH_3 molecule to the P-atom. The concept of selectively addressing only one mode of molecular motion is highly interesting for the field of molecular devices and machines. Several compounds with two 2,6-dimethylphenyl rotators positioned on the opposite side of the molecule (the 6,6' positions on the binol core) than the two hydroxyl groups were prepared and the rotation rates of the rotators investigated before and after chemically modifying the two hydroxyl groups (Fig 4b). The rotation was studied in two solvents in order to investigate a possible solvent effect. Although of measurable rate, the rotation of the 2,6-dimethylphenyl groups did not appear to undergo any significant change upon chemically modifying the hydroxyl groups. The choice of solvent did not seem to make any difference either, with the exception of a cyclic phosphoramidite derivative

Summary

that exhibited a significantly lower rotation barrier in toluene-d_8 than in DMSO-d_6. The concept of affecting the rotation rate by a mere change of solvents is rather exciting and requires additional research. The concept of using noncovalent interaction to remotely affect the rotation rate was also investigated (Fig 4b,c). (*R*)-Binol equipped with two 2,6-dimethylphenyl rotators at the 6,6' positions was studied in separate mixtures with (*S*)-2-amino-3-phenyl-1-propanol and (*R*)-2-amino-3-phenyl-1-propanol as this aminoalcohol is known to form hydrogen bonded complexes with biphenols. In CDCl$_3$ the rotation barrier in the presence of the (*S*)-aminoalcohol was found to be significantly lower than in its absence. The possibility of controlling the rotation rate through the formation of supramolecular complexes is exciting. Moreover, the idea of addressing a molecule on one side and affecting the properties of its rotators on the other side of the molecule is a highly interesting concept. The (*R*)-aminoalcohol was found to have the same effect on the rotation rate of the rotators as the (*S*)-aminoalcohol.
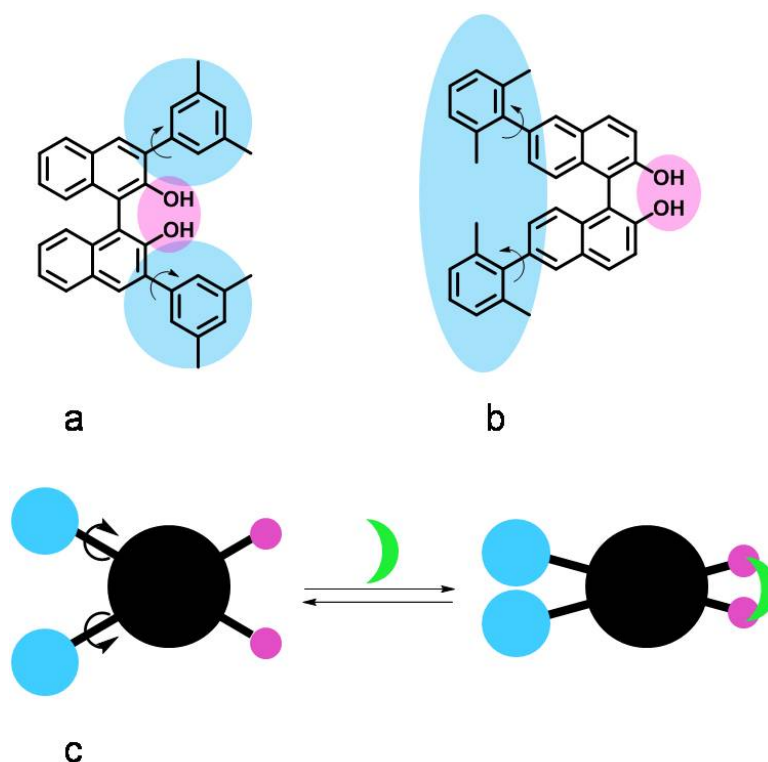
Figure 4. Design of binol–based molecular rotors as discussed in Chapter 6; highlighted in pink are the areas that can be chemically altered and highlighted in blue are the rotors whose rotation rate may be affected by the chemical change in the pink region.

Overall, the research presented in this thesis contributes to the better understanding of motion-related behaviour of molecules. Various molecular systems have been investigated and several ways of controlling motion have been identified. The insight and knowledge gained will bring nanoscience one step closer to the realization of harnessing motion and performing work at the molecular and submolecular level paving the way for numerous practical applications.

Samenvatting

Ondanks alle wetenschappelijke vooruitgang door de jaren heen staan wetenschappers nog steeds voor een raadsel als het gaat om sommige van de meest fundamentele aspecten van de biologische systemen waarop leven is gebaseerd. De wijze waarop de moleculen die aan de basis van de biochemie staan hun functie uitvoeren in een uitermate complexe omgeving als een cel is voor het grootste deel nog steeds een raadsel. Een beter begrip van deze natuurlijke systemen op moleculair en zelfs submoleculair niveau is nodig om ze te beïnvloeden en veranderen op een gecontroleerde wijze. Dit is zeer belangrijk om bijvoorbeeld bepaalde ziektes te behandelen. Het is zeer ingewikkeld om uit te vinden hoe biologische systemen precies in elkaar zitten op moleculair niveau, en ze te manipuleren, niet alleen vanwege de grootte van deze complexe moleculen maar ook door het feit dat op die schaal andere fysische processen een rol spelen.

Desalniettemin is het controleren van de beweging van moleculen een belangrijk doel in de moderne scheikunde. Geïnspireerd door de natuur zijn wetenschappers begonnen om simpele systemen te maken met als doel controle te verkrijgen over beweging op (sub)moleculair niveau. Moleculaire rotors, motoren, shuttles en schakelaars zijn uitgebreid getest in pogingen om de beweging van moleculen te beheersen. Dit effent de weg naar een andere extreem belangrijke doelstelling in de moderne wetenschap, namelijk het verrichten van werk op moleculair niveau.

Het introductiehoofdstuk van dit proefschrift geeft een overzicht van de talrijke pogingen van wetenschappers om kunstmatige motorsystemen te ontwikkelen, waarvan het merendeel is geïnspireerd door de systemen uit de natuur. De focus ligt op rotatiebeweging en responsieve moleculen op oppervlakken. In het eerste deel wordt de ontwikkeling van moleculaire rotors uiteengezet, en hoe de rotatie mogelijk kan worden beheerst. In het tweede deel wordt de voortgang in het onderzoek naar responsieve moleculen op oppervlakken beschreven, van de studie van eenvoudige moleculen tot nanovoertuigen van immer toenemende complexiteit. Hoewel er al veel onderzoek is verricht in dit veld, zijn er nog steeds voldoende nieuwe doelstellingen. Dynamische systemen waarin gekoppelde rotatie plaatsvindt zijn nog niet uitvoerig bestudeerd, en het aansturen van slechts één rotor in een complex moleculair systeem met meerdere rotors is nog steeds een wetenschappelijke uitdaging. En hoewel er een elektrisch aangedreven nano-auto is ontwikkeld, die zelfs met licht-aangedreven moleculaire motoren is uitgerust, is het nog steeds niet mogelijk om licht te gebruiken als brandstof voor beweging over een oppervlak. Bovendien zal het een vereiste zijn dat de efficiëntie van deze systemen verhoogd wordt om ze daadwerkelijk te kunnen toepassen. Verder onderzoek in dit veld is dus noodzakelijk.

Samenvatting

Het onderzoek dat wordt beschreven in dit proefschrift is gericht op het beheersen van beweging op moleculair en submoleculair niveau. Het ontwerp en de synthese van nieuwe moleculen wordt beschreven, evenals spectroscopie van de moleculen in oplossing, met als doel een beter begrip te ontwikkelen van hoe deze moleculen zich gedragen en bewegen op oppervlakken. Ook wordt beschreven hoe nieuwe rotors zijn ontworpen, gesynthetiseerd en bestudeerd om de rotatiesnelheid te kunnen controleren.

In Hoofdstuk 2 van dit proefschrift staan het ontwerp, de synthese en karakterisatie van de nieuwe azobenzeenmoleculen **1** en **2** (Figuur 1) beschreven, alsmede hun eigenschappen in oplossing. Moleculen **1** en **2** zijn ontworpen met respectievelijk drie en vier lichtgevoelige schakelaars (Figuur 1), om uiteindelijk hun schakelgedrag op een oppervlak te kunnen bestuderen. Dit type moleculen met meerdere schakelaars is slechts weinig bestudeerd en hun gedrag wordt nog niet volledig begrepen. Dankzij de hoge symmetrie was het mogelijk om de moleculen via convergente syntheseroutes te maken. De fotochemie van beide moleculen in oplossing werd uitvoerig bestudeerd met UV−Vis en NMR spectroscopie. Beiden vertonen schakelgedrag typerend voor azobenzenen; de azobenzeengroep kan met licht worden geïsomeriseerd van de *E* naar de *Z* isomeer en *vice versa*, en de *Z* isomeer kan ook thermisch worden omgezet in de stabielere *E* isomeer. De kinetiek van de thermische isomerisatie werd onderzocht bij verschillende temperaturen en uit de resultaten werd een mechanisme voor de thermische isomerisatie afgeleid. Beide moleculen vertonen dezelfde fotochemische eigenschappen en het schakelen van de azobenzeengroepen gebeurt onafhankelijk van de rest van het molecuul. Op basis van het gedrag van deze moleculen in oplossing zijn de moleculen goede kandidaten voor verder onderzoek op oppervlakken. De eerste experimenten op een oppervlak worden inmiddels uitgevoerd.
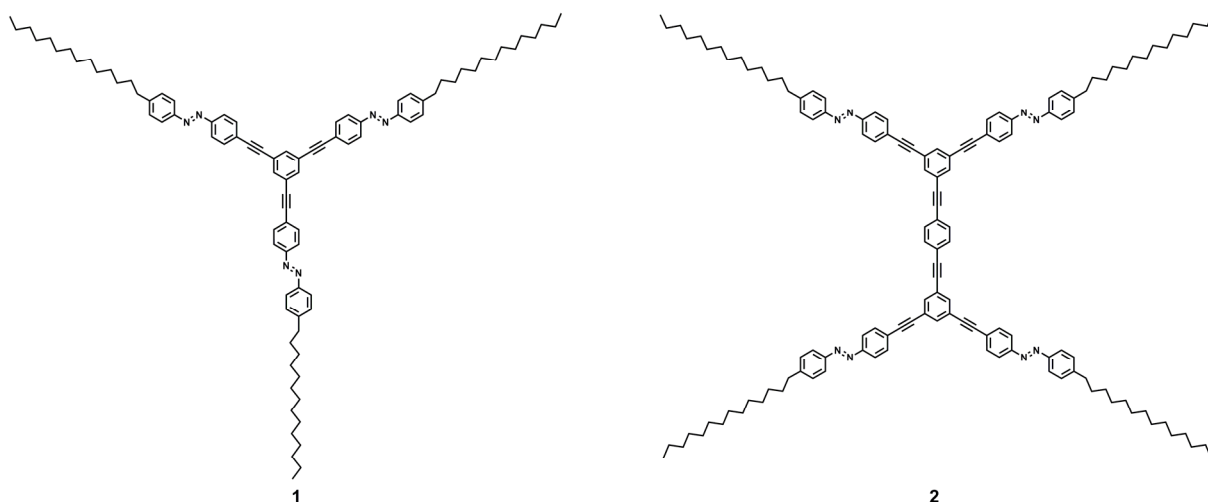

Figuur 1. De nieuwe moleculen met meerdere azobenzeengroepen beschreven in Hoofdstuk 2.

Hoofdstukken 3 en 4 richten zich op het ontwerp, de synthese, karakterisatie en het bestuderen van de eigenschappen in oplossing van die nieuwe nanovoertuigen

3a,b en **4** uitgerust met trifenylsilylgroepen als wielen en één of twee azobenzeengroepen (Figuur 2). Zowel de azobenzeenschakelaars als de wielen zijn verbonden met een centrale carbazoolgroep en de moleculen verschillen behalve in het aantal azobenzeengroepen ook in de positionering van de wielen (Figuur 2). De moleculen zijn ontworpen om bestudeerd te worden op oppervlakken, om te kijken of de moleculen zich kunnen voortbewegen over het oppervlak, en om bij te dragen aan de ontwikkeling van nanovoertuigen die met licht kunnen worden aangedreven. Aangezien het bekend is dat meerdere azobenzeengroepen samen werk kunnen verrichten wordt verwacht dat molecuul **4**, beschreven in Hoofdstuk **4**, zich anders gedraagt op een oppervlak dan moleculen **3a,b** die staan beschreven in Hoofdstuk 3. De moleculen werden gemaakt via convergente syntheseroutes. De fotochemische eigenschappen in oplossing van de nieuwe moleculen werden uitgebreid bestudeerd met UV−Vis en NMR spectroscopie. De moleculen vertonen allen schakelgedrag typerend voor azobenzenen; de azobenzeengroep kan met licht worden geïsomeriseerd van de *E* naar de *Z* isomeer en *vice versa*, en de *Z* isomeer kan ook thermisch worden omgezet in de stabielere *E* isomeer. In het geval van bisazobenzeen **4** trad echter ook een onomkeerbare nevenreactie op, waardoor dit molecuul mogelijk minder geschikt is voor toepassing in studies op oppervlakken. De kinetiek van de thermische isomerisatie werd bestudeerd bij verschillende temperaturen en hieruit werd afgeleid dat isomerisatie in oplossing via een inversiemechanisme plaatsvindt voor moleculen **3a,b** en een mechanisme tussen rotatie en inversie voor molecuul **4**. Moleculen **3a,b** hebben beiden één azobenzeengroep en verschillen alleen in de positie van de wielen en vertonen dezelfde fotochemische eigenschappen. Molecuul **4**, met twee azobenzeengroepen, lijkt daarentegen meer op de moleculen **1** en **2** uit Hoofdstuk 2 wat betreft thermische isomerisatie. In beide monoazobenzenen **3a,b** is het normale isomerisatiegedrag van de azobenzeengroep behouden gebleven en deze moleculen zijn goede kandidaten voor oppervlaktestudies. Zowel metingen op het grensvlak van een oppervlak met een oplosmiddel als metingen onder ultrahoog vacuüm worden uitgevoerd.
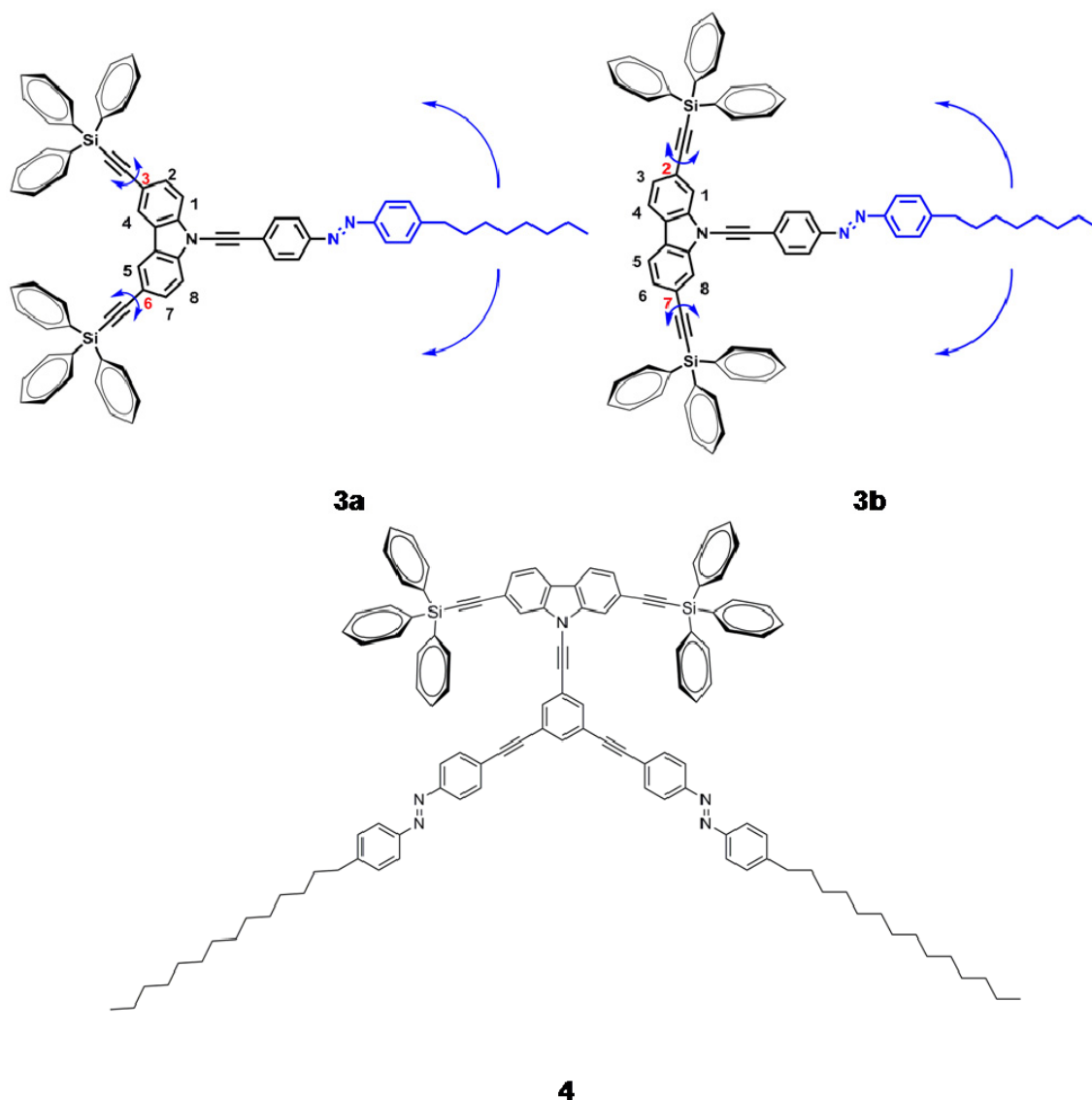
Figuur 2. De nieuwe moleculen gericht op verplaatsing over een oppervlak beschreven in Hoofdstukken 3 en 4.

Hoofdstuk 5 van dit proefschrift gaat over unidirectionele, door licht aangedreven moleculaire rotatiemotoren gebaseerd op sterisch gehinderde alkenen (Figuur 3). De bijzondere eigenschappen van deze moleculen maken ze toepasbaar in nanotechnologie. Veel potentiële toepassingen zouden echter kunnen profiteren van een hogere rotatiesnelheid. Daarom werd de nieuwe moleculaire motor **5** ontworpen en gesynthetiseerd en werden zijn eigenschappen bestudeerd met verscheidene spectroscopische technieken. In Figuur 3 is te zien dat de nieuwe motor bestaat uit fluoreengroep in de onderhelft en cyclopenteenring in de bovenhelft; deze is gefuseerd met een *p*-xylylgroep en heeft een *tert*-butylgroep op het stereocentrum. De kinetiek van de thermische isomerisatie werd bestudeerd met zowel UV−Vis spectroscopie bij lage temperatuur als met transient absorptie spectroscopie bij kamertemperatuur. Uit deze metingen bleek dat het gebruik van de *tert*-butylgroep én de *p*-xylylgroep aan de vijfring leidt tot een toename van de rotatiesnelheid van de moleculaire motor die groter is dan als slechts één van deze groepen wordt gebruikt.

Bovendien ligt het evenwicht in de fotoisomerisatie van de nieuwe motor **5** zeer gunstig en is de rotatie unidirectioneel.

stabiel (*R*)-(*M*)-**5**   instabiel (*R*)-(*P*)-**5**

instabiel (*R*)-(*P*)-**5**   stabiel (*R*)-(*M*)-**5**
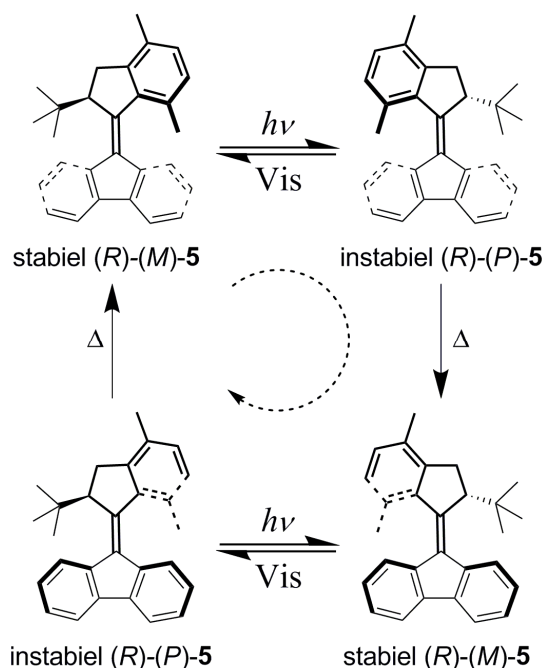
Figuur 3. De nieuwe moleculaire motor **5** ondergaat unidirectionele rotatie onder invloed van licht zoals beschreven in Hoofdstuk 5.

Hoofdstuk 6 beschrijft het ontwerp en de synthese van, en metingen aan, een serie nieuwe moleculaire rotors gebaseerd op binaftyl met als doel het controleren van de rotatiesnelheid door middel van sterische hinder (Figuur 4a) en allosterische regulatie (Figuur 4b,c). De hier beschreven moleculen zijn voorzien van meerdere rotors, waardoor ze kunnen worden gebruikt om gekoppelde rotatie te onderzoeken en mogelijk ook in experimenten om selectief één van de rotors te beïnvloeden. Verscheidene verbindingen met twee 3,5-dimethylfenyl-rotators op de koolstofatomen naast de hydroxylgroepen van binol (de 3,3'-posities) werden gesynthetiseerd en de rotatiesnelheid werd bestudeerd voor en na chemische modificatie van de hydroxylgroepen. De rotatie van de 3,5-dimethylfenylgroep bleek echter een zodanig lage barrière te hebben dat de rotatie in beide gevallen te snel was om te meten in alle verbindingen. De rotatie van de bis(1-fenylethyl)aminogroep rond de P−N binding (met het P-atoom gebonden aan beide O-atomen van binol) was echter traag genoeg om gemeten te kunnen worden en werd aanzienlijk versneld door een molecuul BH_3 aan het P-atoom te binden. Het concept van selectief één rotor in een ensemble beïnvloeden is erg interessant vanuit het oogpunt van de nanotechnologie. Verscheidene verbindingen met 2,6-dimethylfenyl-rotators aan de andere kant van het molecuul ten opzichte van de hydroxylgroepen (de 6,6'-posities van binol) werden gesynthetiseerd en de rotatiesnelheden werden bepaald voor en na chemische modificatie van de hydroxylgroepen (Figuur 4b). De rotatiesnelheid werd gemeten in twee verschillende oplosmiddelen om een mogelijk oplosmiddeleffect waar te nemen. Hoewel de rotatiesnelheden in dit geval wel

konden worden gemeten, werd er geen verschil gevonden bij chemische modificatie van de hydroxylgroepen. Het oplosmiddel leek niet van invloed te zijn, behalve in het geval van een cyclisch fosforamidiet-derivaat dat een aanmerkelijk lagere rotatiesnelheid had in tolueen-d_8 dan in DMSO-d_6. Het kunnen aanpassen van de rotatiesnelheid door simpelweg het oplosmiddel te veranderen is een interessant concept dat verder onderzocht dient te worden. Het idee om niet-covalente interacties te gebruiken om de rotatiesnelheid te beheersen werd ook onderzocht (Figuur 4b,c). (*R*)-Binol gesubstitueerd met twee 2,6-dimethylfenyl-rotators op de 6,6'-posities werd bestudeerd in mengsels met zowel (*S*)-2-amino-3-fenyl-1-propanol als (*R*)-2-amino-3-fenyl-1-propanol omdat van dit aminoalcohol bekend is dat het door middel van waterstofbruggen complexen vormt met bifenolen. De barrière voor rotatie in CDCl$_3$ was aanzienlijk lager in aanwezigheid van (*S*)-2-amino-3-fenyl-1-propanol. De mogelijkheid om de rotatiesnelheid te kunnen beïnvloeden door het vormen van een supramoleculair complex biedt mogelijkheden. Bovendien is het zeer interessant om aan de ene kant van het molecuul iets te binden, wat vervolgens de eigenschappen van de rotors aan de andere kant van het molecuul beïnvloedt. Het (*R*)-aminoalcohol had hetzelfde effect op de rotatiesnelheid als het (*S*)-aminoalcohol.
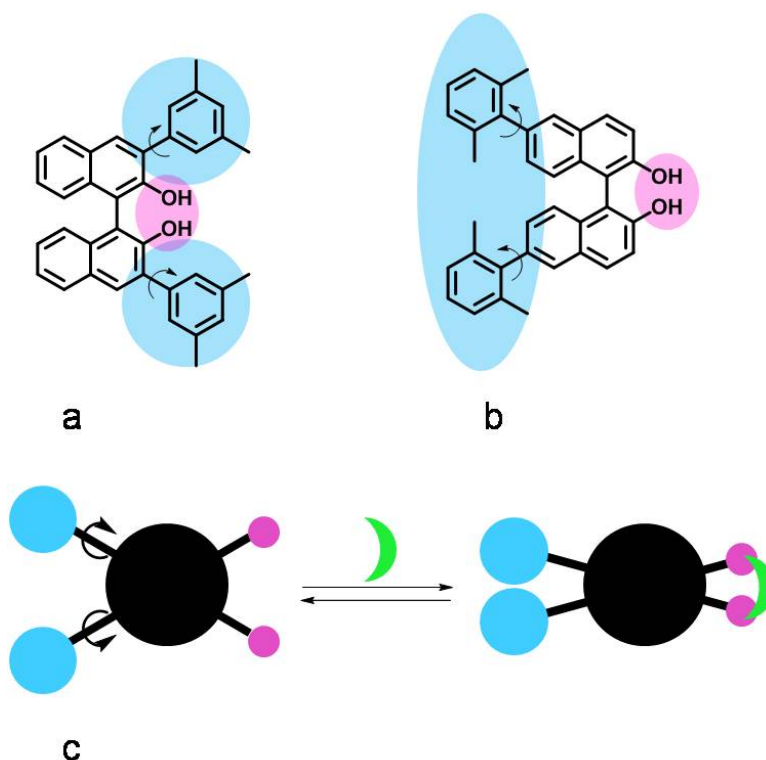
Figuur 4. Ontwerp van moleculaire rotors gebaseerd op binol zoals beschreven in Hoofdstuk 6; de groepen die chemisch kunnen worden gemodificeerd zijn aangegeven met roze, de rotors die kunnen worden beïnvloed door de modificatie in de roze gebieden zijn aangegeven met blauw.

Al met al draagt het onderzoek dat wordt beschreven in dit proefschrift bij aan een beter begrip van de beweging van moleculen. Verscheidene moleculaire systemen zijn onderzocht en er werden verschillende manieren gevonden om deze

bewegingen te kunnen beheersen. De nieuwe inzichten en kennis brengen de nanowetenschap een stap dichter bij het beheersen van beweging en het verrichten van werk op moleculair en submoleculair niveau en dit effent de weg voor talloze toepassingen.

Acknowledgements

In this final section of my thesis I intend to place the work described herein in a social context as opposed to the scientific context present throughout the remainder of the thesis. The research presented here is not a mere result of being locked away in a laboratory for five years but rather a result of years of research intertwined with extensive interaction with other people, be it in terms of purely scientific contributions, completely non-work related support or anything in between.

Dear Ben, you cannot imagine the joy I felt when you first accepted me as a PhD student in your group. I was on my way to conquer the world! Soon thereafter I actually started my PhD and for the five years that followed that feeling of pure enthusiasm suffered many ups and downs. There were times when I found my PhD utterly pointless and then there were times when I felt proud of the work I carried out. As my supervisor you have always approached my projects, as well as chemistry in general, with admirable enthusiasm and, at times, almost naive optimism both of which are something I have tremendous respect for. I do wish though that we had had more time for discussion than your far too hectic schedule allowed for. I also wish we had been successful in establishing a much needed external collaboration for some of the projects. At the end of the day, however, I am happy to say that I hold no regrets about my PhD nor about the time I spent in Groningen and would hereby genuinely like to thank you for your part in that.

I would like to extend my gratitude to the people who directly took part in the research presented herein. Thom and Jos, the calculations that you performed as part of my research projects on molecular rotors and motors, respectively, have given the experimental results an added value. I appreciate your efforts and am thankful for all the inspiring discussions during our work together. Lili, I am grateful for your contribution to the investigation of my new molecular motor. The measurements that you performed have significantly contributed to the project and will hopefully result in a nice publication. Lourens-Jan, you worked as my student on the „jumping jack" project, as you liked to call it, and obtained some nice results which are also presented in this thesis. Apart from genuinely enjoying working with you, guiding you in the lab rekindled my passion for teaching and working with students. I am grateful for the experience as well as for your efforts on the project. Xiaoyan and Arjen, you both made a great effort to examine my molecules on the surface by means of STM. It is rather unfortunate, however, that you were not see able to see the molecules on the surface. Nevertheless, your efforts are greatly appreciated.

Questioning results, providing feedback, suggesting experiements and considering crazy ideas are essential for scientific progress. The work presented in this thesis is, in its entirety, indebted to the indisputable contributions of the motor subgroup and all its members. Many others have also made a significant impact on the work presented herein. In the course of research on molecular rotors, presented in chapter 6 of this thesis, prof. Scheek generously offered his help with the data

Acknowledgements

analysis. I truly enjoyed our extensive discussions from which I feel that I have learnt a great deal. I do regret, however, that it was not before the last few months of my PhD that we started working together. Had we had more time to work on that project, I feel that our collaboration could have been even more fruitful. Be that as it may, I would like to express my gratitude for all your help in the short time that we worked together. Furthermore, in their capacity of members of the reading committee, prof. Browne, prof. Broer and prof. Minnaard are gratefully acknowledged for critically yet promptly evaluating this thesis which has improved it in many aspects.

An often understated yet, in my opinion, highly important part of the PhD program was the problem session. Discussing chemical problems and conundrums in front of the blackboard as well as preparing a set of problems for other problem solvers was something I truly enjoyed and found very useful and instructive. Needless to say, Miriam's delicious home-made cakes made the experience all the more delightful. I am grateful to everyone who contributed to the problem sessions in one way or another.

Petra and Arjen, I feel genuinely happy about having you as my paranymphs. Were it possible to have three paranymphs, Erik would surely be the third one. All three of you have been of tremendous help with my thesis, promotion and celebration. Arjen, your view, feedback and advice on almost everything in this thesis have been of extreme significance to me. Petra, your efforts with the organization of the day of the promotion as well as with advising me on how (not) to dress have not gone unnoticed. Erik, your help with the design of the cover of this thesis as well as with so many other things regarding the promotion itself means a great deal to me. I feel that having the three of you by my side around the time of the finalization of my PhD is the next logical step from friendships that have been built throughout my time in Groningen and beyond. Arjen, spending time with you in the lab as well as outside of it has been a lot of fun; conversations about virtually everything, ranging from utterly insignificant everyday things to the big questions in life, never seem to bore us, do they? However, I miss those find-as-many-spelling-mistakes-in-the-presentation contests that we used to play during talks when we would compete to see who would find more spelling mistakes in the presentation slides of illiterate mortals. Petra, exploring new restaurants together and attending classical music concerts or theatrical performances afterwards has been a true delight. Erik, we may have had some communication issues while working alongside each other in the lab but spending time outside the lab has always been so much fun; attending concerts and exhibitions, travelling and taking photos together and countless other activities make truly nice memories. Getting together for foursomes has also been most fun. It is rather intriguing, however, that it takes a total of three men to handle a full evening of Petra (and that is only after meeting beforehand for a few shots of strong liquor).

The atmosphere in Ben's group as well as in adjoining groups has always been highly stimulating, both in terms of research and in the social aspect. Playing soccer is but one example of the fun activities I was engaged in. I thank everyone who

contributed to the nice environment at the institute. The C-wing, however, deserves a special word of gratitude. Neither the stimulating working atmosphere nor the fun social activities will easily escape my memory. The movie making, the lunch breaks with Chinese food accompanied by enlightening discussions, indulging in Petra's tasty home-made cakes, checking for the newest fail compilations and spying on the pornguy were but a few of countless activities that made work more fun. I would like to thank all members of the C-wing for the nice atmosphere. Some people, however, made a more prominent impact on me. Romina, having coffee breaks with you was always a special experience for me, even if it meant just standing idle next to the coffee machine or sitting in silence in the canteen. You are by far the most interesting non-talking person I have met. I appreciate all the nice times together. Jos, we both know you should have been assigned to our lab. Conversing with you has always been a true joy for me. Sometimes I would get no response from my labmates on certain matters and at those times I knew I could always turn to you in search of guidance. You would always be more than happy to engage in an exchange of thoughts with me and that is something I am deeply grateful for. Matea, it was nice having you around the lab. Having someone to complain about the Dutch to was surely an asset. It was also nice being your neighbour for a while. Robby, thank you for having me as your paranymph. It was an honour and, more importantly, a really fun day. Mahthild, it was nice having you as a wingmate. Thank you for opening up the sizzling hot microwave meals for me so that I would not burn my hands.

Despite my strong belief that mere words would simply fail to describe the true atmosphere in my former lab, I shall nevertheless make an attempt here to address this significant part of my time in Groningen. Before my arrival in the Netherlands, little did I know how stimulating my immediate working environment would be for the years that followed. Jochem, Jort and Thom, as my new labmates, you allowed me to express my inner (and outer) self to the fullest. This was by no means a one-way process as I also found myself privileged to get to know each and one of you through the frequent *would you rather* quizzes. These not only revealed much about you but also initiated discussions that would, more often than not, take us where no human mind had ever gone before. Needless to say, I was overwhelmed. Each of you, however, has pursued their own talents and interests as well. Jochem, your passion and devotion to master the Croatian language has left many native speakers speechless. I feel honored to have had the opportunity to assist you in realizing your potential. Thom, your affection towards badgers is only surpassed by your love for tea. I hope one day you manage to (safely) combine the two passions. Jort, your passion for sports is admirable but your long list of injuries is rather scary. I wonder how many of those have been caused by tripping over oversized socks. Jochem, Jort and Thom, I enjoyed every moment spent in the lab with you. Our jokes reflect four different types of humor yet they appear to synchronize perfectly when we join forces. I could not possibly imagine better labmates during my PhD.

Taiwan! I feel happy to have received some support outside of work as well. My, doing sports with you has been of tremendous help in getting rid of all the stress that has piled up in these final moments before graduating, and spending time with you has meant more to me than you probably realize. I appreciate all the nice times together and thank you for bearing with me and my endless PhD related frustrations. Monique, my fellow hedonist, shaking and swirling with you has been a fun distraction. Under the watchful eye of the no-eyes smiley face I have indeed managed to finish my PhD. Thank you for your support.

I feel lucky to have received some support from Croatia as well. This mostly appeared in form of old friendships that could never be broken my a mere relocation within Europe. I value these old friendships the most. Senada, keeping virtual contact throughout the years has been really important to me and our endless walks and never-ending talks during my visits in Zagreb are most dear to me. Diana, it feels reassuring knowing that there is someone keeping an eye on the 'hood. There is nothing more fun than going out to meet you for some ice cream every time I am in Zagreb. Pavle, meeting you for a pile of food and some guy talk accompanied by stupid jokes is always a special treat for me. Ilija, I regret that you are too far away now for weekend pop-ins but it helps to know you are doing well in the States. Maja, we have kept the most regular contact over the years and have been there for each other in sickness and in health. What is more, we have been on so many trips together which have all formed truly nice memories. Somehow we always get along with ease. Thank you for your support over the years.

In the end I feel that I owe a special word of gratitute to my family. Dear mom and dad, you have been there with me for the whole ride, sharing joyful moments when things went well, as well as frustrating moments when things did not seem to work out for one reason or another. I greatly appreciate all the support.

Having written the acknowledgement section I realize that being concise is by no means one of my virtues. Ironically enough, when I first started my PhD, I considered the acknowledgement section utter nonsense and intended to completely omit it from my thesis. Pondering on the question whether I have changed over the last five years, however, seems like a perfect way to close.

Jurica